OPTIMAL MANAGEMENT AND CONTROL OF RENEWABLE ENERGY BASED GENERATION RICH INTEGRATED TRANSMISSION AND DISTRIBUTION ELECTRIC GRID

by

Olalekan Olasunkanmi Ogundairo

A dissertation submitted to the faculty of
The University of North Carolina at Charlotte
in partial fulfillment of the requirements
for the degree of Doctor of Philosophy in
Electrical Engineering

Charlotte

2023

Approved by:

_____
Dr. Sukumar Kamalasadan

_____
Dr. Valentina Cecchi

_____
Dr. Abasifreke Ebong

_____
Dr. Badrul Chowdrury

_____
Dr. Srinivas Akella

ABSTRACT

OLALEKAN OLASUNKANMI OGUNDAIRO. Optimal Management and control of Renewable Energy Based Generation Rich Integrated Transmission and Distribution Electric Grid. (Under the direction of DR. SUKUMAR KAMALASADAN)

Renewable energy resources advancement and offerings are steadily increasing, a major factor leading to its global fast adoption. The connection of these resources to the electric grid, however, needs to be studied to ensure efficiency both from an operational and regulatory standpoint. The IEEE 1547 has been used to establish standards for grid interconnection of some renewable energy resources (RERs). In this dissertation, the operations of RERs connected to the grid with respect to their control, management, and optimization are studied. It is of note that RERs are intermittent in nature and this can have effects on the power quality metrics or utility objectives on either transmission, distribution network separately or collectively. For instance, the stability of the grid can be affected due to the low inertia of these resources, which can impact the voltage or the grid frequency. A novel adaptive controller was developed to damp the oscillations caused by these RERs, the controller was initially tested with RERs in one network architecture, and it offers advantages such as dynamically responsive support to the grid to control the frequency, a frequency spectrum was used to determine the amount of support required in an adaptive manner. The architecture was then expanded to a network model that has both transmission and distribution networks integrated together with the interconnection of multiple RERs connected to the grid, the capabilities of the proposed architecture were evaluated with different test cases with different grid events. The architecture had the capability to control multiple generators as well as damp the oscillations observed during the test cases and simulations performed, by adaptively updating the gain of the power system stabilizers (PSS). On the management side, A new technique was developed with grid-connected RERs that provide real-time visibility of two integrated networks during operation. Presently, the operations don't offer such capabilities as the transmission system operator (TSO) is often times blind to the distribution system operator (DSO). Our technique makes it possible for the transmission network to adjust itself in real-time in case of sudden changes in the distribution network with RERs connected, A stochastic linear optimization technique; Linear decision rule (LDR) that establishes the relationship between the generators in the transmission network and the RERs in the distribution network was implemented, the technique addresses one of the major issues with integrated T&D IEEE networks which is boundary mismatch caused by the reverse power flow from the distribution network, in addition to offering the operational advantages required by most utilities like minimization of voltage deviation, and minimization of cost of operation, as it eliminates the need for curtailing RERs which is

the current implementation used by most utilities, the technique theorem proof was also discussed and The performance of the technique was evaluated using different integrated T&D IEEE networks, with different grid penetration levels of the RERs. Furthermore, Grid Connected RERs are multiperiod in nature, it is therefore imperative to study their behavior at each time interval, the optimization framework was extended to such studies to handle the reverse power flow operation due to the irradiance daily curve, and the optimal power flow formulation was transformed to multiperiod optimal power flow MPOPF. The effectiveness of the proposed architecture was tested with an irradiance curve, and a typical residential load curve, it demonstrated the capability to reduce the boundary mismatch while ensuring the grid objectives for each network were achieved. Finally, the impact of electric vehicle charging was studied and a management approach was developed, electric vehicles (EVs) adoption is also increasing impacts of the distribution network on the transmission network with respect to grid penetration, we developed a two-stage stochastic linear optimization in the integrated T&D to handle the uncertainty with electric vehicle charging and compared with effective EV charging management technique that was developed. A novel approach to handle the uncertainty with EV charging by providing an optimal set-point to charging charging was designed and evaluated, to assist utilities with operational planning.

DEDICATION

To God almighty, for the inspiration and strength. To my Parents, Mum you are a true hero and my siblings Omotola and Oluwatosin, thank you for your support and encouragement.

ACKNOWLEDGEMENTS

I have been very fortunate to get support from many people during my doctoral studies. I want to thank my advisor, Professor Sukumar Kamalasadan, who made this work possible. I would also like to thank the other members of my dissertation committee: Professors Abasifreke Ebong, Professor Valentina Cecchi,Professor Badrul Chowdrury and Professor Srinivas Akella, who have inspired my research. This work was supported by the U.S. National Science Foundation (NSF). I would also like to thank UNC, Charlotte, for the Graduate Assistant Support Plan (GASP) award. Many thanks to my fellow students and friends at UNC, Charlotte, who have directly or indirectly supported my work.

TABLE OF CONTENTS

LIST OF TABLES xi

LIST OF FIGURES xii

LIST OF ABBREVIATIONS xvi

CHAPTER 1: INTRODUCTION 1

1.1. Background 1

1.2. Motivation 1

1.3. Main Contribution of the Dissertation 2

1.4. Intellectual Merit and Broader Impact 3

1.5. Dissertation outline 4

CHAPTER 2: LITERATURE REVIEW 6

2.1. Introduction 6

2.2. Benefits and Challenges of Grid Connected RERs 7

2.2.1. Advantages of Grid Connected RERs 7

2.2.2. Disadvantages of Grid Connected DERs 10

2.3. Conventional Control methods for Grid-connected RERs 12

2.3.1. Damping controllers 13

2.3.2. Harmonic Resonance 13

2.3.3. Operational mode 14

2.3.4. Frequency control 14

2.4. Conventional management methods for Grid-connected RERs 15

2.4.1. Battery 16

2.4.2. Smart-Inverter 16

2.4.3. DERMs 18

2.4.4. PowerSharing 19

2.5. Conventional Integrated T&D optimization method 20

2.5.1. Unified Modeling 20

2.5.2. Co-Simulation Modeling 20

2.6. Summary 22

CHAPTER 3: A NOVEL ADAPTIVE DAMPING CONTROLLER FOR GRID CONNECTED RERS 23

3.1. Introduction 23

3.2. Online Adaptive Damping Controller for Wind Integrated Power Grid 23

3.2.1. DESIGN AND MODELING OF ENERGY SOURCES 24

3.2.2. Synchronous Generators 24

3.2.3. Double Fed Induction Generator Model 25

3.2.4. Mathematical Model of Proposed Damping Controller 27

3.2.5. Discussions and Performance Evaluation 31

3.3. Oscillation Damping of Integrated Transmission and Distribution Power Grid with Renewables Based on Novel Measurement-Based Optimal Controller 34

3.3.1. Main contribution 36

3.3.2. DESIGN AND MODELING OF ENERGY SOURCES 37

3.3.3. RER Integrated Power Distribution System 37

3.3.4. Mathematical Model of Proposed Damping Controller 40

3.3.5. TestSystem:Modified IEEE 123-Bus Test System, Kundu Two Area, Solar PV and WindTurbine 44

3.3.6. Discussions and Performance Evaluation 51

3.4. Summary 52

CHAPTER 4: MANAGEMENT TECHNIQUE: INTEGRATED TRANSMISSION AND DISTRIBUTION NETWORK OPTIMAL POWER FLOW. 54

4.1. Introduction 54

4.2. Integrated Transmission and Distribution Optimal Power Flow Simulation Using Linear Decision Approach 55

4.2.1. Main contribution 56

4.2.2. Model Description: General model 56

4.2.3. Transmission Network OPF model 58

4.2.4. Distribution Network OPF model 60

4.2.5. Co-Simulation using Integrated optimization engine(IOE) with LDR 61

4.2.6. OPF Remarks 63

4.2.7. Discussion and Performance Evaluation 65

4.3. Stochastic Optimization of Integrated Transmission and Distribution Network Considering Distributed Generation With Uncertainties 67

4.3.1. Main contributions 70

4.3.2. Overview of existing model 71

4.3.3. Transmission Network 73

4.3.4. Distribution Network 74

4.3.5. Stochastic optimization with LDR 76

4.3.6. LDR Theorem Proof 78

4.3.7. Results and Discussion 79

4.3.8. Test system I: IEEE 57 TN and IEEE 34 DN 80

4.3.9. Test system II: IEEE 118 TN and IEEE 123 DN 84

4.4. Summary 86

CHAPTER 5: MULTI-PERIOD INTEGRATED TRANSMISSION AND DISTRIBUTION OPTIMAL POWER FLOW SIMULATION USING LINEAR DECISION APPROACH 89

5.1. Introduction 89

5.1.1. Main contribution 91

5.2. Previous and Current Model Challenges 91

5.2.1. Transmission Network MPOPF 92

5.2.2. Distribution Network MPOPF 95

5.2.3. Case studies 97

5.3. Proposed Integrated optimization engine(IOE) architecture 98

5.3.1. OPF Remarks 101

5.3.2. LDR Theorem Proof 102

5.4. Discussion and Performance evaluation 104

5.4.1. Test system IEEE 9 and IEEE 13 104

5.4.2. Test system IEEE 57 and IEEE 34 106

5.4.3. Test system IEEE 118 and IEEE 123 107

5.5. Summary 108

CHAPTER 6: TIME REECEDING OPTIMIZATION OF GRID-CONNECTED RERS WITH MULTIPLE UNCERTAINTIES(PVS & ELECTRIC VEHICLES) 111

6.1. Management and Coordination of Multiple Grid-Connected Renewable Energy Resources 111

6.1.1. Introduction 111

6.1.2. Main Contributions 114

6.1.3. Previous and Current Model Challenges 115

6.1.4. LDR technique with multiple RERs 116

6.1.5. Results and Discussion 118

6.1.6. Test system IEEE 9 and IEEE 13 118

6.1.7. Test system IEEE 57 and IEEE 34 121

6.2. Management of Electric Vehicle Charging Impact on an Integrated Transmission and Distribution Grid 125

6.2.1. Main Contributions 128

6.2.2. Current Approach 129

6.2.3. Proposed EV charging Management technique 130

6.2.4. Results and Discussion 133

6.3. Summary 137

CHAPTER 7: CONCLUSIONS AND FUTURE WORK 138

7.1. Conclusion 138

7.2. Future Works 140

CHAPTER 8: LIST OF PUBLICATIONS 142

REFERENCES 144

APPENDIX A: THEOREM PROOF 156

APPENDIX B: SIMULATION TOOLS 158

LIST OF TABLES

TABLE 3.1: Comparison of Test Results 34

TABLE 3.2: Location and rating of DERs in IEEE 123-bus system 37

TABLE 3.3: Relative Comparison of Grid Frequency Deviations Corresponding to Different Test Cases 52

TABLE 3.4: Comparison of Test Results With and Without Proposed Control: Grid Frequency 52

TABLE 3.5: Comparison of Test Results With and Without Proposed Control: Settling time 52

TABLE 4.1: Parameters Comparison with different PV penetration Levels 67

TABLE 4.2: Voltage Comparison with different PV penetration Levels 68

TABLE 4.3: Boundary Bus mismatch voltage deviation 68

TABLE 4.4: Substation Active and Reactive Power Output and Cost and Loss Comparisons 81

TABLE 4.5: Parameters Comparison with different PV penetration Levels 82

TABLE 4.6: LDR relationship between the TN generator and Solar PVs 82

TABLE 4.7: Substation Active and Reactive Power Output and Cost and Loss Comparisons with solar PV 82

TABLE 4.8: Boundary Bus mismatch voltage deviation 83

TABLE 4.9: Substation Active and Reactive Power Output and Cost and Loss Comparisons with reverse power flow 84

TABLE 4.10: Parameters Comparison with different PV penetration Levels 86

TABLE 4.11: LDR relationship between generator and Solar PVs 87

TABLE 4.12: Boundary Bus mismatch voltage deviation 88

TABLE 5.1: Boundary Bus mismatch voltage deviation 106

TABLE 5.2: Boundary Bus mismatch voltage deviation 108

TABLE 5.3: Boundary Bus mismatch voltage deviation 109

TABLE 6.1: LDR relationship between the TN generator, Solar PVs, and EV charging aggregator 121

TABLE 6.2: LDR relationship between the TN generator, Solar PVs and EV charging aggregator 125

TABLE 6.3: Control Comparison 136

TABLE 6.4: Parameter 137

LIST OF FIGURES

FIGURE 2.1: Several RERs grid connection to the grid 8

FIGURE 2.2: (a) voltage service level limits (b) voltage variation due to the intermittency of renewable resources 11

FIGURE 2.3: Frequency curve and control levels 12

FIGURE 2.4: RERs Grid integration operation techniques 12

FIGURE 2.5: Schematic of a damping controller 13

FIGURE 2.6: Impedance methods schematic for harmonics mitigation 14

FIGURE 2.7: Operational modes of grid-connected RERs 15

FIGURE 2.8: Synchronverters and Inducverter 15

FIGURE 2.9: Grid-Connected Battery 16

FIGURE 2.10: Schematic diagram of volt-var curve of smart inverter. 17

FIGURE 2.11: Operational modes of grid-connected RERs 19

FIGURE 2.12: Droop control for power sharing 20

FIGURE 2.13: Comparison of homogenous and heterogenous integrated networks 22

FIGURE 3.1: Schematic of the proposed damping controller 28

FIGURE 3.2: FFT based proposed controller gain tuning 29

FIGURE 3.3: IEEE modified 13 Bus system 32

FIGURE 3.4: Case A (a) Speed deviation during grid fault, (b) PCC voltage during grid fault, (c) Oscillation frequency identified from frequency spectrum during grid fault, (d) Controller gain calculated based on oscillation frequency during grid fault. 32

FIGURE 3.5: Case B (a) Variable wind speed profile, (b) Speed variations during variable wind speed profile, (c) Proportional gain derived based on oscillation frequency, (d) Integral gain derived based on oscillation frequency. 33

FIGURE 3.6: Case B: Comparison of frequency spectrum with and without damping control. 34

FIGURE 3.7: Case C (a) Speed deviation during load change, (b) PCC voltage during load change, (c) Oscillation frequency identified during load change, (d) Proportional gain derived based on oscillation frequency. 34

FIGURE 3.8: PV and load areas in IEEE 123-bus system. 38

FIGURE 3.9: PV and load areas in IEEE 123-bus system. 39

FIGURE 3.10: Flowchart for the proposed optimal damping controller. 43

FIGURE 3.11: Field implementation framework of Integrated transmission and distribution system with dynamic models of generators and proposed damping controller. 44

FIGURE 3.12: Case 1A: Grid frequency measurements for fault occurrence at Area 1. 45

FIGURE 3.13: Case 1A: Dynamically changing gains. 45

FIGURE 3.14: Case 1B: Grid frequency measurements corresponding to fault occurrence at tie-line. 46

FIGURE 3.15: Case 1B: Dynamically changing gains. 46

FIGURE 3.16: Case 1C: Grid frequency measurements corresponding to fault occurrence in distribution system. 47

FIGURE 3.17: Case 1C: Dynamically changing gains. 47

FIGURE 3.18: Case 2: Varying wind speed and irradiance profile. 48

FIGURE 3.19: Case 2: Grid frequency measurements corresponding to change in irradiance and wind profile. 48

FIGURE 3.20: Case 2: Dynamically changing gains. 49

FIGURE 3.21: Case 3: Grid frequency corresponding to sudden load change. 50

FIGURE 3.22: Case 3: Dynamically changing gains. 50

FIGURE 3.23: Case 4: Grid frequency measurements corresponding to harmonic loads. 51

FIGURE 3.24: Case 4: Dynamically changing gains. 51

FIGURE 4.1: Types of the interconnected network with different boundaries 55

FIGURE 4.2: Integrated $T\&D$ model with master-slave approach 57

FIGURE 4.3: Transmission network - One line 58

FIGURE 4.4: Distribution network- One line 60

FIGURE 4.5: Integrated T&D model for IEEE 9bus and IEEE 13bus 66

FIGURE 4.6: Case A: 25% penetration level 66

FIGURE 4.7: Case B: 60% penetration level 66

FIGURE 4.8: Case C: 80% penetration level 67

FIGURE 4.9: Boundary bus mismatch reduction with LDR 68

FIGURE 4.10: Schematic diagram of an integrated $T\&D$ system. 72

FIGURE 4.11: One line diagram of the transmission network. 73

FIGURE 4.12: One line diagram of the distribution network 75

FIGURE 4.13: Integrated optimization engine 77

FIGURE 4.14: Integrated T&D model for IEEE 57bus and IEEE 34bus 80

FIGURE 4.15: Voltage profile for IEEE 57 bus TN compared to the state-of-the-art 81

FIGURE 4.16: Voltage profile for IEEE 34 bus DN compared to the state-of-the-art 81

FIGURE 4.17: Generation cost comparison with SILP, no LDR, and with no DERs connected 83

FIGURE 4.18: Voltage profile for IEEE 57bus system 84

FIGURE 4.19: IEEE 118bus and IEEE 123bus Integrated T&D model 84

FIGURE 4.20: Voltage profile comparisons for IEEE 118 bus network 85

FIGURE 4.21: Voltage profile comparisons for IEEE 123 bus network 85

FIGURE 4.22: Generation cost comparison with SILP, and conventional NLP. 86

FIGURE 4.23: Bus voltage profile IEEE 118bus network. 88

FIGURE 5.1: A schematic of Integrated T&D model with master-slave approach 92

FIGURE 5.2: Transmission network - One line 92

FIGURE 5.3: Distribution network- One line 95

FIGURE 5.4: IEEE 9bus voltage levels 98

FIGURE 5.5: Cost and irradiance levels before&after curtailing the SolarPVs 98

FIGURE 5.6: irradiance and Load demand profiles for 24hr 104

FIGURE 5.7: Integrated T&D model for IEEE 9bus and IEEE 13bus 105

FIGURE 5.8: 24hr TN bus voltage profiles with no solar PVs connected 105

FIGURE 5.9: Total demand in TN and Total Solar active power 106

FIGURE 5.10: Generation cost comparison with and without curtailment 106

FIGURE 5.11: Boundary bus mismatch reduction with LDR 107

FIGURE 5.12: Integrated T&D model for IEEE 57bus and IEEE 34bus 107

FIGURE 5.13: Generation cost comparison with and without curtailment 107

FIGURE 5.14: Boundary bus mismatch reduction with LDR 108

FIGURE 5.15: Integrated T&D model for IEEE 118bus and IEEE 123bus 108

FIGURE 5.16: Generation cost comparison with and without curtailment 109

FIGURE 5.17: TN Generation power comparison with and without curtailment 109

FIGURE 5.18: Boundary bus mismatch reduction with LDR 110

FIGURE 6.1: Grid integration of Electric Vehicles with RERs 115

FIGURE 6.2: Proposed Architecture with Agents 116

FIGURE 6.3: INL Electric Vehicle residential daily load curve 116

FIGURE 6.4: irradiance and Load demand profiles for 24hr 119

FIGURE 6.5: Integrated IEEE 9bus and IEEE 13bus T&D model 119

FIGURE 6.6: Voltage profile for IEEE 9 bus TN compared to the state-of-the-art 120

FIGURE 6.7: Voltage profile for IEEE 13 bus DN compared to the state-of-the-art 120

FIGURE 6.8: 24hr TN bus power demand with no DERs connected 121

FIGURE 6.9: Generation cost comparison with and without RERs connection 121

FIGURE 6.10: Total generation in TN with and without RERs connection 122

FIGURE 6.11: EV charging profiles expected and sudden 122

FIGURE 6.12: Total demand in TN before and after sudden operations 122

FIGURE 6.13: Boundary bus mismatch reduction with LDR 123

FIGURE 6.14: Integrated IEEE 57bus and IEEE 34bus T&D model with the interconnection of solarPV and Electric vehicle aggregator 123

FIGURE 6.15: Voltage profile for IEEE 57 bus TN compared to the state-of-the-art 124

FIGURE 6.16: Voltage profile for IEEE 34 bus DN compared to the state-of-the-art 124

FIGURE 6.17: 24hr TN bus power demand with no DERs connected 124

FIGURE 6.18: Generation cost comparison with and without RERs connection 125

FIGURE 6.19: Total generation in TN with and without RERs connection 125

FIGURE 6.20: Total demand in TN before and after sudden operations 126

FIGURE 6.21: EV charging profiles expected and sudden 126

FIGURE 6.22: Boundary bus mismatch reduction with LDR 126

FIGURE 6.23: A schematic of smart charging infrastructure [1] 130

FIGURE 6.24: Typical EV charging curve 130

FIGURE 6.25: Load profiles for 24hr 133

FIGURE 6.26: Integrated T&D model for IEEE 9bus and IEEE 13bus 134

FIGURE 6.27: 24hr TN bus voltage profiles 134

FIGURE 6.28: 24hr TN generator active power 135

FIGURE 6.29: Dispatch for charging station passive control 135

FIGURE 6.30: Dispatch for charging station active control 135

FIGURE 6.31: Energy delivered with different controls 136

FIGURE 6.32: Power demand with different controls 136

FIGURE 6.33: Cost impact of different charging controls 137

LIST OF ABBREVIATIONS

ψ_{qs} stator flux

A exponential zone amplitude (V)

C capacitance of the DC converter

C_{in} input Capacitance

C_{out} output Capacitance

D duty cycle input of the converter

E_0 battery voltage constant (V)

F_{HP} flow high pressure

F_{LP} flow low pressure

H inertia

i battery current (A)

i^* filtered current (A)

$i_{d/q}$ d-axis and q-axis inverter output current

K polarization constant (V/Ah)

$k^L_{PSS,i}$ lower bound value of the PSS gain

$k^U_{PSS,i}$ upper bound value of the PSS gain

K_a exciter gain

K_f stabilizer gain

K_{PSS} PSS gains

L inductance of the DC converter

L_{inv} inverter inductance

L_{in} filter input inductance

L_{rr} exciter gain

P_{batt} rotor resistance

P_{CH} position of chest delay

P_{ch} rotor inductance

P_{CO} position of crossover

P_{disch} rotor resistance

P_{GV} position of Governor value

P_{RH} position of reheater

R internal resistance of the battery

r_r rotor inductance

T_ω wash filter time constant

T_{CH} chest delay time constants

T_{CO} cross over delay time constants

T_{sm} reference of voltage

T_{sr} reference of voltage

V_{bat} internal battery voltage (V)

$V_{d/q}$ d-axis and q-axis inverter output voltage

V_{dc} voltage at dc-link

V_{dl} d-axis voltages across the inverter L_{inv}

V_f stabilizer emf

V_{pcc} voltage at PCC

V_{pss} output reference of the power system stabilizer

V_{ql} q-axis voltages across the inverter L_{inv}

V_{ref} reference of voltage

V_r input filter emf

b_2, b_1, b_0 Cost coefficient of generators

c_2, c_1, c_0 Cost coefficient of generators

m_2, m_1, m_0 Generator cost coefficient

u_i Magnitude of square voltage for bus i

$\mathcal{G}$ Network graph

$\mathcal{L}$ Set of all branches in the network

$\mathcal{N}$ Set of all buses in the network

Φ_{ij} Phases in the line ij

Φ_{ij} Set of the phases of line ij

DN Distribution network

e_k k-th basis vector

$i_{d/q}$ d-q axis grid current

$i_{ds/r}$ stator and rotor side current d-frame

I_{ij} Current flow across the line ij

I_{ij} Current flow from line ij

I_{pq} Current flow across the line pq

$i_{qs/r}$ stator and rotor side current q-frame

l_{ij} Magnitude of square current flow from line ij

l_{ij} Square current flow from line ij

l_{pq} Magnitude of square current flow on line pq

P_{agg} Aggregrate charging station bus

P_{ev} Power consumed by each EV

P_j^d/Q_j^d Bus j active/reactive power load

P_j^g/Q_j^g Bus j active / reactive power generated

$P_{K,D}/Q_{K,D}$ Active/Reactive demand power at the bus k

$P_{k,RP}$ Reverse active power from distribution network

P_k^g/Q_k^g Active/Reactive power generation at the bus k

$P_{m,RP}$ Reverse active power into TN

P_m^d/Q_m^d Power demand active/reactive at the bus m

P_m^g/Q_m^g Power generated active/reactive from the bus m

S_{ij} Apparent power flow through line ij

S_{ij} Apparent power flow between bus i and j

S_{jk} Complex power flowing through line jk

S_{km} Apparent power flow between bus k and m

S_{load}^{S} Total load distribution network

S_{mn} Apparent power flowing through line mn

S_{pq} Complex power flowing through line pq

S_{pv} Apparent power of solar PV

S_{pv} Complex power flow of solar PV

S_S DN total complex power

S_S Total apparent power demand by DN

S_s Complex power flow of the feederhead

TN Transmission network

u_0^{abc} Distribution network feeder head voltage

u_0^{abc} Feeder voltage abc

$V_{d/q}$ d-q axis grid voltages

$V_{d1/q1}$ d-q axis output voltages of the inverter

$V_{ds/r}$ stator and rotor side voltage d-frame

V_i,V_j Vector of bus voltages at bus i and bus j

V_j Bus j nodal vector voltage

V_k Bus k nodal vector voltage

V_K^B Voltage at the boundary bus

V_m Nodal voltage vector for bus m

V_n Nodal voltage vector for bus n

V_{pcc}^{abc} Boundary bus voltage

$V_{qs/r}$ stator and rotor side voltage q-frame

$X(i)$ Charging station setpoint

x, y Decision variables if load or boundary bus exist

y_j Shunt capacitance at node j

Y_k Auxiliary variables admittance at bus k

Y_{line} Line admittance

Y_{lm} Series admittance

Y_m Auxiliary variables admittance at bus m

Y_{nm} Admittance of transmission line between node n and node m

y_n Shunt capacitance at node n

z_{ij} Line impedance

z_{jk} Impedance of line jk

z_{mn} Impedance of line mn

DERS Distibuted energy resources

DG Distributed generation

RERs Renewable energy resources

CHAPTER 1: INTRODUCTION

1.1 Background

Recent trends in electricity generation include the interconnection of several resources with the traditional power grid. Amongst the new resources, renewable energy resources (RERs) are gaining fast adoption, because of their economic, environmental, and sustainability benefits. In addition, many policies are major drivers for the adoption of RERs [2, 3]. The electricity delivery frequency determines the point of interconnection for these resources, depending on the type of RER. For instance, wind turbines are connected to the transmission layer. At the same time, small-scale or residential solar systems can be connected to the distribution layer, which can be referred to as distributed generation (DG). Studies show there are 12 million DG units across the United States with a total capacity of 200GW [4]. RERs can be operated in both a grid-connected mode and an off-grid mode. In a grid-connected mode, the traditional grid is transformed from a unidirectional flow into a bidirectional flow, which increases the network complexity. In most RERs, power generation varies due to the intermittency/variability of the source. For example, wind speed variability results in wind turbine frequency and power output fluctuations [5]. This variability can have a significant impact on the grid. These impacts can be more severe, depending on the level of renewable energy penetration. Some of these impacts result in violation of power quality standards, such as the voltage ANSI value (0.95-1.05pu) or the frequency, which should be kept between 59.5-60.5Hz, so the system does not lose stability. Power quality is assumed to be good if the aforementioned metrics remain at an acceptable, steady value of voltages and frequency, with a smooth sinusoidal waveform. This showcases the need for effective control and management strategies.

1.2 Motivation

Renewable energy has led to a lot of cutting-edge innovation and the advent of new technological devices in the energy industry, The resources making this feasible are unique in their operations and are largely dependent on their sources. For instance, a wind turbine's power output is largely influenced by the wind speed, and so is the sun irradiance determining the amount of power a Solar PV can produce. double fed induction generators (DFIG) is one the major types of wind turbine generators used owing to their operational efficiency, with two back-to-back PWM converter. Even though wind turbines have low or no inertia, the increased penetration of wind turbines can offer great benefits and disadvantages for both

power system damping and sensitivity modes of the system. WTG don't produce inertia response during grid disturbances and hence with high penetration levels of wind turbines, the impacts might be severe. Solar PV's operations are similar to that of wind turbines with respect to low inertia support, the efficiency can also be influenced by AC/DC converters. Since these resources offers a lot of advantages, both economically and environment, there is a need to evaluate the control and management technology needed to achieve a smooth operation. On the control, most of the existing architecture doesn't account for the fast-changing nature of RERs and there makes it difficult to adequately reduce such impacts which can cause frequency oscillation. Another major challenge with grid-connected RERs is their management in an integrated T&D framework, the existing grid architecture doesn't provide the transmission network insights into the distribution network where most RERs are connected. With the increasing penetration of these resources, there is a need for this visibility into both networks, so the generating resources can readjust themselves quickly to avoid grid quality issues.

A lot of research work has been done on integrated T&D power flow, However, utilities still have specific grid objectives to achieve and hence the need for an optimal power flow framework, to satisfy this objectives.

1.3 Main Contribution of the Dissertation

- An adaptive damping controller which exhibits superior performance during dynamic grid conditions when compared to conventional vector control, due to its adaptive tuning capability.

- Battery integrated control architecture that ensures improved secondary response characteristics, based on a damping controller requirement.

- An optimal damping controller that can augment generator controllers and/or PSS, which can effectively damp the oscillations in transmission and distribution networks.

- Optimal controller architecture that can dynamically adjust the gain values based on linear optimization that modulates the generator excitation to effectively damp the oscillation.

- A linear decision rule LDR that addresses the challenges with reverse power flow of an integrated transmission and distribution network and reduces the boundary bus voltage mismatch.

- An Extension of the LDR for integrated $T\&D$ in a receding time horizon optimal power flow, with multiple RERs and uncertainties.

- A charging management technique using setpoints control form optimal power flow to manage uncertainty with EV charging.

1.4 Intellectual Merit and Broader Impact

The intellectual merit of this work is

1. The project provides a technique that is used to offer damping support to the grid in a real-time manner, the technique is adaptive to the changes occurring in the grid either natural or sudden. The project uses a spectrum to identify the torque needed to reduce the frequency oscillation. The approach was evaluated with different scenarios to test its effectiveness.

2. This project provides a novel architecture with observability and controllability capabilities while using an optimal sharing strategy for multiple generating resources to provide damping support to the grid, this was evaluated in an integrated T&D framework. A mathematical optimization to dynamically change some of the static parameters of the resources is implemented.

3. One of the major drawbacks of integrated T&D with huge penetration of renewable energy resources is intermittency or reverse power flow, which is currently being addressed through the curtailment of these resources, a new technique is developed that provides real-time insights of this resources to the generators on the integrated network, to observe and adjust accordingly.

4. The operation of the power grid is in a multi-period framework, which involves optimal power flow solutions solved at defined intervals, the capabilities of the stochastic linear optimization for an integrated T&D is then extended to multiperiod OPF to establish the versatility and capability to operate efficiently at different intervals with other resources.

5. The possibility of several intermittent resources interacting with the grid is the fundamental of smart-grid, a novel approach is developed to handle the uncertainty by several of these interconnected resources and keep the grid operating smoothly within its boundary conditions.

6. Electric vehicle charging is a major issue for utilities due to the uncertainty with respect to charging, a new methodology was developed to assist utilities in providing setpoints to charging stations to assist with planning and other objectives.

The broader impact of this work

1. Control systems and architecture can be designed to be adaptive in nature to accommodate the changes by RERs which can lead to fast or sudden changes in the grid.

2. PMU's data can be used as a source for a real-time controller, providing a damping torque for grid oscillation.

3. Distribution system operator (DSO) with several resources can provide insights to the Transmission system operator (TSO) in real-time to handle the changes before scheduling intervals.

4. The maximum offerings of grid-connected RERs can fully be exploited on every occasion reducing the need to curtail or isolate these resources.

5. Utilities can improve their planning efforts, as well as grid-stability issues with respect to the uncertainty of EV charging.

1.5 Dissertation outline

In Chapter 2 a comprehensive literature review on the state-of-the-art of control methods that are used to address the dynamic changes caused by RERs was analyzed, we compared the performance of the existing controls and identified their shortcoming,. We studied the implementation of three different widely used approaches and their offerings, we also tested the approach with different scenarios to validate our hypothesis on the need for better control implementation. Furthermore, we also explored the management of grid-connected RERs by reviewing some of the approaches that are been used and clearly identified the need for the technique to improve operational efficiency.

Chapter 3 an adaptive damping controller was developed which ensures that the dynamics from RERs are adequately managed to avoid deviations with respect to frequency or voltage on the grid. The controller was further extended into an integrated T&D system with different RERs and different grid resource conditions.

In Chapter 4 a management technique for an integrated T&D, which enables the system to operate efficiently despite the sudden change due to RERs eliminating the need for curtailment of DERs which led to cost efficiency and minimization of voltage deviation. A linear decision rule (LDR) technique was used to establish the relationship between the two networks and provide insights into the distribution network to the transmission network, In Chapter 5 The new architecture of our LDR technique for an integrated T&D, to a multiperiod framework, which is time-receding horizon and larger networks to further test the versatility of our approach. Chapter 6, The number of uncertainties in the integrated T&D was increased and extended the scope of the newly proposed methodology to handle multiple uncertainties and different time intervals.

Finally, the conclusion about our work is presented in Chapter 7, while in Chapter 8, future work to be done were discussed.

CHAPTER 2: LITERATURE REVIEW

2.1 Introduction

The modernization of the power grid involves a lot of new technologies interplaying at all the layers involved in the generation of electricity to the point of consumption. These new technologies are been implemented at generation, transmission, distribution, and even consumption. The technological advancement though offers numerous benefits ranging from sustainability, cost, and environmental benefits. This is also transforming the distribution network into a more complex interconnected network, the traditional unidirectional flow of electricity has now been replaced with bidirectional flows due to the advancements. The new technologies coupled with the existing traditional grid are commonly referred to as Smart Grid. Smart grid comprises distributed energy resources (DERs) which are rapidly increasing in penetration with the existing grid and have led to distributed generation.

Recent studies revealed that there are 12 million distributed generation DG units across the united states with a total of 200 GW [6, 7]. The growth of the distributed energy resources DERs can be attributed to climate change and the declining cost of DERs, some of these DERs technologies include distributed generation e.g. solar PVs, wind generation, or battery storage systems like electric vehicles, flywheels, or demand response is referred to as DERs which can interplay at any of the levels in the electricity chain (Generation to consumption). The Grid integration of these resources can however have significant effects on important power quality metrics in distribution such as voltages and frequency. These issues are from the variability nature of the sources of most DERs, for instance, wind speed can vary the amount of power generated by the wind turbine and can impact the grid frequency, concurrently overvoltageâs and Undervoltage can be caused by the varying irradiance profile. The level of impact can be adverse if the penetration level of the DERs is high, which therefore necessitates a need for efficient control and management techniques for Grid-connected DERs. [6, 8]The IEEE 1547 standards form the basis of the interconnection of DGs with the distribution network. In accordance with these standards, a parameter such as voltage should be kept within the limits of the ANSI value (0.95-1.05pu), the frequency should also be within the limits be 59.5-60.5 Hz. The optimal coordination and management of the smart grids is an imperative action to implement to maximize the benefits DERs proposes in terms of cost, sustainability, and resiliency.

Due to the volume of DERs been integrated into the grid, their management should be done at the device levels, and they can receive instruction in groups for efficient management.

The group-level management can be done by the DSO which communicates to the DERMS which coordinates at the device level. The most advanced method of managing DERs is the DER aggregator which makes use of an alternating direction method of multipliers (ADMM) for distributed controls but has the limitation of not having access to the accurate system model and are completely unaware of the system constraints, these limitations are the propositions that the distributed energy resource management systems offer, as it an intelligent platform that enables all the capabilities of the system without violating the constraints, as well utilizing the resources to solve already violated constraints and return the system to stability.

The distribution network include resources transforming the grid into an active network (ADNs)[9],[10] leading to a reverse power flow to the TN, These resources are dynamic, and can lead to a sudden change or transient operation [11] if not well captured in a day ahead forecast due to their nature. Their level of penetration [12] in the grid can have some significant effects which influences key power quality metrics of the grid (voltage, frequency, and many more) during such times of variations. The optimal power flow (OPF) computation can be performed within specified intervals or a day ahead schedule for efficient planning. However, with the recent trends the solution seems not efficient [13] any more due to the increase in the number of resources (distributed generation) [14], inter-playing and controls on the DN. This studies enable us to ensure that the transmission system operator (TSO) and distribution system (DSO) operators are not been almost blind to each other controls or coordination [15], especially during these dynamic operations [16]

These all call for new architectures to balance the real-time generation and demand efficiently and to ensure proper coordination due to the new relationship existing between the generators, customers, and network operators, and provide optimal benefits.[17]. The existing controls and management approaches currently being used to achieve a smooth operation of the integrated grid is discussed in this chapter.

2.2 Benefits and Challenges of Grid Connected RERs

Most of the Grid-connected RER issues discussed above can be managed using a DERMS platform. Even though DERs integration offers many benefits to the existing grid infrastructure which will be discussed it is important to discuss some power quality issues [18] that occur due to the integration of RERs needs to be discussed extensively as well.

2.2.1 Advantages of Grid Connected RERs

Grid-connected DERs have general benefits to utilities and electricity consumers such as generation operation Cost reduction, environmental friendly, sustainability, Grid resiliency. However, a further look into its benefits to utility DERs are used for grid ancillary services,

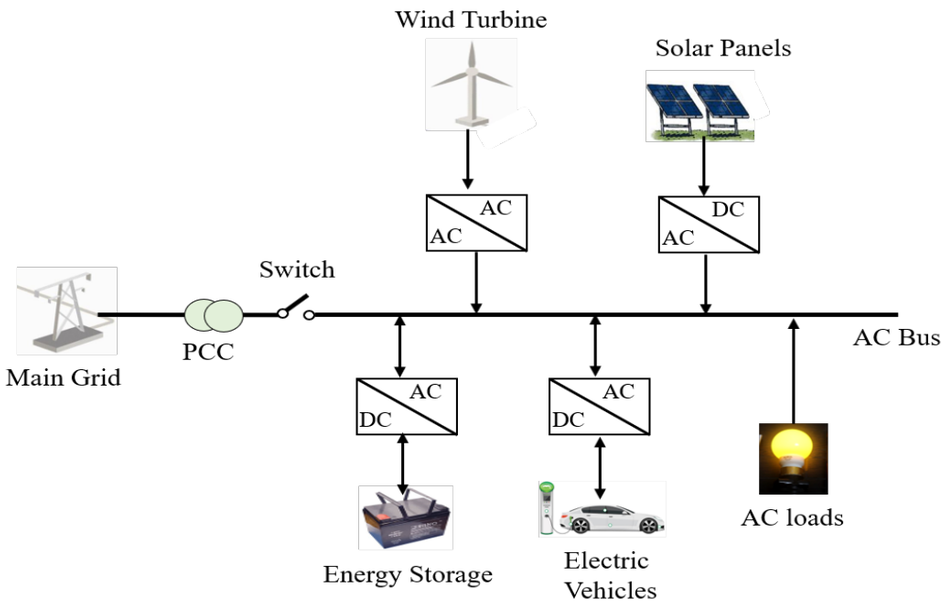

Figure 2.1: Several RERs grid connection to the grid

some of which are discussed below:

2.2.1.1 Volt-Var Optimization

The voltage levels from the feeder in the network can be optimized especially in a situation where the loads are voltage sensitive loads and this is done to ensure that the voltages can be maintained within the service level limits of (0.95-1. 05p.u), which can help reduce the amount of power been consumed and directly lower the cost of generation. DERs smart inverters coordinate with existing legacy devices capacitor banks, load-tap changers, and voltage regulators to perform this function. The Volt Var optimization (VVO) optimizes the set points of the legacy devices and the DERs smart inverters using real-time measurement of the grid from the DERMS. Apart from the objective of using the VVO to reduce the power consumption of the feeder which is known as conservative voltage reduction, it can also perform objectives as loss minimization and regulate feeder voltages. Before the implementation of VVO, existing approaches such as Volt var control (VVC)[19–21]and integrated volt var control (IVVC)[22] could only optimize the operation of legacy control devices, but the increasing penetration of DERs and integration of distributed generation which comprises smart inverters employ the joint optimization of all the devices in a framework known as VVO. [23] VVO has been evaluated through a bi-level approach with two optimization techniques was combined was used. Level 1 which uses mixed-integer linear programming (MILP) optimization technique objective was to minimize the power consumption for the feeder by controlling the legacy devices such as the voltage regulators, capacitors banks, and smart inverters and providing a setpoint, Level 2, therefore, uses a Nonlinear programming technique (NLP) with the set points in Level 1 to perform a power flow solutions, which can vary only the smart inverter setpoints obtained from the previous level, while ensuring that

the setpoints for both the capacitor banks and voltage regulators are constant. The bi-level approach ensures that each system is optimized at each node, to reduce the computational burden and reduce the risk of single-point failure for centralized control. An improved performance was observed when the VVO approach was used as Conservation voltage reduction (CVR) concerning the power reduction consumed and losses.

2.2.1.2 Peak demand management

The demand profile for most electricity consumers varies frequently, and one important as well as a critical phase to plan for is the peak demand period[24]. Even though these do not occur for a long duration, if not properly managed can cause have significant adverse effects on the grid. Hence, even though most utilities have baseload consumption, generation, studies have shown that capacity planning is based on the peak load demand. This also impacts the costs of electricity generation from the perspective of high-ramp power generation, also the generation components as generators, transformers, switchgear, protection systems need to plan for in terms of peak demand requirements which leads to an increased cost. DERs can be used to support peak demand requirements, the generation support from the DERs will have a competitive cost advantage rather than increasing existing generation sources and supporting equipmentâs capacity. Peak load management is done using DERs such as PVs, battery, and Electric vehicles and has been evaluated by several studies [25–29], in [24] where a commercial load management algorithm was implemented that combined a scheduling algorithm of EVâs, to optimally provide peak management support with PVâs and batteries combined.

2.2.1.3 Service Restoration during faults

Fault occurrence can lead to the outage on the grid and can pose a significant effect on the grid, as well as damages to electricity consumers downstream to the grid, who might also have some critical loads. Faults can also distort the frequency on the grid, and lead to instability issues. Fault occurrence is often high-impact low probability events know as Grid resilience. Outages experienced in the US costs the economy 18 to 33 billion per year[30]. Even though, their lots of devices to help reduce the effects such as switches, reclosers, and circuit breakers, during fault occurrence, can still lead to a significant number of outages, Most times a new feeder can be reconnected and reconfigured to reduce the number of outages. Grid-connected DERs and smart switches can be coordinated together and used for restoration. The feeder is reconfigured such that the customers experiencing the outage are connected to a neighboring DER(s) and are restored. A lot of studies have been written to improve grid resilience using DERs and microgrids but didnât include post-restoration failures. The studies carried out by [31, 32] use a spanning tree algorithm to restore critical

loads and maximize the duration time.[33] The distribution system is sectionalized into a self-sustained microgrid to supply power after a service. An approach was proposed by[34] where a distributed service restoration algorithm is used to reduce the number of outages after fault occurrence occurs in a large feeder network.

2.2.2 Disadvantages of Grid Connected DERs

We have discussed some advantages of Grid-connected DERs in the previous section. This interconnection leads to some power quality issues. High penetration levels of for instance by solar PVs can lead to overvoltages, wind energy conversion systems generation is also intermittent and non-dispatchable which can lead to high fluctuations caused by wind turbine[35][36]. The power supply is said to be of good quality if it remains constant at acceptable steady-state voltage values and frequency with smooth sinusoidal waveform[37][38]. Power quality affects the overall reliability of power grids which are power fluctuations, frequency fluctuations, voltage fluctuations, and harmonic distortions[39–43] and some mitigation techniques[41, 42]. have been reviewed in the literature. However, two of the major issues that are mostly caused by grid-connected DERs include voltage distortion and frequency imbalance.

2.2.2.1 Voltage level

Increasing penetration of DERs in the Grid has significant impacts on the voltage level on the grid. This impact can be more severe in networks with high DER penetration, in other for loads to properly, voltage has to be within the service limit of 0.95-1. 05p.u. Hence, the need for voltage management impediment in grid-connected DERs, Voltage management devices such as capacitor banks, voltage regulators, and load tap changers still offers the advantages of controlling the voltage level on the grid, however, the intermittent nature of DERs, like irradiance with solar PVs can vary suddenly and cause overvoltageâs if it increases suddenly and Undervoltage when the irradiance level is very low. Capacitors banks even though majorly serves the purpose of reducing losses on the system, can also improve the voltage profile on the grid, and several other new devices such as the smart inverters with volt-var, volt-watt control mechanisms are been used to improve the voltage levels, by controlling reactive power or active power from the DERs. Battery banks are connected with inverters to improve the voltage profile on the grid. Several control architectures are used for voltage management.[44] an optimal online voltage management algorithm, that makes use of a combination of battery energy storage, PV active power curtailment, controllable loads, and voltage regulators. [45] authors propose the use of static var compensators and smart inverters to address the overvoltage and under-voltage problem. Figure (a) below shows the different operating regions of the grid voltage from over-voltage, allowable limits,

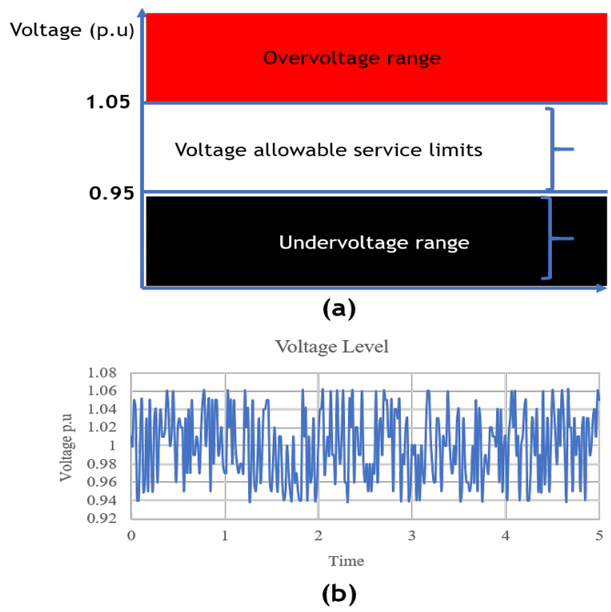

Figure 2.2: (a) voltage service level limits (b) voltage variation due to the intermittency of renewable resources

and Undervoltage. While figure (b) shows the voltage levels with DERs connected to the grid and if not properly managed can lead to grid voltage level issues as shown Fig.2.2.

2.2.2.2 Frequency distortion issues

Frequency stability is a major requirement in the operation of the power grid, this challenge often time arises as a result of the imbalance between power supply and power demand. Grid frequency is an important metric to access the health of the grid[46, 47]. Synchronous generators have a huge amount of inertia from the rotating mass can assist in reducing the rate of change of frequency (ROCOF), thus inertia helps to prevent frequency extortion issues and can serve as the first means of control. The primary control then assists after the inertia, has been tried, and another layer of control that helps mitigate this is the secondary control. Primary frequency control actions are initiated by the synchronous generators, while the secondary frequency control can be from the grid operators which can employ the use of devices such as batteries. In the primary control, the actions are taken based on the deviation in the speed, by measuring the local frequency from the generator itself, while the second is based on the data collected through telemetry systems. The figure below shows the interaction of the control mechanism. M is the inertia constant, ΔW represents the change in local frequency measurements, B is the frequency bias, R is the droop coefficient of the generator, D is the load damping constant, ΔP_{tie} is the change in power from one area to another, ΔP_L is the load change, ΔP_m is the generator output changes, ΔP_b is the change in DERS such as a battery, T_{ch} and T_g are the time constants of the prime mover and speed governor. ACE is the area control error that provides a notification of the deviation from the nominal frequency. All the interaction and time of response for different control mechanism is shown below as shown Fig.2.3.

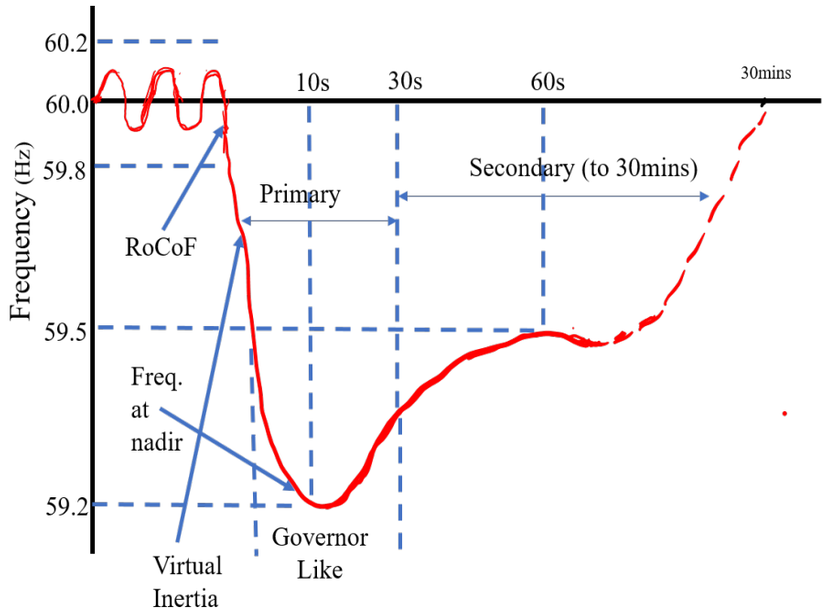

Figure 2.3: Frequency curve and control levels

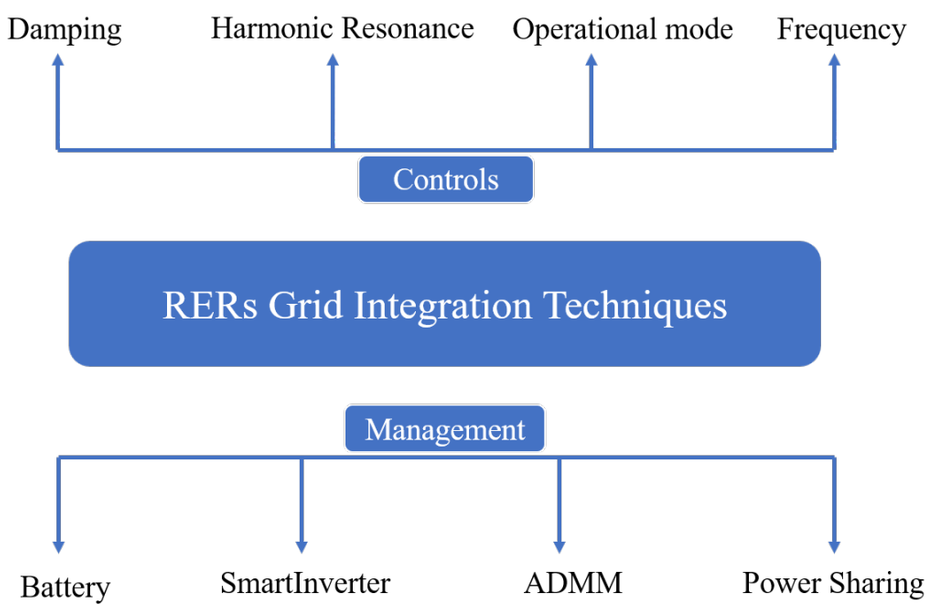

Figure 2.4: RERs Grid integration operation techniques

Other issues experience in grid-connected RERs include Power fluctuations which have been widely mitigated using energy storage systems like batteries, ultracapacitors [48–50] and non-energy storage systems[51, 52] such as pitch angle control and DC link voltage control methods in the wind turbines[53, 54]. Another issue is harmonics which is the distortion of voltage and current waveforms caused by nonlinear loads, this issue is mitigated by filters which kind either be passive or active filters or by using virtual impedance method[55] to shape the control impedance through harmonic compensation[56]

2.3 Conventional Control methods for Grid-connected RERs

In this section, some control techniques used in grid-connected renewable energy resources Fig.2.4 shows the classification of some of the techniques implemented for controls and management of these grid-connected resources.

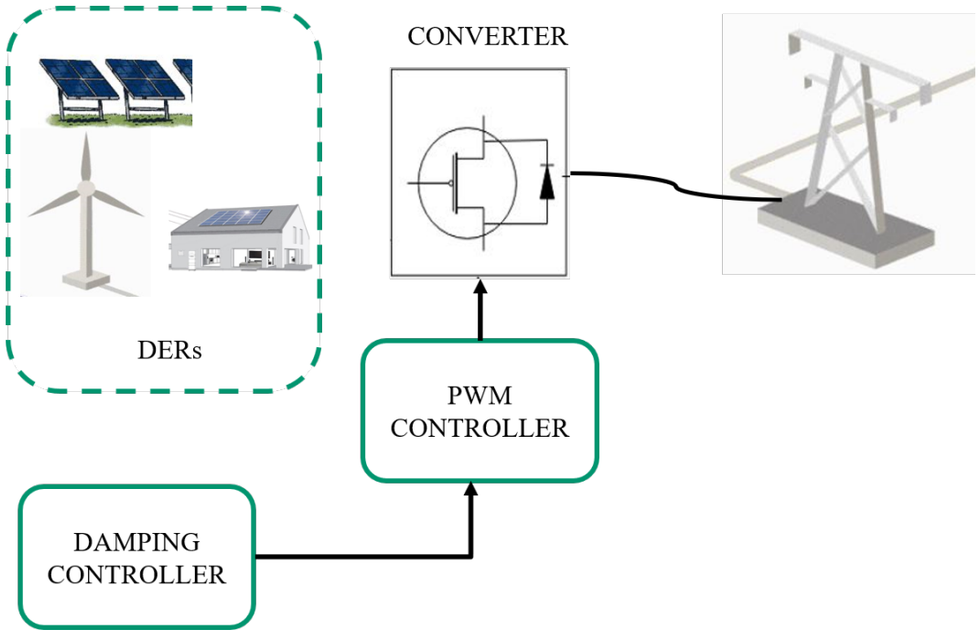

Figure 2.5: Schematic of a damping controller

2.3.1 Damping controllers

Grid-connected RERs are susceptible to issues such as frequency distortion. frequency oscillation issues are caused mostly by variations in the active power. Since the power generated by RERs varies based on their sources of generation the likelihood of the occurrence of this kind of issue is high. For instance, wind power generation varies with wind speed leading to frequency distortion which can lead to a major grid disturbance if sustained for a long duration. Fault occurrences are also known to cause frequency distortion. A couple of studies have been done to assist with the mitigation of this issue, frequency scanning methods have been used to analyze the relationship between frequency and impedance of the compensation network, to further improve grid stability, grid-connected DFIG damping strategies are implemented to control DFIG with and without batteries. Battery energy storage system (BESS) and advanced control management are critical enablers for grid ancillary support. Damping Controllers operate by providing an additional source of power to the converters, which might be supplied as additional current, to damp the oscillation on the grid by reducing the rate of change of frequency to disturbance. This is implemented by measuring the deviation in the frequency on the grid, as an input into a controller to provide an additional current to the converters of the Grid Connected RERs. A lot of methods can be implemented with the damping techniques such as adaptive damping controller[57], and some work has also been done using fuzzy logic.

2.3.2 Harmonic Resonance

RERs uses converter systems to interface with the grid, the output side of the filter (LCL) of these converters can interact with the impedance on the line, which can lead to negative increment impedance [58] causing stability issues concerning the frequency and

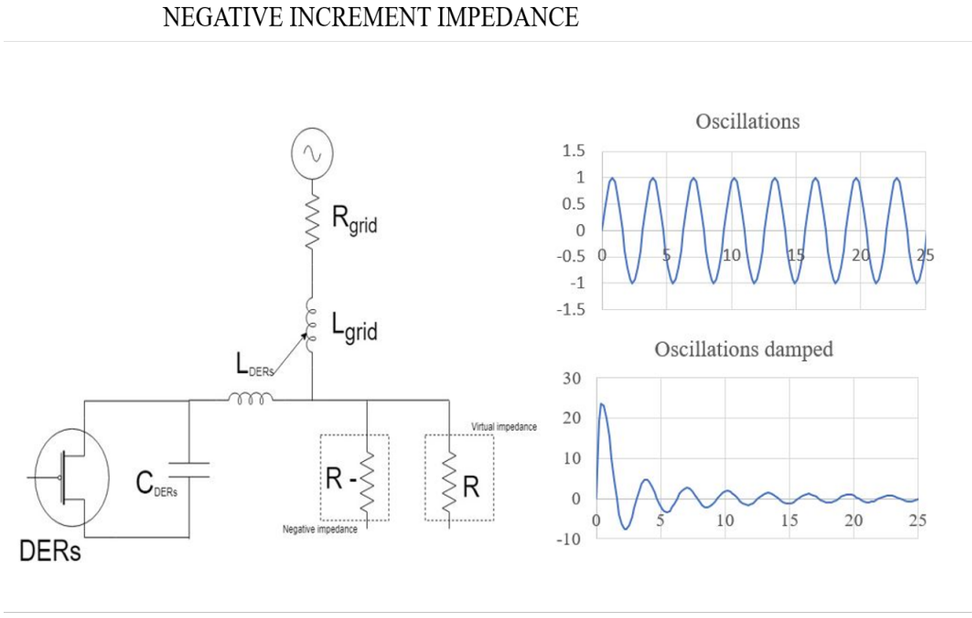

Figure 2.6: Impedance methods schematic for harmonics mitigation

can cause a major challenge (subharmonics or Harmonics). Various studies and approaches have been carried out on how to mitigate these issues. [59] Impedance based approach predicts the system stability at the point of interconnection based on the ratio of output impedance to equivalent system impedance, a more straightforward stability analysis using frequency domain, it is however limited to small-scale power electronics system and neglects network dynamics and cannot adequately estimate the system impedance.[60,61] Component Connection method is a form of state-space model, where the state matrix can be estimated using eigen properties, the interaction of components and critical system parameters can be easily determined, but the challenges of this method is the complexity in relating the system and component. Output impedance reshaping can also be done by using a virtual impedance lossless circuit for harmonic compensation sharing between multiple DERs[62].

2.3.3 Operational mode

DERs can operate in both grid forming mode and grid feeding mode[63]. The transitioning of the grid-connected inverters during these modes can create some frequency, voltage, or current disturbances, A couple of control schemes have been implemented to assist with these transients and to aid smooth transition[64–66]. Phase-locked Loop PLL and virtual resistors are used to mitigate this disturbance, the major challenge with a phase-locked loop is that it deals with the outer power loop and synchronization, however, some issues can still occur because of internal current or voltage loops which is not accounted for by the approach.

2.3.4 Frequency control

Unlike traditional synchronous generators which have a large amount of inertia to mitigate frequency disturbance, most RERs have little or no inertia, this means that small disturbances can increase the rate of change of frequency ROCOF and may lead to load

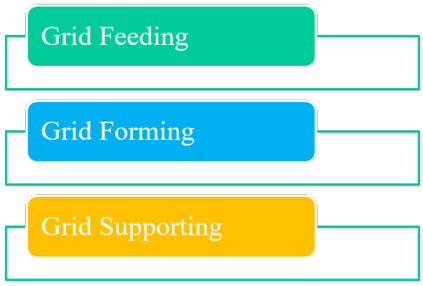

Figure 2.7: Operational modes of grid-connected RERs

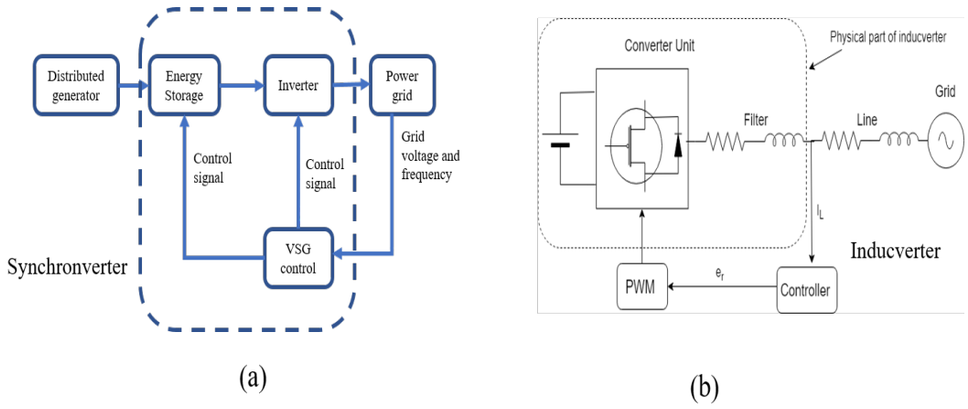

Figure 2.8: Synchronverters and Inducverter

shedding to maintain a balance. A lot of control approaches as been used to provide inertia so that issues caused by the disturbance can be minimized. A conventional method is to use Superconductive Magnetic Energy Storage (SMES), which has a superconducting coil that stores energy in a magnetic field created by the DC to minimize output frequency fluctuation[67], the major challenges with implementing SMES is the high capital cost[54]. The virtual inertia approach is also, Synchronverters[67, 68] this mimics the Synchronous Generators (SG), Use a control algorithm to behave like a synchronous generator, it uses mathematical equations to form a PLL which makes it capable of maintaining synchronism with the terminal voltage, the issues with synchronverters frequency levels distortion is a bit steeper with respect to nadir frequency, even though it has faster settling. [69]Virtual synchronous generators (VSG) are more suitable for grid operations and provides better minimum frequency deviation, higher energy exchange due to higher settling time, various implementation of VSG concept is explained in [70–74]. VSG can also be further optimized with particle swam optimization[75] where the voltage angle deviation VAD is kept within the limit of operation to maintain stability. Inducverter [76, 77] A new control topology that mimics induction generator behavior in power systems, helps auto-synchronization with the grid without information about the grid voltage, it also eliminates the need for synchronization units and PLL.

2.4 Conventional management methods for Grid-connected RERs

In this section, some management techniques used in grid-connected renewable energy resources were discussed, as shown in Fig.2.4.

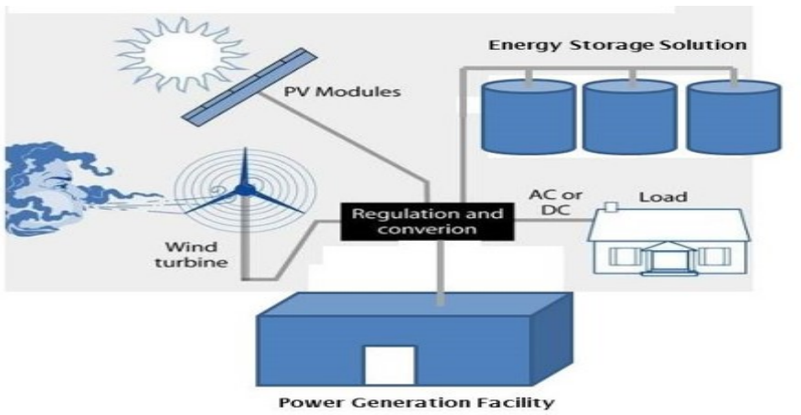

Figure 2.9: Grid-Connected Battery

2.4.1 Battery

Batteries help to avoid waste and any deficit between generation and demand which can result in delayed delivery of power to loads. The battery allows intermittent renewables to substantially contribute to the energy mix for our national grid. Therefore the need for a dispatchable generation and storage devices, these storage devices offer benefits such as providing spinning reserve, correcting frequency, or provision for new transmission and or generation capacity. In some situations, the battery is connected to the converters of the Renewable energy resources.

2.4.2 Smart-Inverter

Smart inverters have been proposed as a solution[78, 79] for most voltage problems that could arise from the integration of DERs into distribution grids. The several functionalities of smart inverters are a testament to their versatility. A report published by the Electric Power Research Institute (EPRI) groups functionalities of smart inverters into different categories based on control drivers and the purpose of each functionality [8]. However, for voltage-related issues the most commonly implemented functionality is the volt-var and volt-watt functions of the smart inverter are been implemented to ensure that the grid-network voltage level at all locations is within the acceptable limits of operation.

Volt-watt and volt-var functionalities of smart inverters have been widely considered for solving voltage problems due to high DER penetration levels. The volt-watt function enables control of the DERâs active power output as a function of the bus voltage being observed while the volt-var function enables reactive power control, each of the functions can either inject or absorb reactive/active power depending on the functionality been implemented. According to the EPRI smart inverter functions report, both functions are classified under the autonomous function category meaning that once the desired control actions have been configured, the smart inverter responds on its own based on observed grid conditions. Typically, volt-watt curves and volt-var curves are used to specify the desired performances for smart

inverters operating in these modes. It is worth mentioning that the volt-watt curve used in the study is quite aggressive. However, this is not a major concern in this study as desired settings can be configured for real-world smart inverters to meet specified requirements.

A study was carried out on overvoltage correction in active distribution grids using the smart inverter (SI). The volt-var curve used for the smart inverter are is as shown in fig. 6.4, for some more adverse scenarios that reactive power support from SI couldnt handle, we enabled the volt-watt functionality. The voltage values for the volt-var curve were set following guidelines specified in the IEEE 1547 standards [9]. For the volt-var curve, the Deadband region was set between 0.99 p.u. and 1.01 p.u. When the voltage goes out of this range, the smart inverter starts injecting or absorbing reactive power as required. Although both volt-var and volt-watt functions are enabled, the generation of active power takes precedence over the generation or absorption of reactive power. Hence, active power is curtailed when reactive power absorption is unable to mitigate the overvoltage problem. An investigation was done on a IEEE 13Bus network, analysis was performed first to see which bus location is better to connect the smart inverter to mitigate the issue.[80] The smart inverter operates by monitoring the voltage at the point of interconnection (VPOI) of the DERs with the grid. If VPOI $>$ 1.05, the smart inverters absorb reactive power, thereby correcting over-voltage conditions. Likewise, if the VPOI $<$ 0.95, reactive power is injected to improve the under-voltage condition. As shown in Figure 2, the capacitive region is used when absorbing reactive power and the inductive region while supplying reactive power. The reactive power being absorbed or injected is a function of the amount of reactive power available which is calculated using equation (1).

$$Kvar_{available} = \sqrt{(KVA_{rating})^2 - (KW_{present})^2} \tag{2.1}$$

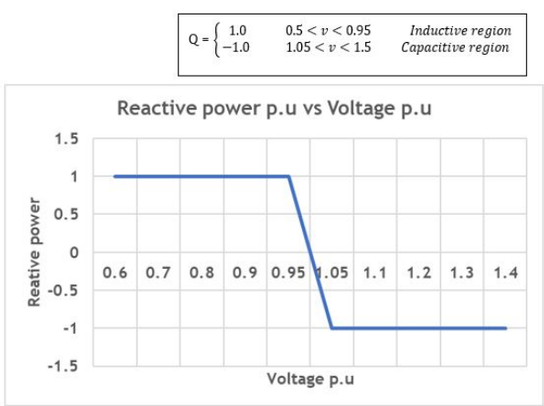

Figure 2.10: Schematic diagram of volt-var curve of smart inverter.

Smart inverters are capable of other functionalities like the dynamic reactive current function, fixed power factor function, maximum generation limit function. Dynamic current

function differs from volt-var because its mode of operation is dynamic unlike the volt-var whose operations is at steady-state which infers that the decision factor is the change in voltage rather than the change in voltage level, it operates by providing capacitive reactive currents. Fixed power function makes the smart inverters perform the role of been a voltage regulator, while the maximum generation limits function limits the amount of power the PV can supply to the grid.

Apart from the functions of a smart Inverter, there are also certain features that they possess to demonstrate its intelligent capabilities. Five features have been identified by some literature, and are discussed below:

- Plug and Play: Enable easy communication and seamless integration with the grid[81–84].

- Adaptability: Should be able to operate during fault occurrence [85–88] in certain conditions especially when critical loads are involved. They should be able to detect islanding mode operation of DERs[89–91].

- Self-Awareness: Smart inverter self-awareness features is divided into three concepts[79, 92, 93], they can perform diagnostics to know where issues during operation are originating from, they can also carry out prognosis to estimate when a fault is going to happen and finally, they should also have condition monitoring capabilities to know the health and status of the component.

- Autonomy: Smart inverters should be able to operate by switching their mode of operation from grid forming to grid feeding modes[63], it should also aid controls that assist with the sharing of power based on the ratings of the inverter when we have multiple inverters.

- Cooperativeness: Smart inverters have the capabilities to assist in reactive power-sharing, this has been discussed in some of the functions of the smart inverters. They also possess the capability to assist with ramp rate control.

2.4.3 DERMs

Grid-connected DERs management and coordination are achieved with advanced distributed management systems (ADMS). ADMS is a software platform that offers a couple of advantages over the DMS as it combines the capabilities of existing distribution management software (DMS), Supervisory control and data acquisition (SCADA), geographical information system, output management system (OMS), meter data management system. DMS is used to manage legacy voltage regulating devices such as the capacitor banks, transformer taps, and voltage regulators, while the ADMS platform incorporates distributed PV

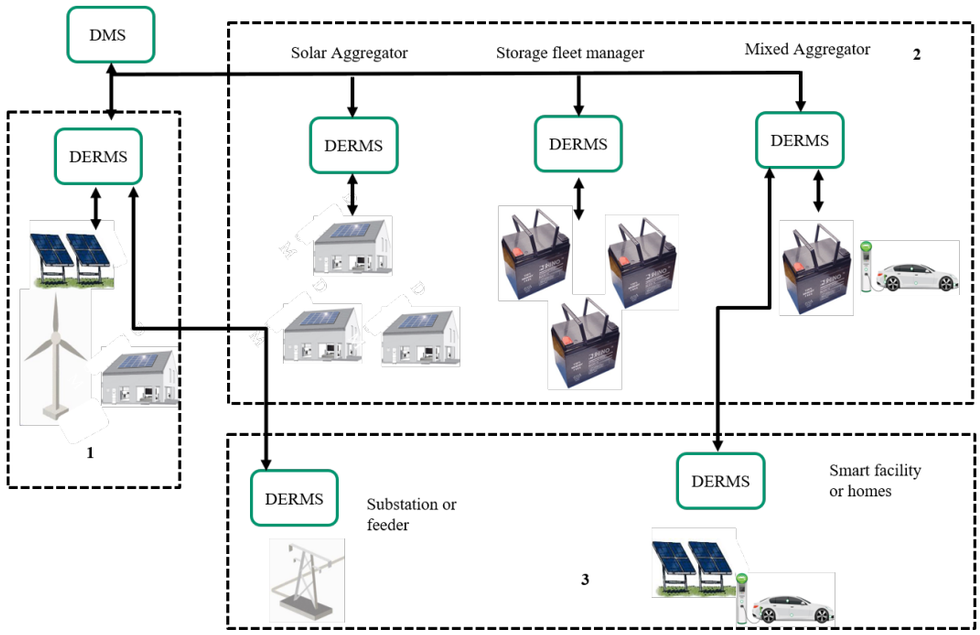

Figure 2.11: Operational modes of grid-connected RERs

generation and other inverter-based resources. A conventional DMS performs power flow analysis frequently to determine the setpoints and optimal settings of legacy voltage regulating devices based on the utilities need at a particular point, while the ADMS under which distributed energy resource management (DERMS) platform falls categorically, incorporates the services of DERs with algorithms to help that provides a better optimal solution. DMS makes use of sensors on the power systems to know the operational status, and limits and compare itâs with operational goals and priorities at any given time. Some DMS are DERMS ready and hence a communication link is made available as seen in fig. 2.11, DMS is then defined to determine what services are requested while DERMS provides the services as requested or alternatively, DMS carries out grid-level service functions, DERMS performs the device-level function capabilities

2.4.4 PowerSharing

The increasing penetration of RERs has led to the interfacing of several inverters to the grid, this has lead to the need for a control method to share active and reactive power efficiently amongst the resources.[94–96] A droop control method has been widely used to enable active power-sharing between parallel-connected inverters[97–101], which has advantages over master-slave control method as it eliminates the need for a communication link, and also over active current distribution control where a current reference is provided for each inverter but faces the challenges of the failure of one inverter leading to an entire system failure, the shortcomings of the droop-control method is that reactive power is not shared adequately, and the harmonic current.[62] A virtual impedance loop is used to enable the sharing of reactive power between the inverters, this employs the use of virtual impedance loops to compensate for the inverter output and line impedance unbalances, since the reac-

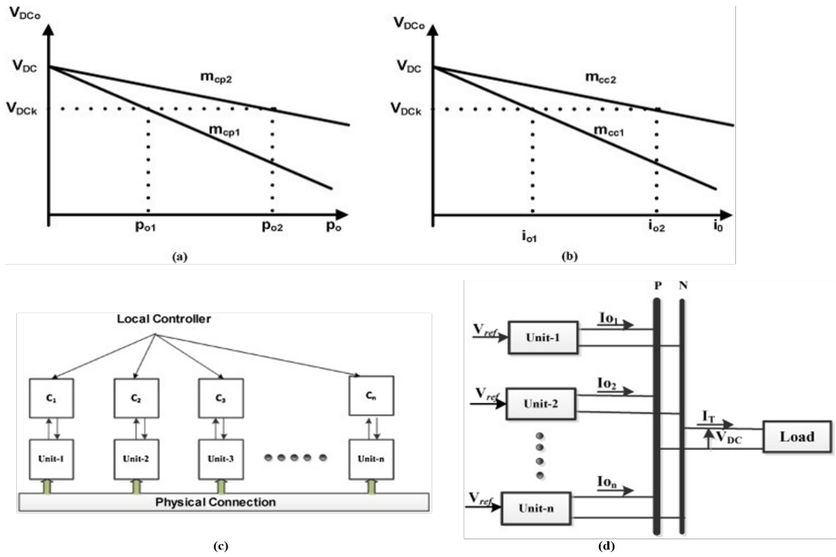

Figure 2.12: Droop control for power sharing

tive power sharing is dependent on the impedance of DG feeders and output side impedance of L-C-L filters, the shortcoming of this approach is that large of impedance can be required which can degrade the voltage quality especially in weak islanded Grid.[102–104]

2.5 Conventional Integrated T&D optimization method

Before discussing some of the optimization methods of conventional Integrated T&D. methods, we need to look at the advancement in the modeling of the integrated T&D.Alot of techniques have been developed for the modeling of the techniques which are discussed below.

2.5.1 Unified Modeling

Unified modeling is such that the same framework is used for the modeling of both networks and a common model is developed which has all the measurements of both networks either from energy management systems (EMS), supervisory control and data acquisition (SCADA), A couple of techniques has been discussed like Graph trace analysis, or using a synthetic distribution system model combined with the transmission system using a top-bottom approach. A global power flow method based on the master-slave technique has also been deployed where the computation is done iteratively, to improve the efficiency of the solution a contingency selection is performed, DC power flow approximation, and approximation of the distribution system network. Alternatively, the transmission system network can be modeled as a positive sequence network and the distribution is modeled as a three-phase network, in which an NR solver can be used for its solution.

2.5.2 Co-Simulation Modeling

Co-simulation offers the advantages of some visibility and explores the economic benefits of the DGs connected to the network, co-simulations allow for special domain tools while exchanging time-synchronized boundary variables. Integrated grid modeling system(IGMS)

is one of the tools that is used for co-simulation that uses a python-interface to communicate between two controllers for the transmission system in MATPOWER and the distribution system in GridLAB-D.Another tool is the Hierarchical Engine for Large Scale Infrastructure Simulation (HELICS), which is used for both transmission and distribution networks as well as the communication protocols and control interface, finally a co-simulation tool used for transactive energy applications is the Framework for network co-simulation (FNCS).

For the optimal power flow solutions of integrated T&D, a direct idea for solving the problem is to use centralized optimization, which may encounter some practical difficulties for current power systems: a) As stated in the characteristics of DGs differ from those of transmission generators because they are more dispersed throughout the network in a larger number thus, they are difficult to centrally control on a transmission level. b) Because a transmission system operator (TSO) and distribution system operator (DSO) function independently, the parameters of the network and generators of the transmission and distribution network are currently always non-observable to each other; thus, it is difficult to establish a centralized TDCED model for current power systems. Only the information at the boundary buses, such as the power values and LMPs, can be mutually observable. Thus, a centralized TDCED solution may not be computationally efficient for current practical applications. Another idea is the use of decentralized optimization to solve TDCED. One possible method is the direct adoption of existing algorithms that are developed for solving coordinated regional transmission systems (RTSs). The algorithm used can be classified into two: the Lagrangian relaxation family (LR-F) and the optimality condition decomposition family (OCD-F). The LR-F primarily includes traditional LR the auxiliary problem principle (APP) alternating direction of multipliers (ADMM) and analytical target cascading (ATC) Generally, the drawbacks of the LR-F algorithms are the low convergence rate and an inconvenient parameter tuning process the OCD-F primarily includes a synchronous iteration that was proposed by Conejo et al. and extended in and an asynchronous iteration version proposed by Biskas et al. The synchronous version has a better convergence property, whereas the asynchronous version is easier for practical implementation and has been tested in the Balkan system as the two typical OCD algorithms are aimed at the coordination of RTSs with similar characteristics, their decomposition formats are homogeneous, that is, the messages passed among the subsystems have similar components. Specifically, as shown in the figure below, each subsystem with the same boundary information is called homogeneous decomposition. Each computational unit sends its boundary voltage angles and multipliers to the connected subsystems and receives others' boundary voltage angles and multipliers in each iteration. However, unlike the interaction characteristics of interconnected RTSs, those of the transmission and distribution networks are âheterogeneousâ: from the transmis-

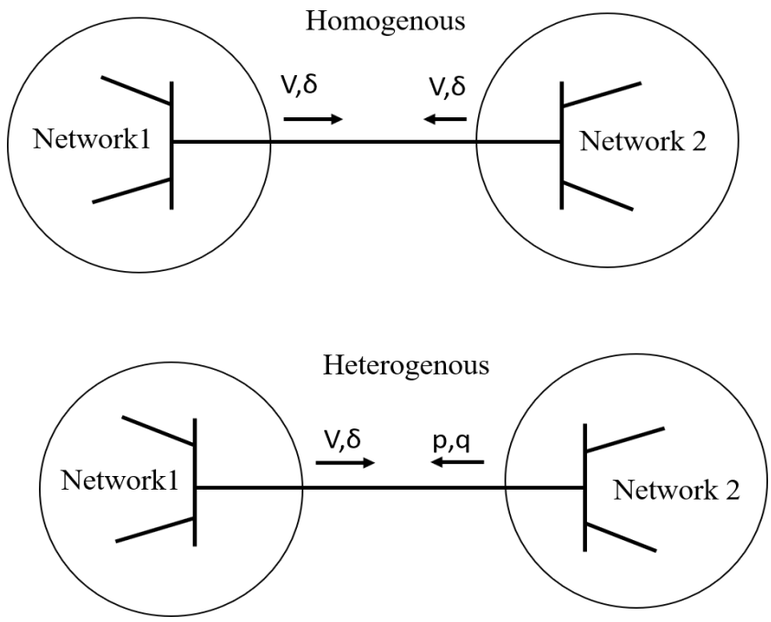

Figure 2.13: Comparison of homogenous and heterogenous integrated networks

sion perspective, the distribution is usually regarded as load injections at boundary buses; conversely, from the distribution perspective, transmission is usually regarded as a virtual source generating at the price of LMPs. Therefore, it is helpful to know whether there might be a new algorithm to take full advantage of the heterogeneous qualities.

2.6 Summary

In this chapter, grid-connected RER is reviewed. The advantages as well benefits of grid-connected RERs are discussed as pertaining to their utilization to achieve certain grid objectives. The challenges associated with grid-connected RERs in regard to power quality metric issues were also evaluated. Furthermore, some of the conventional control and management techniques to handle the challenges of RERs being connected to the grid are discussed, and the shortcomings of the techniques and limitations are also discussed.

CHAPTER 3: A NOVEL ADAPTIVE DAMPING CONTROLLER FOR GRID CONNECTED RERS

3.1 Introduction

The upsurge in renewable energy generation has led to the modernization of electric power distribution systems, and the integration of renewable energy resources into the grid is changing the operation of the grid with respect to controls and management. Renewable energy sources, such as wind farms are often more reliable but are also prone to power quality problems such as frequency distortion, and voltage variations, during grid operations, which occur during overloading conditions, intermittency, and fault occurrences. The stability and resiliency of the network grid are also impacted due to the nature of these resources, the interconnection of these resources will make the grid experience decreased inertia. Numerous research studies have focused on improving grid damping, including the lack of inertia, due to the integration of renewable energy resources.

3.2 Online Adaptive Damping Controller for Wind Integrated Power Grid

In recent years, most utility companies have been exploring renewable energy generation to improve the resiliency and reliability of their networks. The integration of these renewable resources into the grid has, therefore, changed certain operational requirements for power systems, despite the advantages of reduced cost in the long run by the distributed energy resources (DERs), some power quality challenges are faced with the integration, such as frequency variation, voltage issues during load changing dynamics and fault occurrence. Wind energy is at the forefront of renewables, due to its economic advantages over other resources[105]. The major challenges in the time past with wind energy have been the operation of wind energy conversion systems (WECS) with variable speed as opposed to fixed wind speed. The variability of the wind speed causes fluctuation in the power output of the wind turbine and its frequency.[5]. Fixed wind speed also causes instability during the short circuit condition in connecting networks due to the high level of reactive power absorbed.

The application of a doubly-fed induction generator (DFIG) wind generation system has been widely used to solve these challenges owing to its reduced robustness in the converter system, which leads to minimum power losses. It also offers a much better generation system than the other WECS. Besides, DFIG has advantages such as high energy efficiency and controllability for the variable speed wind turbine. [106]. Various control techniques have

been implemented to control the doubly-fed induction generation in grid-connected mode and islanded mode of operation. A cyclo-converter-based control for decoupled control of active and reactive power for the DFIG was proposed in [107]. Some studies based on frequency scanning methods have also been used to analyze the relation between frequency and impedance of compensation network [108]. To further improve the stability, grid-connected DFIG damping control strategies are implemented to control DFIG, with and without batteries [109–113]. Battery energy storage systems (BESS) and advanced control management are critical enablers for grid ancillary support [18,57,114]. BESS in some studies is integrated into the V_{dc} link of the PWM back-to-back converters to improve the power quality issues. The main drawback associated with these architectures is that they cannot adaptively damp the frequency oscillations. In this chapter, a method is proposed to adaptively damp the oscillations based on an online controller. This is accomplished by dynamically changing and tuning the damping controller parameters by measuring the frequency at every interval. The proposed controller is implemented both in the grid-side control of the DFIG and the battery system connected to the DC-link. The controller performance is then evaluated for scenarios, such as during faults, varying wind speed, and load dynamics. Major contributions of this work include:

- An online adaptive frequency damping controller.
- The proposed architecture exhibits superior performance during dynamic grid conditions compared to conventional vector control, due to its adaptive tuning capability.
- Battery integrated control architecture that ensures improved secondary response characteristics.

3.2.1 DESIGN AND MODELING OF ENERGY SOURCES

The modeling and design of the three main energy sources used in the test system are discussed in this section. It includes a synchronous generator, DFIG, and battery system.

3.2.2 Synchronous Generators

The test system has two main synchronous generator types, the slack Generator, and the PV Generator. The PV generator is connected to bus 692, which supplies the loads downstream to the point of interconnection (i.e., loads at bus 692 and 675, while the slack generator is responsible for supplying the remaining power demand on the grid and management of the grid frequency. The steam turbine governor is used for the control of the active power, while the excitation control is used for voltage management. The active power is controlled (maintained constant) by the steam turbine governor, which controls the frequency and the speed of the generator, while the grid voltage is controlled using the exciter.

$$\frac{d}{dt}\begin{bmatrix}\Delta W_r\\ \Delta P_{SR}\\ \Delta P_{GV}\\ \Delta P_{CH}\\ \Delta P_{RH}\\ \Delta P_{CO}\end{bmatrix} = \begin{bmatrix}\frac{-K_D}{TSR} & 0 & 0 & \frac{F_{HP}}{2H} & \frac{F_{IP}}{2H} & \frac{F_{LP}}{2H}\\ \frac{-K_{GS}}{TSR} & 0 & 0 & 0 & 0 & 0\\ 0 & \frac{1}{T_{SM}} & \frac{-1}{T_{SM}} & 0 & 0 & 0\\ 0 & 0 & \frac{1}{T_{CH}} & \frac{-1}{T_{CH}} & 0 & 0\\ 0 & 0 & 0 & \frac{1}{T_{RH}} & \frac{-1}{T_{RH}} & 0\\ 0 & 0 & 0 & 0 & \frac{1}{T_{C0}} & \frac{-1}{T_{C0}}\end{bmatrix} \begin{bmatrix}\Delta W_r\\ \Delta P_{SR}\\ \Delta P_{GV}\\ \Delta P_{CH}\\ \Delta P_{RH}\\ \Delta P_{CO}\end{bmatrix} + \begin{bmatrix}0 & \frac{-1}{2H}\\ \frac{1}{T_{SR}} & 0\\ 0 & 0\\ 0 & 0\\ 0 & 0\\ 0 & 0\end{bmatrix} \begin{bmatrix}\Delta P_{ref}\\ \Delta P_L\end{bmatrix} \tag{3.1}$$

The steam turbine governor control ensures the stability of the power reference for the synchronous generators and gives an output of P_m, the mechanical power input to the generator, while the excitation controller provides the generator with the field voltage reference. A voltage stabilizer is used as well to improve the voltage on the grid according to the IEEE-DC4B and IEEE-STIA. The dynamic equations guiding the synchronous generator model are shown in (3.1).

$$\begin{aligned} V_f &= k_A(V_{ref} + V_{pss} - V_r)\\ V_{fmin} &\leq V_f \leq V_{fmax} \end{aligned} \tag{3.2}$$

$$\frac{V_{fmin}}{K_a} \leq V_{PID} \leq \frac{V_{fmax}}{K_a} \tag{3.3}$$

$$V_{PID} = (V_{ref} + V_{pss} - V_t - \frac{K_f}{T_f}[V_f - V_{stab}]) \tag{3.4}$$

where V_{ref} is the reference voltage,K_a is the exciter gain, V_f is stabilizer emf, V_{stab} is the stabilizer voltage, V_{pss} is the output reference of the power system stabilizer, K_f is the stabilizer gain, and V_r is the input filter emf.

3.2.3 Double Fed Induction Generator Model

The voltage equations of DFIG in the synchronous rotating ($d-q$ frame) model are described below:

$$v_{qs} = -r_s i_{qs} + w_e \psi_{ds} + p\psi_{qs} \tag{3.5}$$

$$v_{ds} = -r_s i_{ds} + w_e \psi_{qs} + p\psi_{ds} \tag{3.6}$$

$$v_{qr} = -r_r i_{qr} + (w_e - w_r)\psi_{dr} + p\psi_{qr} \tag{3.7}$$

$$v_{dr} = -r_r i_{dr} + (w_e - w_r)\psi_{qr} + p\psi_{dr}. \tag{3.8}$$

where $v_{ds/r}$, $i_{ds/r}$ and $v_{qs/r}$, $i_{qs/r}$ are the stator side and rotor side voltage and current in the $d-q$ frame, respectively.

Grid side converter (GSC): The GSC controls the DC-link voltage constant. It is also used to regulate and provide reactive power support to the grid, which is done through the implementation of stator voltage-oriented control. The q-axis component of the stator voltage is set to 0, while the d-axis component is aligned to the stator voltage, for control of the reactive power. The equations for control of the GSC in the $d-q$ frame are shown below:

$$\begin{bmatrix} v_d \\ v_q \end{bmatrix} = R \begin{bmatrix} i_d \\ i_q \end{bmatrix} + L\rho \begin{bmatrix} i_d \\ i_q \end{bmatrix} + Lw_e \begin{bmatrix} -i_q \\ i_d \end{bmatrix} + \begin{bmatrix} v_{d1} \\ v_{q1} \end{bmatrix} \tag{3.9}$$

The active and reactive power from the GSC controller are given as:

$$\begin{bmatrix} P \\ Q \end{bmatrix} = \begin{bmatrix} v_q i_q \\ v_q i_d \end{bmatrix} \tag{3.10}$$

where i_d and i_q are the $d-q$ axis currents from the inverter, v_d and v_q are the $d-q$ axis grid voltages, and v_{d1} and v_{q1} are the $d-q$ axis output voltages of the inverter.

Rotor side converter (RSC): The main objective of the RSC is to control the speed of the turbine to ensure that the machine operates at maximum power point tracking (MPPT), even during varying wind speeds. The rotor side converter also ensures that the active power and reactive power track their reference, which is accomplished by controlling the excitation voltage. Vector control of RSC is based on stator flux oriented frame ($\psi_{qs} = 0$, $v_{qs} = v_s$). The equations governing the control of the converter outer loop and inner loop control are presented below,

The stator active and reactive power in terms of the rotor current are stated as,

$$P_s = v_{qs} * \frac{L_m}{L_{rr}} i_{qr} \tag{3.11}$$

$$Q_s = v_{qs} * \frac{L_m}{L_{rr}} i_{qr} + \psi_{ds}. \tag{3.12}$$

with rotor voltage equations as,

$$v_{qr} = v_{qr}^{*} + (w_e - w_r)(\sigma L_{rr} i_{dr} + \frac{L_m}{L_s}\psi_{ds}) \tag{3.13}$$

$$v_{dr} = v_{dr}^{*} - (w_e - w_r)(\sigma L_{rr} i_{qr}). \tag{3.14}$$

where L_{rr} and r_r represents the rotor inductance and resistance and $\sigma = 1 - \frac{L_m^2}{L_s L_r}$.

3.2.3.1 Battery system

The battery system is connected to the DC link of the two PWM converters, where the energy storage system acts to mitigate power fluctuations and consequently power quality problems. It operates by measuring the dc-link voltage, which is kept constant, but the current flowing through the battery varies, hereby, changing its mode of operation for either charging or discharging. The battery is designed with filter parameters (e.g., inductance L_{in}, input capacitance C_{in}, and output capacitance C_{out}). The controller is implemented to function in a buck-boost mode of operation. It has two cascaded controllers. The inner loop acts to control the current and provide the duty cycle reference for the generating switching pulses, whereas the outer loop control is responsible for maintaining the V_{dc} constant, where V_{pcc} is the per unit value of the V_{dc} constant. The battery control equation is show in (3.33):

$$P_{batt} = \begin{cases} P_{disch} & V_{pcc} < 1 \\ 0 & V_{pcc} = 1 \\ P_{ch} & V_{pcc} > 1 \end{cases} \tag{3.15}$$

where P_{batt} is the status of the battery, P_{disch} indicates discharging, and P_{ch} represents charging.

$$V_{pcc} = \frac{V_{dc}}{V_{base}} \qquad\qquad V_{base} = 1128V \tag{3.16}$$

3.2.4 Mathematical Model of Proposed Damping Controller

The objective of the proposed architecture is to damp the grid frequency oscillations by modulating the active power output from the DFIG. As explained in Section 3.2.3, the GSC (operating under the voltage oriented reference frame) utilizes the quadrature axis current component to control the active power output, thereby maintaining the DC-link voltage constant. Hence, the proposed GSC damping control loop is designed to modulate the quadrature axis current reference (using $I_{gsc_{damp}}$, as shown in Fig. **??**) to the GSC control considering the frequency deviation. Thus, the proposed GSC control modulates the active

power to damp the oscillation utilizing the energy stored in the DC-link capacitor. In order to enhance the performance and operating region of the proposed control and overcome the limited available power from DC-link for modulation, a battery control is integrated into the architecture that can modulate the power output from the battery using $I_{batt_{damp}}$. This ensures excellent damping capability and improved secondary response.

The equation governing with the implementation of the proposed damping control loop for active power/dc-link control with the GSC is represented by,

$$v_{d1} = Ri_d + æLi_d + i_{gsc_{damp}} - !_eLi_q + v_d \tag{3.17}$$

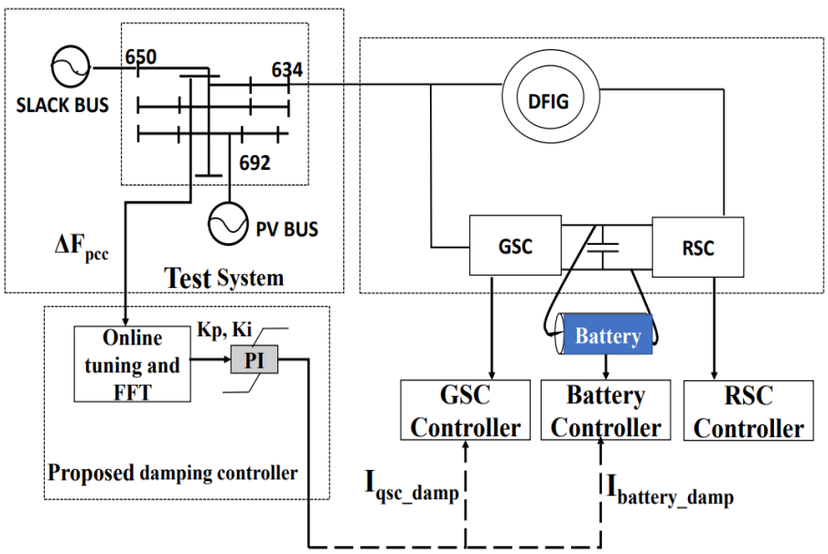

Figure 3.1: Schematic of the proposed damping controller

where R and L are the line inductance and resistance, respectively. Additionally, $!_e$ is the angular frequency of the supply voltage, i_d and i_q are the d-axis and q-axis currents from the inverter, v_{d1} and v_{q1} are the $d-q$ axis output voltages of the inverter, v_d and v_q are the $d-q$ axis grid voltage and $\rho = \frac{d}{dt}$. Similarly, the battery control equation with the proposed loop is shown in (3.18), where $I_{batt_{damp}}$ and $I_{gsc_{damp}}$ are the supplementary current control signals.

$$F_{sw} = \frac{1}{H}\frac{V_{dc}}{V_{batt}+V_{dc}}\cdot - \frac{V_{batt}^2}{RC(V_{batt}+V_{dc})} + 4\frac{I_{dc}}{t_s} \tag{3.18}$$

$$\begin{cases} discharge\ mode & I_{dc} > 0 \\ standby\ mode & I_{dc} = 0 \\ charge\ mode & I_{dc} < 0 \end{cases} \quad I_{dc} = I_c + I_{batt} + I_{batt_{damp}} \tag{3.19}$$

3.2.4.1 Frequency Spectrum based tuning of supplementary damping control loop gains

The control gains of the proposed damping controller are tuned dynamically based on the oscillation frequency of the closed-loop system. A frequency spectrum-based analysis is

performed to identify the oscillation frequency of the system and then modify the controller gain values to perform optimal desired damping. The associated steps for the proposed tuning method are depicted in Algorithm 8 and Fig. 3.2.

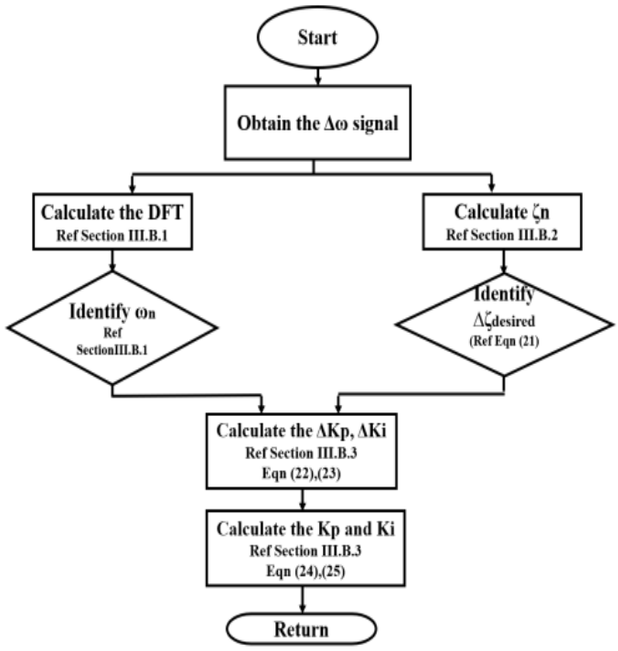

Figure 3.2: FFT based proposed controller gain tuning

Algorithm 1: Controller Gain Tuning

1 -
2 Compute the speed/frequency deviation signal, $x[n] = \Delta\omega$.
3 Compute the frequency spectrum of the frequency signal, $X[k]$ (via the FFT (6.33)), then obtain the spectrum magnitude $P[k]$ via (3.21) and corresponding frequencies $[f_x, P[k]]$.[115–117]
4 Calculate damping coefficient of $X[k]$ using logarithmic decrement method per (3.22) and (3.23).
5 Desired change in damping coefficient is calculated per (3.24), respectively.
6 Desired change in controller gains is calculated per (3.25) and (3.26), considering the identified oscillation frequency and desired change in damping.
7 Calculate the final control gains per (3.27) and (3.28)

The proposed frequency spectrum-based tuning includes the following steps.

3.2.4.2 Calculate the DFT of the measured $\Delta\omega$ signal and identify the natural frequency of oscillation

Let us consider the frequency representation of measured $\Delta\omega$ be represented as $x[n]$. The Fast Fourier Transform (FFT) is performed on the measured input signals to determine its frequency spectrum. The FFT of the input $x[n]$ gives the frequency spectrum $X[k]$ per [118, 119].

$$X[k] = \sum_{n=0}^{N-1} x[n] \cdot \exp\left(\frac{-i2\pi kn}{N}\right) \qquad 0 \leq k \leq N-1 \tag{3.20}$$

The spectrum magnitude $P[k]$ is shown in (3.21), where N is the length of $X[k]$. The energy signal frequency spectrum $X[k]$ can then be expressed in terms of frequency (f_x) and corresponding magnitude ($P[k]$), such that $X[k] \rightarrow [f_x, P[k]]$.

$$P[k] = \frac{2 \cdot |X[k]|}{N} \tag{3.21}$$

The frequency (f_x) corresponding to the maximum peak of ($P[k]$) represents the dominant oscillation frequency calculated at that instance.

3.2.4.3 Identify the desired damping

The controller gains should be adjusted to damp these oscillation frequencies. For that, the existing damping coefficient is identified from the measured $\Delta\omega$ signal using the logarithmic decrement method [120, 121]. This method identifies the damping ratio using the amplitude information of adjacent peaks of an underdamped system. Logarithmic decrement is obtained as the natural log of the ratio of amplitudes of two successive peaks.

$$\delta = \frac{1}{n} ln \frac{x_i - x_f}{x_{i+n} - x_f} \tag{3.22}$$

where n represents the n^{th} peak after the first peak, x_i and x_{i+n} represent the amplitude of the i^{th} peak and the $(i+n)^{th}$ peak, and x_f represents the final steady state value. The damping ratio is then calculated from the logarithmic decrement as,

$$\zeta = \frac{1}{\sqrt{1 + (\frac{2\pi}{\delta})^2}} \tag{3.23}$$

Thus, from (3.23) current damping ratio is obtained. Now the goal is to improve this damping to an ideal desired value (i.e., 0.8 is considered in this work) and is obtained as,

$$\Delta\zeta_{desired} = \zeta_{desired} - \zeta \tag{3.24}$$

3.2.4.4 Calculate the gains for the proposed damping controller

Using this desired change in damping, ζ and identified oscillation frequency, the desired change in controller gains are calculated as,

$$\Delta K_p = 2 * \Delta\zeta_{desired} * \omega_n \tag{3.25}$$

$$\Delta K_i = 2\pi(\Delta\omega_n)^2 \tag{3.26}$$

where $\Delta\omega_n$ represents the change in the identified oscillation frequency from the previous instant. The new controller gains are modified by accommodating the required change in controller gains as shown,

$$K_p[k] = K_p[k-1] + \Delta K_p \tag{3.27}$$

$$K_i[k] = K_i[k-1] + \Delta K_i. \tag{3.28}$$

3.2.5 Discussions and Performance Evaluation

The simulations were done in MATLAB/SIMULINK using the IEEE 13 Bus system (modified to consider as a sub-transmission network), with three-phase loads across the load buses (Fig. 3.3). The test system includes a DFIG at Bus 634 via a transformer, a slack generator at bus 650 (to maintain the grid frequency), and a PV Generator at bus 692 (to feed the local loads at buses 692 and 675). The PV generator is modeled such that it supplies only the power demand by the loads that are local to it. In our system design, the power demanded is at bus 675 and 692 of the test system shown in Fig.3.3. The power reference for the PV generator is, therefore, obtained from the measurement of the total power demanded at the bus 675 and 692.

The simulations were performed for different conditions, while implementing the proposed controller and the grid frequency were observed during different system dynamic conditions. The grid frequency, measured at bus 632, was observed to be uniform across all the buses on the grid.

3.2.5.1 Case A: Performance during a grid fault

This test scenario validates the performance of the proposed damping controller during a three phase fault applied at 7s for a duration of 150ms at bus 671 of the test system.

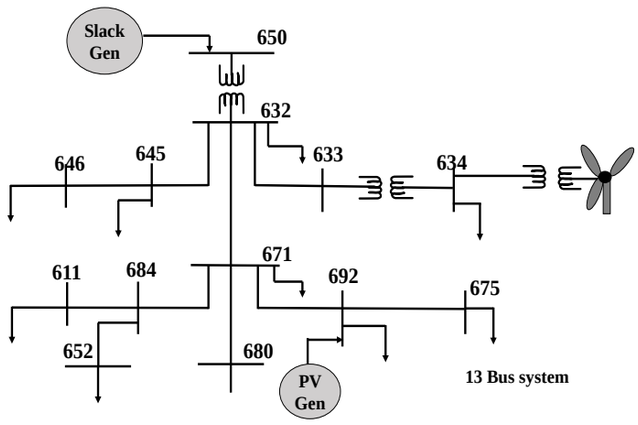

Figure 3.3: IEEE modified 13 Bus system

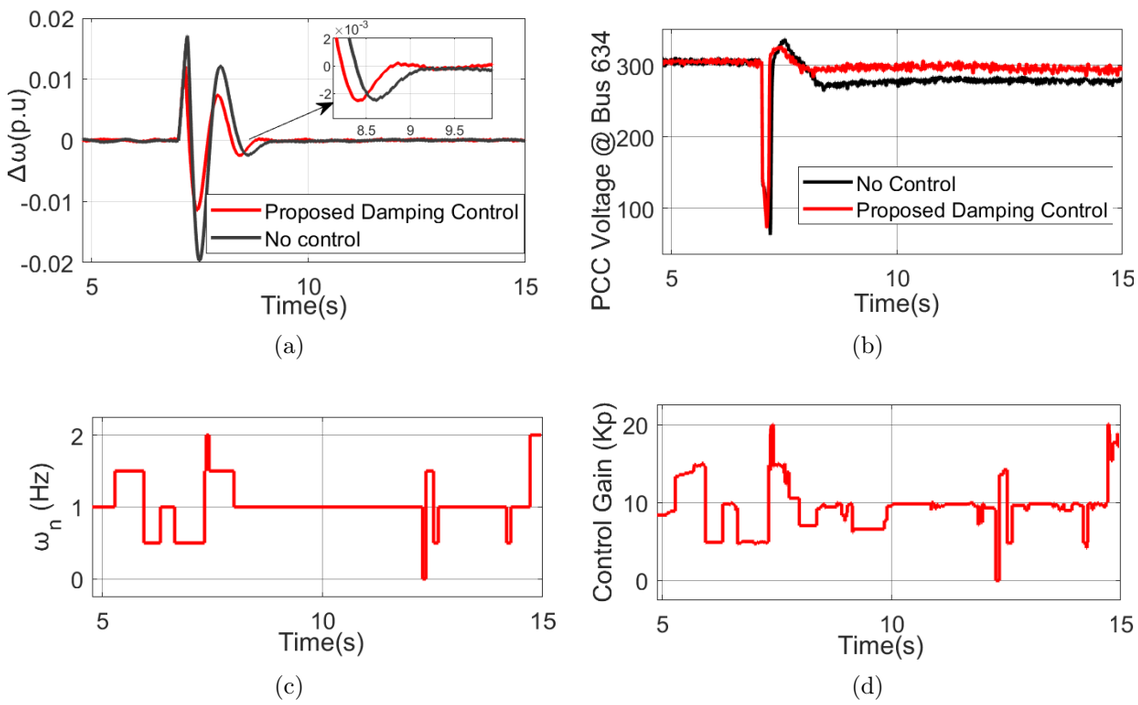

Figure 3.4: Case A (a) Speed deviation during grid fault, (b) PCC voltage during grid fault, (c) Oscillation frequency identified from frequency spectrum during grid fault, (d) Controller gain calculated based on oscillation frequency during grid fault.

Fig. 3.4a shows the improvement in frequency deviation with the proposed control. Fig. 3.4a depicts the superiority of the proposed control in damping the oscillations and faster settling time. A 33% improvement in damping and 11% improvement in settling time was observed with the proposed control approach. Fig. 4.6 shows the superior ability of the proposed control to regulate the voltage to the nominal value after the fault when compared to the scenario without control. The identified oscillation frequency and the online tuning of the controller gains (based on the frequency) are shown in Fig. 4.7 and Fig. 4.8, respectively.

3.2.5.2 Case B: Performance during variable wind speed profile

This test scenario validates the performance of the proposed damping controller during a variable wind speed profile. The wind profile used for testing is shown in Fig. 3.5a. The ability of proposed control to maintain the frequency tightly to the nominal value by providing the necessary damping is depicted in Fig. 3.5b. The derived controller gains, corresponding to the identified oscillation frequency, are shown in Fig. 3.5c and Fig. 3.5d. Fig. 3.6 shows a comparison of the frequency spectrum for this case with and without the damping controller. The dominant frequencies identified in the configuration without the controller are damped when the proposed damping controller is included.

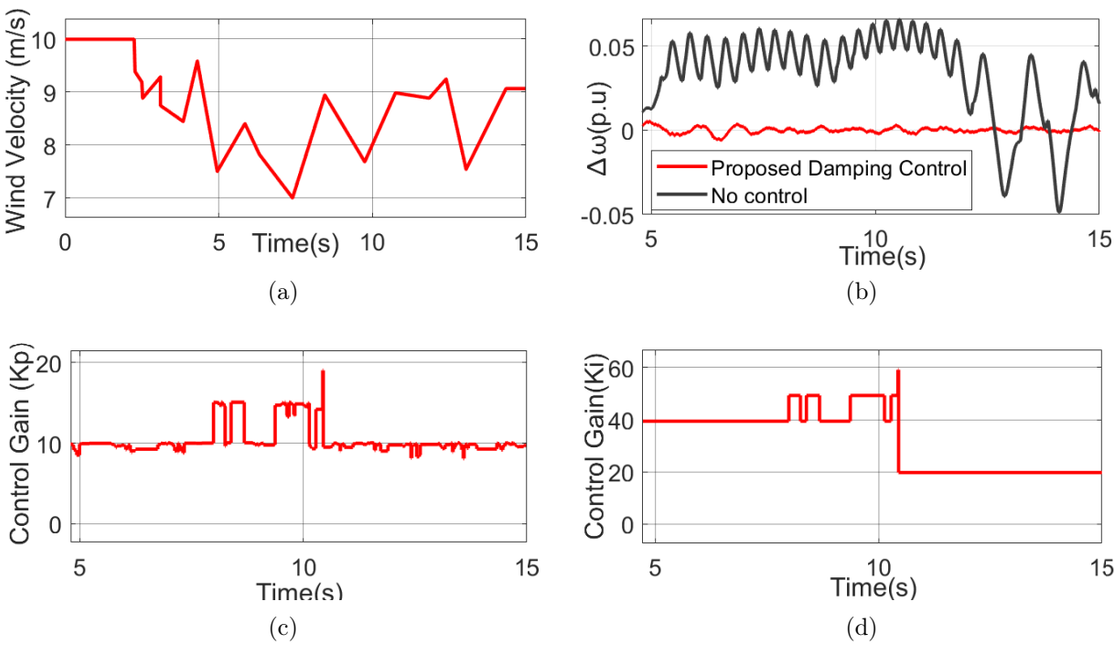

Figure 3.5: Case B (a) Variable wind speed profile, (b) Speed variations during variable wind speed profile, (c) Proportional gain derived based on oscillation frequency, (d) Integral gain derived based on oscillation frequency.

3.2.5.3 Case C :Performance during a Sudden Load Change

This test scenario validates the performance of the proposed damping controller during a sudden load change initiated at 7s for a duration of 2s at bus 634 of the test system. A 50% improvement in frequency deviation was observed during 7s to 9s, as shown in Fig. 3.7a. The identified oscillation frequency and the derived controller gains are shown in Fig. 3.7b

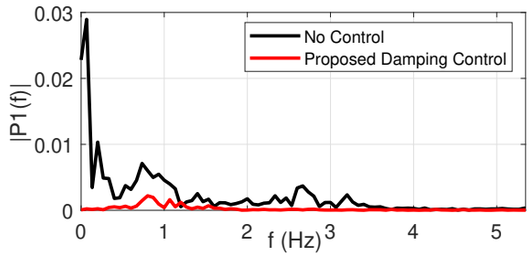

Figure 3.6: Case B: Comparison of frequency spectrum with and without damping control.

and Fig. 3.7c, respectively.

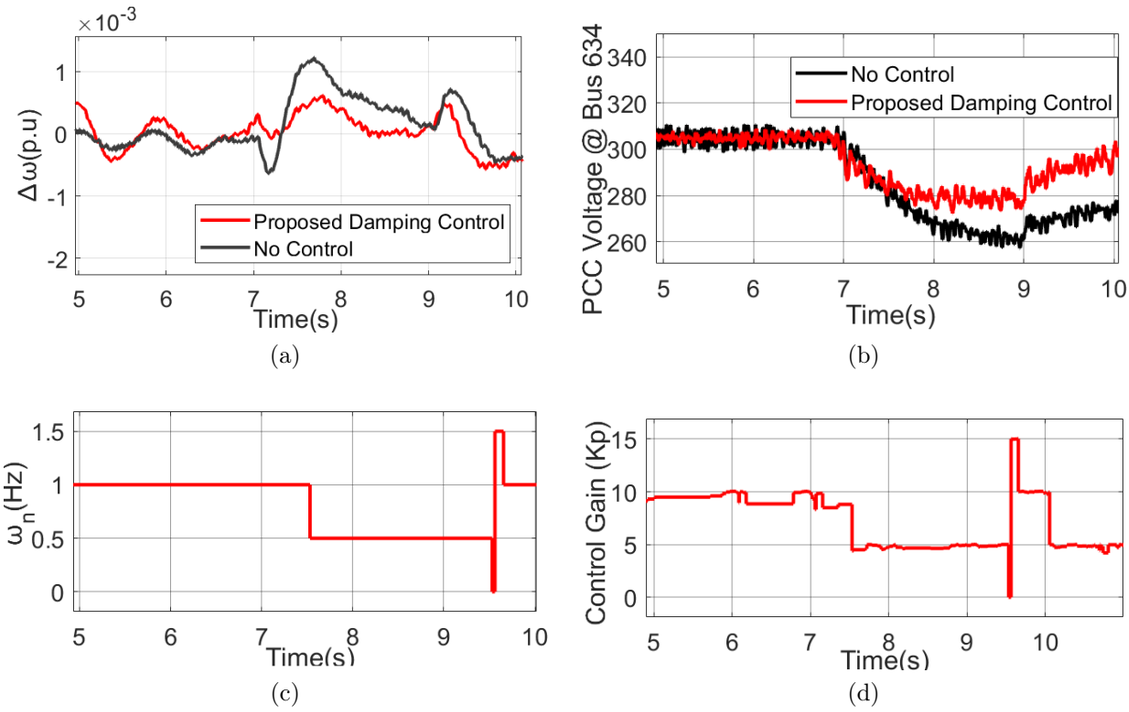

Figure 3.7: Case C (a) Speed deviation during load change, (b) PCC voltage during load change, (c) Oscillation frequency identified during load change, (d) Proportional gain derived based on oscillation frequency.

TABLE 3.1: Comparison of Test Results

Parameter	No Control(NC)	Proposed Control
Case A: % of Δf	2%	1%
Case A: Settling time	1.45s	2.15s
Case A: % improvement in Vpcc	-	6% compared to NC
Case B: % of Δf	5%	0.05%
Case C: % of Δf	0.1%	0.05%

3.3 Oscillation Damping of Integrated Transmission and Distribution Power Grid with Renewables Based on Novel Measurement-Based Optimal Controller

Recent trends in electricity generation include the interconnection of several resources with the traditional power grid. Amongst the new resources, renewable energy resources (RERs) are gaining fast adoption, because of their offered economic, environmental, and sustainability benefits. In addition, many policies are major drivers for the adoption of

RERs [2, 3]. The electricity delivery frequency determines the point of interconnection for these resources, depending on the type of RER. For instance, wind turbines are connected to the transmission layer. At the same time, small-scale or residential solar systems can be connected to the distribution layer, which can be referred to as distributed generation (DG). Studies show there are 12 million DG units across the United States with a total capacity of 200GW [4]. RERs can be operated in both a grid-connected mode and an off-grid mode. In a grid-connected mode, the traditional grid is transformed from a unidirectional flow into a bidirectional flow, which increases the network complexity. In most RERs, power generation varies due to the intermittency/variability of the source. For example, wind speed variability results in wind turbine frequency and power output fluctuations [5]. This variability can have a significant impact on the grid. These impacts can be more severe, depending on the level of renewable energy penetration. Some of these impacts result in violation of power quality standards, such as the voltage ANSI value (0.95-1.05pu) or the frequency, which should be kept between 59.5-60.5Hz, so the system does not lose stability. Power quality is assumed to be good if the aforementioned metrics remain at an acceptable, steady value of voltages and frequency, with a smooth sinusoidal waveform. This showcases the need for effective control and management strategies.

Battery energy storage devices are one of the approaches that have been widely implemented for load frequency control (LFC) [122]. Batteries are also being used for smoothing of RERs, which can be connected to the DC-link of solar PVs or the DC-link capacitance of a wind turbine. Despite the advantages of the interconnection of batteries by charging and discharging, the fast-changing behavior of ambient sources and the capacity of the battery plays a major role in addressing these issues. During the short circuit condition that occurs while connecting networks, fixed wind speeds can also result in instability, because of the high level of reactive power that is absorbed. Other methods to mitigate frequency fluctuation include superconductive magnetic energy storage systems (SMEs). Despite the advantages of higher long life and density, this solution is quite expensive to implement. Lack of inertia is another major challenge with the interconnection of these resources and the reason that they are susceptible to frequency fluctuations.

In terms of power generation, wind energy is harvested using wind energy conversion systems (WECS). Unlike conventional plants that use synchronous generators, WECS uses different generators, such as squirrel cage induction, doubly-fed induction, and permanent magnet synchronous generators. A doubly-fed induction generator (DFIG) offers improved performance concerning the variability of wind sources, leading to minimized power losses. It also provides generation system improvements over other WECS. Furthermore, DFIGs has several benefits for use with variable speed wind turbines, such as high energy efficiency and

controllability [106]. To control DFIG based generation in both grid-connected and islanded modes of operation, several different control techniques have previously been implemented. For example, a cyclo-converter-based control approach was proposed in [107] for decoupled control of DFIG active and reactive power. To analyze the relation between frequency and impedance of compensation networks, some studies have been based on frequency scanning methods [108]. Grid-connected optimization and control approaches for supporting the grid both with and without batteries, to provide additional stability improvement are reported in [112, 123–125]. For grid ancillary support, a battery energy storage system (BESS) with advanced control management is key [114]. In some studies, to improve power quality, the BESS is integrated with the V_{dc} link of the PWM back-to-back converters. However, the main disadvantage associated with these control architectures is that they cannot adaptively damp the frequency oscillations.

Power system stabilizers (PSSs) are overviewed as supplementary controllers to damp system oscillations. The highly nonlinear and dynamic nature of the power grid impacts the performance of conventional PSSs. Hence, some advanced PSS control architectures based on adaptive neural and fuzzy-based control logic have been discussed by many researchers. An adaptive neuro-fuzzy-based adaptive PSS control is discussed in [126]. The dynamic behavior of the plant is identified and the input link weights of the neural network are adaptively adjusted. While a conventional PSS uses generator speed as the local power signal to damp the oscillations, the idea of improving the observability of the PSS by employing an additional signal is discussed in [127]. A similar approach of a modified PSS to effectively damp the oscillations is presented in [128,129]. While [128] makes use of a recursive gradient algorithm for the adaptive PSS design, the architecture in [129] is based on an inherent dead-band adaptive tune architecture, which can track the system operating modes without any strict prerequisites, as demanded by most architectures.

3.3.1 Main contribution

Major contributions of this work compared to the state-of-the-art are as follows:

- An adaptive damping controller is proposed that can damp oscillations in multiple generators considering variations in both transmission and distribution power grids that include RERs.
- The proposed architecture is based on an optimal control theory, so multiple devices can be controlled with this damping control architecture.
- The approach uses resources considering both centralized and distributed generators in both the transmission and distribution systems.

TABLE 3.2: Location and rating of DERs in IEEE 123-bus system

PV Rating	BESS Rating	NodeIDs
2MVA	1.2MWh	48

- The performance of the proposed control architecture is superior during dynamic grid conditions, as compared with the performance of a conventional approach, because of its adaptive tuning capability and the approach is field implementable.

Moreover, compared to earlier work in [130], advantages of the proposed work include:

- An optimal damping controller that can augment generator controllers and/or PSS, which can effectively damp the oscillations in transmission and distribution networks.
- The architecture can dynamically adjust the gain values based on linear optimization that modulates the generator excitation to effectively damp the oscillations.
- Unlike the previous work, which relies on active power modulation from a DFIG and additional power from a battery for damping, the proposed work can efficiently coordinate the generators, thereby efficiently utilizing the available power from nearby generators to damp the oscillations under dynamic grid conditions.

3.3.2 DESIGN AND MODELING OF ENERGY SOURCES

Some of the energy sources that were discussed in the previous section, had their modeling as the same and were implemented such as synchronous generators, and doubly fed induction generators (DFIG). The network architecture is different as it includes synchronous generators, a DFIG, an AC microgrid, and a battery system. It is designed to simulate an interconnection of a transmission and distribution network. The transmission system is a Kundur two-area network, with a wind turbine connected at the tie lines, while the distribution network is an IEEE 123-bus system, which has a solar PV connected to one of its buses.

3.3.3 RER Integrated Power Distribution System

A large RER is connected to the distribution system, IEEE 123-bus system, where the RER is comprised of a PV farm, battery, and inverter system, as shown in Fig. 3.8. The PV farm is located at bus 48. The PV penetration level capacity is provided in Table 3.2. The RER also has a battery system connected to the DC link bus, which is interconnected with an AC inverter.

3.3.3.1 PV farm

The PV system generates 2MW at the maximum power of operation. The system comprises several solar panels and controllers, such as MPPT to ensure that maximum power is

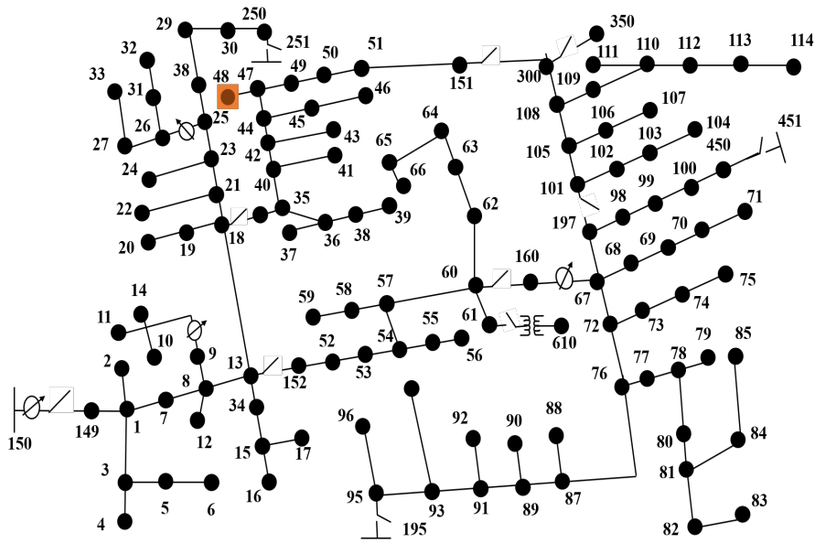

Figure 3.8: PV and load areas in IEEE 123-bus system.

obtained from the resources. The PCC, which can be referred to as the DC-link, has DC power connected to the inverter. The state space representation of the PV system is shown below.

$$\begin{bmatrix} \dot{\bar{i}} \\ \dot{\overline{V}} \end{bmatrix} = \begin{bmatrix} 0 & \frac{-D}{L} \\ \frac{-D}{C} & \frac{-1}{RC} \end{bmatrix} \begin{bmatrix} \bar{i} \\ \overline{V} \end{bmatrix} + \begin{bmatrix} \frac{1}{L} & 0 & \frac{V}{L} \\ 0 & \frac{-1}{C} & \frac{i}{C} \end{bmatrix} \begin{bmatrix} \overline{V_{pv}} \\ \frac{\bar{i}_o}{D_{mpp}} \end{bmatrix} \tag{3.29}$$

$$\begin{bmatrix} V \\ i \end{bmatrix} = \begin{bmatrix} 0 & 1 \\ 1 & 0 \end{bmatrix} \begin{bmatrix} \bar{i} \\ \overline{V} \end{bmatrix} \tag{3.30}$$

In these equations, V_{pv} is the input side voltage, i_o is the output side current, L, C, and D are the inductance, capacitance, and the duty cycle for buck operation of the converter. D_{mpp} is the duty cycle input to the converter for boost operation. Additionally, i, V_g, and V are the inductor current, input voltage, and output voltage, respectively.

3.3.3.2 Battery Model

The battery control system is similar to that of the PV system. The major difference is that, unlike the PV system that does not include a buck mode of operation, the battery can operate in both buck and boost modes for its converter, which depends on the battery mode (i.e., in a mode of discharging or charging). The battery is also responsible for maintaining the DC-link voltage. The battery control system functions as follows. The dc-link voltage, which is maintained as a constant, is measured. However, the current flowing through the battery varies. This results in the battery operation mode changing to either charging or discharging, accordingly. The filter parameters for the battery (e.g., inductance L_{in}, input capacitance C_{in}, and output capacitance C_{out}) are included in the design. The controller, implemented as two cascaded controllers, provides function in a buck-boost operation mode. The inner loop controls the current and provides the duty cycle reference for the generating switching pulses. Whereas, the outer loop control maintains a constant V_{dc} value. The

battery voltage can be represented as,

$$V_{bat} = E_o - K\frac{Q}{Q-it}it - Ri + Ae^{-B\int idt} - K\frac{Q}{Q-it}i^* \tag{3.31}$$

where V_{bat} is the internal battery voltage (V), E_0 is the battery voltage constant (V), K is the polarization constant (V/Ah), K is the polarization constant (V/Ah), Battery capacity (Ah), A is the exponential zone amplitude (V), R is the internal resistance of the battery, $\int idt$ is the actual battery charge (Ah), i is the battery current (A), and i^* is filtered current (A).

The transfer function for the DC-DC converter is given by,

$$\frac{I_i}{d} = \frac{S\frac{V_o}{L} + \frac{V_o}{RLC} + \frac{I_L D'}{LC}}{S^2 + \frac{1}{RC}S - \frac{D^2}{LC}} \tag{3.32}$$

$$P_{batt} = \begin{cases} P_{disch} & V_{pcc} < 1 \\ 0 & V_{pcc} = 1 \\ P_{ch} & V_{pcc} > 1 \end{cases} \tag{3.33}$$

where P_{batt} is the status of the battery, P_{disch} indicates discharging, and P_{ch} represents charging.

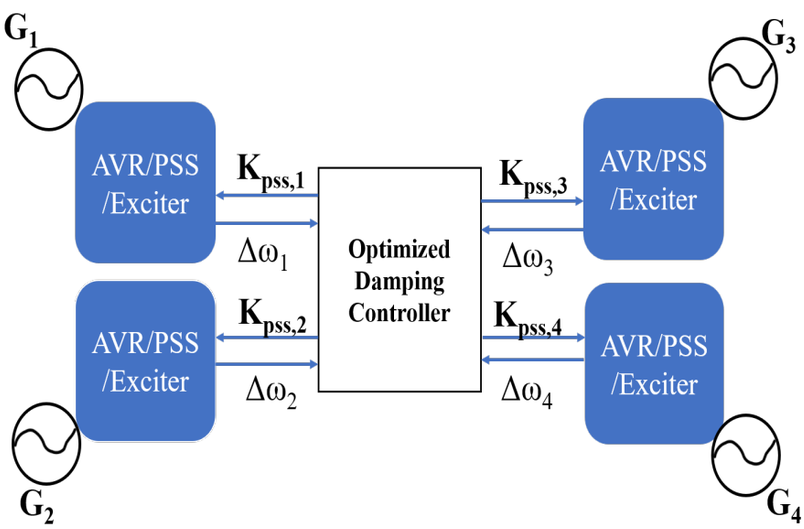

Figure 3.9: PV and load areas in IEEE 123-bus system.

3.3.3.3 Inverter Model

The inverter type has an L filter, referred to as L inverter, where the $d-q$ equations guiding its operations are below,

$$V_{dl} = L_{inv}\frac{di_d}{dt} - wL_{inv}i_q + V_d \tag{3.34}$$

$$V_{ql} = L_{inv}\frac{di_q}{dt} - wL_{inv}i_d + V_q \tag{3.35}$$

where V_{dl},V_{ql} are d-axis and q-axis voltages across inductor L_{inv}, ω is the supply voltage angular frequency, L is the inductance of the L-type filter, i_d, i_q and V_d, V_q are the d-axis and q-axis inverter output current and voltages, respectively. The active and reactive power output when connected to the grid are given by,

$$P = V_d i_d \tag{3.36}$$

$$Q = V_q i_q. \tag{3.37}$$

The state space representation of the inverter equation in a grid connected mode is shown below. If V_d (grid voltage) is kept constant, then i_d and i_q can be used to control the active and reactive power.

$$\begin{bmatrix} i_d \\ i_q \end{bmatrix} = \begin{bmatrix} 0 & \omega \\ \omega & 0 \end{bmatrix} \begin{bmatrix} i_d \\ i_q \end{bmatrix} + \begin{bmatrix} \frac{1}{L_{inv}} & 0 \\ 0 & \frac{1}{L_{inv}} \end{bmatrix} \begin{bmatrix} (V_{dl} - V_d) \\ (V_{ql} - V_q) \end{bmatrix} \tag{3.38}$$

$$\begin{bmatrix} P_{ac} \\ Q_{ac} \end{bmatrix} = \begin{bmatrix} V_d & V_q \\ -V_q & V_d \end{bmatrix} \begin{bmatrix} i_d \\ i_q \end{bmatrix} \tag{3.39}$$

3.3.4 Mathematical Model of Proposed Damping Controller

Considering the power grid models designed in Section II. A finite horizon optimal control framework can be developed if we have a model that relates to a state-space representation of the system as $x_{k+1} = Ax_k + BU_k$.

With the system model in state-space, we can define an optimal control framework by minimizing,

$$J_{obj} = \frac{1}{2} \sum_{k=0}^{N} \left[(x_k)^T Q_c x_k + (u_k)^T R_c U_k \right] \tag{3.40}$$

where Q_c and R_c are symmetric positive (semi-) definite matrices, x_k are the states, u_k is the control input per the control law (e.g., $U_k = K_k x_k$).

With an optimization convergence threshold, ϵ, we can get an optimal solution for this framework with a maximum principle H such that,

$$H = (x_k)^T Q_c x_k + (U_k)^T R_c U_k + \lambda(Ax_k + BU_k) \tag{3.41}$$

where $\lambda_{k+1} - \lambda_k = (\frac{\partial H}{\partial x})^T = Q_c x_k + A^T \lambda_k$ and $U_k = -R_c^{-1} B^T \lambda_k$.

Minimizing (3.41) is equivalent to minimizing (5.24). We can see from the above that $(\frac{\partial H}{\partial x})^T = Q_c x_k + A^T \lambda_k$, $(\frac{\partial H}{\partial \lambda})^T = Ax_k + BU_k$, and $\frac{\partial H}{\partial u} = R_c U_k + \lambda^T B$. Therefore, to minimize H, we should find, A, B, λ, x_k and U_k iteratively and solve each of the derivatives.

3.3.4.1 Measurement Based Optimal Damping Controller Design

Consider two measurements from each generators $\Delta\omega_i$ and ΔV_{Si} with,

$$\Delta\omega_i = \omega_i^m - \omega_i^o \tag{3.42}$$

$$\Delta V_{Si} = V_{Si}^m - V_{Si}^o \tag{3.43}$$

where m and o represent the measured and observed values, respectively. The observed signal is represented as the steady state moving average value from normal operation conditions.

Consider an optimal controller gain for each generator as $K_{PSS,i}$, then this gain can be presented from classical equations as,

$$K_{PSS,i} = \left\{ \left(\frac{p(\Delta V_{S,i})(1+pT_2)}{1+pT_1} + \frac{(\Delta V_{S,i})(1+pT_2)}{T\omega_i(1+pT_1)} \right) * \frac{1}{p\Delta\omega_i} \right. \tag{3.44}$$

where $p = \frac{d}{dt}$. With the deviations in speed and voltage represented as in (3.42) and (3.43) we get,

$$K_{PSS,i} = \left(p(\Delta V_{Si}) + \frac{\Delta V_{Si}}{T\omega_i} \right) * \frac{1}{p\Delta\omega_i}. \tag{3.45}$$

where T is the time constant. To discretize, first, we need to rewrite the deviation of the speed and the control input of the stabilizer per (4.32) and (3.47).

$$Y_{2,i} = \Delta\omega_i \tag{3.46}$$

$$Y_{1,i} = \Delta V_{S,i} \tag{3.47}$$

Each of the stabilizer equations then becomes,

$$K_{PSS,i} = \left(p(Y_{1,i}) + \frac{Y_{1,i}}{T\omega_i} \right) * \frac{1}{pY_{2,i}}. \tag{3.48}$$

Discretization of these equations produces the following,

$$K_{PSS,i} = \frac{\Delta Y_{1,i} + bY_{1,i}}{\Delta Y_{2,i}} \tag{3.49}$$

$$\Delta Y_{2,i} * K_{PSS,i} = \Delta Y_{1,i} + bY_{1,i} \tag{3.50}$$

where $b = \frac{\Delta t}{\Delta T\omega_1}$.

Then rewrite (3.50) as,

$$\Delta Y_{1,i} = -bY_{1,i} + K_{PSS,i} * \Delta Y_{2,i}. \tag{3.51}$$

Algorithm 2: Proposed Adaptive Damping Controller

```
-
Identify all the devices in the network (e.g., generators, wind turbines, and solar PVs)
  and measurement points.
Initialize the system parameters and K_pss, K_pss^U, K_pss^L, ΔY_2^U, ΔY_2^L and ΔY_1 for all
  the controllable generators.
Compute the speed/frequency deviation signal, Δω, as shown in (3.42).
Obtain the measure Δω for each generator, n, and set the value for ϵ.
From step 3, calculate Δω_T, as Δω_T = Σ_{i=1}^{N} Δω_i.
for k = 1 : N do
    while i ≤ n
    Calculate the A, B, x_k, and U_k using (3.52) and (3.53)
    if Δω_T ≥ ϵ then
        Minimize Δω_T using (3.41). For this
        Find K^k_{pss,i} using (4.12)-(3.57)
        Calculate P_k and λ_k using (3.58)
        Update U_k using (3.53)
        Calculate Δω_T using (3.52)
    else
        if Δω_T < ϵ then
            K^k_{pss,i} = K^{k-1}_{pss,i}
        end
    end
end
```

For multiple generators, (3.51) can be written as (3.52).

$$\overbrace{\begin{bmatrix} \Delta Y_{1,i} \\ \vdots \\ \Delta Y_{1,n} \end{bmatrix}}^{x_{k+1}} = -\overbrace{\begin{bmatrix} b_1 \\ \vdots \\ b_n \end{bmatrix}}^{A}\overbrace{\begin{bmatrix} Y_{1,i} \\ \vdots \\ Y_{1,n} \end{bmatrix}}^{x_k=\Delta\omega_i} + \overbrace{\begin{bmatrix} I \end{bmatrix}}^{B}\overbrace{\begin{bmatrix} K_{PSS,i}\Delta Y_{2,i} \\ \vdots \\ K_{PSS,n}\Delta Y_{2,n} \end{bmatrix}}^{U_k=K_{PSS,i}\Delta V_i} \tag{3.52}$$

From the above, it can be seen that with the help of measurements we can find A, B, x_k, and U_k iteratively. Thus, (3.42) can be written as $\min_{x_1,\ldots x_T} \Delta\omega_T = \sum_{i=1}^{N} \Delta\omega_i$, where $H = \Delta\omega_T$.

3.3.4.2 Framework to Calculate U_k, λ, and K_{PSS}

For this control application, (3.52) can be substituted in (3.42). Derivatives for minimizing (3.42) can be calculated only if we can find λ and U_k. From (3.52) it can be seen that,

$$U_k^i = \Delta Y_{2,i} * K_{PSS,i}. \tag{3.53}$$

However, we have to calculate $K_{PSS,i}$ from U_k^i. To solve this, considering an upper and lower limit for $K_{PSS,i}$ as $K_{PSS,i}^U$ and $K_{PSS,i}^L$ and for $\Delta Y_{2,i}$ as ${\Delta Y_{2,i}}^U$ and ${\Delta Y_{2,i}}^L$ we can apply four additional McCormick constraints to (3.42) considering,

$$U_{k+1}^i \geq K_{PSS,i}^L * \Delta Y_{2,i} + K_{PSS,i} * {\Delta Y_{2,i}}^L - K_{PSS,i}^L * {\Delta Y_{2,i}}^L \tag{3.54}$$

$$U_{k+1}^{i} \geq K_{PSS,i}^{U} * \Delta Y_{2,i} + K_{PSS,i} * {\Delta Y_{2,i}}^{U} - K_{PSS,i}^{U} * {\Delta Y_{2,i}}^{U} \tag{3.55}$$

$$U_{k+1}^{i} \leq K_{PSS,i}^{U} * \Delta Y_{2,i} + K_{PSS,i} * {\Delta Y_{2,i}}^{L} - K_{PSS,i}^{U} * {\Delta Y_{2,i}}^{L} \tag{3.56}$$

$$U_{k+1}^{i} \leq K_{PSS,i} * {\Delta Y_{2,i}}^{U} + K_{PSS,i}^{L} * \Delta Y_{2,i} - K_{PSS,i}^{L} * {\Delta Y_{2,i}}^{U} \tag{3.57}$$

where i represents damping controller identification number. Therefore, the bilinear terms for the McCormick envelope are ($K_{PSS,i}$, $Y_{2,i}$). From these constraints U_k^i can be found from existing and previous values of $K_{PSS,i}$ and $\Delta Y_{2,i}$, where ${K_{PSS,i}}^{L} = \min_{x_1,\ldots x_T} K_{PSS,i}$ and ${\Delta Y_{2,i}}^{L} = \min_{x_1,\ldots x_T} \Delta Y_{2,i}$ from the last ten samples. Similarly, we can find the ${K_{PSS,i}}^{U}$ and ${\Delta Y_{2,i}}^{U}$ with maximum values of the previous samples.

Finally, λ_k is calculated as,

$$\lambda_k = -P_k x_k \tag{3.58}$$

where P_k is the solution of the Riccati equation for the k-step $= Q_c + K_{PSS,i}^{T} R_c K_{PSS,i} + (A + BK_{PSS,i})^{T} P_{k-1} (A + BK_{PSS,i})$. For the simulation, we used four power system stabilizers hence, $i = 1...4$. Using the equations above, the gains of the damping controller, K_{PSS}, are updated at each time interval, based on the deviations seen on the grid. A flowchart of the proposed optimal damping controller algorithm is provided in Fig. **??** and the corresponding optimal adaptive algorithm that dynamically adjusts the gains of the PSS is shown in Algorithm 8.

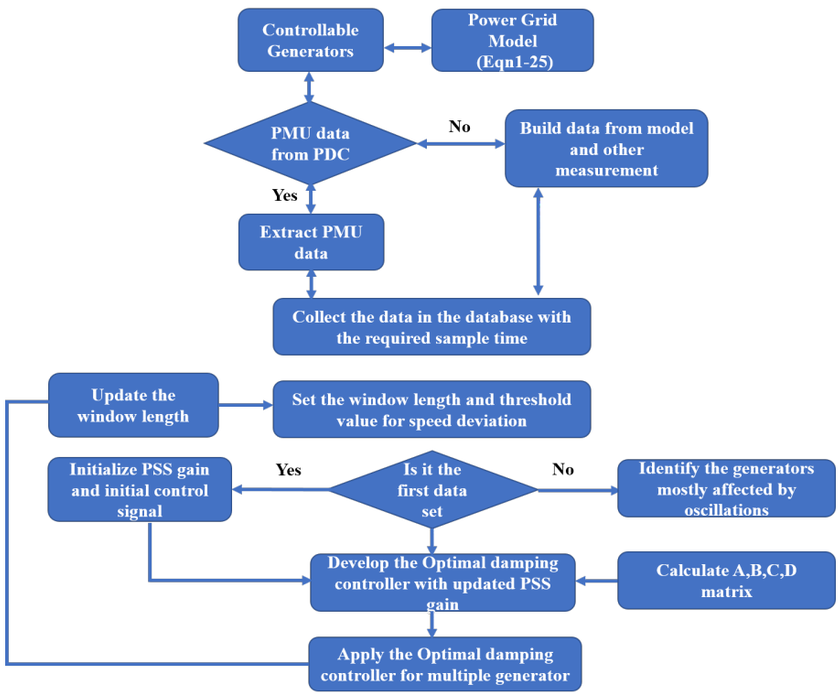

Figure 3.10: Flowchart for the proposed optimal damping controller.

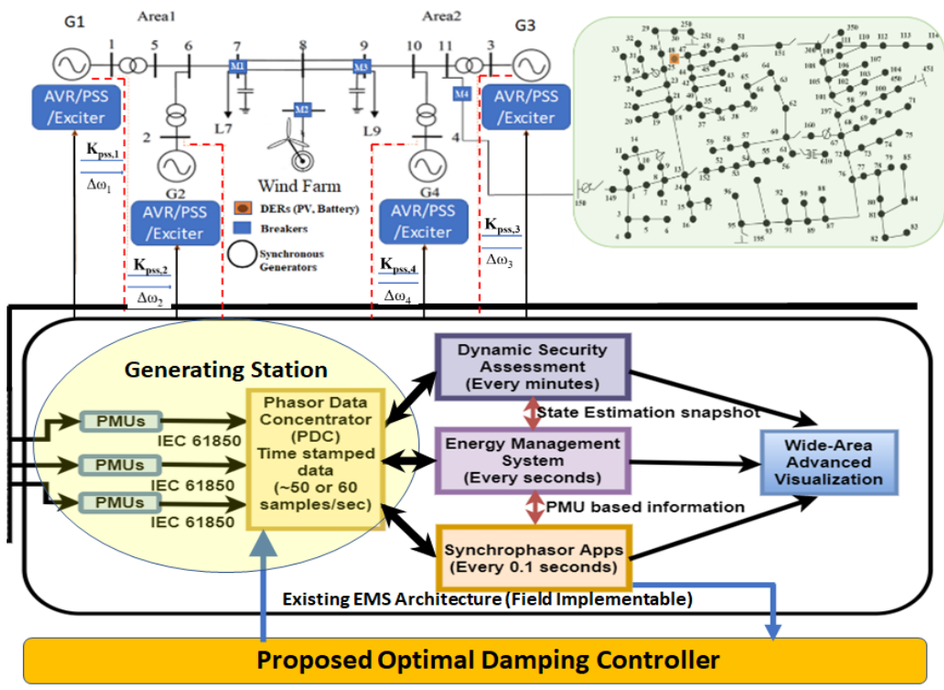

Figure 3.11: Field implementation framework of Integrated transmission and distribution system with dynamic models of generators and proposed damping controller.

3.3.5 TestSystem:Modified IEEE 123-Bus Test System, Kundu Two Area, Solar PV and WindTurbine

The proposed optimal oscillation damping controller is tested under different scenarios and the frequency is measured at each of the points, as shown in Fig. 3.11, to validate the performance. Three test cases scenarios are discussed. Case 1 analyzes the performance of the proposed approach for a fault. Case 2 analyzes the response during dynamic variations of the irradiance profile and wind speed profile. Case 3 analyzes the performance for a sudden load change. Case 4 shows the operational performance during a harmonic load change. The system architecture involves the modeling and design of the four main energy sources. It includes synchronous generators, a DFIG, an AC microgrid, and a battery system. The network architecture is designed to simulate an interconnection of a transmission and distribution network. The transmission system is a Kundur two-area network, with a wind turbine connected at the tie lines, while the distribution network is an IEEE 123-bus system, which has a solar PV connected to one of its buses

3.3.5.1 Scenario: Fault

In Case 1, performance of the proposed adaptive PSS architecture is tested for a three phase to ground fault triggered at 10s at different locations of the test system for a duration of 250ms.

3.3.5.2 Case 1A

In this case, the performance of the proposed adaptive PSS architecture is tested for a three-phase to ground fault triggered at Area 1. The frequency of the generators correspond-

ing to the test scenario is shown in Fig. 3.12. The results showcase the ability of the proposed controller to provide faster damping of oscillations following a disturbance, as compared with the conventional control approach. The performance of the corresponding dynamic control gain derived by the optimization algorithm for this test case is detailed in Fig. 3.13. With a fault at Area 1, the contribution of the generators in Area 1 is similar, while the contributions between area generators are different. Also, the control gains for Area 2 are changing more dynamically, even though the magnitude is lower. Fig. 3.13 depicts the contribution of the algorithm that dynamically adjusts the control contributions from each of the generators following the event at 10s.

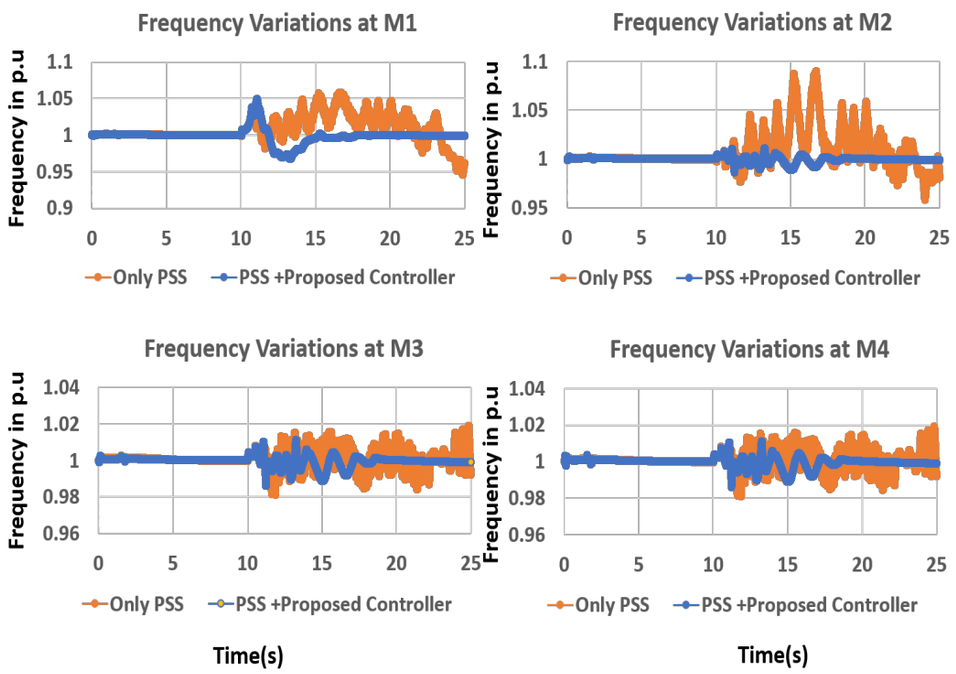

Figure 3.12: Case 1A: Grid frequency measurements for fault occurrence at Area 1.

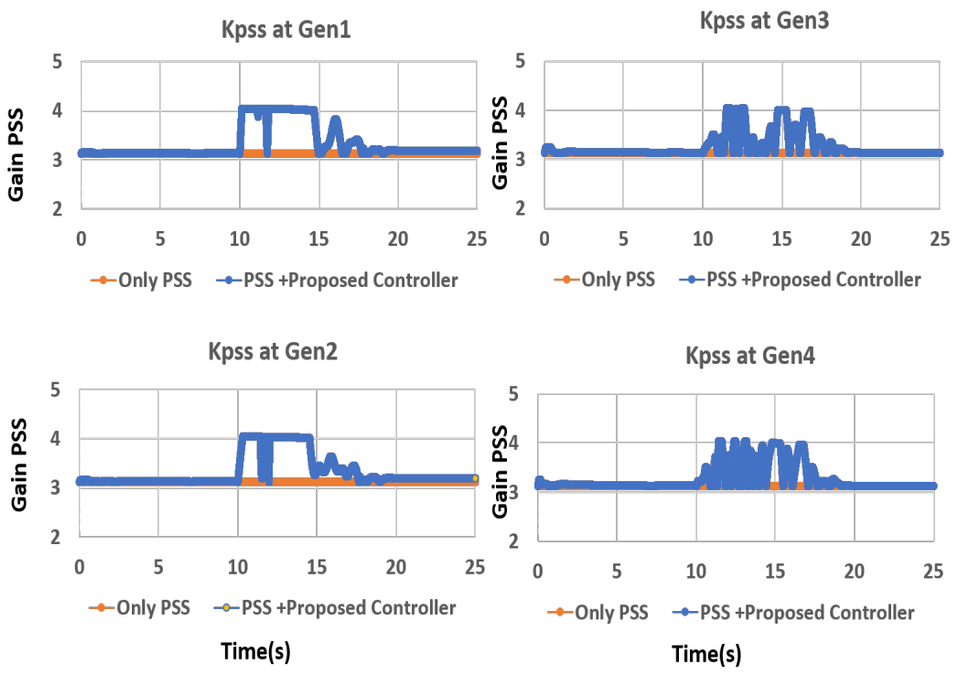

Figure 3.13: Case 1A: Dynamically changing gains.

3.3.5.3 Case 1B

In this case, the fault occurrence is on the tie-line. The damping action for all four measurement points shown in Fig. 3.11 is depicted in Fig. 3.14. It can be seen that the damping is similar in all the parts of the grid, which is expected due to the reason that the areas are balanced in power transfer, with an overall improvement of around 1%. The dynamic gains generated by the algorithm in Fig. 3.15 show that all generators participate equally towards maintaining the grid frequency when the fault is located at the tie-line.

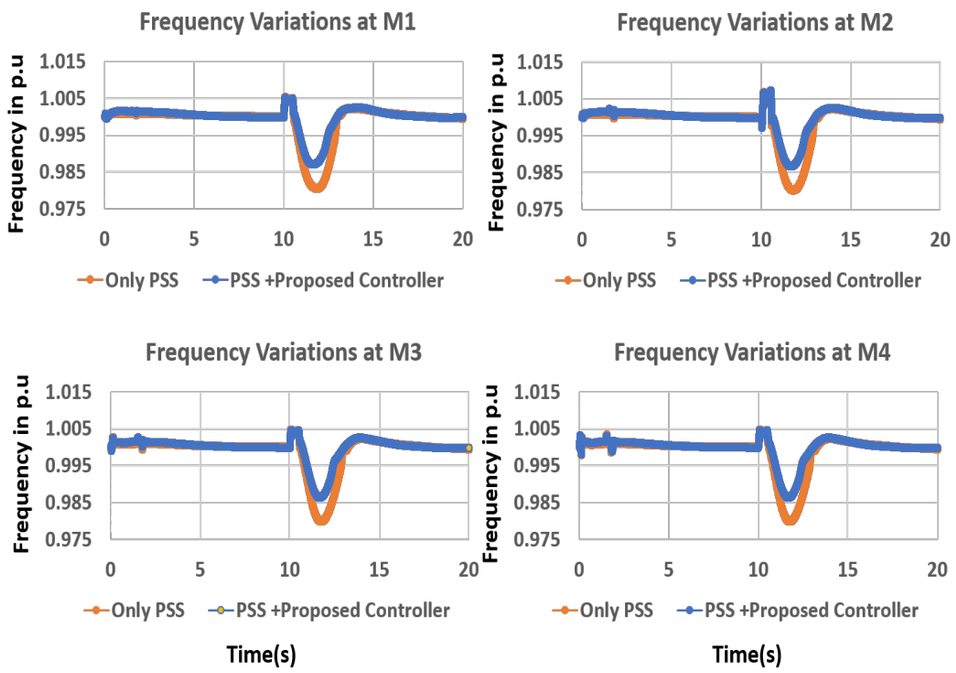

Figure 3.14: Case 1B: Grid frequency measurements corresponding to fault occurrence at tie-line.

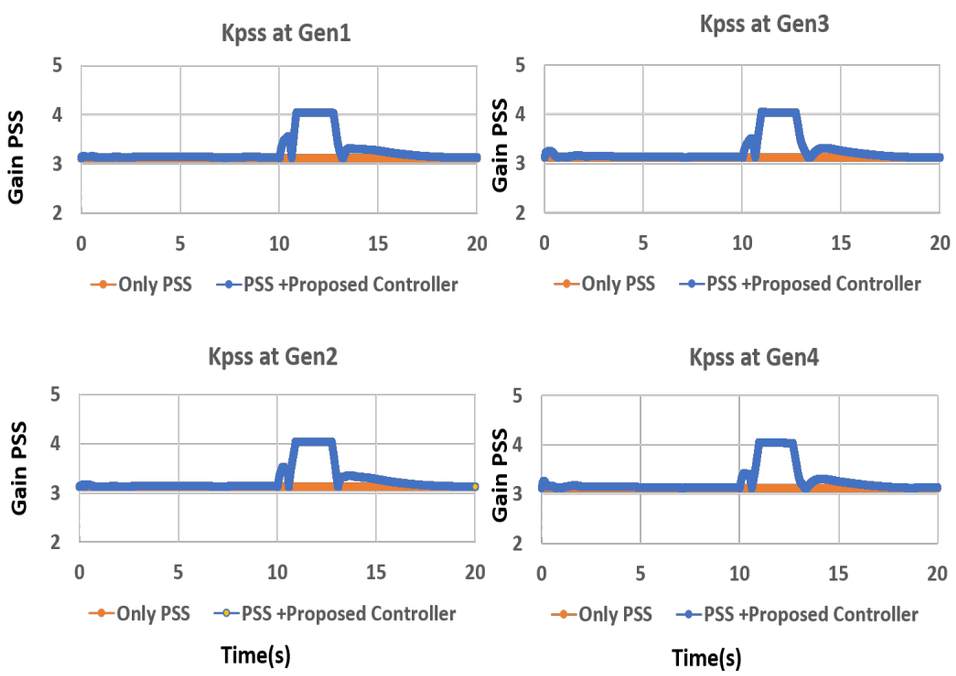

Figure 3.15: Case 1B: Dynamically changing gains.

3.3.5.4 Case 1C

In this case, a fault scenario is developed in the distribution system and the controller performance for a fault located at the distribution system is detailed in Fig. 3.16 and Fig. 3.17, respectively. With the proposed control, the contributions from the generator are dynamically adjusted contrary to the conventional PSS, as shown in Fig. 3.17, resulting in faster damping of oscillations, as shown in Fig. 3.16.

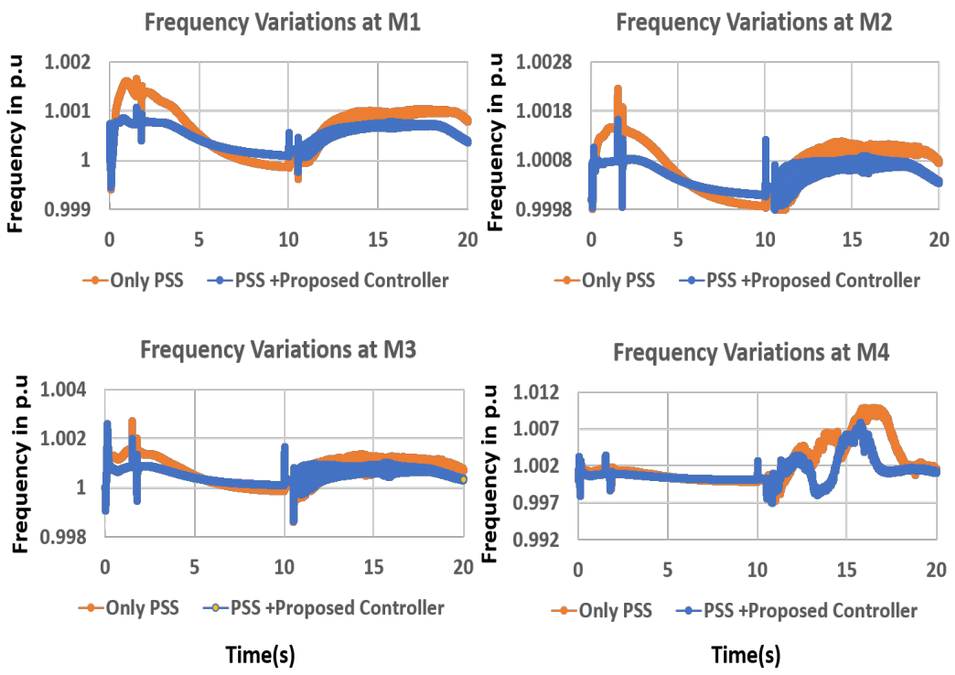

Figure 3.16: Case 1C: Grid frequency measurements corresponding to fault occurrence in distribution system.

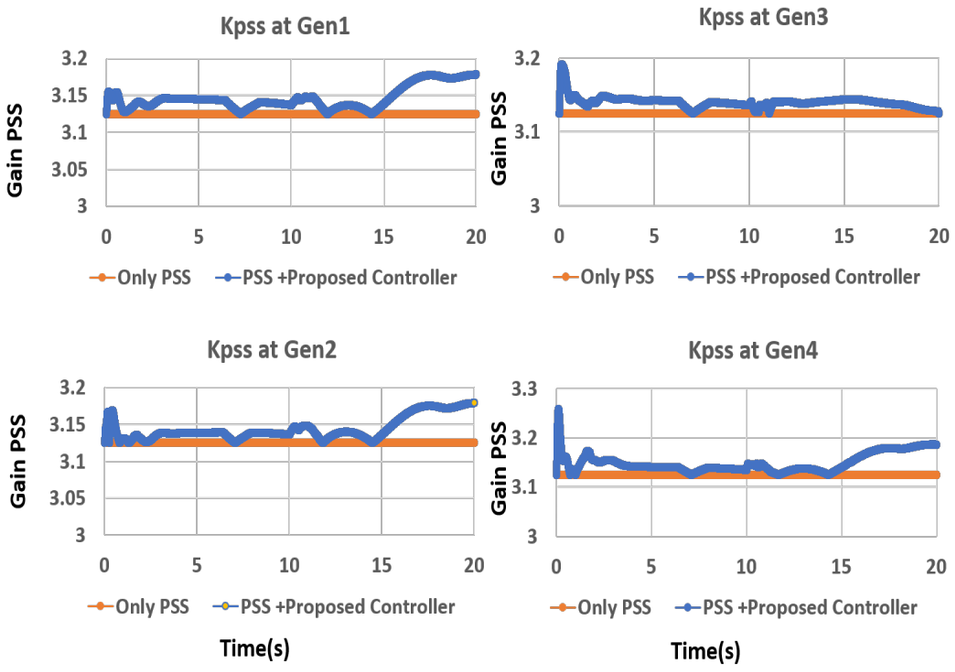

Figure 3.17: Case 1C: Dynamically changing gains.

3.3.5.5 Scenario: Varying wind speed and irradiance scenario

3.3.5.6 Case 2

In this scenario, the output from solar PVs and the wind turbine is assumed to be varying, due to the variation in irradiance and wind profile, respectively as shown in Fig. 3.18. The corresponding frequency deviations are showcased in Fig. 3.19 and the controller gains are illustrated in Fig. 3.20. The results show the ability of the proposed control architecture to tightly maintain the grid frequency to the nominal value, even during highly dynamic input profiles. The larger size of the wind farm shows a much wider low-frequency oscillation in transmission system areas ($M_1 - M_4$). It can be seen that when the PV irradiance is varied (at 10s), the frequency starts oscillating. With the proposed damping controller the frequency deviation is close to zero indicating a stable system.

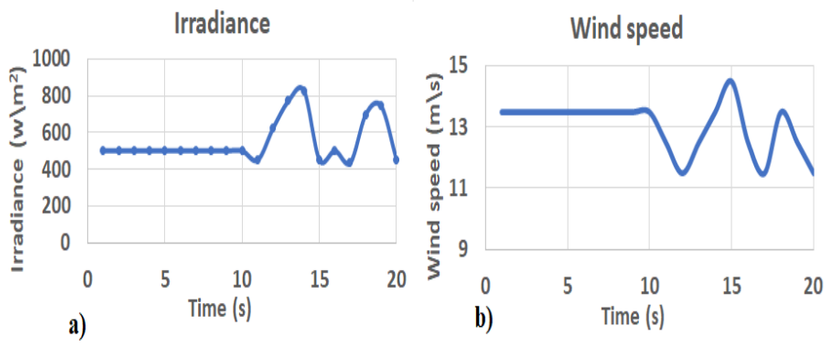

Figure 3.18: Case 2: Varying wind speed and irradiance profile.

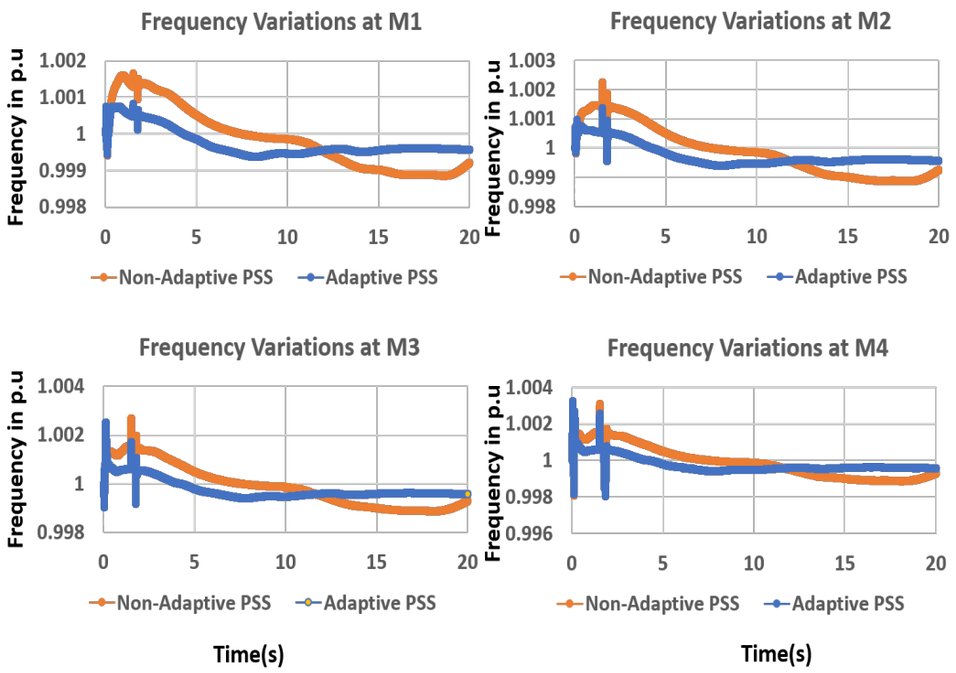

Figure 3.19: Case 2: Grid frequency measurements corresponding to change in irradiance and wind profile.

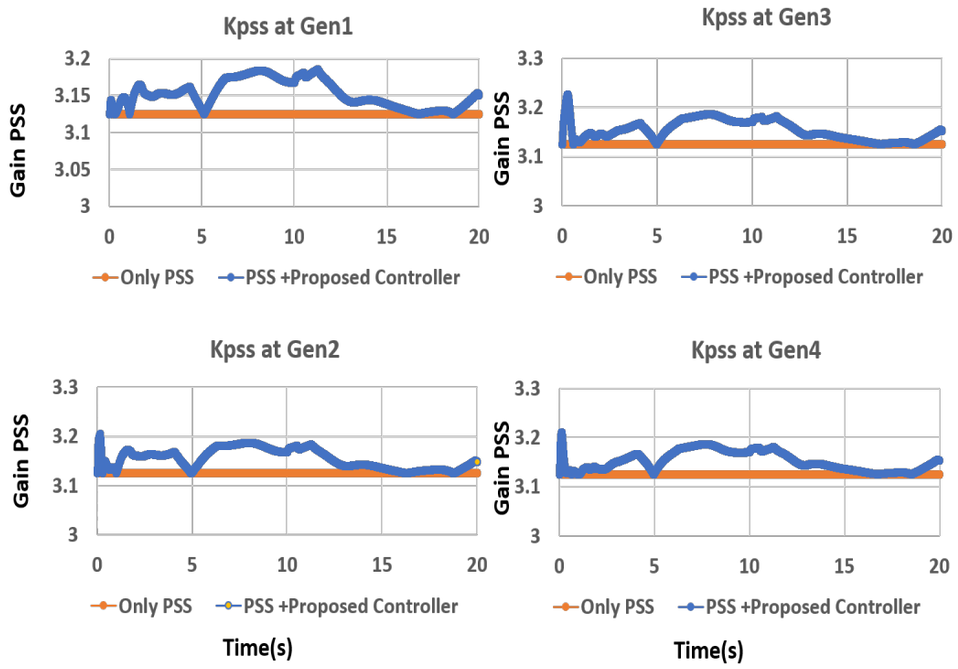

Figure 3.20: Case 2: Dynamically changing gains.

3.3.5.7 Scenario: Sudden load change scenario

3.3.5.8 Case 3

In this scenario, the controller performance was tested for a sudden load change initiated at Area 2. The grid frequency observed at each measurement point is showcased in Fig. 3.21. The proposed optimization could tightly maintain the frequency around 1p.u. shortly following the dynamic event. The ability of the proposed optimization algorithm to dynamically adjust the gain following the load change event at 10s is showcased in Fig. 3.22. A 47% improvement settling time is observed with the proposed approach compared to the conventional approach.

3.3.5.9 Scenario: Harmonic loads

3.3.5.10 Case 4

In this case, a harmonic fault scenario has been tested with the proposed controller. To this end, second-order harmonic conditions are created at 12s during the simulation. The load model is as follows.

$$V_{load} = V_S - I_1 Z_S sin(\omega_1 t + \theta_1) - ...I_n sin(n\omega_1 t + \theta_n)(R + jnX) \tag{3.59}$$

This was initiated by bringing a load online that operates at a different frequency than the grid frequency. The frequency deviation, as observed from the grid, is shown in Fig. 3.23. It can be seen that at 12s, the frequency deviations occur due to the switching of these loads. Also, it can be noted that with the proposed damping controllers the oscillations in the frequency are reduced. Table 3.4 and Table 3.5 quantitatively summarizes the effect of

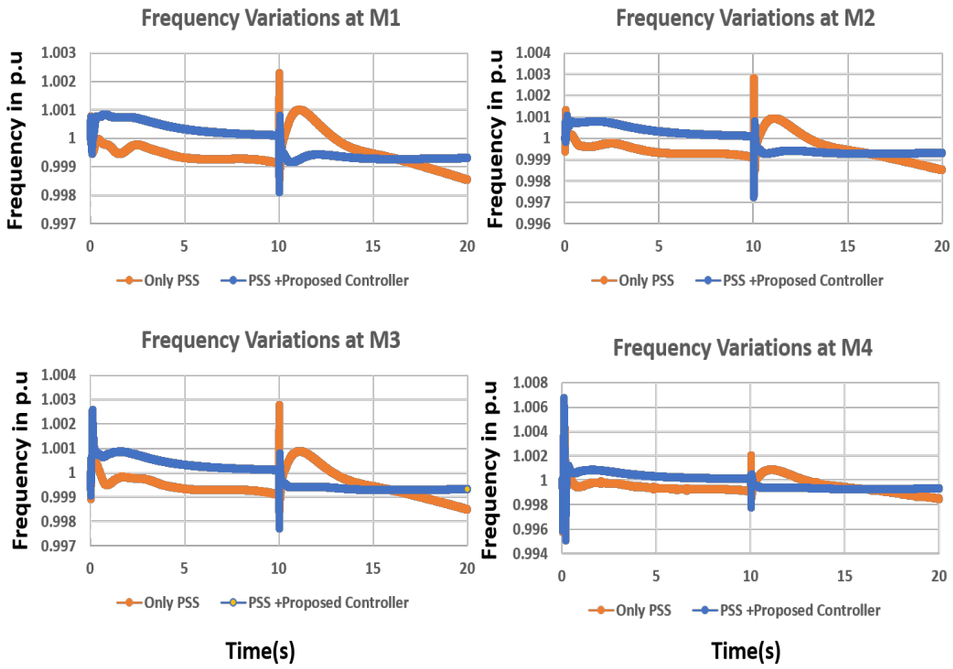

Figure 3.21: Case 3: Grid frequency corresponding to sudden load change.

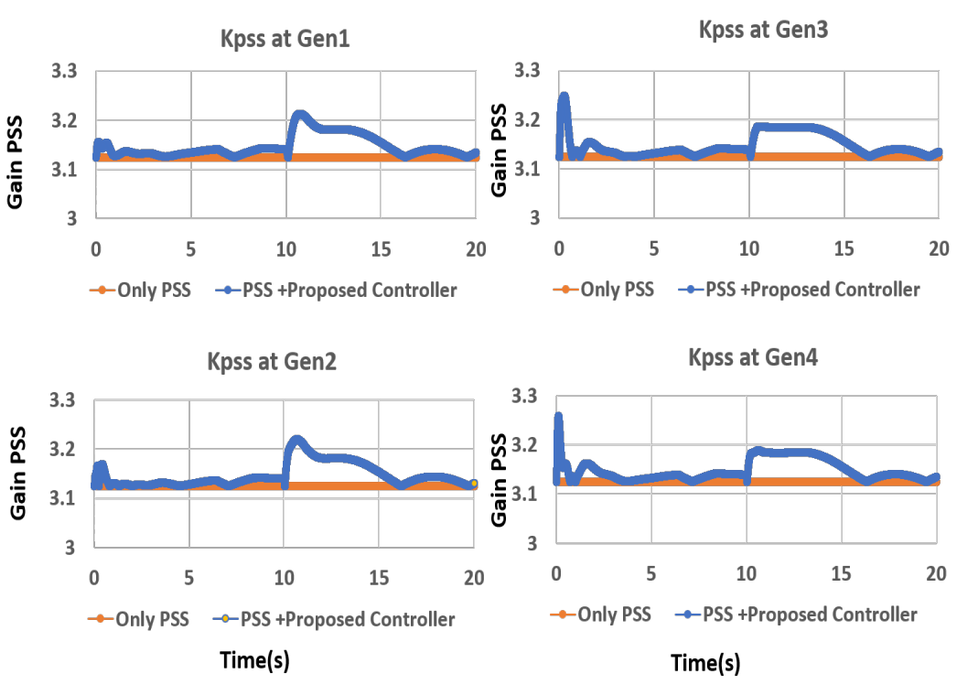

Figure 3.22: Case 3: Dynamically changing gains.

the proposed controller.

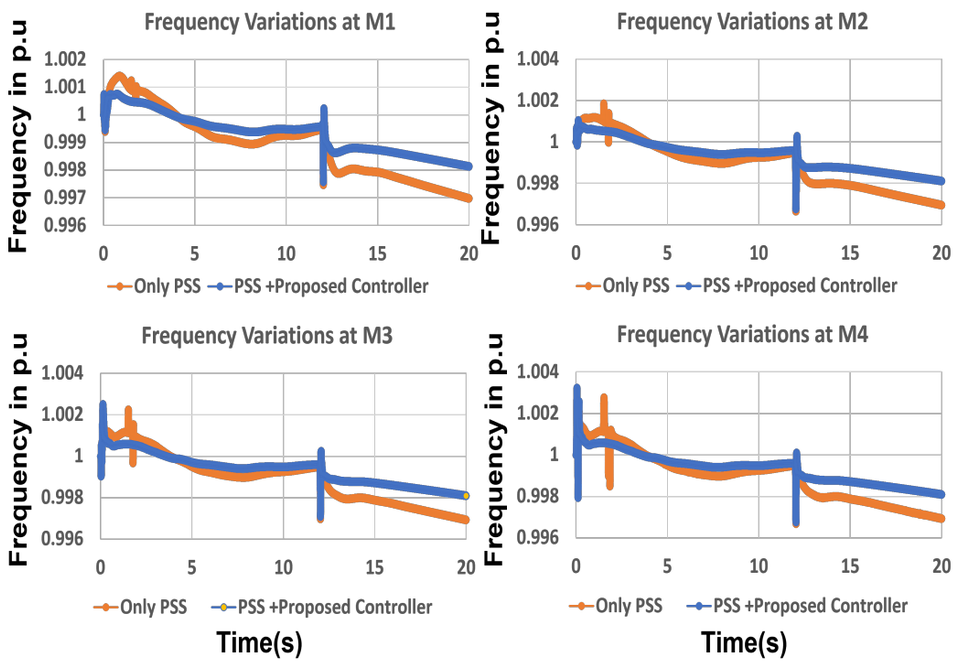

Figure 3.23: Case 4: Grid frequency measurements corresponding to harmonic loads.

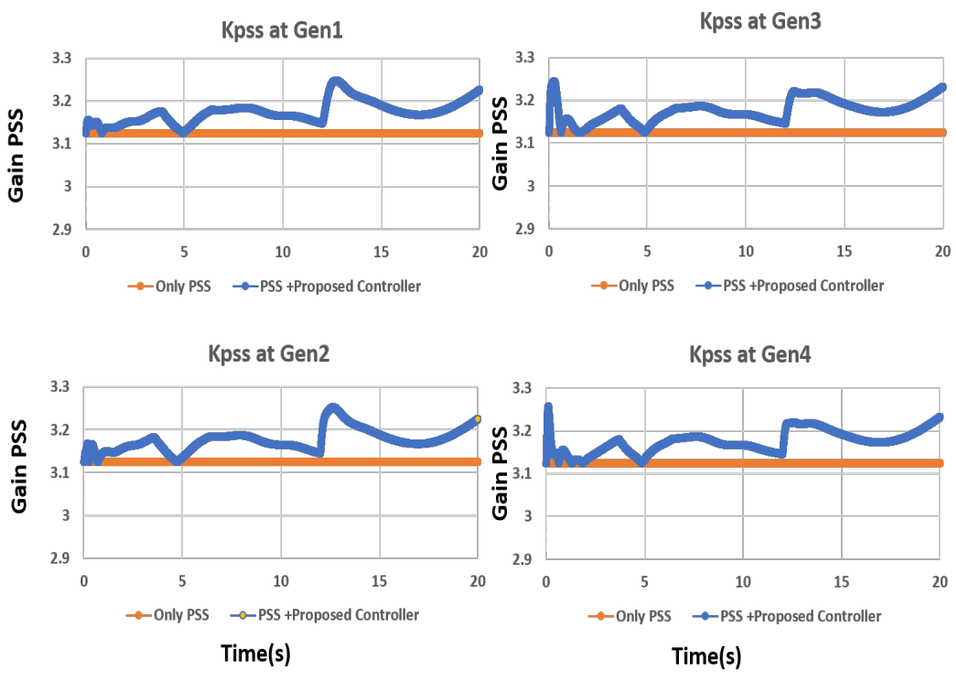

Figure 3.24: Case 4: Dynamically changing gains.

3.3.6 Discussions and Performance Evaluation

As seen from the results provided Table 4.11, Table 3.4, and Table 3.5, performance of our previous damping controller in [130] and the conventional controller (state-of-the-art) are similar. However, with the proposed damping controller, significant improvements in terms of frequency oscillations and settling times have been noticed. Power system stabilizers have the advantages of improved damping and stability of the system by providing additional action to the excitation controller to damp electromechanical oscillations but have the disadvantages of

TABLE 3.3: Relative Comparison of Grid Frequency Deviations Corresponding to Different Test Cases

Case	Measurement	Non-Adaptive	Adaptive	% Error
Case 1A	M_1	1.060	0.994	6.23%
	M_2	1.091	0.989	9.35%
	M_3	1.015	1.00	1.48%
	M_4	1.013	1.00	1.28%
Case 2	M_1	0.9985	0.9998	0.13%
	M_2	0.999	0.9995	0.13%
	M_3	0.995	0.999	0.4%
	M_4	0.9985	0.9998	0.14%
Case 3	M_1	1.0012	0.9999	0.13%
	M_2	1.001	0.9998	0.12%
	M_3	1.003	0.998	0.3%
	M_4	1.0015	0.999	0.25%

TABLE 3.4: Comparison of Test Results With and Without Proposed Control: Grid Frequency

Cases	CC	PC	% Improvement
Fault Case 1	1.0900	0.9895	7.50%
Fault Case 2	1.01	1.001	0.90%
Fault Case 3	0.9751	0.9878	1.28%
Varying Wind-Solar Profile	0.9985	0.9998	0.13%
Load Change	1.0015	0.9998	0.15%
Harmonic load	0.996	0.998	0.21%

Notes: CC is conventional control with only PSS
PC is PSS + Proposed Control

TABLE 3.5: Comparison of Test Results With and Without Proposed Control: Settling time

Cases	CC	PC	% Improvement
Fault Case 1	17s	25s	15.0%
Fault Case 2	16s	16.8s	4.76%
Fault Case 3	11.8s	14.9s	20.81%
Varying Wind-Solar Profile	12.2s	14.2s	14.08%
Load Change	10.7s	14.4s	25.7%
Harmonic load	12.7s	13.5s	5.93%

Notes: CC is conventional control with only PSS
PC is PSS + Proposed Control

a longer settling time attributed towards apriori modeling and tuning. The main significant advantage of the proposed architecture is that it can be implemented online, auto-tunes, and can be applied to multiple generators considering both transmission and distribution dynamics.

3.4 Summary

An optimal damping control framework is designed and implemented on an integrated transmission and distribution system with bulk power and distributed renewable-based generation. The major contribution and goal are to develop a methodology that can manage the frequency oscillation in an integrated transmission and distribution network, with interconnected renewable energy resources. The approach relies on an optimal damping control architecture that is adaptive and at the same time optimal. In addition, an optimization

technique is implemented to help ensure optimum performance of the controller, while minimizing the deviation of the grid frequency. The approach is implemented on synchronous generators that can be used to augment the existing stabilizers or other damping controllers. Also, a field implementation methodology is discussed in this chapter. The results from simulations on real-life feeders validate the superiority of the proposed control method, as compared with a conventional control approach, to provide an improved grid frequency response for a range of anticipated dynamic conditions (e.g., wind speed variations, faults, and load changes). Overall a 10% improvement in damping and settling time is observed. Future work will focus on the implementation of the proposed method with the integration of other renewable sources (e.g., energy storage devices, such as supercapacitors, battery banks, and impacts of electric vehicles charging and discharging on the grid) will also be addressed using the proposed approach to keep the grid operation in normal operating conditions. Finally, the hardware implementation of this proposed controller will be performed using the real-time simulator

CHAPTER 4: MANAGEMENT TECHNIQUE: INTEGRATED TRANSMISSION AND DISTRIBUTION NETWORK OPTIMAL POWER FLOW.

4.1 Introduction

The modernization of the grid involves many resources interplaying at different layers of the grid, most of these resources have gained significant adoption because of their advantages and the need to achieve a clean and sustainable environment. Several enabling policies and technological advancements, including improved performance and reduced costs of computing, connectivity, and communication technologies, are providing the benefits of maximizing the potential of these resources. Renewable energy resources are one of the major devices amongst these resources either as SolarPVs, wind turbines, battery banks, or electric vehicles. Beyond providing power to the immediate resource owners, these resources are capable of supplying power to the grid hereby providing an alternative source of income to the resource owner as well as decarbonizing the grid. The grid is an interconnected system with mainly two networks, the transmission and distribution network, the endpoint electricity consumer is connected to the distribution network, and this where most of the RERs are been connected to the grid, although some resources can be connected to the transmission network based on their capacity. Recent experiences are showing that these resources can have an impact on the transmission network due to their increasing capacity, and penetration levels with the grid. This can affect power quality parameters on the grid such as voltage or the boundary bus of interconnection of the transmission and distribution network. Interconnection of the grid is an established phenomenon and can be easily modeled for two networks that have the same boundary variables, however, their complexity increases when the boundary variables of exchange are different, this is shown in the figure below. Visibility is one of the major challenges utilities are facing with this interconnection, as the transmission network is not visible to the operation of the distribution where most of the renewable energy resources are behind the meter. Despite improved load forecasting models, used in power flow simulations by utilities, the stochastic of renewable energy resources is a major thing to consider these days, especially with the interaction of humans which is difficult to model, or control which might have offered better solutions. In this chapter, we studied the impact of renewable energy resources on the grid and developed a new technique to address some of the challenges that the uncertainty and reverse flow from the distribution network due to renewable energy resources can cause to the grid.

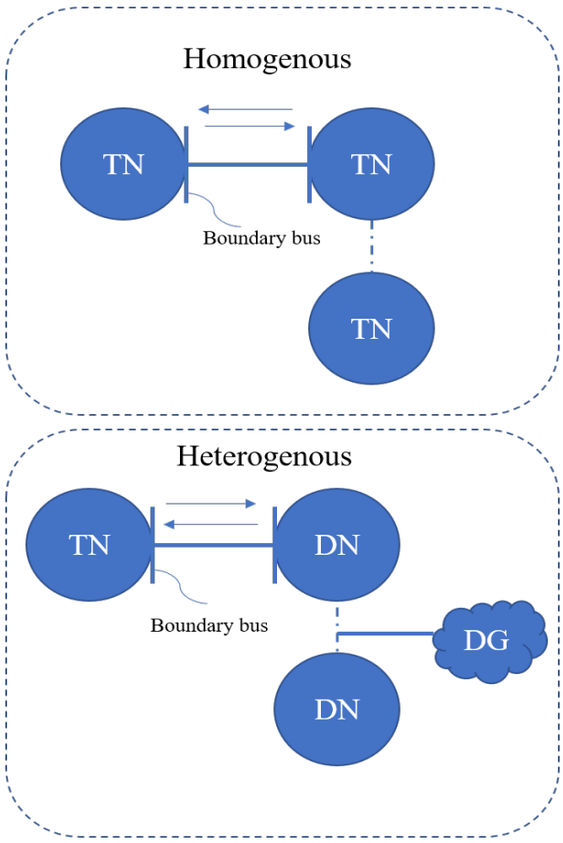

Figure 4.1: Types of the interconnected network with different boundaries

4.2 Integrated Transmission and Distribution Optimal Power Flow Simulation Using Linear Decision Approach

The distribution network include resources transforming the grid into an active network (ADNs)[9],[10] leading to a reverse power flow to the TN, These resources are dynamic, and can lead to a sudden change or transient operation [11] if not well captured in a day ahead forecast due to their nature. Their level of penetration [12] in the grid can have some significant effects which influences key power quality metrics of the grid (voltage, frequency, and many more) during such times of variations. The optimal power flow (OPF) computation can be performed within specified intervals or a day ahead schedule for efficient planning. However, with the recent trends the solution seems not efficient [13] any more due to the increase in the number of resources (distributed generation) [14], inter-playing and controls on the DN. This studies enable us to ensure that the transmission system operator (TSO) and distribution system (DSO) operators are not been almost blind to each other controls or coordination [15], especially during these dynamic operations [16]. Several frameworks including Framework for Network Co-Simulation (FNCS)[131], Integrated Grid Modeling System (IGMS)[132, 132, 133], HELICS [134] have been developed to facilitate T&D simulations. IGMS is a power system modeling platform for integrated T&D analysis through a co-simulation approach. The frameworks have issues of loosely performing the coupling of T&D systems while exchanging the boundary variables once and not intuitively allowing for convergence at every time step.

A lot of research work has been done on the power flow simulations of integrated T&D networks [135], when compared with OPF. For OPF, the objectives of each network may differ, for instance TN objective might be economic dispatch or loss minimization, whereas often times the primal objective of the DN is loss minimization. The benefits of developing a technique for integrated T&D is to efficiently manage the operations of distributed generation in the interconnected network rather than curtail DG [136] to prevent issues such as transformer overloading (TFO), voltage violation,which could have offered benefits like cost minimization and voltage correction. Relaxation techniques is used when solving OPF due to the non-linearity of powerflow equation. In this chapter we used the SDP framework, the method can be deployed as a branch flow method (BFM) mostly used for the DN, or bus injection method (BIM) for TN. The SDP technique operates based on rank solution method, which is exact when there is no duality gap. The SOCP method uses branch flow methods, and performs its relaxation using a cone for the non-linear terms in the constraint [137]. In this chapter we have developed a technique that simulated the integrated T&D OPF, which ensures each network objective is achieved while ensuring the TN networks operate efficiently with reverse power from DN.

4.2.1 Main contribution

The main contribution of this section includes the following:

- An integrated model T&D that considers the interaction of the transmission and distribution, including their control devices and load models.
- A linear decision rule LDR was implemented to help the co-simulation address the heterogeneous relationship between the transmission and distribution system.
- An LDR technique can be used to ensure that DGs are utilized optimally for an economical operation.

4.2.2 Model Description: General model

The integrated T&D has a general model known as master-slave structure [138, 139] as shown in Fig. 4.2. All the devices and components in the TN aside from the boundary bus are referred to as the master system, while all the devices and components in the DN including the boundary bus are referred to as the slave system. The boundary bus is the interconnecting bus between both networks, since, the variables exchanged at the boundary are different the integrated network can be referred to as a heterogeneous network. The model that involves independent transmission OPF and independent distribution OPF is known as the TDOPF. The objective functions is (1), operational constraints for TN are in (2), (3), (5) and for DN are in (6), (7). The boundary bus power flows are in (8), (9), and

(10).

$$Objfunction : min \quad C_M(U^M, U^B, X^M, X^B) + C_S(U_S, X_B, X_S) \tag{4.1}$$

subject to

$$f_M(U^M, X^M, X^B) = 0 \tag{4.2}$$

$$g_M(U^M, X^M, X^B) \geq 0 \tag{4.3}$$

$$f_B(U^B, X^S, X^M X^B) = 0 \tag{4.4}$$

$$g_B(U^B, X^B) \geq 0 \tag{4.5}$$

$$f_S(U^S, X^B, X^S) = 0 \tag{4.6}$$

$$g_S(U^S, X^B, X^S) \geq 0 \tag{4.7}$$

Boundary bus power balance

$$P^B + f_{pMB}(X^M, X^B) = f_{pBS}(X^B, X^S) \tag{4.8}$$

$$f_{MB}(U^B, X^M, X^B) = y^{BS} \tag{4.9}$$

$$y^{BS} = f_{BS}(X^B, X^S) \tag{4.10}$$

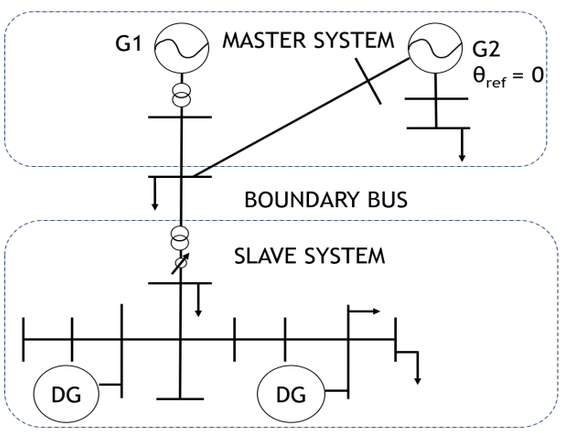

Figure 4.2: Integrated $T\&D$ model with master-slave approach

U represents vector of the control variables, for instance the active and reactive power control from devices such as generators, voltage regulators, shunt capacitor, **X** is the vector of state variables which is voltage magnitude and angles. where **f** is the equality constraints such as power flow and the **g** is the inequality constraints that establishes network constraints such as bus voltages and line flows.

At PCC, the voltage of the transmission (boundary) bus is the feeder voltage (magnitude

and angle) for the distribution network u_0^{abc}

$$u_0^{abc} = V_{pcc}^{abc} \tag{4.11}$$

The TDOPF optimality conditions can be rewritten using the Lagrangian multiplier.

$$A = -\lambda_M^T f_M - w_M^T f_M - w_M^T g_M - \lambda_{MB}^T (f_{MB} - y^{BS}) \tag{4.12}$$

$$B = c_M + c_s - w_B^T g_B - \lambda_S^T f_S - w_S^T g_S - \lambda_{BS}^T (y_{BS} - f^{BS}) \tag{4.13}$$

$$L = A + B \tag{4.14}$$

4.2.3 Transmission Network OPF model

The technique used for solving the transmission network OPF is a bus injection method [140]. The objective of the OPF is to reduce the cost of generation and minimize losses. The one-line representation of the transmission network is shown Fig. 4.3.

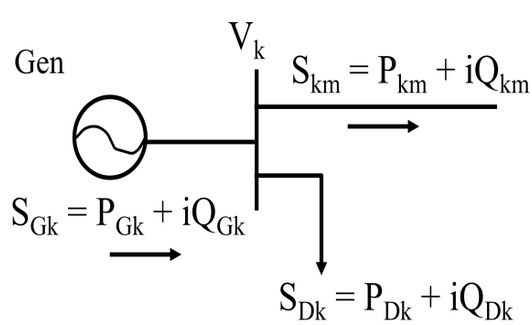

Figure 4.3: Transmission network - One line

The Non - Convex AC OPF equations are below

$$min \quad f_k(P_{G_K}) = c_{k2} P_{G_k}^2 + c_{k1} P_{G_k} + c_{k0} \tag{4.15}$$

The constraints are below

$$Powerbalance : S_{G_K} - S_{D_K} = diag(\bar{V_k}) \bar{Y}_{kbus}^{*} \bar{V_k}^{*} \tag{4.16}$$

$$Lineflow : \bar{Y}_{kline} \bar{V_k} \leq Iline, max \tag{4.17}$$

$$Apparentflow : Q_k \bar{V_k} \leq Iline, max \tag{4.18}$$

$$GenActivePower : P_k^{min} \leq P_{G_k} \leq P_k^{max} \tag{4.19}$$

$$GenReactivePower : Q_k^{min} \leq Q_{G_k} \leq Q_k^{max} \tag{4.20}$$

$$Voltagelimits : V_k^{min} \leq V_k \leq V_k^{max} \tag{4.21}$$

The equations are then re-written with SDP relaxation.

$$\sum_{k\epsilon G} C_{k2}(TrY_kW + P_{D_k})^2 + C_{k1}(TrY_kW + P_{D_k}) + C_{k0} \tag{4.22}$$

The constraints are below

$$P_k^{min} \leq TrY_kW \leq P_k^{max} \tag{4.23}$$

$$Q_k^{min} \leq Tr\bar{Y}_kW \leq Q_k^{max} \tag{4.24}$$

$$(V_k^{min})^2 \leq TrM_kW \leq (V_k^{max})^2 \tag{4.25}$$

$$-P_{lm}^{max} \leq TrY_{lm}W \leq P_{lm}^{max} \tag{4.26}$$

$$TrY_{lm}W^2 + Tr\bar{Y}_{lm}W^2 \leq (S_{lm}^{max})^2 \tag{4.27}$$

$$\tag{4.28}$$

The auxiliary variables used in the equations above are obtained as follows

$$Y_{lm} = (\bar{y}_{lm} + y_{lm})e_l e_l^T - (y_{lm})e_l e_m^T \tag{4.29}$$

$$Y_k = e_k e_k^T Y \tag{4.30}$$

$$Y_k = \frac{1}{2}\begin{bmatrix} R_e(Y_k + Y_k^T) & I_m(Y_k^T - Y_k) \\ I_m(Y_k - Y_k^T) & R_e(Y_k + Y_k^T) \end{bmatrix} \tag{4.31}$$

$$Y_{lm} = \frac{1}{2}\begin{bmatrix} R_e(Y_{lm} + Y_{lm}^T) & I_m(Y_{lm}^T - Y_{lm}) \\ I_m(Y_{lm} - Y_{lm}^T) & R_e(Y_k + Y_k^T) \end{bmatrix} \tag{4.32}$$

$$\bar{Y_k} = \frac{-1}{2}\begin{bmatrix} I_m(Y_k + Y_k^T) & R_e(Y_k - Y_k^T) \\ R_e(Y_k^T - Y_k) & I_m(Y_k + Y_k^T) \end{bmatrix} \tag{4.33}$$

$$M_k = \begin{bmatrix} e_k e_k^T & 0 \\ 0 & e_k e_k^T \end{bmatrix} \tag{4.34}$$

Applying the Schur's complement

$$\begin{bmatrix} c_{k1}T_r(Y_kW) - \alpha_k + a_k & \sqrt{c_{k2}}T_r(Y_kW) + b_k \\ \sqrt{c_{k2}}T_r(Y_kW) + b_k & -1 \end{bmatrix} \leq 0 \tag{4.35}$$

Such that a_k = c_{k0} + $c_{k1}P_{D_k}$ b_k = $\sqrt{c}$_k2P_D_k

Algorithm 3: Transmission network BIM-SDP OPF

```
-
Determine the total number of buses n_b and branches n_br in the network
Identify all the devices in the network (Generators, transformers)
Initialize all the sdpvar variables (l_ij,u_i,S_ij)
Develop a Ybus of the network and find the auxiliary variables using system
  parameters.
for x = 1 : n_b do
    if if x is a bus,then then
        Formulate the bus constraint using the equation 9&10.
    else
        if if branch x is a voltage regulator, then then
            Formulate the branch constraint using the equation 23
        end
    end
end
Solve the BIM SDP OPF using MOSEK solver.
for x = 1 : n_br do
    if if rank = 1 ,then then
        W is positive semi-definite.
    else
        if if rank > 1, then then
            W is not a positive semi-definite.
        end
    end
end
```

4.2.4 Distribution Network OPF model

SDP branch flow method (BFM) [141] was used for simulation analysis at the DN, with the OPF objective being loss minimization. The formulation accommodates different numbers of bus-phases in the network and the interconnection and the representation of the network as one line is shown in the figure 4.4 below.

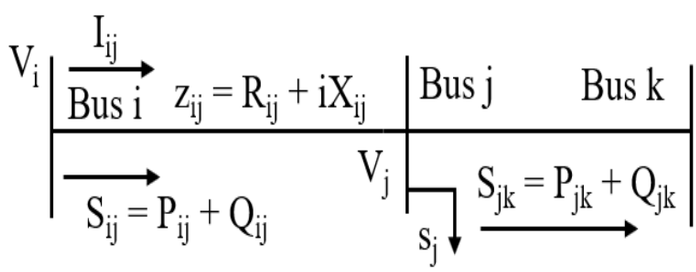

Figure 4.4: Distribution network- One line

$$V_i = [V_i^a, V_i^b, V_i^c]^T \tag{4.36}$$

$$V_j = [V_j^a, V_j^b, V_j^c]^T \tag{4.37}$$

The assumption is that bus i and j both have 3-phases which might not be in some cases.

$$Minimize \sum real(z_{ij} l_{ij}) \tag{4.38}$$

$$\sum diag(S_{ij} - z_{ij} l_{ij}) + s_j + y_j u_j = \sum diag(S_{jk})^{\phi_j} \tag{4.39}$$

$$u_j = u_i^{\phi_{ij}} - (S_{ij} z_{ij}^H + S_{ij}^H z_{ij}) + z_{ij} l_{ij} z_{ij}^H \tag{4.40}$$

$$u_i <= diag(u_i) <= u_i \tag{4.41}$$

$$u_0 = V_0^{ref} (V_0^{ref})^H \tag{4.42}$$

Positive semidefinite (PSD) constraint

$$\begin{bmatrix} u_i^{\theta_{ij}} & S_{ij} \\ S_{ij}^H & l_{ij} \end{bmatrix} \geq 0 \tag{4.43}$$

PSD is set to be equal to 1.

4.2.5 Co-Simulation using Integrated optimization engine(IOE) with LDR

The proposed approach ensures integrated T&D network operates efficiently, the transmission network readjusts itself to the total power consumed at the distribution network and there is no need or curtailment of DG. The TOPF is therefore re-written to accommodate for the changing dynamics in the distribution network leading to the reverse power flow in the transmission network, **k** is a constant, which is power from DG and undispatchable. The equation is written below

$$TOPF = min \quad C_M(U^M, U^B, X^M, X^B, K_{DG}^S) \tag{4.44}$$

The objectives of each of the networks are written below

$$TOPF = min \quad (a_k(P_{Gk}^2) + b_k(P_{Gk}) + C_k) \tag{4.45}$$

$$DOPF = min \quad Re(S_{ij} - Z_{ij} I_{ij}^2) \tag{4.46}$$

The active power from the generators is a combination of loads P_D, the losses P_{loss} in the

Algorithm 4: Distribution network BFM-SDP OPF

```
-
Determine the total number of buses n_b and branches n_br in the network
Identify all the devices in the network (Generators, regulators, transformers)
Determine the total number of phases in each branch and buses in the network
Develop a Ybus of the network based on the parameters
Initialize all the sdpvar variables (l_ij,u_i,S_ij)
for x = 1 : n_br do
    if if branch x is a line, then then
        Formulate the branch constraint using the equation 23.
    else
        if if branch x is a voltage regulator, then then
            Formulate the branch constraint using the equation 23
        end
    end
end
for x = 1 : n_b do
    Formulate the bus constraint using the equation 23
    formulate other boundary constraints
end
Solve the BFM SDP OPF using MOSEK solver.
for x = 1 : n_br do
    if if equation 27 is satisfied, then then
        The solution is local optimum.
    else
        if if equation 28 is satisfied, then then
            global optimum is the solution.
        end
    end
end
```

Algorithm 5: Steps for Integrated Optimization engine

```
Initialize the interconnected network by setting the system parameters for
computation
while tol > ϵ do
    forall t ∈ TN do
        solve the transmission network OPF.
        obtain the system parameters. (Voltage and angle)
        Check if power quality parameters are violated
        if yes, apply LDR. Use the parameters as setpoints for the DN feeder at PCC
    end
    forall d ∈ DN do
        solve the distribution network OPF.
        obtain the total load demand with losses at the distribution network
        update the load at PCC of the T&D network.
    end
    Obtain the new tolerance error using equation 23
    Check for convergence.
end
end
```

transmission network, and the reverse active power P_{RP}

$$\sum_{k=1}^{n_b} P_{Gk} = \sum_{k=1}^{n_b} P_{k,D}^{M} + \sum_{k=1}^{n_{br}} P_{km}^{M} + \sum_{k=1}^{n_{br}} P_{km,loss}^{M} - \sum_{k=1}^{n_b} P_{k,RP}^{M} \tag{4.47}$$

The reverse power flow into the TN is obtained as thus.

$$S^{M}_{k,RP} = S_S - S_{PV} \tag{4.48}$$

$$P^{M}_{k,RP} = Re(S^{M}_{k,RP}) \tag{4.49}$$

$$Initialization : S^{M(0)}_{B} = S^{load}_{S} \tag{4.50}$$

$$V^{abc}_{pcc} = u^{abc}_{0} \tag{4.51}$$

$$Minimize \quad \Delta S^{e}_{B} = S^{M(0)}_{B} - S_S \tag{4.52}$$

$$S_S = S^{load}_{S} + S^{losses}_{S} - S_{PV} \tag{4.53}$$

$$S_M = S^{G}_{M} + S^{load}_{M} + S^{losses}_{M} \tag{4.54}$$

The model of the solar PV is below

$$S^2_{PV} = P^2_{PV} + Q^2_{PV} \tag{4.55}$$

A linear decision rule is used to provide the TN insights into the DN. Several analysis was obtain to establish the relationship between TN generators and DN solar PVs as written in the form below. The general implementation of the Linear decision rule.

$$Y = a + bX \tag{4.56}$$

where Y is the P_{PG} active power from the generators in the transmission system, X is the P_{PV} active power generated by the solar PVs.

$$Gen(i) : \quad P_{G(i)} = a + bP_{PV} \tag{4.57}$$

Where i is the generator number.

4.2.6 OPF Remarks

The detailed proof of the global optimality and the exactness of the SDP-OPF model in transmission network is discussed in this section.

$$P_{injk} = X^T Y_k X \tag{4.58}$$

$$P_{injk} = T_r[X^T Y_k X] \tag{4.59}$$

Applying the trace operator multiplicity property

$$P_{injk} = T_r[Y_k X X^T] \tag{4.60}$$

Introducing the W matrix

$$W = [X X^T] \tag{4.61}$$

for equ (12) the unit operator K_{th} basis vector was implemented.

$$e_k e_k^T = 1 \tag{4.62}$$

The W matrix can be decomposed into the following

$$W = [R\{V\}I\{V\}]^T[R\{V\}I\{V\}] \tag{4.63}$$

$$W = XX^T \tag{4.64}$$

This approach works for rank(W) = 1 and 2 only.

For rank(W)=2, eigen decomposition using Molzahn approach.

$$W_{opt} = \rho_1 E_1 E_1^T + \rho_2 E_2 E_2^T \tag{4.65}$$

$$X_{opt} = \sqrt{\rho_1^{opt}} E_1^{opt} + \sqrt{\rho_2^{opt}} E_2^{opt} \tag{4.66}$$

Where E_1 and E_2 are Eigenvectors, and $\rho\_1, \rho\_2 are the first and second large stabsolute eigenvalue of W.$

Finally, we applied Schur's complement, which is used to transform polynomial constraints into quadratic constraints and that the semi-definite constraints equal quadratic constraints. Such that H $\in S^n$

$$H = \begin{bmatrix} X & Y \\ Y^T & P \end{bmatrix} \tag{4.67}$$

$$S = P - Y^T X^{-1} Y \tag{4.68}$$

The Schur complement of X in H

- H > 0 if and only if X > 0 and S > 0
- X > 0 then H ≥ 0 and S ≥ 0

The apparent branch flow constraint equations (10e)

$$\begin{bmatrix} -(\bar{S}l_m)^2 & T_r(Yl_mW) & T_r(\bar{Y}l_mW) \\ T_r(Yl_mW) & -1 & 0 \\ T_r(\bar{Y}l_mW) & 0 & -1 \end{bmatrix} \leq 0 \tag{4.69}$$

Applying the multiplicity trace operator

$$T_r(Yl_mW) = (-1)T_r(Yl_mW) \tag{4.70}$$

$$\begin{bmatrix} \bar{S}l_m^2 & T_r(Yl_mW) & T_r(\bar{Y}l_mW) \\ T_r(Yl_mW) & 1 & 0 \\ T_r(\bar{Y}l_mW) & 0 & 1 \end{bmatrix} \geq 0 \tag{4.71}$$

Comparing this with equation (50)

$$\begin{bmatrix} 1 - \frac{T_r(Yl_mW)^2}{Sl_m^2} & \frac{T_r(\bar{Y}l_mW)T_r(Yl_mW)}{Sl_m^2} \\ \frac{T_r(\bar{Y}l_mW)T_r(Yl_mW)}{Sl_m^2} & 1 - \frac{T_r(Yl_mW)^2}{Sl_m^2} \end{bmatrix} \geq 0 \tag{4.72}$$

$$\bar{S}l_m^2 - T_r\{Yl_mW^2\} - T_r\{Yl_mW^2\} \geq 0 \tag{4.73}$$

4.2.7 Discussion and Performance Evaluation

Our approach was tested on the interconnection of IEEE 9bus and IEEE 13bus as shown in the Fig. 4.5. The results were first benched-marked with IEEE test cases simulation MATPOWER results. To increase the penetration level of the solarPV in DN to TN, the system was modified such that 20 times the base load values of the DN was connected to the TN. As seen in the integrated system inFig. 4.5 the boundary bus is bus 4. A base case simulation was done, after which the system was tested with different penetration levels.

The LDR relationship between each of the generators on the TN and the solar PV's

$$Gen(1): \quad P_{G(1)} = 89.80 - 0.45 * P_{PV} \tag{4.74}$$

$$Gen(2): \quad P_{G(2)} = 134.32 - 0.07 * P_{PV} \tag{4.75}$$

$$Gen(3): \quad P_{G(3)} = 94.19 - 0.25 * P_{PV} \tag{4.76}$$

4.2.7.1 Case 1

In this scenario, the penetration level of the solarPVs with respect to the DN was 25%, the simulation was performed on different irradiance levels of 0.5p.u, 0.9p.u and 1.0p.u respectively,this enables us to see how the TN parameters was influenced by the solar PV. The impacts was observed on the grid voltages and the cost of power generation.

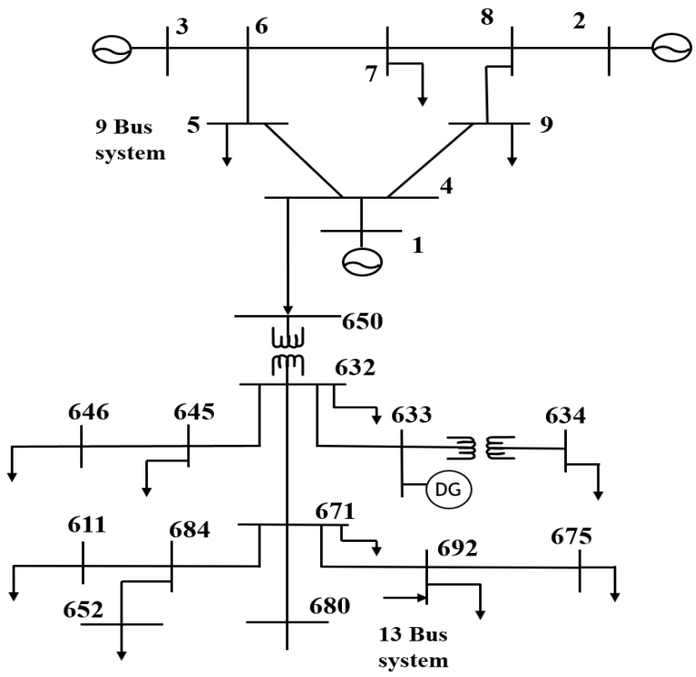

Figure 4.5: Integrated T&D model for IEEE 9bus and IEEE 13bus

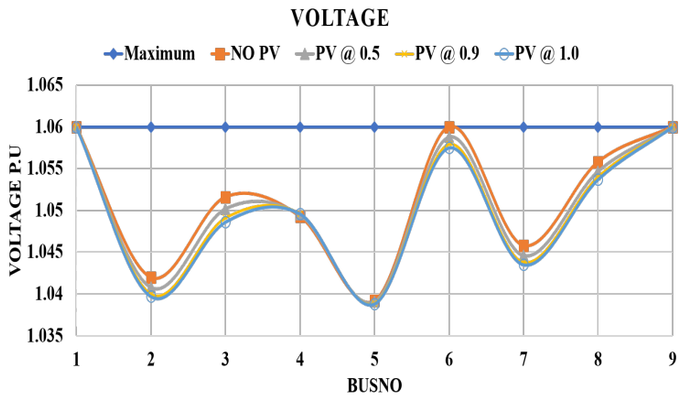

Figure 4.6: Case A: 25% penetration level

4.2.7.2 Case 2

The penetration level of the solarPVs with respect to the DN was 60%, the simulation was performed on the same irradiance levels in case 1, this enables us to see how the TN parameters was influenced by the solar PV. The impacts was observed on the grid voltages and the cost of power generation

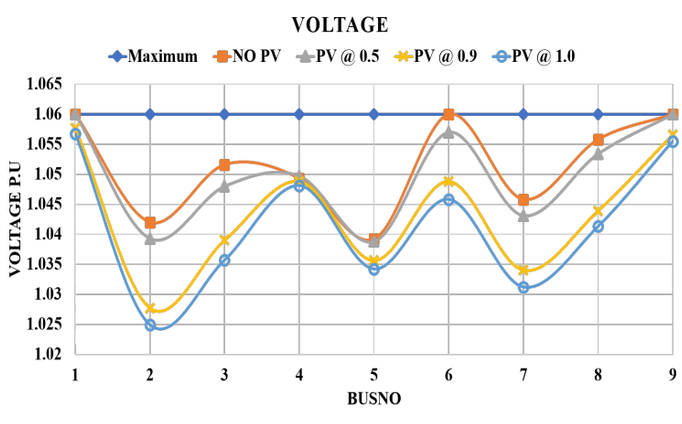

Figure 4.7: Case B: 60% penetration level

4.2.7.3 Case 3

In this scenario, the penetration level of the solarPVs with respect to the DN was 80%, the simulation was performed on the same irradiance levels in case 1, It was seen that at a higher penetration level of 80% and increased irradiance level to 1.0, the voltage was closer to the nominal value of 1.0 p,u, and the cost of generation reduced significantly in case B and case C. As compared with 25% penetration level and 1.0p.u irradiance level, cost of generation dropped from 3,790 $/MWh to 3153 $/MWh as well as the bus with worse voltage from 1.575p.u to 1.044p.u. The minimum deviation is at 80% penetration at bus 2, while the maximum is at 25% penetration at bus 6. Please refer to Figs. 4.6, 4.7, 4.8.

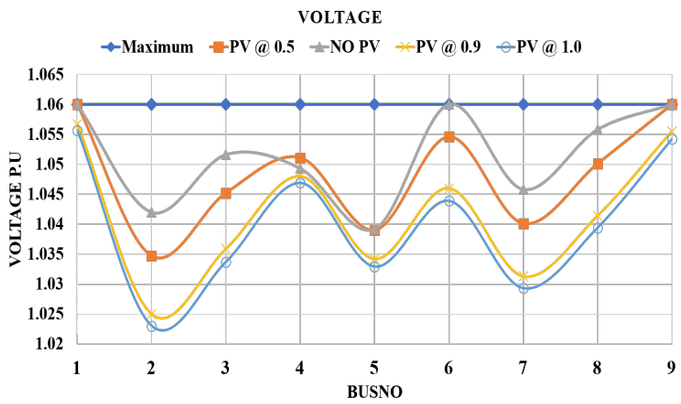

Figure 4.8: Case C: 80% penetration level

TABLE 4.1: Parameters Comparison with different PV penetration Levels

Penetration	Irradiance level	Solar PVs Power Flow(MW)	Generation Cost($/MWh)
25%	0.5	8.33	4.027
	0.9	14.50	3.901
	1.0	16.66	3.857
60%	0.5	20.00	3.790
	0.9	38.00	3.446
	1.0	50.00	3.229
80%	0.5	27.21	3.649
	0.9	48.96	3.248
	1.0	54.40	3.153

4.3 Stochastic Optimization of Integrated Transmission and Distribution Network Considering Distributed Generation With Uncertainties

The electricity grid value chain from generation to consumption has two networks, these networks Transmission network (TN) and distribution network (DN) are physically coupled together. To meet the growing need for a sustainable environment and address global climate change challenges, policies are calling for more renewable energy resources to be connected to the grid and used as sources of energy. RERs also offer numerous advantages to the grid and to the utilities [142],[143]. The democratization of these resources makes it permissible

TABLE 4.2: Voltage Comparison with different PV penetration Levels

Penetration	Bus No	Voltage level no Solar PVs	Voltage level Irrad 1.0 p.u	% Deviation from 1.0 p.u
25%	2	1.042	1.039	3.9%
	3	1.052	1.048	4.8%
	6	1.060	1.058	5.8%
	7	1.046	1.044	4.4%
	8	1.056	1.054	5.4%
60%	2	1.042	1.025	2.5%
	3	1.052	1.036	3.6%
	6	1.039	1.034	3.4%
	7	1.046	1.031	3.1%
	8	1.056	1.042	4.2%
80%	2	1.042	1.023	2.3%
	3	1.052	1.034	3.4%
	6	1.060	1.044	4.4%
	7	1.046	1.029	2.9%
	8	1.056	1.039	3.9%

TABLE 4.3: Boundary Bus mismatch voltage deviation

Parameter	Scenario 1	Scenario 2	Scenario 3
Reverse Power Flow (MW)	0	10.57	17.50
Voltage at PCC with LDR(p.u)	1.041	1.029	1.049
Voltage at PCC without LDR(p.u)	1.041	1.051	1.065

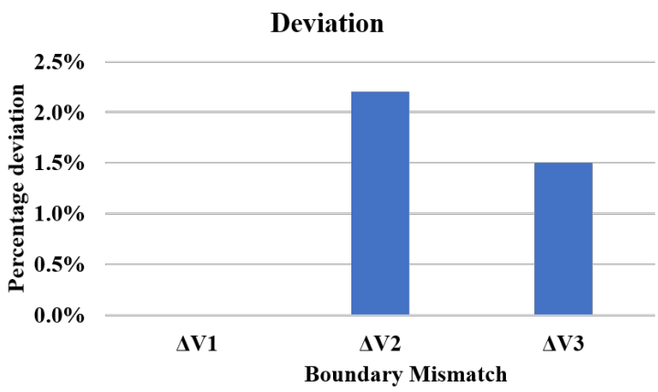

Figure 4.9: Boundary bus mismatch reduction with LDR

for them to be integrated at different layers of the network i.e. either at the customer side or utility scale. On a wider scale based on the number of resources, most RERs are connected to the distribution network and this integration is transforming the grid into an active network (ADNs),[10], [144]. ADNs often causes reverse power flow to the TN. RERs are dynamic, despite planning using accurate forecasts they are still susceptible to a sudden change [11], [145], due to their intermittent nature.

This stochasticity in operations in large-scale couple T&D networks can cause boundary mismatches and impact the security analysis performed by the distribution system operator. Additionally, when a sudden change occurs based on their penetration level with regards to

the integrated grid [146], [147] some significant power quality metrics of the grid[148] can be affected such as grid frequency, harmonics, voltages, and many more. The simulation for the grid network's optimal power flow (OPF) performed at defined time intervals during the day or a day ahead condition for efficient planning. RERs are also a major factor when considering the tightness of this simulation due to their stochastic nature as increasing the number of resources (distributed generation) [14], inter-playing with several controls on the DN, these ultimately calls for more automation devices, There is always a need for network reconfiguration that is dependent on the root node complex voltages, which despite being estimated with phasor measurements units (PMU) can be prone to errors due to the opening and closing loop if the characteristics of the transmission network aren't properly considered. For example, it is reported that the high penetration of DGs in California will create difficulties for TSO due to their separate management structure. An incident in 2011 Arizona southern California outage event, was reported by the Federal Electricity Regulatory Commission (FERC) and North America Electric Reliability (NERC) as an occurrence due to a lack of coordination between TSO and DSO. Therefore the need for studies to enable us to ensure that the TSO and DSO are not almost blind to each other controls or coordination [15], especially during these dynamic operations. Thus a coordination between TN and DN has become mandatory in current grid operation. Current tools that perform the coordination demonstrated by various entitites [149] such as Hierarchical Engine for Large-scale Infrastructure Co-Simulation (HELICS), Framework for Network Co-Simulation (FNCS), Integrated Grid Modeling System (IGMS)[132], and GridSpice[150] are either not performing TN and DN in real-time and/or optimized together.

Power flow simulations of integrated T&D networks [151] have been extensively studied, when compared with OPF. However, for OPF [152], each network has different objectives set by utilities. DN networks are widely known to have an objective of loss minimization while TN objective might be cost efficiency coupled with loss minimization. The challenge RERs cause due to their stochastic nature is not allowing utilities to maximize their benefits, as the utility tries to account for scenarios such as transformer overloading (TFO), and voltage violation, the current technique has been used is the curtailment of distributed generation [136] to prevent such occurrences. The intermittent nature of RERs which makes them uncertain requires stochastic optimization [153], and the integrated T&D are a two-stage stochastic program due to the power generated by the RERs and generators in TN. It has been proven that for a feasible variable of reverse power flow, the generator power output can be determined using a linear decision rule[154],[155].

In this section, focus was on the maximum allowable reverse power flow from the DN into the TN, which indicates that power is exchanged over the distribution transformer in

a bidirectional manner. AC Power flow equations are non-linear [156], [157] hence the need for relaxation techniques to obtain a feasible solution. Amongst the different relaxation techniques, SDP framework is used [158]. Specifically, for the distribution network we used the SDP branch flow method (BFM), while for the transmission network, we used the SDP bus injection method (BIM). Another known relaxation technique is the SOCP method which uses branch flow methods and performs its relaxation using a cone for the non-linear terms in the constraint [137]. The SDP technique operates based on the rank solution method, the solution is feasible and exact when there is no duality gap. For integrating TN and DN, a stochastic linear optimization is implemented in an integrated optimization engine that performs the objective of each network and has its own objective of minimizing boundary errors. The linear optimization constraint (LDR) is used as an additional constraint to ensure that the uncertainties with RERs are managed especially reverse power flow from the distribution network to the transmission network

4.3.1 Main contributions

The main contributions of SILP with state-of-the-art include:

- An optimization technique that co-simulates integrated T&D with heterogeneous boundary variables and ensures each network objective is achieved.
- A technique that handles the boundary variables impact of integrated transmission and distribution network due to uncertainties by RERs.
- The technique is based on stochastic linear optimization which uses a complete recourse formulation to develop the constraint.
- A management approach that uses the linear decision rule constraints to provide the transmission network and its resources insights into the distribution network operations.

As compared to our work in the previous section, the main advantages of this section includes the following:

- The theorem proof for stochastic linear optimization used for the integrated T&D co-simulation is discussed.
- Unlike our previous work that considered only the voltage profile deviation in the TN, the technique handled the voltage profile deviation in the TN and the boundary bus voltage violation during reverse power flow into the TN.
- The impacts of RERs curtailment and no curtailment on the integrated T&D network with and without our developed technique is discussed.

- The stochastic linear optimization proposed is able to handle larger networks of integrated T&D models.

4.3.2 Overview of existing model

Presently grid-coupled networks have two major entities controlling their operations using effective management and co-ordination strategies. The transmission system operator(TSO) coordinates the TN while the distribution system operator coordinates the DN, The integrated T&D has a general model known as master-slave structure [138,139] as shown in Fig. 4.10 and the system is referred to as an heterogeneous network since the boundary variables exchanged are different otherwise it would have been a homogeneous network. The master system is a collection of all the devices and components existing in the transmission network aside from the boundary bus. On the other hand, the slave system comprises devices and components interplaying in the distribution network. The point of common coupling (PCC) is the bus of interconnection of the transmission network and the feeder head bus of the distribution network, this bus is referred to as the boundary bus. The two variables exchanges include voltages for the DN feeder and total power demand by the DN. A general representation of independent transmission OPF and independent distribution OPF is known as the TDOPF [138], the model has an objective function as shown in (4.77), operational constraints for TN are in (4.78), (4.79), (4.81), and for DN are in, (4.80), (4.82), and (4.83) respectively. The boundary bus power flows are in (4.84), (4.85), and (4.86).

$$min \sum \quad c_M(U^M, U^B, X^M, X^B) + c_S(U_S, X_B, X_S) \tag{4.77}$$

subject to

$$f_M(U^M, X^M, X^B) = 0 \tag{4.78}$$

$$g_M(U^M, X^M, X^B) \geq 0 \tag{4.79}$$

$$f_B(U^B, X^S, X^M X^B) = 0 \tag{4.80}$$

$$g_B(U^B, X^B) \geq 0 \tag{4.81}$$

$$f_S(U^S, X^B, X^S) = 0 \tag{4.82}$$

$$g_S(U^S, X^B, X^S) \geq 0 \tag{4.83}$$

$$P^B + f_{pMB}(X^M, X^B) = f_{pBS}(X^B, X^S) \tag{4.84}$$

$$f_{MB}(U^B, X^M, X^B) = y^{BS} \tag{4.85}$$

$$y^{BS} = f_{BS}(X^B, X^S) \tag{4.86}$$

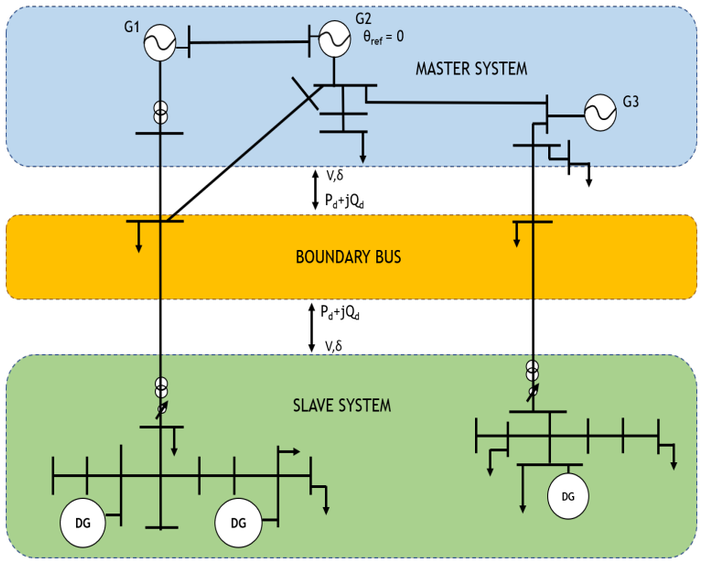

Figure 4.10: Schematic diagram of an integrated $T\&D$ system.

The TDOPF network comprises a vector of control **U** and state **X** variables. The controlled devices are generators, voltage regulators, and shunt capacitors whose active and reactive power can be controlled, while the states are voltage magnitude and angle. **f(*)** is the equality constraints such as power flow and the **g(*)** is the inequality constraints that establish network constraints such as bus voltages and line flows. The optimality condition for the independent model using Lagrangian multiplier is shown in (4.87).

$$A = -\lambda_M^T f_M - w_M^T f_M - w_M^T g_M - \lambda_{MB}^T (f_{MB} - y^{BS}) \tag{4.87}$$

$$B = c_M + c_s - w_B^T g_B - \lambda_S^T f_S - w_S^T g_S - \lambda_{BS}^T (y_{BS} - f^{BS}) \tag{4.88}$$

$$L = A + B \tag{4.89}$$

At the bus of interconnection, the transmission (boundary) bus voltage is the feeder voltage (magnitude) for the distribution network u_0^{abc}

$$u_0^{abc} = V_k^B \tag{4.90}$$

4.3.3 Transmission Network

The technique used for solving the transmission network OPF is SDP bus injection method (BIM) [140], with the representation diagram shown in Fig. 4.11 . The objective of the OPF is to reduce the cost of generation. In a given network graph $\mathcal{G}$ =($\mathcal{N}$, $\mathcal{E}$), where $\mathcal{N}$ is the number of nodes in the network such that k $\in \mathcal{N}$ is the node in the network, $\mathcal{E}$ represents the branches in the network connecting an ordered pair of buses (k, m), addition $\mathcal{L}$ is used for scenarios where the branches are duplicated, i.e. $(k, m) \in \mathcal{E}$ = (m,k),(k,m) $\in \mathcal{L}$. The admittance for the node k is Y_k.

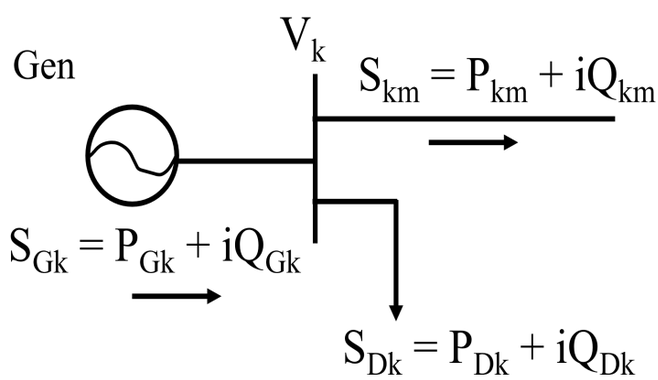

Figure 4.11: One line diagram of the transmission network.

The non-convex AC OPF equations can be represented as

$$min \quad c^T P_G c^T P_G = c_{k2} P_{G_k}^2 + c_{k1} P_{G_k} + c_{k0} \tag{4.91}$$

subject to

$$S_{G_K} - S_{D_K} = diag(\bar{V_k}) \bar{Y}_{kbus}^{*} \bar{V}_k^{*} \tag{4.92}$$

$$\bar{Y}_{km} \bar{V}_k \leq I_{km,max} \tag{4.93}$$

$$\bar{V}_k \bar{Y}_{km} \bar{V}_k^{*} \leq S_{km,max} \tag{4.94}$$

$$0 \leq P_{G_k} \leq P_k^{max} \tag{4.95}$$

$$Q_k^{min} \leq Q_{G_k} \leq Q_k^{max} \tag{4.96}$$

$$V_k^{min} \leq V_k \leq V_k^{max} \tag{4.97}$$

Rewriting (4.91) and (4.92)-(4.97) using SDP formulation gives

$$\sum_{k \epsilon G} C_{k2} (Tr Y_k W + P_{D_k})^2 + C_{k1} (Tr Y_k W + P_{D_k}) + C_{k0} \tag{4.98}$$

subject to

$$P_k^{min} \leq TrY_kW \leq P_k^{max} \tag{4.99}$$

$$Q_k^{min} \leq Tr\bar{Y}_kW \leq Q_k^{max} \tag{4.100}$$

$$(V_k^{min})^2 \leq TrM_kW \leq (V_k^{max})^2 \tag{4.101}$$

$$-P_{lm}^{max} \leq TrY_{lm}W \leq P_{lm}^{max} \tag{4.102}$$

$$TrY_{lm}W^2 + Tr\bar{Y}_{lm}W^2 \leq (S_{lm}^{max})^2 \tag{4.103}$$

Obtaining the auxiliary variables $Y_{lm}$and Y_k using the following

$$Y_{lm} = (\bar{y}_{lm} + y_{lm})e_l e_l^T - (y_{lm})e_l e_m^T \tag{4.104}$$

$$Y_k = e_k e_k^T Y \tag{4.105}$$

$$Y_k = \frac{1}{2}\begin{bmatrix} R_e(Y_k + Y_k^T) & I_m(Y_k^T - Y_k) \\ I_m(Y_k - Y_k^T) & R_e(Y_k + Y_k^T) \end{bmatrix} \tag{4.106}$$

$$Y_{lm} = \frac{1}{2}\begin{bmatrix} R_e(Y_{lm} + Y_{lm}^T) & I_m(Y_{lm}^T - Y_{lm}) \\ I_m(Y_{lm} - Y_{lm}^T) & R_e(Y_k + Y_k^T) \end{bmatrix} \tag{4.107}$$

$$\bar{Y}_k = \frac{-1}{2}\begin{bmatrix} I_m(Y_k + Y_k^T) & R_e(Y_k - Y_k^T) \\ R_e(Y_k^T - Y_k) & I_m(Y_k + Y_k^T) \end{bmatrix} \tag{4.108}$$

$$M_k = \begin{bmatrix} e_k e_k^T & 0 \\ 0 & e_k e_k^T \end{bmatrix} \tag{4.109}$$

Finally, applying the Schur's complement

$$\begin{bmatrix} c_{k1}T_r(Y_kW) - \alpha_k + a_k & \sqrt{c_{k2}}T_r(Y_kW) + b_k \\ \sqrt{c_{k2}}T_r(Y_kW) + b_k & -1 \end{bmatrix} \leq 0 \tag{4.110}$$

such that

$$a_k = c_{k0} + c_{k1}P_{D_k} \tag{4.111}$$

$$b_k = \sqrt{c_{k2}}P_{D_k} \tag{4.112}$$

4.3.4 Distribution Network

The distribution network optimal power flow is modeled using SDP branch flow method (BFM) [141] relaxation technique, with the representation diagram shown in Fig. 4.12 and the objective is to minimize the overall loss in the distribution system. The formulation

accommodates for different number of bus-phases in the network and the interconnection. In a given network graph $\mathcal{G}$ =($\mathcal{N}$, $\mathcal{E}$), where $\mathcal{N}$ is the number of nodes in the network such that $i \in \mathcal{N}$, $j \in \mathcal{N}$ are the nodes in the network, $\mathcal{E}$ represents the branches in the network connecting an ordered pair of buses (i, j), addition $\mathcal{L}$ is used for scenarios where the branches are duplicated, i.e. $(i, j) \in \mathcal{E} = (j, i), (i, j) \in \mathcal{L}$. The line admittance y_{ij}=g_{ij} + jb_{ij}, (i, j) $\in \mathcal{L}$. The apparent power and current flowing from bus $i \in \mathcal{N}$ to $j \in \mathcal{N}$ is S_{ij} and I_{ij} respectively. Other representations used for second-order decision variables are $u_i = V_i V_i^H$, $l_{ij} = I_{ij} I_{ij}^H$, where Φ_{ij} is the set of phases of the line ij, H is the hermitian transpose. The details are presented using Fig. 4.12.

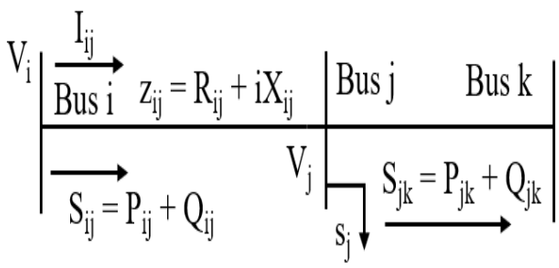

Figure 4.12: One line diagram of the distribution network

$$V_i = [V_i^a, V_i^b, V_i^c]^T V_j = [V_j^a, V_j^b, V_j^c]^T \tag{4.113}$$

The assumption is that bus i and j both have 3-phases which might not be in some cases.

$$min \sum real(z_{ij} l_{ij}) \tag{4.114}$$

$$\sum_{i:i\rightarrow\ j} diag(S_{ij} - z_{ij} l_{ij}) + s_j + y_j u_j = \sum_{k:j\rightarrow\ k} diag(S_{jk})^{\phi_j} \tag{4.115}$$

$$u_j = u_i^{\phi_{ij}} - (S_{ij} z_{ij}^H + S_{ij}^H z_{ij}) + z_{ij} l_{ij} z_{ij}^H \tag{4.116}$$

$$u_i <= diag(u_i) <= u_i \tag{4.117}$$

$$u_0 = V_0^{ref} (V_0^{ref})^H \tag{4.118}$$

Considering a positive semidefinite (PSD) constraint

$$\begin{bmatrix} u_i^{\theta_{ij}} & S_{ij} \\ S_{ij}^H & l_{ij} \end{bmatrix} \geq 0 \quad i \rightarrow\ j \tag{4.119}$$

Rank-1 criteria can be defined as

$$\begin{bmatrix} u_i^{\theta_{ij}} & S_{ij} \\ S_{ij}^H & l_{ij} \end{bmatrix} = 1 \tag{4.120}$$

Algorithm 6: Stochastic Linear Optimization

```
-
Initialize IOE input S^S_load, other TN and DN data
Initialize the variables for LDR
Run several simulations of the integrated network with different irradiance levels
Use a regression model to obtain the constants a and b
Add the LDR constraints to the TN OPF
while tol > ϵ do
    forall t ∈ TN do
        Solve the transmission network OPF.
        Extract the system parameters.(Voltage and angle)
        Check if V^m_k is violated
        If step 6 is yes, apply LDR in equation(40)
        Else use equation(33)
    end
    forall d ∈ DN do
        Solve the distribution network OPF.
        Extract the total load demand with losses at the DN
        Update the boundary variables at PCC with new demand.
    end
    Obtain the new tolerance error using equation (36)
    Check for convergence.
end
end
```

4.3.5 Stochastic optimization with LDR

Stochastic linear optimization is utilized for the proposed co-simulation with details discussed in Appendix B. The proposed approach is operated within an integrated optimization engine (IOE) which is represented in Fig. 4.13. A global optimization algorithm is used to solve each network based on its objective, which then converges to a bidirectional set point for each of the networks based on the integrated optimization engine. In the IOE the TN has real-time insights to the DN and it is able to readjust itself based on the linear decision rule constraints. To enable the insights of both networks, the TOPF is re-written to accommodate for the changing dynamics in the distribution network leading to the reverse power flow in the transmission network, **k** is a constant, due to the power from DG and nondispatchable. With the addition of **k** the TOPF is modified as

$$TOPF = min \quad C_M(U^M, U^B, X^M, X^B, K^S_{DG}) \tag{4.121}$$

Considering this, the objective of each network is redefined as

$$TOPF = min \sum_{g=1}^{N_G} (b_2(P^g_k)^2 + b_1(P^g_k) + b_0) \tag{4.122}$$

$$DOPF = min \quad Re(S_{ij} - Z_{ij} I^2_{ij}) \tag{4.123}$$

For a specific bus k the generator active power P^g_k as shown below is an arithmetic of $P_{k,D}$

which is the load connected, the line losses $P_{km,loss}$, and the reverse active power $P_{k,RP}$ from the DN.

$$P_k^g = P_{k,D}^M + \sum_{m:k\rightarrow\ m} P_{km}^M + \sum_{m:k\rightarrow\ k} P_{km,loss}^M + P_{k,RP}^B \tag{4.124}$$

With this the reverse power flow into the TN is obtained as

$$P_{K,RP}^B = Re(S_{K,RP}^B) \tag{4.125}$$

The integrated optimization engine uses the following set of equations:

$$Initialization : S_{K,RP}^{B(0)} = S_{load}^{S(0)} \tag{4.126}$$

$$V_{pcc}^{abc} = u_0^{abc} \tag{4.127}$$

$$u_0^{abc} = 1.0p.u \tag{4.128}$$

$$Objective : Min \quad \Delta V_{pcc} \tag{4.129}$$

$$\Delta V_{pcc} = V_K^B - V_{pcc} \tag{4.130}$$

$$S_{K,RP}^B = \sum_{i=1}^{n_b} \left[S_{i,D}^S + Re(\sum_{j:i\rightarrow\ j} (S_{ij} - Z_{ij} I_{ij}^2)) - S_{i,pv}^S \right] \tag{4.131}$$

Distributed Energy Resource (DER) considered is solar PV with a general representation as

$$S_{pv}^2 = P_{pv}^2 + Q_{pv}^2 \tag{4.132}$$

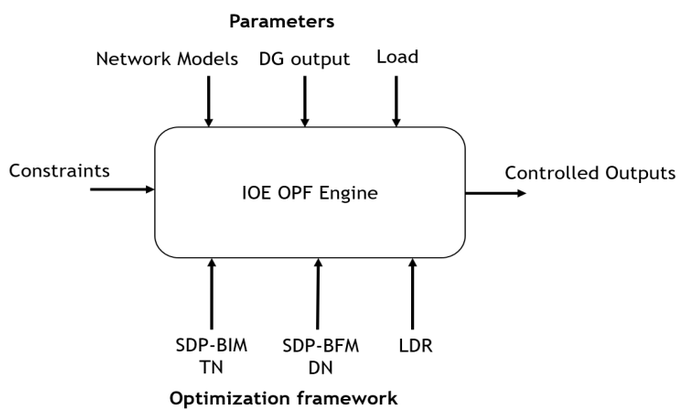

Figure 4.13: Integrated optimization engine

A linear decision rule (LDR) technique is implemented using the theorem discussed in appendix B. The stochastic nature of renewable energy resources is accounted for by ensuring the Transmission network has insight into the operations of the distribution network. Using different irradiance levels analysis was performed to derive the linear relationship between

TN generators and DN solar PVs in the form written below.

$$Y = a + bX \tag{4.133}$$

In (6.14, Y represents transmission network generators' active power for a specific bus k P_k^g, and X is the P_{pv} active power generated by the solar PVs. The representation to accommodate several generators and several RERs can therefore be written as the equation below. For this study, our RERs is solar PV. k is the bus the generator is connected to in the TN while i is the bus the solar PV is connected to in the DN, where a and b are constants. Thus,

$$P_k^g = a + bP_{i,pv} \tag{4.134}$$

4.3.6 LDR Theorem Proof

In this section, the proof of the LDR- model is discussed.

A stochastic model can be formulated as below:

$$\begin{aligned} min \quad & \mathbf{c}'\mathbf{x} + E(Q(\mathbf{x}, \bar{\mathbf{z}})) \\ s.t. \quad & \mathbf{A}\mathbf{x} = \mathbf{b} \\ & \mathbf{x} \geq \mathbf{0} \end{aligned} \tag{4.135}$$

with the $\mathbf{x}$ as vectors and other bold lower case, $\tilde{x}$ as a random variable, bold upper case such as $\mathbf{A}$ are the matrices.

where,

$$\begin{aligned} Q(\mathbf{x}, \mathbf{z}) = min \quad & \mathbf{f}'\mathbf{w} \\ s.t. \quad & \mathbf{T}(\mathbf{z})\mathbf{x} + \mathbf{W}\mathbf{w} = \mathbf{h}(\mathbf{z}), \\ & w_i \geq 0, \quad \forall i \in I \subseteq \{1, ...n_2\} \end{aligned} \tag{4.136}$$

Additionally, $\mathbf{c}$, $\mathbf{f}$ and $\mathbf{b}$ are known vectors in $\Re^{n_1}$, $\Re^{n_2}$ and $\Re^{m_1}$, $\mathbf{T}(\tilde{z})$, $\mathbf{h}(\tilde{z})$ are assumptions for affine data dependency.

$$\mathbf{T}(\bar{\mathbf{z}}) = \mathbf{T^0} + \sum_{\mathbf{k=1}}^{\mathbf{N}} \mathbf{T^k}\tilde{\mathbf{z}}_\mathbf{k}, \quad \mathbf{h}(\tilde{\mathbf{z}}) = \mathbf{h^0} + \sum_{\mathbf{k=1}}^{\mathbf{N}} \mathbf{h^k}\tilde{\mathbf{z}}_\mathbf{k} \tag{4.137}$$

$$\begin{aligned} Z_{STOC} = min \quad & \mathbf{c}'\mathbf{x} + E(\mathbf{f}'\mathbf{w}, (\bar{\mathbf{z}})) \\ s.t. \quad & \mathbf{A}\mathbf{x} = \mathbf{b}, \\ & w_i(\tilde{\mathbf{z}}) \geq 0, \quad \forall i \in I, \\ & \mathbf{x} \geq \mathbf{0} \\ & \mathbf{w}(\tilde{\mathbf{z}}) \in \mathcal{Y} \end{aligned} \tag{4.138}$$

Translating into LDR

$$\mathbf{w}(\bar{z}) = \mathbf{w}^0 + \sum_{k=1}^{N} \mathbf{w}^k \bar{z}_k \tag{4.139}$$

The stochastic model approximation is then written in the LDR

$$\begin{aligned} Z_{LDR} = min \quad & \mathbf{c}'\mathbf{x} + \mathbf{f}'\mathbf{w^0} \\ s.t. \quad & \mathbf{A}\mathbf{x} = \mathbf{b}, \\ \mathbf{T^k}\mathbf{x} + \mathbf{W}\mathbf{w^k} = \mathbf{h^k} \quad & \forall k \in \{0, ...N\}, \\ w_i(\mathbf{z}) \geq 0 \quad & \forall \mathbf{z} \in W, \forall i \in I, \\ & \mathbf{x} \geq \mathbf{0}, \\ & \mathbf{w}(.) \in \mathcal{L} \end{aligned} \tag{4.140}$$

$$\begin{aligned} & w_i(\mathbf{z}) \geq 0 \quad \forall Z \in W \\ & w_i^0 \geq \sum_{j=1}^{N} (z_j s_j + \tilde{z}_j t_j) \end{aligned} \tag{4.141}$$

If the solution at equation(62) is feasible, then it will be in equation(60), $Z_{STOC} \leq Z_{LDR}$, with $\mathcal{W}$ = [-z, $\tilde{z}$]. for some $\mathbf{s}$,$\mathbf{t} \geq 0$ satisfying s_j-$t_j = w_i^j$. Relating the above variables and uncertainties to our integrated T&D model, the variable w is the P_{PG}, the variable x is the $\mathrm{P}_{k,RP}$, while the uncertainty $\tilde{Z}$ is the P_{PV}

4.3.7 Results and Discussion

Different distribution test cases have been simulated and analyzed of which two test systems are presented. Test system 1 is IEEE 57 bus TN integrated with IEEE 34 bus DN. Test system 2 is IEEE 118 bus TN integrated with IEEE 123 bus DN. The detailed method is modeled and simulated using the MATLAB platform's YALMIP optimization toolbox [159]. The YALMIP toolbox used the MOSEK [160] solver to solve the optimization models. For the regression models with LDR, python package was used. The three-phase unbalanced model was implemented for the distribution network and the positive sequence model for the transmission network.

4.3.8 Test system I: IEEE 57 TN and IEEE 34 DN

First, the proposed SILP is tested on an integrated network with the transmission network as IEEE 57bus and the distribution network as IEEE 34bus. The coupled system is illustrated in fig.4.14.

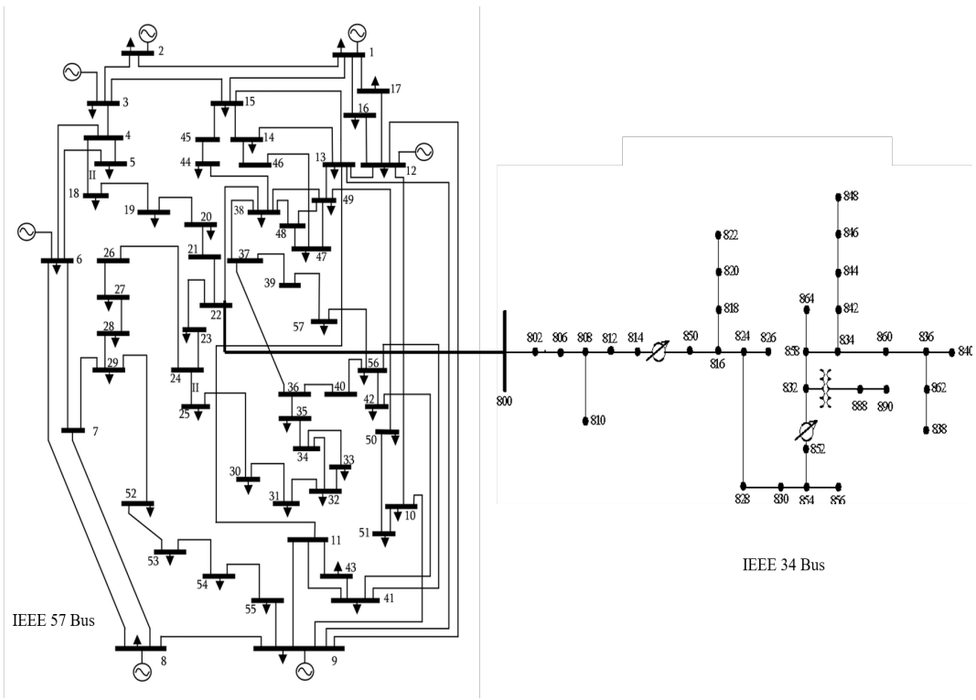

Figure 4.14: Integrated T&D model for IEEE 57bus and IEEE 34bus

Three cases are performed on this realistic network to discuss the advantages of the proposed SILP.

4.3.8.1 Case 1-Integrated Model Analysis without Solar PV

In this case, the proposed integrated SILP model is simulated with the objective of cost minimization for the TN and loss minimization for DN. The optimization model is compared with the conventional NLP models that are run separately for TN and DN. For the conventional NLP modeling MatPower software (used in the field as a state-of-the-art) is utilized.

Fig. 4.15 illustrates the comparison between the TN part of the proposed integrated SILP model and a stand-alone conventional NLP model. It can be seen the voltage profile almost matches with the conventional NLP which shows the exactness of the SILP.

Similarly, Fig. 4.16 illustrates the comparison between the DN part of the proposed integrated SILP model and a stand-alone conventional NLP model. It can be seen the voltage profile almost matches with the conventional NLP which shows the exactness of the SILP showing the exactness.

Further, the substation power and the objective functions are compared with the state-of-the-art for this case as illustrated in Table 4.4. It can be seen that the generation cost for the proposed SILP is lower when compared the TN and DN simulation performed separately.

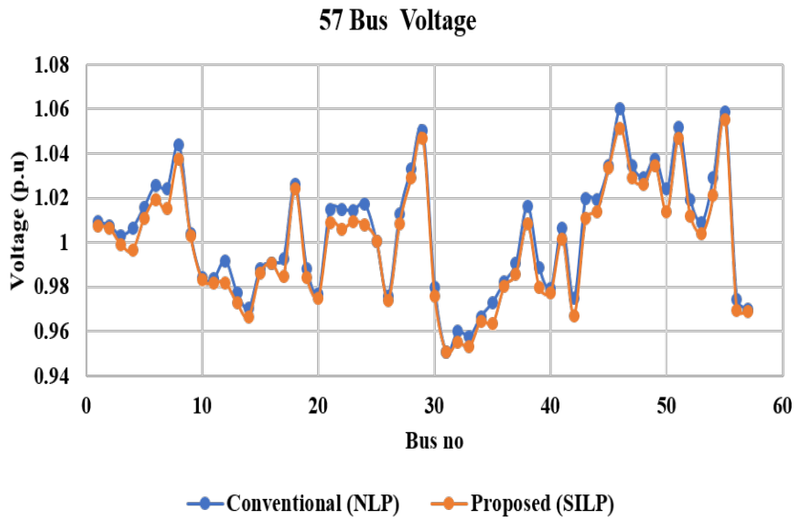

Figure 4.15: Voltage profile for IEEE 57 bus TN compared to the state-of-the-art

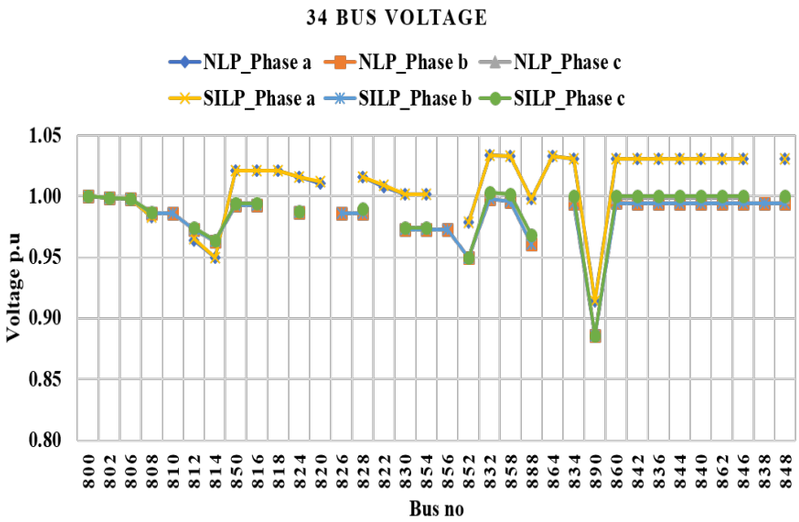

Figure 4.16: Voltage profile for IEEE 34 bus DN compared to the state-of-the-art

Also the power loss is lower as well when compared to the state-of-the-art bu around 5%.

TABLE 4.4: Substation Active and Reactive Power Output and Cost and Loss Comparisons

	$P_{sub}(MW)$	$Q_{sub}(MVar)$	$P_{loss}(MW)$	$Gencost$
IEEE 57-bus test case				
NLP-OPF	1311.40	285.91	20.735	43,583.41
Proposed-SILP	1310.345	286.10	19.685	43,550.60
IEEE 34-bus test case				
NLP-OPF	45.625	5.88	5.25	-
Proposed-SILP	45.860	5.80	5.46	-

4.3.8.2 Case 2- Integrated Model Analysis with Solar PV

To demonstrate the impact of the sudden changes by the solar PV located at DN on the TN, the penetration level of the DN to TN was modified such that 20 times the base load value of the DN was connected to the TN at the boundary bus, bus 22. Test cases with different irradiance and penetration levels was performed and discussed in Table 4.5. The solar PV was connected to bus 824 of the distribution network with a capacity of 50MVA. After

TABLE 4.5: Parameters Comparison with different PV penetration Levels

Penetration	Irradiance level	PVs Power Flow(MW)	Generation Cost($)	P(MW) @PCC	Q(MVAR) @PCC
25%	0.5	6.063	43,349	34.798	6.10
	0.9	10.913	43,118	29.948	6.05
	1.0	12.125	43,061	28.735	5.98
60%	0.5	14.550	42,947	26.310	5.95
	0.9	26.190	42,410	14.670	5.88
	1.0	29.100	42,276	11.760	5.86
90%	0.5	21.825	42,610	19.035	5.90
	0.9	39.285	41,814	1.575	5.85
	1.0	43.650	41,617	-2.79	5.80

running several simulations with different irradiance levels, the linear relationship between the solar PVs and each generator in the transmission network was obtained. The summary of the parameters obtained using a linear regression method done in python. The relationship is as seen in Table 4.6. The IEEE 57bus system has 7 generators, so the relationship was obtained for each generator as

$$Gen(i): \quad P_{G(i)} = a_{(i)} + b_{(i)} P_{PV} \tag{4.142}$$

Table IV illustrates the generation cost and the losses in both TN and DN with the proposed

TABLE 4.6: LDR relationship between the TN generator and Solar PVs

Generator	Bus No	a	b
1	1	106.312	-0.561
2	2	99.989	-0.296
3	3	56.895	-0.280
4	6	65.476	0.168
5	8	410.465	1.164
6	9	100.021	-0.069
7	12	420.504	-5.794

SILP and the conventional NLP. It can be seen that the proposed SILP have a better cost value compared to the NLP.

TABLE 4.7: Substation Active and Reactive Power Output and Cost and Loss Comparisons with solar PV

	$P_{sub}(MW)$	$Q_{sub}(MVar)$	$P_{loss}(MW)$	$Gencost$
IEEE 57-bus test case				
NLP-OPF	1,280.06	273.72	17.504	42,276
Proposed-SILP	1,279.55	273.25	17.250	42,225
IEEE 34-bus test case				
NLP-OPF	11.76	5.86	1.31	-
Proposed-SILP	11.77	5.79	1.35	-

4.3.8.3 Case 3- Integrated Model Analysis with Solar PV During Reverse Power Flow Condition

The scenario with reverse power flow was performed and its impact on the boundary variables was observed. For the proposed system, this scenario was only possible with the penetration level of the DN to be 90% of the TN and the irradiance level of the solarPV was also set to be 1.0 p.u (See Table 4.5).

Table 4.8 shows the boundary bus voltage deviation with the proposed SILP for all three cases. It can be seen that with the proposed SILP the voltage deviation at the boundary bus (DN integrated substation) is less than 5 %. The technique also offered a comparative

TABLE 4.8: Boundary Bus mismatch voltage deviation

Parameter	Case 1	Case 2	Case 3
Reverse Power Flow (MW)	0	0	2.79
Voltage at PCC with LDR(p.u)	None	None	1.012
Voltage at PCC without LDR(p.u)	1.015	1.013	1.060
% Voltage deviation at PCC	0	0	4.53%

advantage with respect to the cost of generation, since it eliminates the need for curtailing solar PV during reverse power operation the cost of generation dropped from $41,738 to $41,617 as shown in the Fig. 4.17.

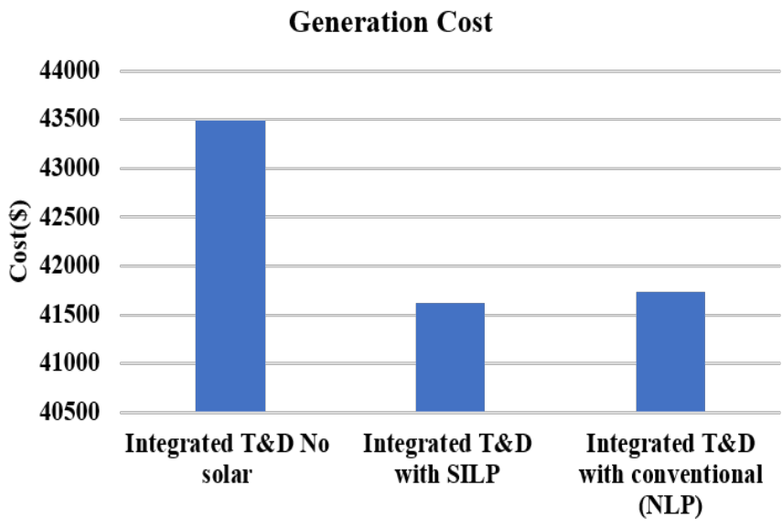

Figure 4.17: Generation cost comparison with SILP, no LDR, and with no DERs connected

The voltage profiles during the reverse power is illustrated in Fig. 4.18. It can be seen that with the proposed SILP the voltage profile is within the limit when compared to the state-of-the-art but violations can be seen when the state-of-the-art model is used.

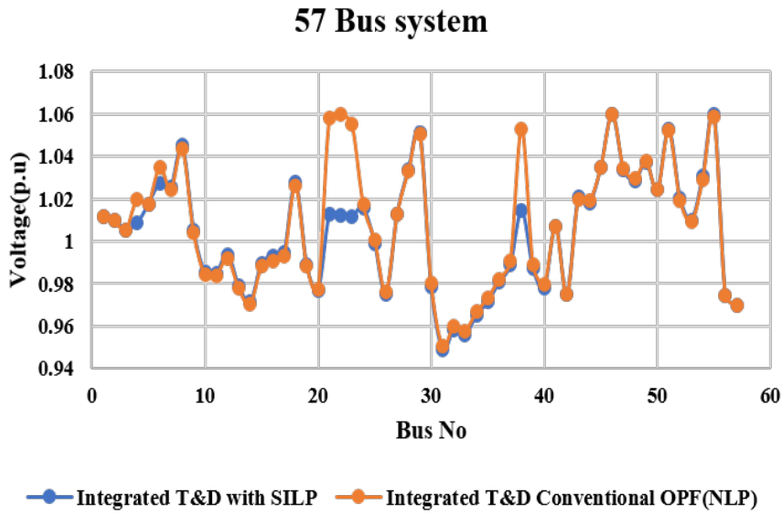

Figure 4.18: Voltage profile for IEEE 57bus system

TABLE 4.9: Substation Active and Reactive Power Output and Cost and Loss Comparisons with reverse power flow

	$P_{sub}(MW)$	$Q_{sub}(MVar)$	$P_{loss}(MW)$	$Gencost$
IEEE 57-bus test case				
NLP-OPF	1,267.31	270.56	16.513	41,737.79
Proposed-SILP	1,264.31	269.87	16.299	41,617.20
IEEE 34-bus test case				
NLP-OPF	- 2.79	-	-	-
Proposed-SILP	- 2.79	-	-	-

4.3.9 Test system II: IEEE 118 TN and IEEE 123 DN

Our approach was further implemented on the interconnection of IEEE 118bus and IEEE 123bus as shown in Fig.4.19. As seen in the integrated system the boundary bus is bus 38.

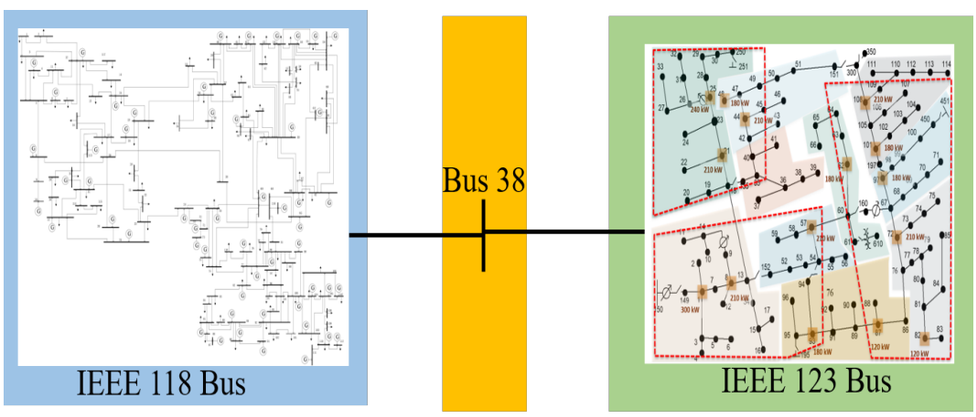

Figure 4.19: IEEE 118bus and IEEE 123bus Integrated T&D model

4.3.9.1 Case 1-Integrated Model Analysis without Solar PV:

Simulations were performed without the interconnection of solar PVs and the results were first benched-marked with conventional NLP performed using MatPower. The results shown below are a comparison of simulations with the proposed SILP and the MATPOWER(NLP) of the transmission network voltages and cost both approaches had the same objective of cost minimization. Fig. 10 illustrates the TN comparisons and Fig. 11 illustrates the DN

comparisons. It was observed that the voltages were closely matching in both scenarios.

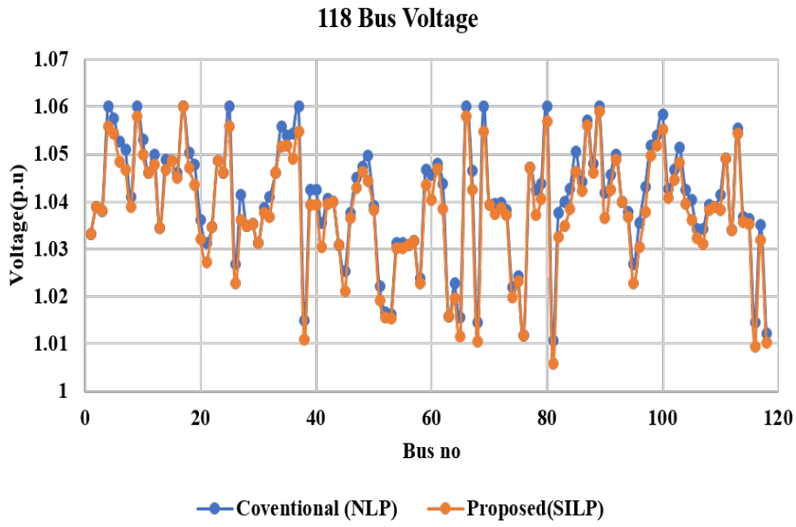

Figure 4.20: Voltage profile comparisons for IEEE 118 bus network

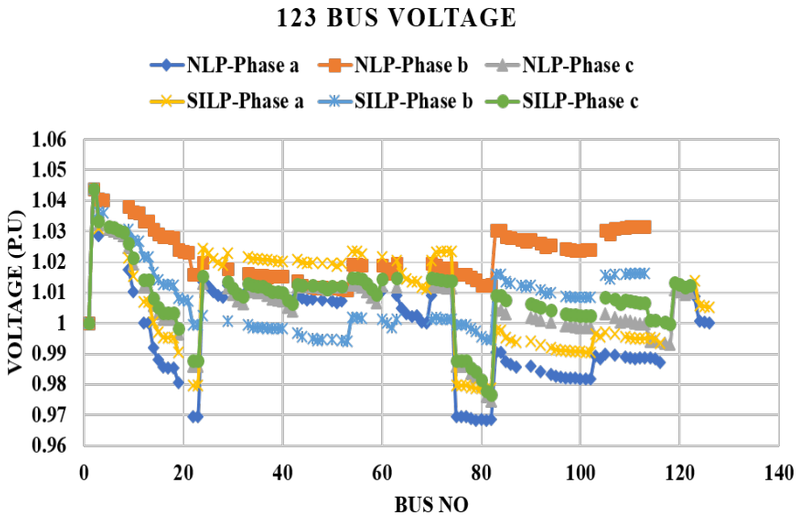

Figure 4.21: Voltage profile comparisons for IEEE 123 bus network

4.3.9.2 Case 2- Integrated Model Analysis with Solar PV

To increase the penetration level of the solar PV in DN to TN, the system was modified such that 20 times the base load values of the DN were connected to the TN. A base case simulation was done, after which the system was tested with different penetration levels as shown in 4.11. The solar PV was connected to bus 56 of the distribution network and it had a capacity of 100 MVA. Similarly, the linear relationship was obtained for each of the generators in the TN and the solar PVs, the IEEE 118bus has 54 generators connected to the network.

4.3.9.3 Case 3- Integrated Model Analysis with Solar PV During Reverse Power Flow Condition:

The scenario with reverse power flow was created and its impact on the boundary variables was observed. This was only possible with the penetration level of the DN to be 90% and

TABLE 4.10: Parameters Comparison with different PV penetration Levels

Penetration	Irradiance level	PVs Power Flow(MW)	Generation Cost($)	P(MW) @PCC	Q(MVAR) @PCC
25%	0.5	11.88	132,103	60.13	25.38
	0.9	21.38	131,701	50.63	24.88
	1.0	23.75	131,621	48.25	24.75
60%	0.5	28.50	131,420	43.50	24.50
	0.9	51.30	130,499	20.70	23.30
	1.0	57.00	130,259	15.01	23.00
90%	0.5	42.75	130,859	29.25	23.75
	0.9	76.95	129,449	-4.95	21.95
	1.0	85.50	129,102	-13.50	21.50

the irradiance levels of 0.9p.u and 1.0p.u (see Tale VII). The LDR technique was effective as seen in the table and the boundary voltage mismatch as shown in Table VIII.

The steepest variations was seen when irradiance is at 1.0p.u and 90% penetration level. Since our technique also eliminated the need for curtailing solar PV the cost of generation dropped from $129,660 to $129,102 as shown in the Fig. 4.22. The reduction in voltage boundary bus mismatch is also achieved through the LDR technique shown in Table 4.12. Fig. 13 illustrates that without SILP, the voltage violation occurs at the boundary bus.

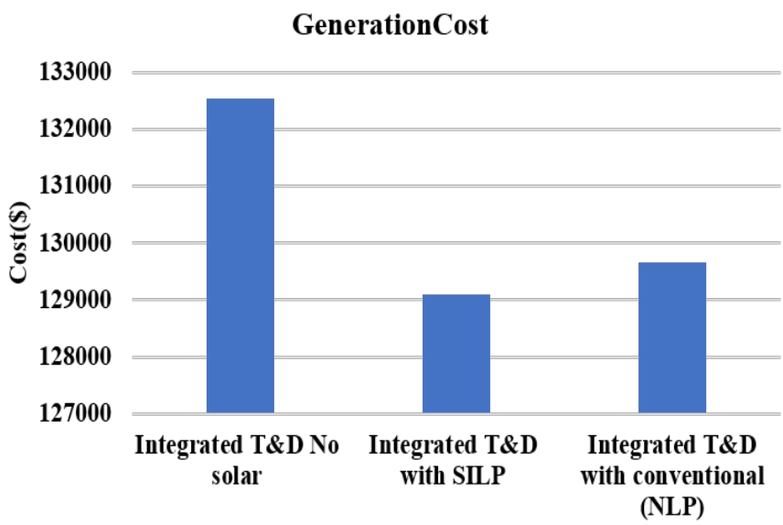

Figure 4.22: Generation cost comparison with SILP, and conventional NLP.

4.4 Summary

The proposed methodology for the co-simulation of an integrated T&D system ensures that the transmission system can adequately capture the changes occurring in the distribution system due to the RERs and operate optimally. Our framework ensures that the grid objectives are achieved for both networks, the formulation can also be implemented in power flow simulations. With this technique, the boundary mismatch challenges in the integrated grid are minimized, which can therefore allow for safe and reliable operations without the need for curtailing the resources. The methodology ensures that the boundary voltage

TABLE 4.11: LDR relationship between generator and Solar PVs

Generator	Bus No	a	b
1	1	28.76	-0.03
2	4	$3.03e^{-5}$	$8.75e^{-8}$
3	6	2.03	$-2.5e^{-2}$
4	8	$2.84e^{-5}$	$7.62e^{-8}$
5	10	403.71	-0.026
6	12	86.10	-0.0041
7	15	25.02	-0.058
8	18	16.75	-0.05
9	19	25.21	-0.051
10	24	$2.96e^{-5}$	$9.71e^{-8}$
11	25	194.57	-0.011
12	26	280.95	-0.017
13	27	11.85	-0.027
14	31	7.27	$-2.8e^{-4}$
15	32	16.96	-0.03
16	34	17.92	-0.18
17	36	22.31	-0.161
18	40	55.27	-0.08
19	42	43.68	-0.04
20	46	19.12	$1.13e^{-3}$
21	49	193.95	-0.009
22	54	49.63	-0.001
23	55	33.70	-0.022
24	56	34.24	-0.024
25	59	150.13	-0.006
26	61	148.91	-0.007
27	62	$1.61e^{-5}$	$-5.95e^{-8}$
28	65	353.65	-0.02
29	66	350.11	-0.018
30	69	455.14	-0.02
31	70	$8.54e^{-5}$	$-1.4e^{-7}$
32	72	$9.52e^{-5}$	$-1.25e^{-7}$
33	73	$1.33e^{-4}$	$-4.78e^{-7}$
34	74	18.35	-0.02
35	76	24.02	-0.016
36	77	$1.96e^{-6}$	$7.23e^{-8}$
37	80	432.02	-0.017
38	85	$8.76e^{-6}$	$-3.83e^{-8}$
39	87	3.63	$-7.3e^{-5}$
40	89	502.5	-0.01
41	90	$1.14e^{-6}$	$4.96e^{-8}$
42	91	$1.04e^{-5}$	$4.54e^{-8}$
43	92	$8.14e^{-6}$	$4.54e^{-8}$
44	99	$1.46e^{-6}$	$6.11e^{-8}$
45	100	231.6	-0.004
46	103	38.28	0.046
47	104	$2.24e^{-4}$	$6.97e^{-7}$
48	105	5.67	$-7.00e^{-3}$
49	107	29.291	$-3.72e^{-3}$
50	110	7.318	$-4.1e^{-3}$
51	111	35.25	$-1.4e^{-4}$
52	112	36.622	-0.002
53	113	1.57e-4	-3.9e-7
54	116	$9.89e^{-6}$	$-3.99e^{-8}$

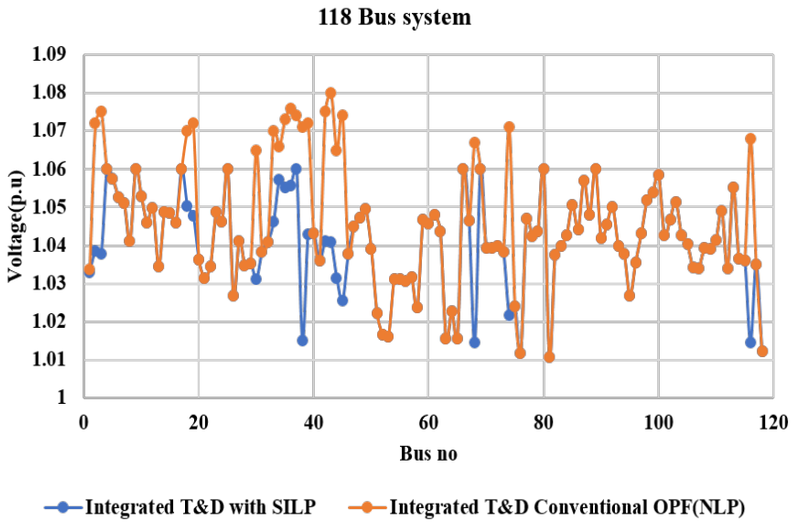

Figure 4.23: Bus voltage profile IEEE 118bus network.

TABLE 4.12: Boundary Bus mismatch voltage deviation

Parameter	Scenario 1	Scenario 2	Scenario 3
Reverse Power Flow (MW)	0	4.98	13.50
Voltage at PCC with LDR(p.u)	None	1.015	1.016
Voltage at PCC without LDR(p.u)	1.014	1.070	1.075
% Voltage deviation at PCC	0 %	5 %	5.5 %

is tightened, and other voltages in the network which are easily susceptible to change are within allowable limits and the need for several iterations for convergence is eliminated. In the future, the scope of our work will be extended to a larger time window and add other renewable energy resources to the network, as well as evaluate other grid objectives.

CHAPTER 5: MULTI-PERIOD INTEGRATED TRANSMISSION AND DISTRIBUTION OPTIMAL POWER FLOW SIMULATION USING LINEAR DECISION APPROACH

5.1 Introduction

The recent developments in the electric grid introduced some changes to steady state solution of the optimal power flow and created the need for a multiperiod optimal power flow (MPOPF) solution. These changes are due to the progressive increase in load and introduction of renewable energy resources into the grid which has led to the deregulation of the electric energy system. Hence, the modern grid has a lot of varying devices operating at each interval. Utilities still have a major objective to operate the grid in a cost-efficient manner, which is achieved through optimal power flow simulations (OPF). OPF solutions provide the optimal operating point for the electric grid based on specified objectives which can either be cost or loss minimization. The solutions can be solved on a day ahead where the utilities make use of known models and provided or needed data to compute the OPF, these simulations is performed for each iteration within a defined interval based on the variations of the devices connected to the network, however, to operate efficiently real-time OPF is also performed by most utilities to address the sudden changes that can occur on the grid. Real-time OPF is performed within 15mins intervals by most utilities, though some of the occurrences by renewable energy resources are sudden and occurs before within each interval. MPOPF asides from achieving the utility objectives must satisfy the technical constraints of the grid such as power-flow equations, active and reactive powers, limits on the generators, line flow limits, MPOPF are also needed because the current grid comprises time coupled devices and for planning purposes. In situations where the size of these resources is large, a reverse power flow into the TN can occur and if not adequately planned for can have significant effects on the power quality metrics in the transmission network such effects can be on the voltage, frequency, and other metrics. Some of the techniques used to address the intermittency of renewable energy resources are the use of grid-storage devices which comes with a few challenges of cost, and operational efficiency. OPF algorithm has been extensively established using different techniques and relaxations dues its non-convexity, such as Linear programming, Non-Linear programming Newton-Raphson, quadratic programming, and interior point method, cite. The introduction of time into the optimal power flow equations increases the simulation computational burden, several techniques have been utilized such as combining receding horizon with different power flow models like DC power flow, SDP relaxations, standard solutions strategies for MPOPF adopting general purpose nonlinear

programming (NLP) methods, usually employed for the solution of non-convex optimization problems, the computational time for solving MPOPF is spent in the solution of Karush-Kuhn-Tucker(KKT). The devices connected to the grid leading to the need for MPOPF are mostly introduced at the distribution networks and they are transforming the integrated grid into an active network[9],[10]. Some research work has been done to extend the OPF work to multiperiod framework, Warrington et all [161] used the Lagrangian decomposition method to solve MPOPF with storage and ramp constraints, Gayme and Topcu [162] considered OPF problems with storage by extending the work of Lavaei and Low. The basic applications in the tools used for simulations with Transmission system operators and Distribution system operators are power flow, and a couple of other techniques and tools have been developed for the co-simulation of the integrated network such as Framework for Network Co-Simulation (FNCS)[131], Integrated Grid Modeling System (IGMS)[132, 132], HELICS [**?**, **?**], the uncertainty of the boundary variables due to renewable energy resources makes the solutions not tight. The differences in the device types also make it difficult to coordinate the coupled network from a single operator, additionally, the only information for both networks is provided at the boundary bus such as power demand, voltage magnitude, voltage angles, and locational marginal prices [163,164]. Some decentralized approaches have been implemented for the integrated networks also which are classified as either Lagrangian relaxation (LR) and Optimality condition decomposition (OCD), the LR involves the use of the alternative direction of method multipliers (ADMM) [165], analytical target cascading (ATC), the shortcomings of the LR approach is the low convergency rate and complex parameter tuning process. The OCP can be deployed either as a synchronous iteration[166] or asynchronous iteration[167]. The synchronous has the advantage of better convergence while the asynchronous is simpler in its implementation. The major challenges for the OCD approach are the inability to work with the exchange of variables with different characteristics. The co-simulation of integrated T&D considering the heterogenous characteristics have also been studied [168,169], the solutions are however still complex. These issues are why the integrated T&D OPF are not been implemented yet, in addition to helping prevent challenges arising as transformer overloading (TFO), grid voltage violation due to the reverse power flow into the TN, and eliminating the need to curtail DG [136], which also offers benefits with regards to cost. This chapter is a further expansion of our work where we implemented our approach for steady-state operations of the integrated network [170]. The relaxation techniques implemented is semidefinite programming (SDP) branch flow method (BFM)and bus injection method (BIM) for the non-linear terms in the constraint [137], The static OPF equations were modified to operate as MPOPF, while ensuring that in each interval the TN devices provide optimum operating points to achieve the grid objectives, using the LDR

methodology to have insights to the DN operations

5.1.1 Main contribution

The main advantages of the technique discussed in this chapter

- Eliminating the need to curtail DERs during uncertainties.
- Providing transmission network insights of distribution network operations at every time.
- Ability to achieve multiple grid objectives within each network and ensure no violation of grid quality metrics.

The main contribution our work in this section includes :

- An technique that co-simulates integrated T&D network considering all the time-varying parameters connected to the grid.
- An approach that minimizes boundary voltage mismatch due to reverse power flow from DN especially at times when the irradiance level of the solarPV is high.
- A linear decision rule LDR is utilized to maximize the cost benefits and voltage management offerings of DERs at each time interval of operation.

5.2 Previous and Current Model Challenges

In most electricity value chain, the management and co-ordination of the operations of the grid is done seperately, the TN is managed by the TSO while the DN is managed by the DSO, The TSO can co-ordinate the voltages exchanged in the boundary power injection, while the DSO regulates the power injection based on the boundary voltage. Most of the techniques available involve similar exchange variables and they are computationally complex. Furthermore, since the variables exchanged at the boundary of integrated T&D are different the network can be referred to as a heterogeneous network. The integrated T&D has a general model known as master-slave structure [138, 139] as shown in Fig. 5.1. All the devices and components in the TN asides from the boundary bus are referred to as the master system, while all the devices and components in the DN including the boundary bus are referred to as the slave system. The boundary bus is the interconnecting bus between both networks, since, the variables exchanged at the boundary are different the integrated network can be referred to as a heterogeneous network.

At PCC, the boundary voltage is the transmission bus voltage which is the feeder voltage (magnitude and angle) for the distribution network u_0^{abc}

$$u_0^{abc}(t) = V_{pcc}^{abc}(t) \tag{5.1}$$

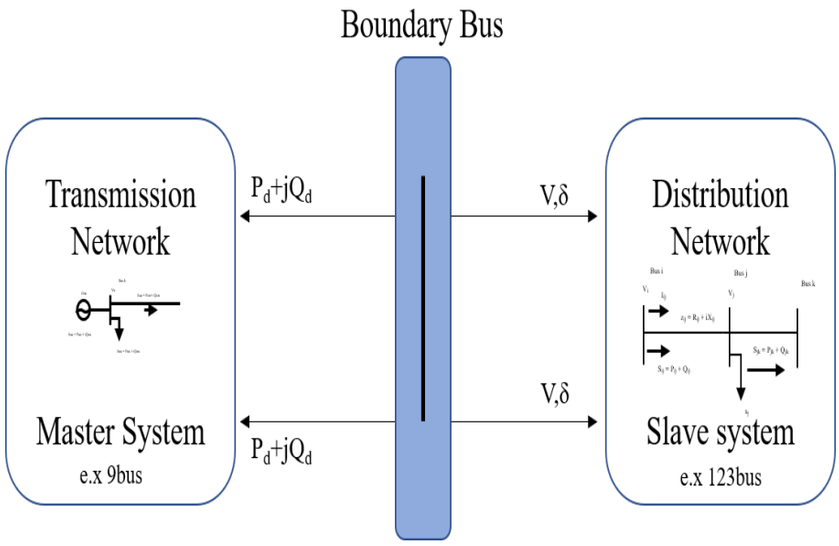

Figure 5.1: A schematic of Integrated T&D model with master-slave approach

5.2.1 Transmission Network MPOPF

Considering the general model of transmission network with the optimal objective of reducing the cost of generation. For a given network graph $\mathcal{G}$ =($\mathcal{N}$, $\mathcal{E}$), where $\mathcal{N}$ is the number of nodes in the network such that m $\in \mathcal{N}$ is the node in the network as shown in the figure below, $\mathcal{E}$ is used to represent the number of branches in the network. Depending on the bus number m or n, V_m is voltage of m $\in \mathcal{N}$. The active power and reactive power of the generation and load are represented as P_m^g,Q_m^g and P_m^d,Q_m^d respectively. The approach used for the solution in the transmission network is a semi-definite relaxation (SDP) bus injection method [140], the one-line representation is as shown in Fig. 5.2.

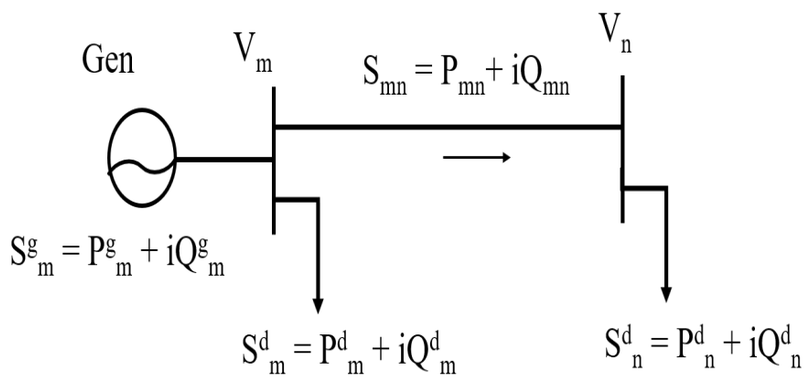

Figure 5.2: Transmission network - One line

The non-convex AC OPF equations are below

$$min \sum_{t=1}^{T_t} (c_2^m (P_m^g(t))^2 + c_1^m P_m^g(t) + c_0^m) \tag{5.2}$$

subject to

$$P_m^g(t) - P_m^d(t) = x(t)^T Y_m x(t) \tag{5.3}$$

$$Q_m^g(t) - Q_m^d(t) = x(t)^T Y_m x(t) \tag{5.4}$$

$$P_{mn}(t) = x(t)^T Y_{mn} x(t) \tag{5.5}$$

$$Q_{mn}(t) = x(t)^T Y_{mn} x(t) \tag{5.6}$$

$$P_m^{min} \leq P_m^g(t) \leq P_m^{max} \tag{5.7}$$

$$Q_m^{min} \leq Q_m^g(t) \leq Q_m^{max} \tag{5.8}$$

$$(V_m^{min})^2 \leq x(t)^T M_m x(t) \leq (V_m^{max})^2 \tag{5.9}$$

$$P_{mn}^2(t) + Q_{mn}^2(t) \leq (S_{mn}^{max})^2 \tag{5.10}$$

$$x(t)^T M_{mn} x(t) \leq L_{mn}^{max} \tag{5.11}$$

SDP relaxation is written below

$$min \sum_{t=1}^{T_t} (a_i)(t) \tag{5.12}$$

$$s.t \quad \mathbf{W}(t) \geq 0 \tag{5.13}$$

$$\begin{bmatrix} a_{mo}(t) & a_{m1}(t) \\ a_{m1}(t) & -1 \end{bmatrix} \leq 0 \tag{5.14}$$

$$P_m^{min} \leq P_m^g(t) \leq P_m^{max} \tag{5.15}$$

$$Q_m^{min} \leq Q_m^g(t) \leq Q_m^{max} \tag{5.16}$$

$$P_m^g(t) - P_m^d(t) = T_r(Y_m \mathbf{W}(t)) \tag{5.17}$$

$$Q_m^g(t) - Q_m^g(t) = T_r(Y_m \mathbf{W}(t)) \tag{5.18}$$

$$(V_m^{min})^2 \leq T_r(M_m \mathbf{W}(t)) \tag{5.19}$$

$$T_r(M_m \mathbf{W}(t)) \leq (V_m^{max})^2 \tag{5.20}$$

$$\begin{bmatrix} T_r(M_{mn} \mathbf{W}(t)) \\ T_r(M_{mn} \mathbf{W}(t)) \end{bmatrix} \leq S_{mn}^{max} \tag{5.21}$$

$$T_r(M_{mn} \mathbf{W}(t)) \leq L_{mn}^{max} \tag{5.22}$$

Where (43), after applying the Schur's complement becomes

$$a_{m0}(t) = c_0^m + c_1^m P_m^g(t) - a_m(t), a_{m1}(t) = \sqrt{c_2^m} P_m^k(t) \tag{5.23}$$

The equation above is for the primal formulation, the dual formulation is thus

$$s.t \quad \mathbf{Z}(t) \tag{5.24}$$

$$\begin{bmatrix} 1 & r_m^1(t) \\ r_m^1(t) & r_m^2(t) \end{bmatrix} \tag{5.25}$$

$$\begin{bmatrix} \lambda_m^P(t) & \lambda_m^P(t) \end{bmatrix} \tag{5.26}$$

$$\begin{bmatrix} \lambda_m^Q(t) & \lambda_m^Q(t) \end{bmatrix} \tag{5.27}$$

$$\begin{bmatrix} \alpha_m(t) \end{bmatrix} \tag{5.28}$$

$$\begin{bmatrix} \beta_m(t) \end{bmatrix} \tag{5.29}$$

$$\begin{bmatrix} \lambda_m^V(t) \end{bmatrix} \tag{5.30}$$

$$\begin{bmatrix} \lambda_m^V(t) \end{bmatrix} \tag{5.31}$$

$$\begin{bmatrix} T_r(M_m\mathbf{W}(t)) \\ T_r(M_m\mathbf{W}(t)) \end{bmatrix} \leq S_{mn}^{max} \tag{5.32}$$

$$\begin{bmatrix} \mu_{mn}(t) \end{bmatrix} \tag{5.33}$$

The auxiliary variables used in the equations are based on lavei and low as well as representing e_m as the k-th basis vector.

$$Y_m = e_m e_m^T Y \tag{5.34}$$

$$Y_{mn} = (\bar{y}_{mn} + y_{mn}) e_l e_l^T - (y_{mn}) e_l e_{mn}^T \tag{5.35}$$

$$Y_m = \frac{1}{2}\begin{bmatrix} R_e(Y_m + Y_m^T) & I_m(Y_m^T - Y_m) \\ I_m(Y_m - Y_m^T) & R_e(Y_m + Y_m^T) \end{bmatrix} \tag{5.36}$$

$$Y_{mn} = \frac{1}{2}\begin{bmatrix} R_e(Y_{mn} + Y_{mn}^T) & I_m(Y_{mn}^T - Y_{mn}) \\ I_m(Y_{mn} - Y_{mn}^T) & R_e(Y_{mn} + Y_{mn}^T) \end{bmatrix} \tag{5.37}$$

$$\bar{Y}_{mn} = \frac{-1}{2}\begin{bmatrix} I_m(Y_{mn} + Y_{mn}^T) & R_e(Y_{mn}^T - Y_{mn}) \\ R_e(Y_{mn} - Y_{mn}^T) & I_m(Y_{mn} + Y_{mn}^T) \end{bmatrix} \tag{5.38}$$

$$\bar{Y}_m = \frac{-1}{2}\begin{bmatrix} I_m(Y_m + Y_m^T) & R_e(Y_m - Y_m^T) \\ R_e(Y_m^T - Y_m) & I_m(Y_m + Y_m^T) \end{bmatrix} \tag{5.39}$$

$$M_{mn} = \begin{bmatrix} (e_m - e_n)(e_m - e_n)^T & 0 \\ 0 & (e_m - e_n)(e_m - e_n)^T \end{bmatrix} \tag{5.40}$$

$$M_m = \begin{bmatrix} e_m e_m^T & 0 \\ 0 & e_m e_m^T \end{bmatrix} \tag{5.41}$$

5.2.2 Distribution Network MPOPF

Similarly, as the transmission network for any given distribution network graph G Let us assume that G = (N, E) for a radial distribution network such that N denotes the set of all vertices and E is the set of all branches. The network model comprises the branch variables such as branch current, branch active, and reactive power flow. Let, Vi is the voltage of node i, Sij and Iij is the complex power and current flown through branch i â j, In this case, the SDP approach used for solving the OPF of the distribution network makes use of the branch flow method (BFM) [141]. the one-line representation is as shown in Fig. 5.3.

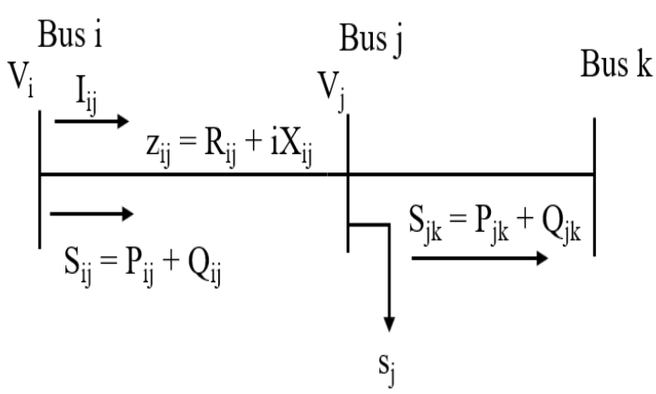

Figure 5.3: Distribution network- One line

Algorithm 7: Optimization steps in the TN

```
-
Determine the total number of buses n_b and branches n_br in the network
Obtain the input data for from bus (fb) and to bus (tb),fb,tb ∈ 𝒩
Identify the network devices (generators, transformers, boundary bus)
Initialize the sdpvar variables (V_m,S_m^g)
Develop the Ybus matrix of the network and obtain the auxiliary variables.
for x = 1 : n_b do
    if if x is a bus, then
        Formulate the bus constraint using the equation 9&10.
    else
        if if branch x is a voltage regulator, then
            Formulate the branch constraint using the equation 23
        end
    end
end
Solve the OPF using BIM SDP technique.
for x = 1 : n_br do
    if if rank = 1 , then
        W is positive semi-definite.
    else
        if if rank > 1, then
            W is not a positive semi-definite.
        end
    end
end
```

The current equation for the branch flow model and the complex power flowing across the branch are shown in the equation below respectively.

$$V_i - Vj = z_{ij} I_{ij} \tag{5.42}$$

$$S_{ij} = V_i I_{ij}^* \tag{5.43}$$

Distribution system modeling can have a different number of phases depending on the nodes, node i below has three-phase lines while node j has two-phase lines.

$$V_i = [V_i^a, V_i^b, V_i^c]^T \tag{5.44}$$

$$V_j = [V_j^a, V_j^b]^T \tag{5.45}$$

If the equation for current and complex power flow is combined together, it will lead to the second-order decision variables which are represented as $\mathrm{u}_i = \mathrm{V}_i \mathrm{V}_i^H, \quad \mathrm{l}_i = \mathrm{I}_{ij} \mathrm{I}_{ij}^H$ which is the squared magnitude of voltage and current respectively.

The objective function is written below as equ(23)

$$Minimize \sum real(z_{ij} l_{ij(t)}) \tag{5.46}$$

Algorithm 8: Optimization steps in the DN

```
-
Determine the total number of buses n_b and branches n_br in the network
Obtain the input data for from bus (fb) and to bus (tb),fb,tb ∈ 𝒩
Identify the network devices (generators, regulators, transformers,DERs)
Determine the total number of phases in each branch and buses in the network
Develop the Ybus matrix of the network.
Initialize all the sdpvar variables (l_ij,u_i,S_ij)
for x = 1 : n_br do
    if if branch x is a line, then
        Formulate the branch constraint using the equation 23.
    else
        if if branch x is a voltage regulator, then
            Formulate the branch constraint using the equation 23
        end
    end
end
for x = 1 : n_b do
    Formulate the bus constraint using the equation 23
    formulate other boundary constraints
end
Solve the OPF using SDP BFM model.
for x = 1 : n_br do
    if if equation 27 is satisfied, then
        The solution is local optimum.
    else
        if if equation 28 is satisfied, then
            global optimum is the solution.
        end
    end
end
```

All the constraints are then written as below

$$\sum diag(S_{ij(t)} - z_{ij} l_{ij(t)}) + s_{j(t)} + y_j u_{j(t)} = \sum diag(S_{jk(t)})^{\phi_j} \tag{5.47}$$

$$u_{j(t)} = u_{i(t)}^{\phi_{ij}} - (S_{ij(t)} z_{ij}^H + S_{ij(t)}^H z_{ij}) + z_{ij} l_{ij(t)} z_{ij}^H \tag{5.48}$$

$$u_{i(t)} \leq diag(u_{i(t)}) \leq u_{i(t)} \tag{5.49}$$

$$u_0 = V_0^{ref} (V_0^{ref})^H \tag{5.50}$$

$$\begin{bmatrix} u_i(t)^{\theta_{ij}} & S_{ij} \\ S_{ij}^H & l_{ij} \end{bmatrix} \geq 0 \tag{5.51}$$

PSD is set to be equal to 1.

5.2.3 Case studies

We performed a snapshot analysis of the integrated system to see the impact of the lack of adequate information sharing between both TSO and DSO, on the cost of generation and the voltage profile of the buses in TN. The test was carried out on an integrated system with IEEE 9 & 13 bus system, the reverse power flow led to the increase in voltage levels

in the TN as shown in Fig. 5.6. The modifications done on the system includes; a large solar PV system of capacity 100MVA was connected to the 13bus distribution network, the DN load was multiplied by 18 times to increase the impact levels of its changes seen at the transmission network.

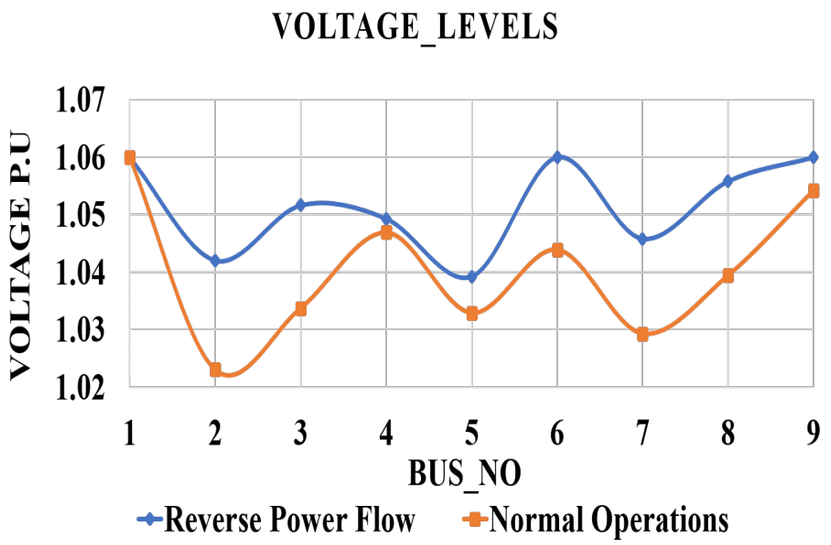

Figure 5.4: IEEE 9bus voltage levels

The approach frequently used to mitigate against the voltage violation Section 6.2.2 involves curtailment of DER, after curtailment the voltage levels were returned to normal operating conditions but the cost of generation was affected.

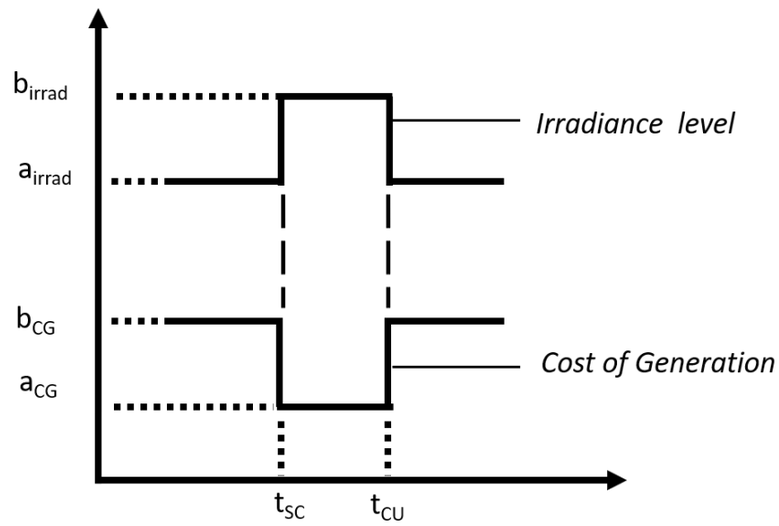

Figure 5.5: Cost and irradiance levels before&after curtailing the SolarPVs

As shown in the fig. **??**, the $a_{irrad} = 0.5$p.u is the irradiance level before the sudden change at time t_{sc} to $b_{irrad} = 0.9$p.u, the solar PV was then curtailed at t_{cu} and the changes on the cost of generation was observed to reduce from b_{CG} to a_{CG}.

5.3 Proposed Integrated optimization engine(IOE) architecture

Our architecture ensures that the grid objectives are achieved, this is made possible by providing the TN insights into the DN at every time while accounting for the heterogeneous

Algorithm 9: Optimization steps for IOE

```
-
Initialize the network data for both integrated systems required for computation.
Obtain the parameters t_p for TN and d_p for DN
while tol > ϵ do
    forall t ∈ 24 do
        forall t_p ∈ TN do
            Solve the TOPF using SDP-BIM.
            Extract the simulation results. (Voltage and angle)
            Check if any bus voltage in TN is violated
            if yes, apply LDR, else
            Use the boundary bus parameters as setpoints for the DN feeder
        end
        forall d_p ∈ DN do
            Solve the DOPF using SDP-BFM.
            Extract the total demand with losses at DN
            Update the DN load demand at PCC of the integrated network.
        end
    end
    Obtain the new tolerance tol, using equation 23
    Check for convergence.
end
```

nature of exchanged boundary variables. The generators on the TN are able to readjust them using our technique in case of a sudden change with the DERs in the DN. Our technique uses a linear decision rule which is a stochastic optimization method, we train the model on the relationship between the active power of the TN generators and active power from the Solar PV in the DN, and we then develop a linear expression of the relationship which has a constant and variable parameter. The expression is then added as a constraint to the TN and provides the generators on the TN insights to the DN, which eliminates the need for the curtailment of the DG at each time. The step-by-step process of our technique is shown in the algorithm table 11. The primary TDOPF model in [139] is modified while ensuring all the conditions for TDOPF optimality and boundary bus power balance are satisfied as shown in the set of equations below. We ensure that the new entity **Z** which is a representation of the reverse power flow into The TN is added in the TOPF. It is important to note the characteristic of **Z** as undispatchable and is a constant once the variable active power from solarPV is generated using the principle of complete recourse stochastic optimization.

The transmission objective is written to accommodates for the new parameter **Z**.

$$min \quad c_M(U^M(t), U^B(t), X^M(t), X^B(t), Z^S_{DG}(t)) \tag{5.52}$$

The TOPF and DOPF objectives equation are written below

$$TOPF = \sum_{t=1}^{T_t} \sum_{g=1}^{N_G} (c_2(P_{m,t}^g)^2 + c_1(P_{m,t}^g) + c_0(t)) \tag{5.53}$$

$$DOPF = min \sum_{t=1}^{T_t} Re(S_{ij}(t) - Z_{ij} I_{ij}^2(t)) \tag{5.54}$$

In the transmission network, active power generated is a combination of power flowing in the lines in the network P_{mn}, the line losses P_{mn}^{loss}, and the reverse active power $P_{m,RP}^{M}$ from DN through the boundary bus p.

$$P_m^g(t) = \sum_{n:m\rightarrow n} P_{mn}^M(t) + \sum_{n:m\rightarrow n} P_{mn,loss}^M(t) + P_{m,RP}^M(t) \tag{5.55}$$

From the distribution system slave network, the reverse power is obtained as below

$$S_{m,RP}^M(t) = S_S(t) - S_{pv}(t) \tag{5.56}$$

$$P_{m,RP}^M(t) = Re(S_{m,RP}^M(t)) \tag{5.57}$$

$$S_S(t) = S_S^{load}(t) + S_S^{losses}(t) \tag{5.58}$$

Note that if $P_{m,RP}^M(t) > 0$ then it is an active power demand and not a reverse power flow.

$$Initialization : S_{m,RP}^{M(0)} = S_S^{load(0)} \tag{5.59}$$

$$DNfeedervoltage : u_0^{abc} = 1.0 \tag{5.60}$$

$$Min \quad \Delta V_{pcc}(t) = V_m^{pcc}(t) - u_0^{abc}(t) \tag{5.61}$$

Solar PV using its apparent, real, and reactive power is modeled as shown in equ(6).

$$S_{pv}^2(t) = P_{pv}^2(t) + Q_{pv}^2(t) \tag{5.62}$$

The steps for the algorithm TOPF and DOPF are discussed in the paper [170].

5.3.0.1 Linear decision rule

A linear decision rule LDR relationship was obtained by running an analysis on the integrated optimization engine with different irradiance data set. After the analysis, a relationship was established between the changing power from the SolarPVs and the response of the generator power in the transmission system. The data sets were divided into training and test data to validate the accuracy of the model. The relationship is then added as an

additional constraint to the integrated optimization engine, to ensure that the output from the generator adjusts to the reverse power flow into the TN due to changing nature of the resources on the DN. The integrated optimization engine has an objective to minimize the deviation errors "boundary bus mismatch" voltage.

The formulation of the Linear decision rule.

$$Y(t) = a + bX(t) \tag{5.63}$$

The $P_m^g(t)$ at each time t is the active power from the generators in the TN which represents the Y term in the LDR, X is the P_{pv} active power generated by the solar PVs connected at the DN.

$$P_m^g(t) = a + bP_{pv}(t) \tag{5.64}$$

5.3.1 OPF Remarks

The detailed proof of the global optimality and the exactness of the SDP-OPF model in transmission network is discussed in this section.

$$P_{injk} = X^T Y_k X P_{injk} = T_r[X^T Y_k X] \tag{5.65}$$

Applying the trace operator multiplicity property

$$P_{injk} = T_r[Y_k X X^T] \tag{5.66}$$

Introducing the W matrix

$$W = [XX^T] \tag{5.67}$$

for equ (12) the unit operator K_{th} basis vector was implemented.

$$e_k e_k^T = 1 \tag{5.68}$$

The W matrix can be decomposed into the following

$$W = [R\{V\}I\{V\}]^T[R\{V\}I\{V\}]W = XX^T \tag{5.69}$$

This approach works for rank(W) = 1 and 2 only.

For rank(W)=2, eigen decomposition using Molzahn approach.

$$W_{opt} = \rho_1 E_1 E_1^T + \rho_2 E_2 E_2^T \tag{5.70}$$

$$X_{opt} = \sqrt{\rho_1^{opt}} E_1^{opt} + \sqrt{\rho_2^{opt}} E_2^{opt} \tag{5.71}$$

Where E_1 and E_2 are Eigenvectors, and $\rho\_1, \rho\_2 are the first and second largest absolute eigenvalue of W.$

Finally, we applied Schur's complement, which is used to transform polynomial constraints into quadratic constraints and that the semi-definite constraints equal quadratic constraints. Such that H $\in S^n$

$$H = \begin{bmatrix} X & Y \\ Y^T & P \end{bmatrix} S = P - Y^T X^{-1} Y \tag{5.72}$$

The Schur complement of X in H

- H > 0 if and only if X > 0 and S > 0
- X > 0 then H ≥ 0 and S ≥ 0

The apparent branch flow constraint equations (10e)

$$\begin{bmatrix} -(\bar{S} l_m)^2 & T_r(Y l_m W) & T_r(\bar{Y} l_m W) \\ T_r(Y l_m W) & -1 & 0 \\ T_r(\bar{Y} l_m W) & 0 & -1 \end{bmatrix} \leq 0 \tag{5.73}$$

Applying the multiplicity trace operator

$$T_r(Y l_m W) = (-1) T_r(Y l_m W) \tag{5.74}$$

$$\begin{bmatrix} \bar{S} l_m^2 & T_r(Y l_m W) & T_r(\bar{Y} l_m W) \\ T_r(Y l_m W) & 1 & 0 \\ T_r(\bar{Y} l_m W) & 0 & 1 \end{bmatrix} \geq 0 \tag{5.75}$$

Comparing this with equation (50)

$$\begin{bmatrix} 1 - \frac{T_r(Y l_m W)^2}{S l_m^2} & \frac{T_r(\bar{Y} l_m W) T_r(Y l_m W)}{S l_m^2} \\ \frac{T_r(\bar{Y} l_m W) T_r(Y l_m W)}{S l_m^2} & 1 - \frac{T_r(Y l_m W)^2}{S l_m^2} \end{bmatrix} \geq 0 \tag{5.76}$$

$$\bar{S} l_m^2 - T_r\{Y l_m W^2\} - T_r\{Y l_m W^2\} \geq 0 \tag{5.77}$$

5.3.2 LDR Theorem Proof

In this section, the proof of the LDR- model is discussed and the theorem is proof is shown:

A stochastic model can be formulated as below:

$$\begin{aligned} min \quad & \mathbf{c}'\mathbf{x} + E(Q(\mathbf{x}, \bar{\mathbf{z}})) \\ s.t. \quad & \mathbf{A}\mathbf{x} = \mathbf{b} \\ & \mathbf{x} \geq \mathbf{0} \end{aligned} \tag{5.78}$$

with the $\mathbf{x}$ as vectors and other bold lower case, $\tilde{x}$ as a random variable, bold upper case such as $\mathbf{A}$ are the matrices.

where,

$$\begin{aligned} Q(\mathbf{x}, \mathbf{z}) = min \quad & \mathbf{f}'\mathbf{w} \\ s.t. \quad & \mathbf{T}(\mathbf{z})\mathbf{x} + \mathbf{W}\mathbf{w} = \mathbf{h}(\mathbf{z}), \\ w_i \geq 0, \quad & \forall i \in I \subseteq \{1, ...n_2\} \end{aligned} \tag{5.79}$$

Additionally, $\mathbf{c}$, $\mathbf{f}$ and $\mathbf{b}$ are known vectors in $\Re^{n_1}$, $\Re^{n_2}$ and $\Re^{m_1}$, $\mathbf{T}(\tilde{z})$, $\mathbf{h}(\tilde{z})$ are assumptions for affine data dependency.

$$\mathbf{T}(\bar{\mathbf{z}}) = \mathbf{T^0} + \sum_{\mathbf{k=1}}^{\mathbf{N}} \mathbf{T^k}\tilde{\mathbf{z}}_\mathbf{k}, \quad \mathbf{h}(\tilde{\mathbf{z}}) = \mathbf{h^0} + \sum_{\mathbf{k=1}}^{\mathbf{N}} \mathbf{h^k}\tilde{\mathbf{z}}_\mathbf{k} \tag{5.80}$$

$$\begin{aligned} Z_{STOC} = min \quad & \mathbf{c}'\mathbf{x} + E(\mathbf{f}'\mathbf{w}, (\bar{\mathbf{z}})) \\ s.t. \quad & \mathbf{A}\mathbf{x} = \mathbf{b}, \\ w_i(\tilde{\mathbf{z}}) \geq 0, \quad & \forall i \in I, \\ & \mathbf{x} \geq \mathbf{0} \\ & \mathbf{w}(\tilde{\mathbf{z}}) \in \mathcal{Y} \end{aligned} \tag{5.81}$$

Translating into LDR

$$\mathbf{w}(\bar{z}) = \mathbf{w}^0 + \sum_{k=1}^{N} \mathbf{w}^k \bar{z}_k \tag{5.82}$$

The stochastic model approximation is then written in the LDR

$$\begin{aligned} Z_{LDR} = min \quad & \mathbf{c}'\mathbf{x} + \mathbf{f}'\mathbf{w^0} \\ s.t. \quad & \mathbf{Ax} = \mathbf{b}, \\ \mathbf{T^k x} + \mathbf{W w^k} = \mathbf{h^k} \quad & \forall k \in \{0, ...N\}, \\ w_i(\mathbf{z}) \geq 0 \quad & \forall \mathbf{z} \in W, \forall i \in I, \\ & \mathbf{x} \geq \mathbf{0}, \\ & \mathbf{w}(.) \in \mathcal{L} \end{aligned} \tag{5.83}$$

$$\begin{aligned} & w_i(\mathbf{z}) \geq 0 \quad \forall Z \in W \\ & w_i^0 \geq \sum_{j=1}^{N} (z_j s_j + \tilde{z}_j t_j) \end{aligned} \tag{5.84}$$

If the solution at equation(62) is feasible, then it will be in equation(60), $Z_{STOC} \leq Z_{LDR}$, with $\mathcal{W}$ = [-z, $\tilde{z}$]. for some $\mathbf{s}$,$\mathbf{t} \geq 0$ satisfying s_j-t_j = w_i^j. Relating the above variables and uncertainties to our integrated T&D model, the variable w is the P_{PG}, the variable x is the $\mathrm{P}_{k,RP}$, while the uncertainty $\tilde{Z}$ is the P_{PV}

5.4 Discussion and Performance evaluation

OOur multiperiod implementation was tested on two different networks, and for a 24hr day interval, the same daily load profile and irradiance profile was used for each of the integrated networks, this is as shown in the Fig. 5.6

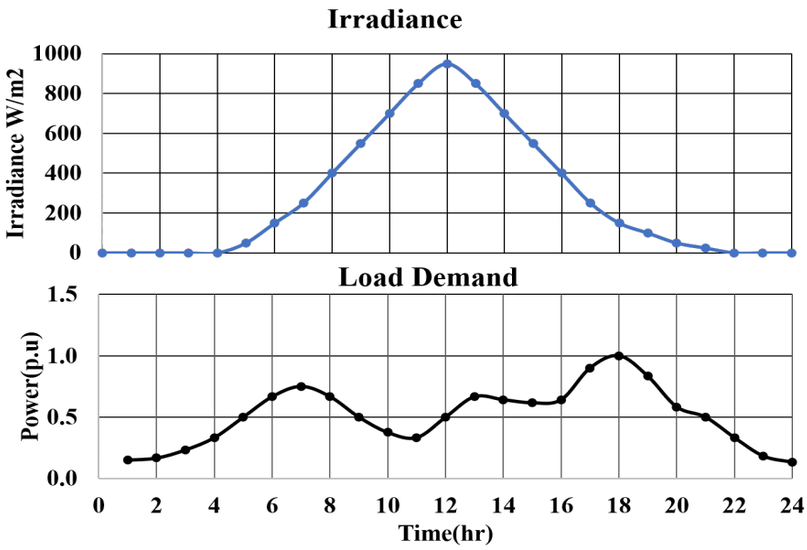

Figure 5.6: irradiance and Load demand profiles for 24hr

5.4.1 Test system IEEE 9 and IEEE 13

We evaluated our technique first on the integrated IEEE 9 & 13 bus system, the system architecture is as shown in Fig. 5.7, with the boundary bus as bus 4. Static OPF analysis

was performed to benched-mark the SDP BIM model with MATPOWER OPF simulation results. The system was modified to enable the changes in the DN to have a significant impact on the TN. A modification was performed on the DN such that 20 times the base load value was connected to the TN, table5.1 shows the linear decision rule relationship after training with over 1000 data sets. The base case simulation with no solarPV connected TN voltages is shown in Fig. 5.8, After the connection the generation cost, boundary voltage error, and the voltage profiles were observed as shown Fig. 5.10, Fig. 5.9 and Fig. 5.11 respectively.

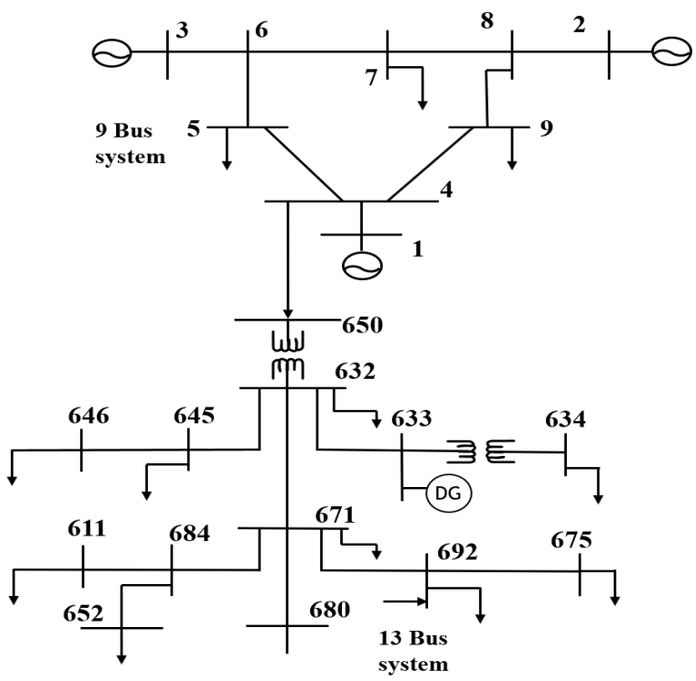

Figure 5.7: Integrated T&D model for IEEE 9bus and IEEE 13bus

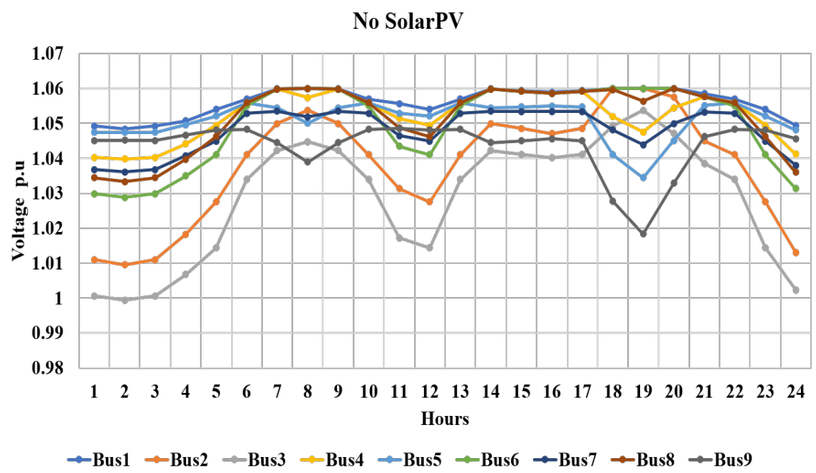

Figure 5.8: 24hr TN bus voltage profiles with no solar PVs connected

The solarPVs were connected to the DN and several simulations were performed on the integrated network, to establish the LDR relationship between the uncertain variables in the network.

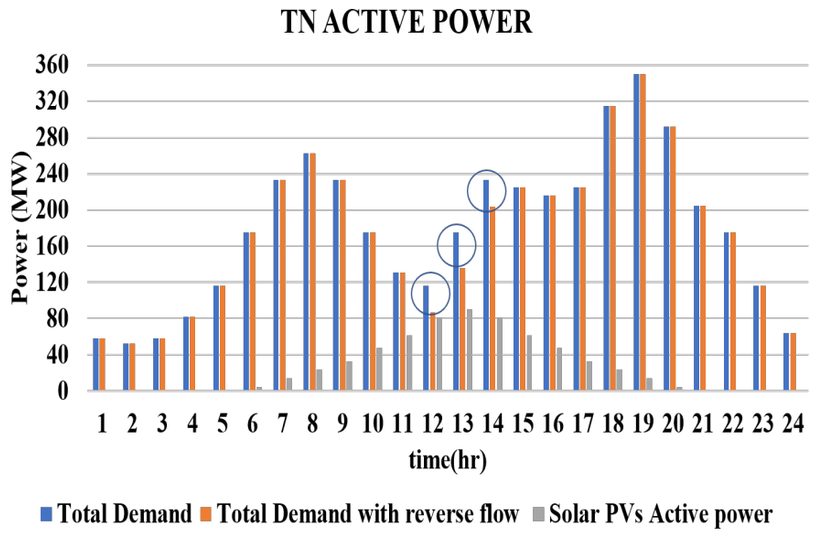

Figure 5.9: Total demand in TN and Total Solar active power

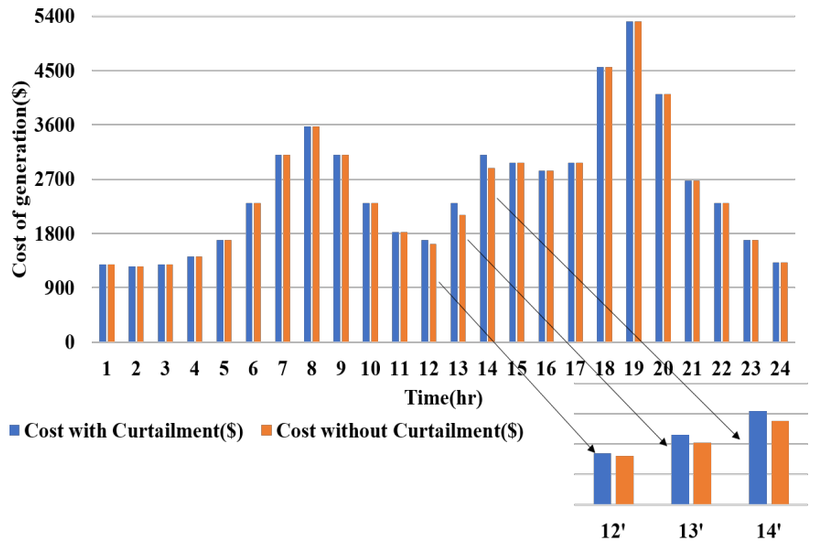

Figure 5.10: Generation cost comparison with and without curtailment

TABLE 5.1: Boundary Bus mismatch voltage deviation

Parameter	Scenario 1	Scenario 2	Scenario 3
Operating hour (hr)	12	13	14
Reverse Power Flow (MW)	43.16	23.48	13.34
Voltage at PCC with LDR(p.u)	1.039	1.038	1.048
Voltage at PCC without LDR(p.u)	1.065	1.060	1.052

5.4.2 Test system IEEE 57 and IEEE 34

Our second test system was integrated IEEE 57 & 34 bus system, the system architecture is as shown in Fig. 5.12with the boundary bus is bus 22, Our static OPF analysis was performed as well to benched-mark the SDP BIM model with MATPOWER OPF simulation results. The system was modified to enable the changes in the DN have a significant impact on the TN. A similar modification on the DN as in the previous case was performed such that 20 times the base load value was obtained was connected to the TN. The Linear decision rule

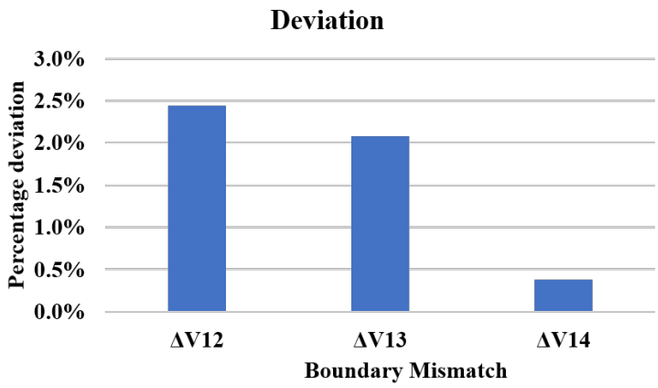

Figure 5.11: Boundary bus mismatch reduction with LDR

parameters were obtained and the constants are shown in the table 5.2. The analysis after integration of the PVs, with respect to generation cost is as shown in Fig. 5.13 and the minimization of boundary voltages mismatch in Fig. 5.14.

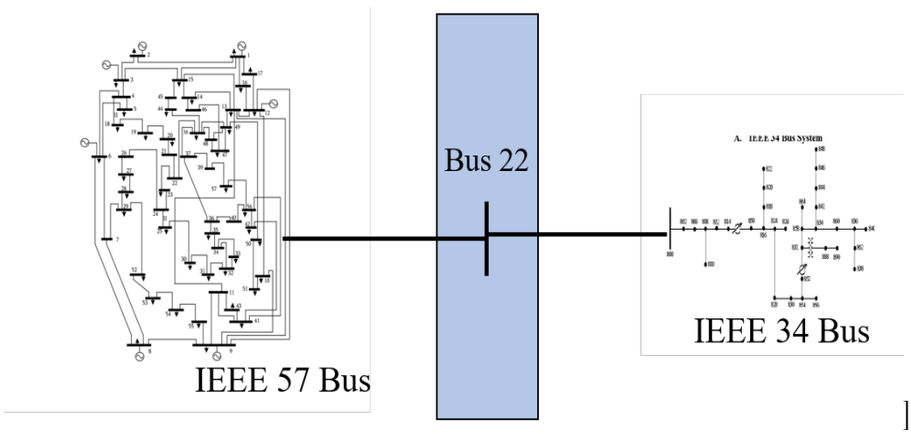

Figure 5.12: Integrated T&D model for IEEE 57bus and IEEE 34bus

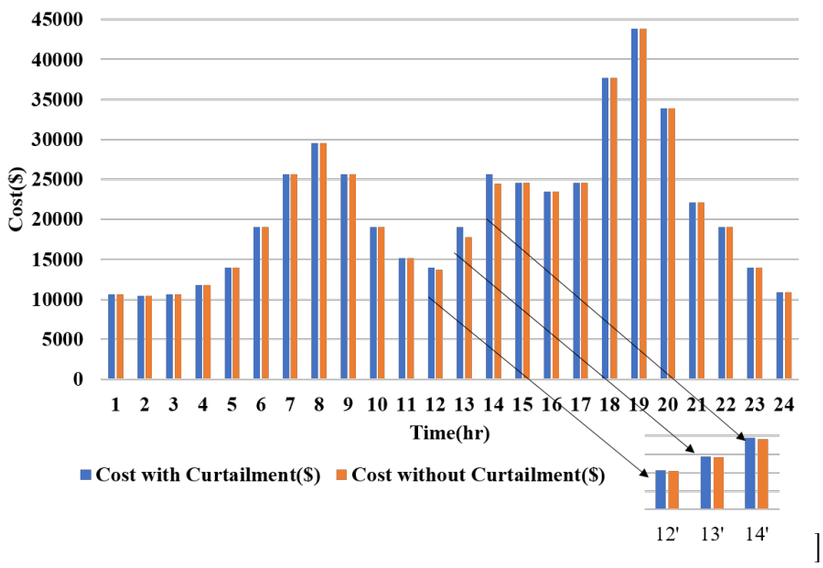

Figure 5.13: Generation cost comparison with and without curtailment

5.4.3 Test system IEEE 118 and IEEE 123

Finally, we evaluated the capabilities of our technique on a larger integrated network which is integrated IEEE 118 & 123 bus system, the system architecture is as shown in Fig.

TABLE 5.2: Boundary Bus mismatch voltage deviation

Parameter	Scenario 1	Scenario 2	Scenario 3
Operating hour (hr)	12	13	14
Reverse Power Flow (MW)	21.03	9.73	4.41
Voltage at PCC with LDR(p.u)	1.021	1.016	1.040
Voltage at PCC without LDR(p.u)	1.060	1.055	1.052

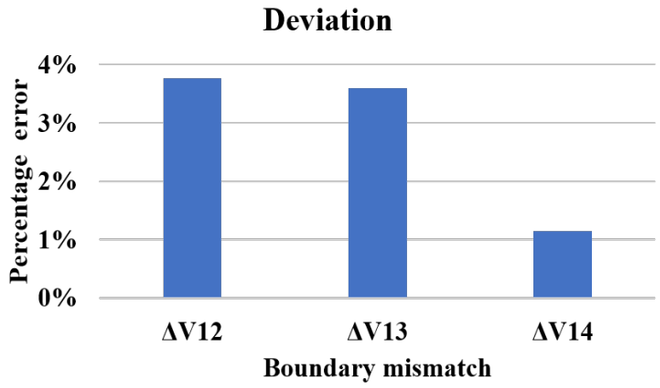

Figure 5.14: Boundary bus mismatch reduction with LDR

5.15with the boundary bus is bus 37, Our static OPF analysis was performed as well to benched-mark the SDP BIM model with MATPOWER OPF simulation results. The system was modified to enable the changes in the DN to have a significant impact on the TN. A similar modification on the DN as in the previous case was performed such that 20 times the base load value was obtained was connected to the TN. The Linear decision rule parameters were obtained and the constants are shown in the table 5.3. The analysis after integration of the PVs, with respect to generation cost is as shown in Fig. 5.17 and the minimization of boundary voltages mismatch in Fig. 5.18.

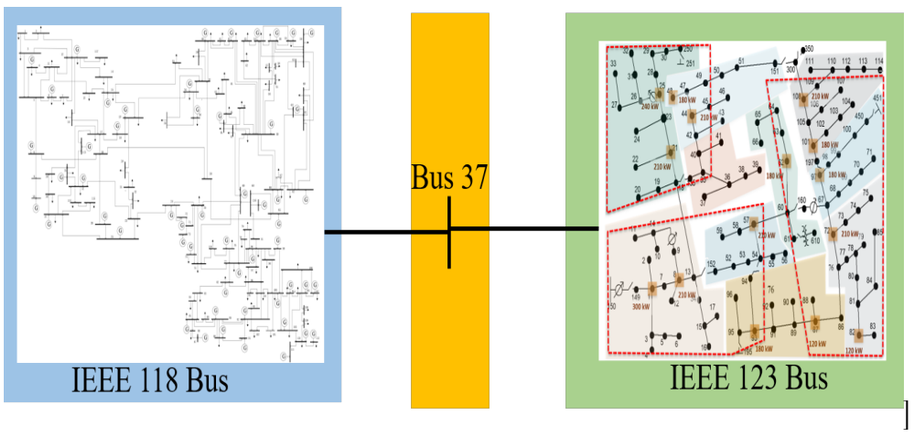

Figure 5.15: Integrated T&D model for IEEE 118bus and IEEE 123bus

5.5 Summary

The versatility of our stochastic linear optimization using the Linear decision rule framework to handle the intermittent nature of renewable energy resources capable of affecting

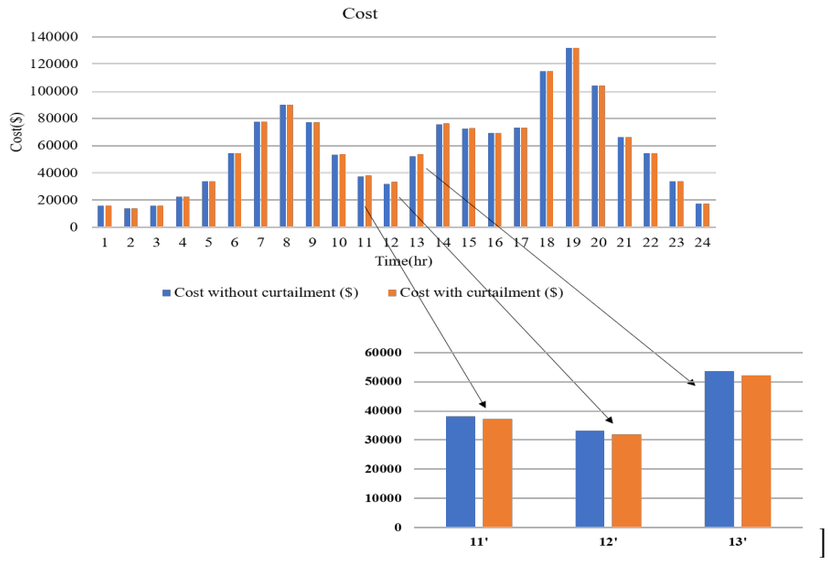

Figure 5.16: Generation cost comparison with and without curtailment

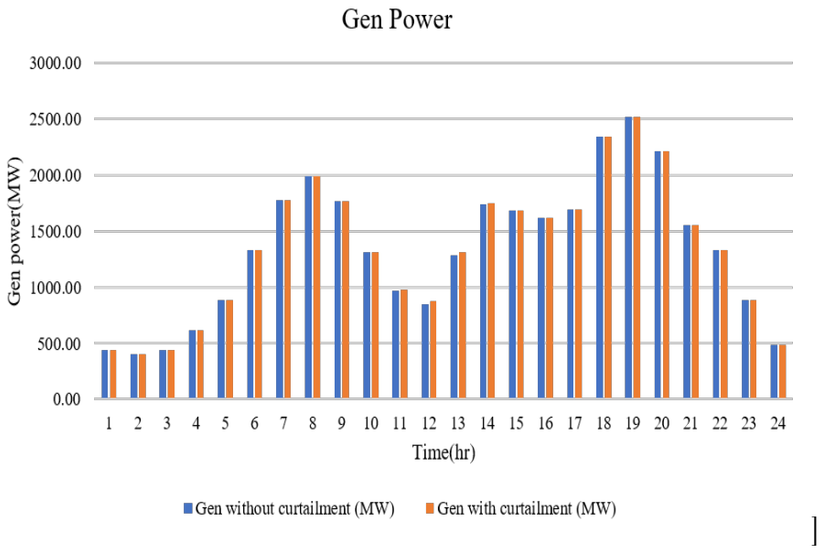

Figure 5.17: TN Generation power comparison with and without curtailment

TABLE 5.3: Boundary Bus mismatch voltage deviation

Parameter	Scenario 1	Scenario 2	Scenario 3
Operating hour (hr)	12	13	14
Reverse Power Flow (MW)	21.03	9.73	4.41
Voltage at PCC with LDR(p.u)	1.021	1.016	1.040
Voltage at PCC without LDR(p.u)	1.060	1.055	1.052

grid quality metrics due to their penetration level at any time was further demonstrated. Our LDR technique ensures that the grid objective for each of the coupled networks is achieved while fully utilizing the offerings of the RERs. Furthermore, it ensures that the TSO now has insights into the operations of the DSO. Allowing more reverse power flow to the transmission network reduces the cost of generation and the proposed approach also shows improvement in the reduction of boundary mismatch errors, by ensuring that the power generated at each interval by the generators in TN adapts to the power generated by the solarPvs with the

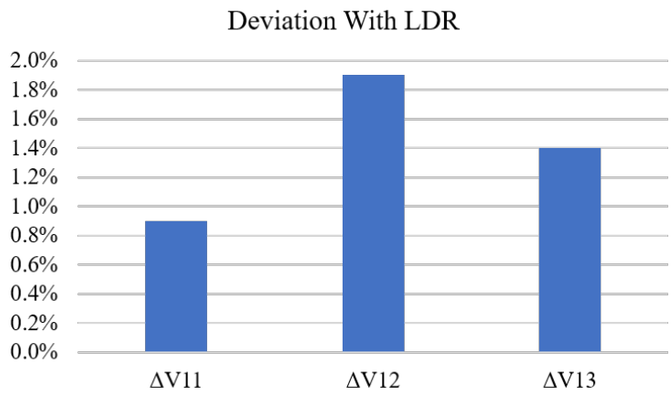

Figure 5.18: Boundary bus mismatch reduction with LDR

linear constraint. Our work will be expanded by adding more uncertainties from other DERs to the integrated grid

CHAPTER 6: TIME REECEDING OPTIMIZATION OF GRID-CONNECTED RERS WITH MULTIPLE UNCERTAINTIES(PVS & ELECTRIC VEHICLES)

Several renewable energy resources are connected to the grid at different intervals, and most of these resources are stochastic in their operations, Electric vehicle is one of the resources that is gaining a lot of traction in the global transportation scene. Plug-in-Electric Vehicles (PEVs) are capable of impacting the grid and a lot of advancements have occurred with electric vehicles such as the Vehicle to grid(V2G), Vehicle to home (V2H) to offer other benefits to utilities for services such as peak shaving, frequency regulations. The impacts of electric vehicle charging need to be studied on networks, and in a large combined manner on the transmission network. Electric vehicles are capable of causing peak-to-peak phenomena or pressure on the grid, during coincidence charging which can have significant impacts on the power grid.

6.1 Management and Coordination of Multiple Grid-Connected Renewable Energy Resources

In this section, a methodology that coordinates the charging of electric vehicles and uses a stochastic optimization framework to manage uncertainties with EV users and other renewable energy resources is developed. The new technique is an extension of our linear optimization work in the previous chapter and an addition of a new variable (new uncertainty), this proof is also shown and discussed in the chapter.

6.1.1 Introduction

The grid now has several resources interacting together with several controls and management techniques. Renewable energy resources (RERs) are one of those new technologies gaining a lot of increasing penetration and traction in the grid. These new technologies are been implemented at generation, transmission, distribution, and even consumption. The technological advancement though offers numerous benefits ranging from sustainability, cost, and environmental benefits.The new technologies coupled with the existing traditional grid are commonly referred to as Smart Grid. Smart Grid comprises distributed energy resources (DERs) which are rapidly increasing in penetration with the existing grid and have led to distributed generation. In [171] studied how the operations EVs can be effectively integrated and how they can play a crucial role in reducing other system impacts and become great resources for smart grid infrastructure. One common phenomenon about these renewable energy resources is their uncertainty or sudden change which can be due to their sources or

the unpredictable nature of humans who have direct control over them and whose decision-making process cannot be accurately forecasted into models or planning by the utilities. The challenges of this occurrence are lately known to have significant effects on the grid, owing to their penetration levels.

Utilitiesâ major goal is to operate the grid in a smooth and reliable manner while meeting the demands of their consumers. However, increasing RERs adoption will influence the demand profile for each distribution network [172–174], posing challenges to its robust operation and infrastructural integrity. For instance, with electric vehicles (EVs) intermittent charging patterns induced by the stochastic operations of several EV users will create load variations and imbalances in the grid components or if several EVs recharge their batteries at the same time, the power grid load impact induced by EV charging scenarios could be outside safe boundaries. Considering these stochastic charging events, the consumption pattern of EV users will have an impact on the energy requirements from the grid causing disruptions, especially with a large number of fleets. In [175] studies were carried out on the infrastructure impact of EV, including system modeling, power flow studies, and demonstration activities utilizing the USC Distribution System as a test system. Since EVs are considered as distributed energy resources this type of mobile energy demand is highly influenced by several factors. These include EV battery State of Charge (SOC), battery type and capacity, charging duration with charge preferences, etc. EVs can be recharged at home or any public charging station with low operational cost given market incentives and regulations. Residential EV charging demand is fairly predictable in nature as the average userâs driving pattern could be identified on a regular basis. However, public EV re-charging scenarios are stochastic and difficult to predict because they are influenced by EV user decisions. Driver behavior is a key factor that determines the energy usage of an EV which is elemental on weather conditions, traffic density, acceleration rate, and maintaining a minimum safe distance between following vehicles. Aside from charging, EV can also supply electricity back to the grid in what we refer to as V2G. V2G is the most promising opportunity to adopt EVs in power systems because of its specific features of feeding energy back to the electric power grid It increases the reliability of power systems and lowers system costs. [176, 177]

Some work has been done to manage the charging of EVs, in [178] an on optimal charging strategy using particle swam optimization(PSO), this focuses more on predicting the charging patterns of EV users, not how to address the uncertainty in charging which is still inherent in EV operations.[179], considered a coordinated charging operation with the status of the charging stations can either be 0 or 1, this is not effective as prevents electric vehicle users from being unsatisfied especially if they need to charge their vehicles urgently. Some of these techniques to coordinate the charging of electric vehicles are complex when there are

to multi-extreme variables or constraints to consider. [180–182]

Determining the Spatial-Temporal Model (STM) of EV charging load across the LV network is critical in the optimal operational efficiency of the entire distribution network. The challenges of large-scale EV integration in the power grid are manifold. First, due to uncontrolled charging schemes adopted by EV users, the power load might increase during peak hours. This can be a source of possible grid failures due to voltage instability, power losses etc. Second, due to the power capacity constraints, the charging stations might not be able to fulfill all EV recharge requests when several EVs recharge at the same time. These interactions between TN and DN pose a complex challenge to the real-time operation and dependencies between the two systems with a higher level of EV penetration, Including the charging load impact of EVs in DN within the mathematical modeling of TN, through coordinated control of coupled networks could improve the operational integrity of the overall system.

Unplanned peak demand issues account for most of the outage issues experienced at the distribution network and since most of these RERs operate as behind-the-meter devices, visibility is important to balance the economic advantages with utility reliability. The economic and sustainability benefits of renewable energy resources are currently been utilized largely by utilities so several strategies are used to ensure an efficient operation of the modern grid. Some legacy devices such as voltage regulators, capacitor banks, smart inverters, and smart switches are currently been used to address the challenges of operating a grid connected with different RERs. Another is the curtailment of RERs during such scenarios when they are posing challenges on the interconnected grid which is typically known as islanding.

Wang et al. in [183] optimized the level of electric vehicle charging station directly, and the coordinated scheduling of wind power and electric vehicle charging is studied in this chapter, however, the established model only constrains the node voltage and transmission power, no constraint considering charging time or charging capacity. Other studies have investigated the effects of large-scale EV integration on power systems. Studies have been done Integrated simulation-based approach to model road traffic and EV battery charging using Multi-agent systems. However, more emphasis has been made on EV agentâs characteristics and behavioral modeling rather than the interrelation between TN and DN. Details of distributed charging station services are not included in the electricity grid. We try to bridge the research gap by considering several aspects of stochastic EV agent behavioral profiles and coupling TN with DN. Moreover, for calculating the cost function of travel time based on traffic flow in transportation network modeling, the current state-of-the-art research in optimal operation of interdependent transportation-power network systems is based on a graph network approach where nodes and edges are represented as the interlinking elements.

The functional characteristic metrics of both TN and PDN are measured by considering methods of network analysis.

Utilities make use of either power flow or optimal power flow (for specific objectives) simulations to keep the grid operating in an efficient manner, to improve the performance of an integrated network that has heterogenous boundary elements visibility is important. This chapter is a further extension of our work [170] where we considered only one RERs, we have extended our work to handle multiple resources and demonstrated the benefits of ensuring that the generators on the transmission network have insights into the real-time solar PV power output and charging dispatch for the charging stations.

6.1.2 Main Contributions

The main advantages the technique developed in this section include

- Coordination of Electric vehicle charging in the grid.
- Minimization of generation cost due to increased demand by multiple RERs.
- Co-simulation of transmission and distribution network and ensuring no violation of grid power quality metrics.

The main contribution of this section includes the following:

- A technique that selects the optimal dispatch control for charging stations.
- Minimization of voltage boundary errors in an integrated T&D model.
- Management of the stochastic nature of several grid-connected renewable energy resources in an integrated T&D network.

6.1.3 Previous and Current Model Challenges

Presently, most utilities perform coordination of the transmission network and distribution network separately, in some of our previous work we have established a simulation technique that offers the capabilities to co-simulate both networks and ensure adequate sharing of information. in [138,139] we considered a steady state simulation analysis, while in [138,139], the simulation was performed in a multiplied framework. Most of this previous work isn't capable of accommodating multiple renewable energy resources that are stochastic in nature, especially with the introduction of electric vehicles. Additional utilities are looking for active ways to control the charging of electric vehicles to manage their stochastic load demand and reduce the operation cost incurred by utilities to meet the growing demand for electricity, as well as reduce the strain on the grid. Here is a structure of what the grid now looks like with many renewable energy resources interplaying[138,139] as shown in Fig. 6.1.

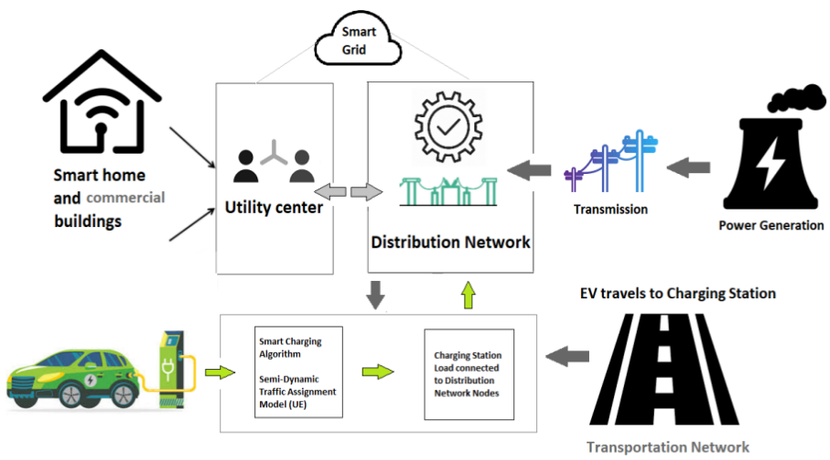

Figure 6.1: Grid integration of Electric Vehicles with RERs

6.1.3.1 Case study Architecture

The architecture comprises of agents; which can either be the EV agent which collects the information of the EV like the battery size and state of charge SOC, also the scheduling agents which determine the decision of integrated T&D optimal power flow, lastly the charging agent which determines the flow of energy when charging.

The load curve is based on INL electric vehicle charging curve for a residential consumer, which provided us with the peak charging time of most electric vehicle users in a 24-hour period.

First, we determine the aggregate charging bus in the distribution network and apply the constraint shown in the equation below.

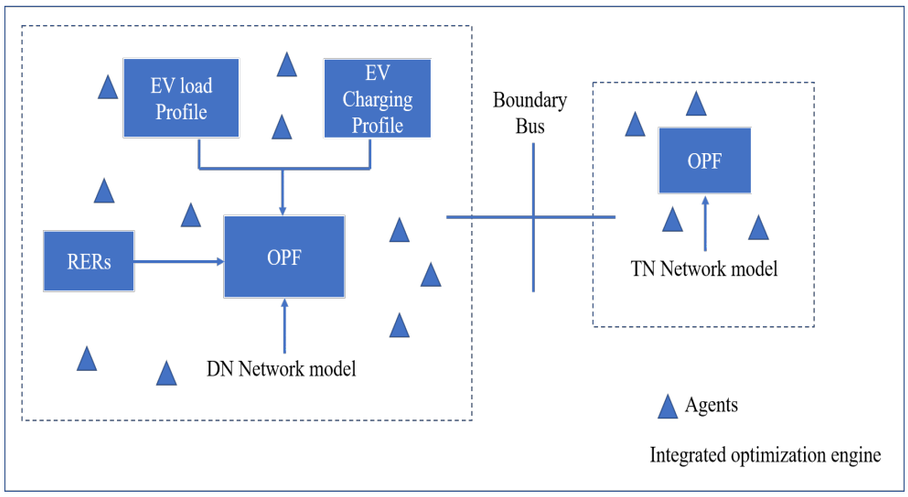

Figure 6.2: Proposed Architecture with Agents

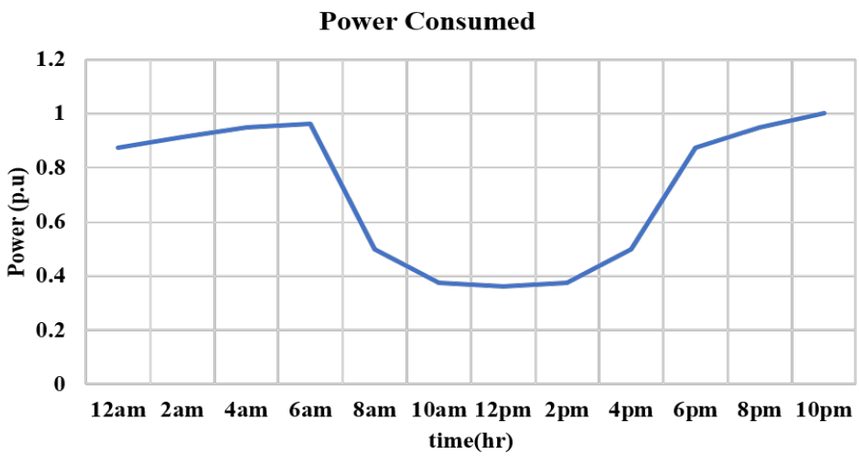

Figure 6.3: INL Electric Vehicle residential daily load curve

$$\forall \quad t = \{1, ...24\}, P_{agg}(t) \leq min \sum_{n=1}^{k} Pc_n \tag{6.1}$$

$$P_{agg}(t) = min \sum_{t=1}^{ev} P_{ev}(t) \tag{6.2}$$

6.1.4 LDR technique with multiple RERs

A stochastic linear optimization technique that allows the transmission network assets to adjust itself to the operations of the distribution network was developed. Our formulation is based on a two-stage complete recourse model, for the purpose of this work two renewable energy resources (solarPV and electric vehicles) are considered.

The objectives of each network are written below and the proof is detailed in the appendix, the TN has the objective of minimizing the cost of generation while the DN is to minimize the losses in the system.

Algorithm 10: Optimization steps for IOE

```
-
Initialize the data for all the devices in the integrated network.
Determine the EVs aggregate bus in the distribution network.
Obtain the parameters t_p for TN and d_p for DN
while tol > ϵ do
    forall t ∈ 24 do
        forall t_p ∈ TN do
            Solve the TOPF using SDP-BIM.
            Extract the simulation results. (Voltage and angle)
            Check if any bus voltage in TN is violated
            if yes, apply LDR, else
            Use the boundary bus parameters as setpoints for the DN feeder
        end
        forall d_p ∈ DN do
            Solve the DOPF using SDP-BFM.
            Extract the total demand with losses at DN
            Update the DN load demand at PCC of the integrated network.
        end
    end
    Obtain the new tolerance tol
    Check for convergence.
end
```

$$TOPF = min \sum_{t=1}^{T_t} \sum_{g=1}^{N_G} (f(P_{m,t}^g)) \tag{6.3}$$

$$where, f(P_{m,t}^g) = c_2(P_{m,t}^g)^2 + c_1(P_{m,t}^g) + c_0(t) \tag{6.4}$$

$$DOPF = min \sum_{t=1}^{T_t} Re(S_{ij}(t) - Z_{ij} I_{ij}^2(t)) \tag{6.5}$$

In the transmission network, active power generated is a combination of power flowing in the lines in the network P_{mn}, the line losses P_{mn}^{loss}, and the power $\mathrm{P}_{m,RP}^{M}$ from TN to DN through the boundary bus.

$$P_m^g(t) = \sum_{n:m\longrightarrow n} P_{mn}^M(t) + \sum_{n:m\longrightarrow n} P_{mn,loss}^M(t) + P_{m,RP}^M(t) \tag{6.6}$$

From the distribution system slave network, the reverse power is obtained as below

$$S_{m,RP}^M(t) = S_S(t) + S_{agg}(t) - S_{pv}(t) \tag{6.7}$$

$$P_{m,RP}^M(t) = Re(S_{m,RP}^M(t)) \tag{6.8}$$

$$S_S(t) = S_S^{load}(t) + S_S^{losses}(t) \tag{6.9}$$

Note that if $P_{m,RP}^M(t) > 0$ then it is an active power demand and not a reverse power flow.

$$Initialization : S_{m,RP}^{M(0)} = S_{S}^{load(0)} \tag{6.10}$$

$$DNfeedervoltage : u_{0}^{abc} = 1.0 \tag{6.11}$$

$$Min \quad \Delta V_{pcc}(t) = V_{m}^{pcc}(t) - u_{0}^{abc}(t) \tag{6.12}$$

Solar PV using its apparent, real, and reactive power is modeled as shown in equ(6).

$$S_{pv}^{2}(t) = P_{pv}^{2}(t) + Q_{pv}^{2}(t) \tag{6.13}$$

A linear decision rule (LDR) technique is one of the frameworks for stochastic optimization, this is a set of rules obtained after performing several analysis of the RERs in an integrated OPF, and a multilinear regression model (MLR) is then developed based on the sample results to obtain the relationship below.

$$Y = a + bX + mC \tag{6.14}$$

In (6.14, Y represents transmission network generators' active power for a specific bus k P_{k}^{g}, and X is the P_{pv} active power generated by the solar PVs, while P_{agg} is the charging capacity demand by all the electric vehicles. The representation to accommodate several generators and several RERs can therefore be written as the equation below. For this study, our RERs used are solar PV and electric vehicles, the uncertainty with these resources can either be with the sources of the resources or individual customer action. k is the bus the generator is connected to in the TN,i is the bus the solar PV is connected to in the DN, while i is the bus in which the charging station aggregator is connected. Furthermore, a, b and m are constants in the equation deduced after several sampling. Thus,

$$P_{k}^{g} = a + bP_{i,pv} + mP_{j,agg} \tag{6.15}$$

6.1.5 Results and Discussion

An analysis was performed on two different integrated networks with, and for a 24hr day interval, the load profile as shown below was implemented, irradiance profile, and EV charging curve were used for each of the integrated networks.

6.1.6 Test system IEEE 9 and IEEE 13

The LDR technique with multiple resources was evaluated first on the integrated IEEE 9 & 13 bus system, the system architecture is as shown in Fig. 6.5, with the boundary bus on the TN as bus 4. The integrated system was modified to enable the changes in the DN

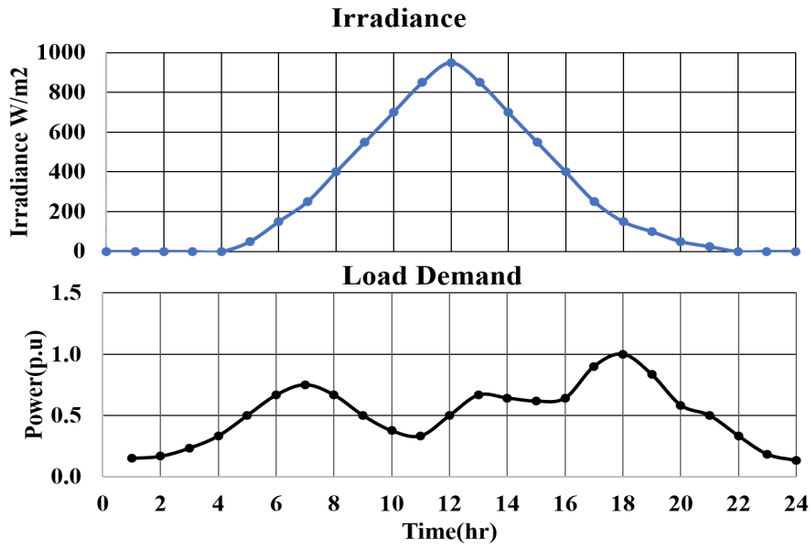

Figure 6.4: irradiance and Load demand profiles for 24hr

to have a significant impact on the TN. A modification was performed on the DN such that 20 times the base load value was connected to the TN. The base case simulation was done with no solarPV and electric vehicles connected to the integrated network and the power generated is shown in Fig. 6.8, After the connection the generation cost, total demand, and boundary voltage error were observed as shown Fig. 6.9, Fig. 6.10 and Fig. 6.13 respectively.

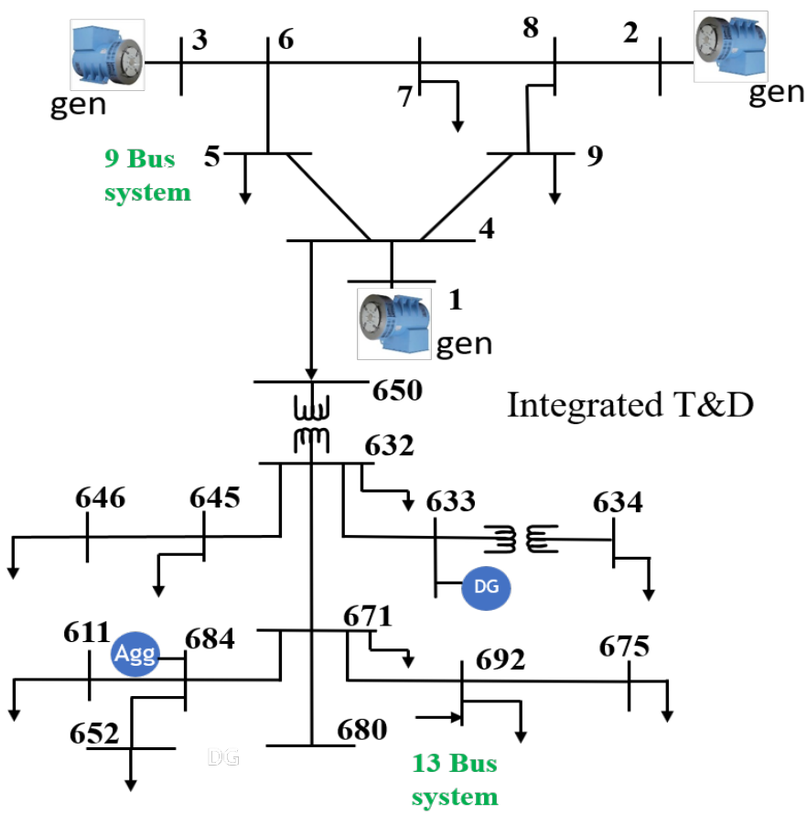

Figure 6.5: Integrated IEEE 9bus and IEEE 13bus T&D model

First, we needed to validate our formulation with the conventional NLP OPF for each network using our formulation, by performing static OPF analysis was performed to benchedmark the SDP BIM model with MATPOWER OPF NLP simulation results.

Fig. 6.6 illustrate the comparison between the TN part of the proposed integrated SILP

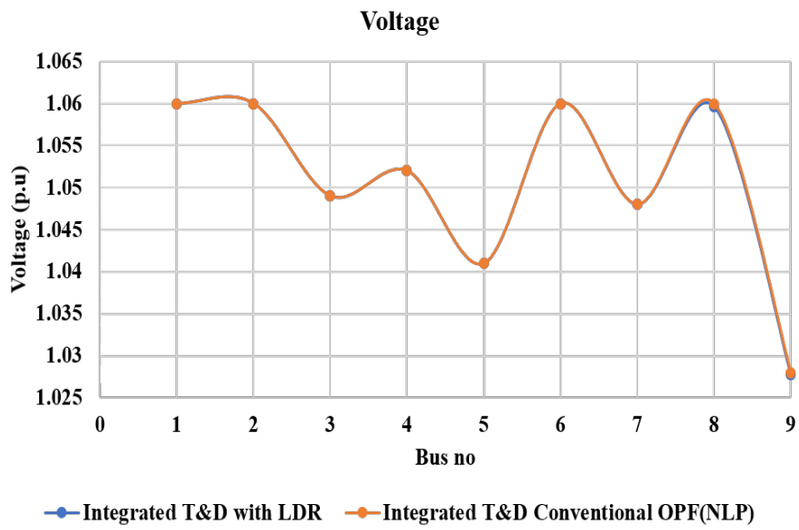

Figure 6.6: Voltage profile for IEEE 9 bus TN compared to the state-of-the-art

model and a stand alone conventional NLP model. It can be seen the voltage profile almost matches with the conventional NLP which shows the exactness of the SILP.

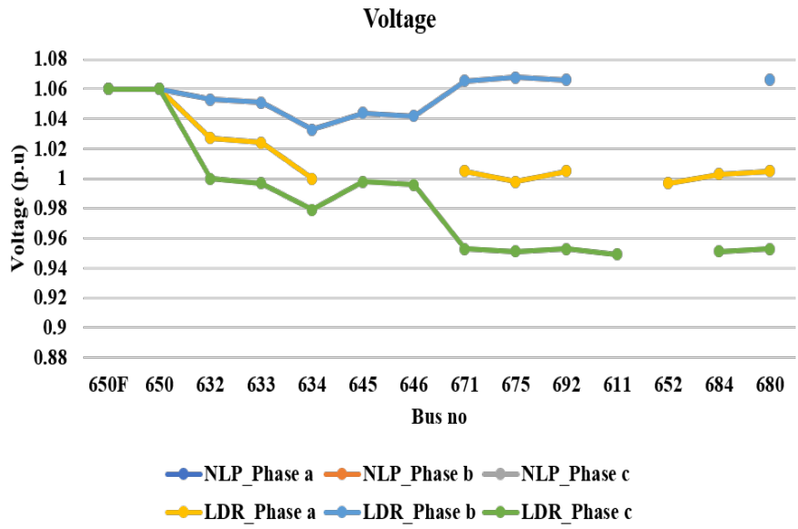

Figure 6.7: Voltage profile for IEEE 13 bus DN compared to the state-of-the-art

Similarly, Fig. 6.7 illustrate the comparison between the DN part of the proposed integrated SILP model and a stand alone conventional NLP model. It can be seen the voltage profile almost matches with the conventional NLP which shows the exactness of the SILP showing the exactness.

The solarPVs were connected to the DN to the bus 633, while the electric vehicle aggregator was connected to bus 684 on the DN, and several simulations were performed on the integrated network, to establish the LDR relationship between the uncertain variables in the network as seen in table6.1 shows the linear decision rule relationship after training with over 1000 data sets.

Finally, we observed the sudden change in the behavior of charging an electric vehicle and its impact on the grid, the changes in the behavior of charging occurred when the Solar PVS was operating at its optimum capacity leading to a higher reverse power flow. The LDR

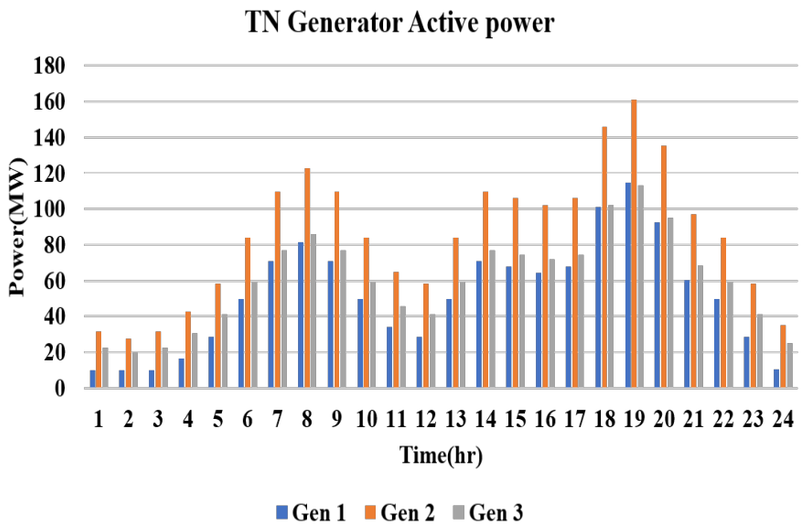

Figure 6.8: 24hr TN bus power demand with no DERs connected

TABLE 6.1: LDR relationship between the TN generator, Solar PVs, and EV charging aggregator

Generator	Bus No	a	b	m
1	1	109.53	-0.117	0.023
2	2	155.67	-0.131	0.065
3	3	109.12	-0.091	0.042

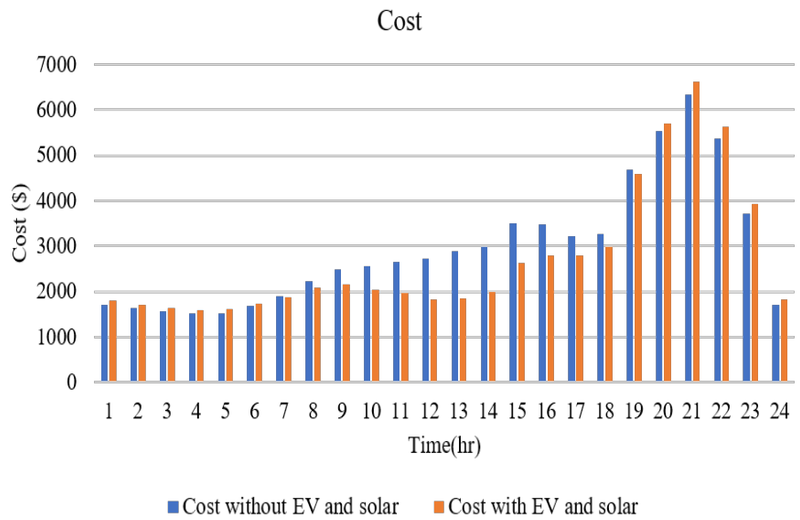

Figure 6.9: Generation cost comparison with and without RERs connection

technique was able to provide the generators with insights into the charging operations and output capacity which led to the reduction in boundary bus mismatch.

6.1.7 Test system IEEE 57 and IEEE 34

We extended the LDR technique with multiple resources to another integrated network IEEE 57 & 34 bus system, the system architecture is as shown in Fig. 6.14, with the boundary bus on the TN as bus 22. The integrated system was modified to enable the changes in the DN to have a significant impact on the TN. Similarly, a modification was performed on the DN such that 20 times the base load value was connected to the TN as well as a base case simulation with no solarPV and electric vehicles connected to the integrated network,

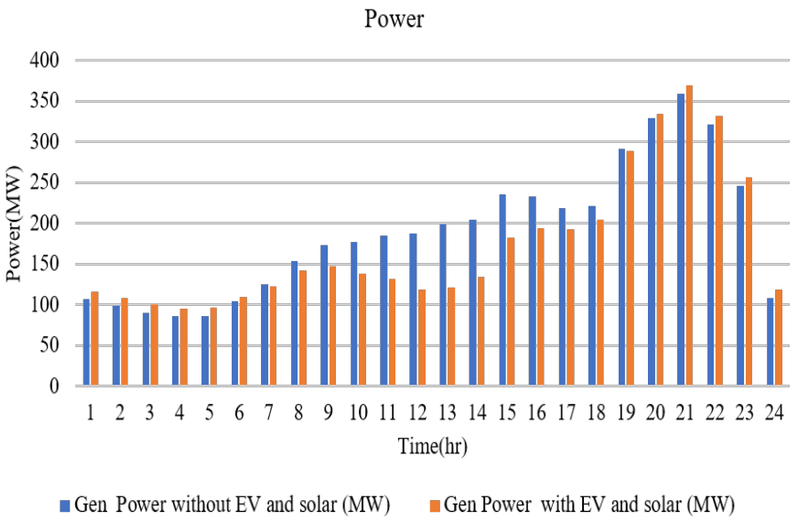

Figure 6.10: Total generation in TN with and without RERs connection

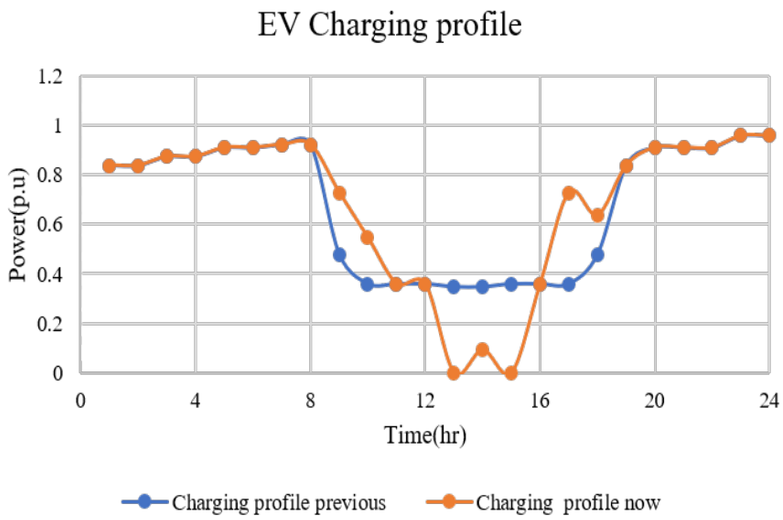

Figure 6.11: EV charging profiles expected and sudden

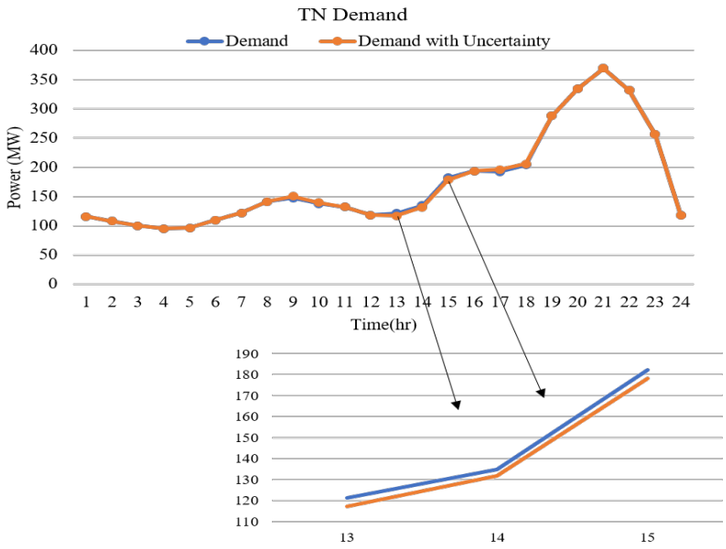

Figure 6.12: Total demand in TN before and after sudden operations

the power generated is shown in Fig. 6.17, After the connection the generation cost, power generation, and boundary voltage error were observed as shown Fig. 6.18, Fig. 6.19 and Fig. 6.22 respectively.

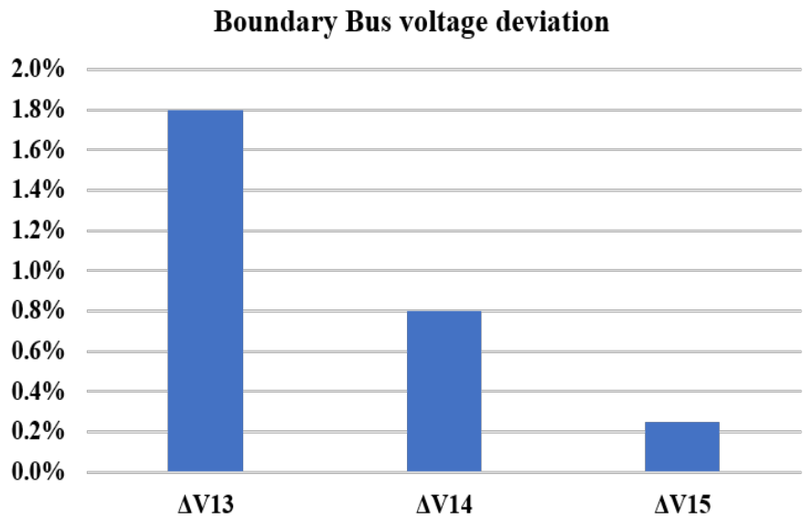

Figure 6.13: Boundary bus mismatch reduction with LDR

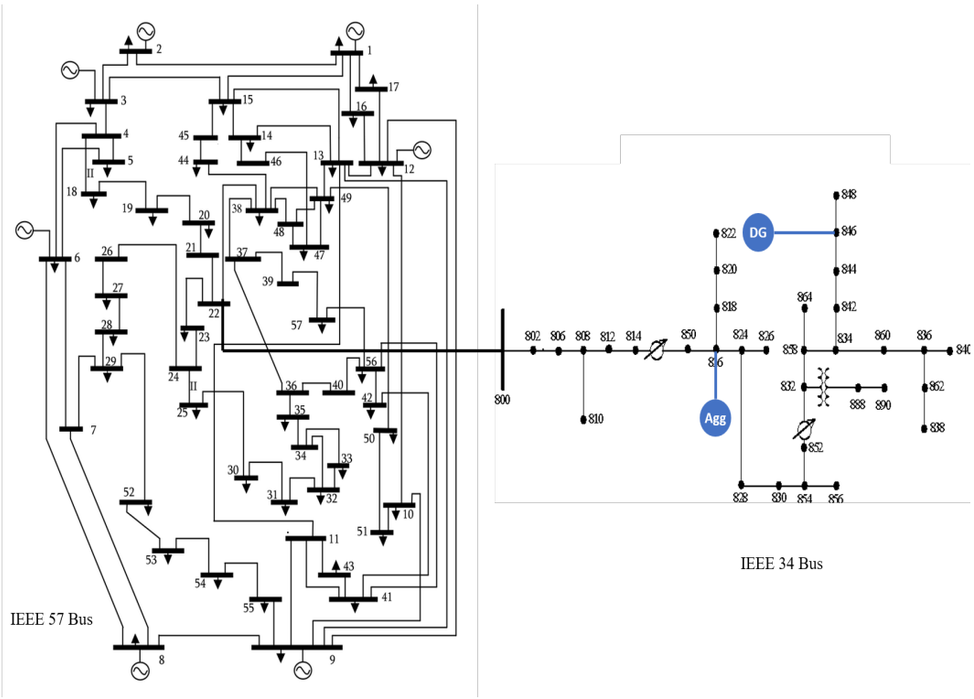

Figure 6.14: Integrated IEEE 57bus and IEEE 34bus T&D model with the interconnection of solarPV and Electric vehicle aggregator

Fig. 6.15 illustrate the comparison between the TN part of the proposed integrated SILP model and a stand alone conventional NLP model. It can be seen the voltage profile almost matches with the conventional NLP which shows the exactness of the SILP.

Similarly, Fig. 6.16 illustrates the comparison between the DN part of the proposed integrated SILP model and a stand-alone conventional NLP model. It can be seen the voltage profile almost matches with the conventional NLP which shows the exactness of the SILP showing the exactness.

The solarPVs were connected to the DN to the bus 828, while the electric vehicle aggregator was connected to bus 816 on the DN, and likewise, several simulations were performed on the integrated network, to establish the LDR relationship between the uncertain variables in the network as seen in table6.2 shows the linear decision rule relationship after training

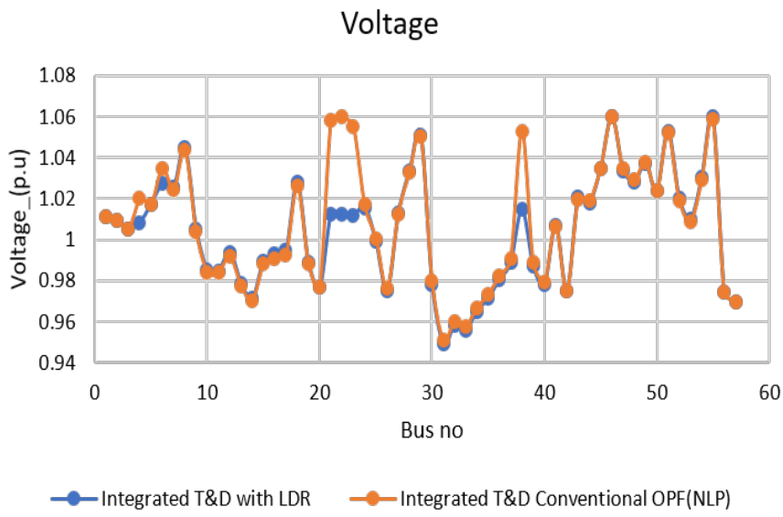

Figure 6.15: Voltage profile for IEEE 57 bus TN compared to the state-of-the-art

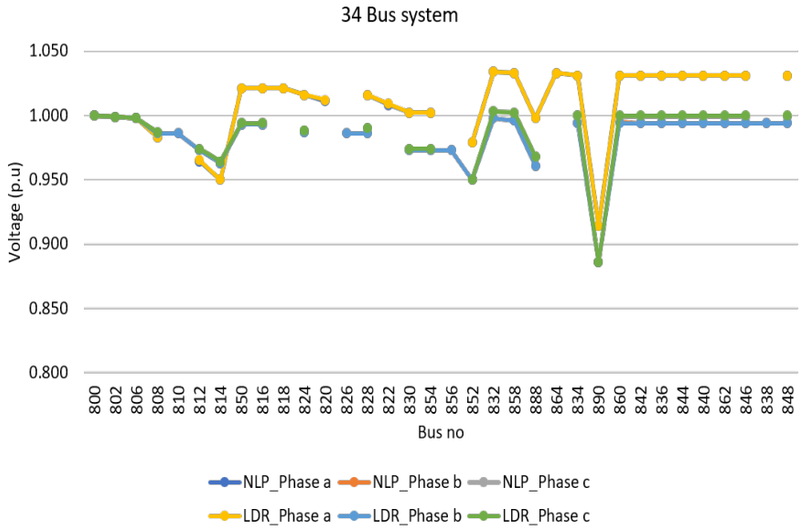

Figure 6.16: Voltage profile for IEEE 34 bus DN compared to the state-of-the-art

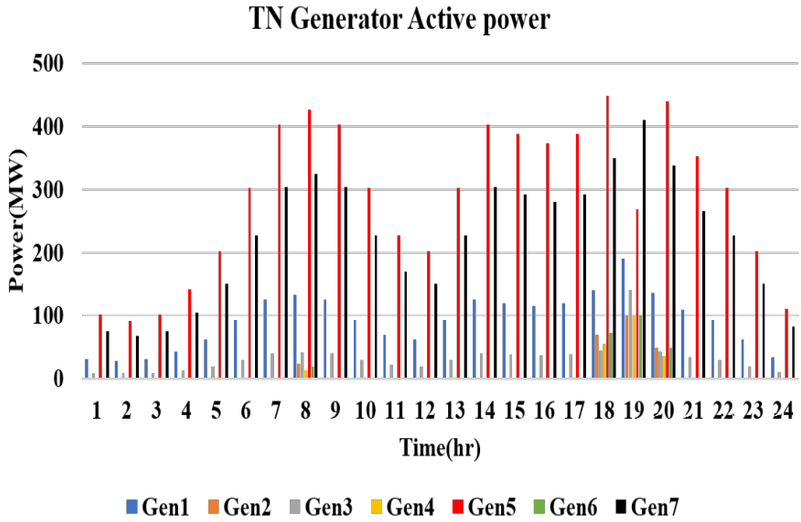

Figure 6.17: 24hr TN bus power demand with no DERs connected

with over 1000 data sets

Finally, we observed the sudden change in the behavior of charging an electric vehicle and its impact on the grid, the changes in the behavior of charging occurred when the Solar PVS

TABLE 6.2: LDR relationship between the TN generator, Solar PVs and EV charging aggregator

Generator	Bus No	a	b	m
1	1	106.312	-0.561	-0.261
2	2	99.989	-0.296	-0.096
3	3	56.895	-0.280	-0.115
4	6	65.476	0.168	0.09
5	8	410.465	1.164	0.571
6	9	100.021	-0.069	-0.003
7	12	420.504	-5.794	-1.005

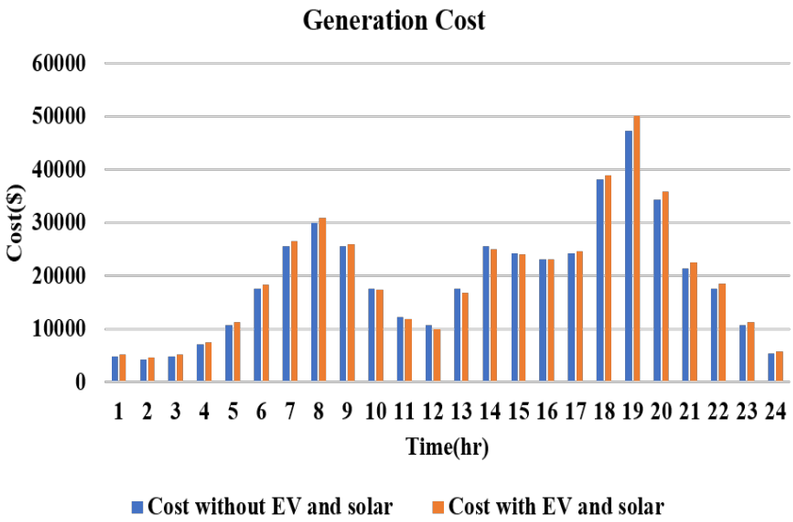

Figure 6.18: Generation cost comparison with and without RERs connection

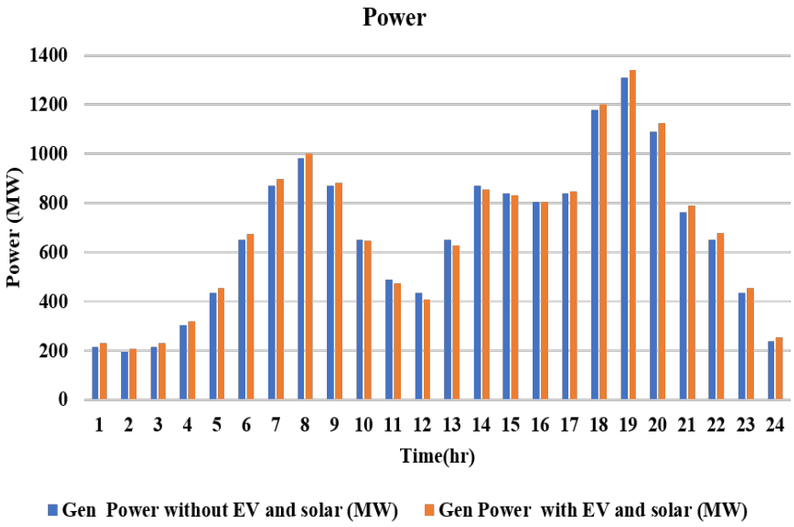

Figure 6.19: Total generation in TN with and without RERs connection

was operating at its optimum capacity leading to a higher reverse power flow. The LDR technique was able to provide the generators with insights into the charging operations and output capacity which led to the reduction in boundary bus mismatch.

6.2 Management of Electric Vehicle Charging Impact on an Integrated Transmission and Distribution Grid

Electric Vehicle is one of the major players in the decarbonization of the grid and tackling climate change calls for the transformation of public transport into a smart electric trans-

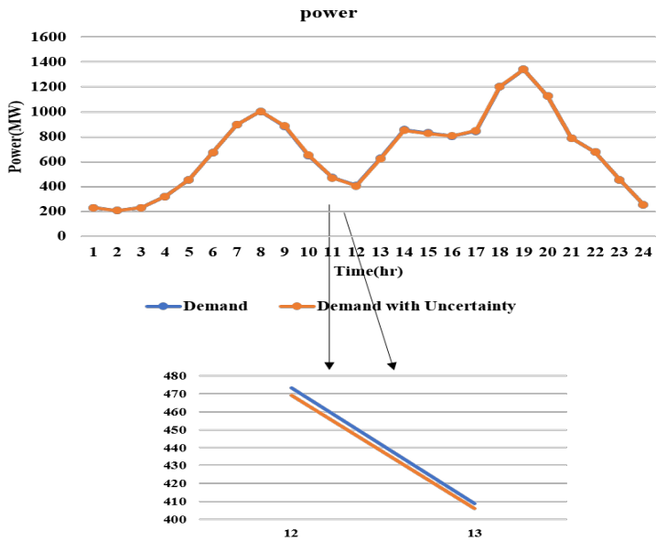

Figure 6.20: Total demand in TN before and after sudden operations

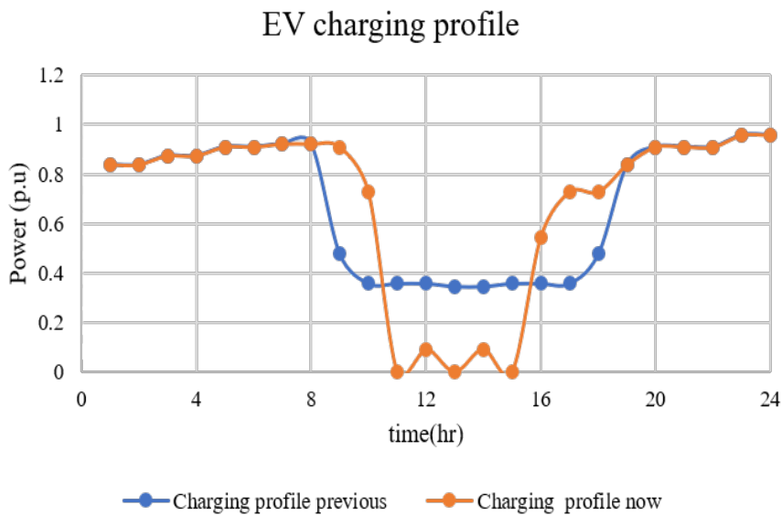

Figure 6.21: EV charging profiles expected and sudden

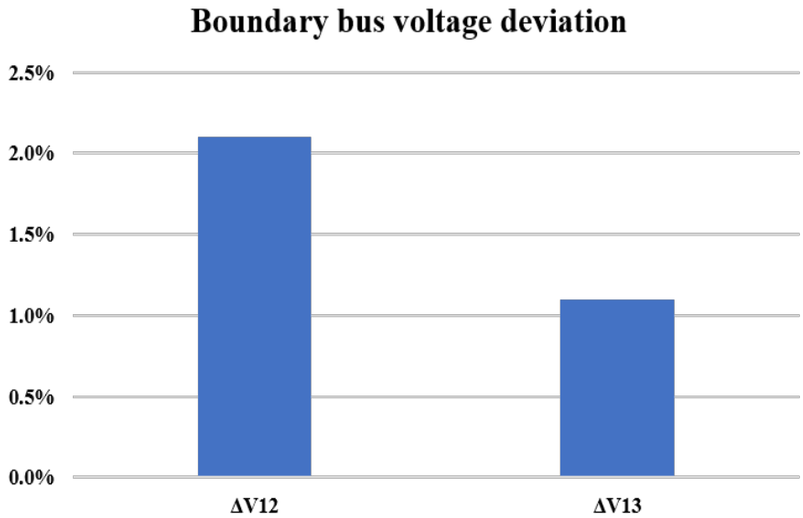

Figure 6.22: Boundary bus mismatch reduction with LDR

portation network, EVs use electrical energy to recharge their batteries instead of burning fossil fuels. Battery technology has grown significantly[177, 184, 185] which has led to the increased adoption of Electric vehicles (EVs) as one of its main applications. A larger EV

penetration will require the installation of more charging stations deployed strategically to meet the demands of EV movement and charging behavior without depleting the EV battery entirely. Also, when several EVs recharge their batteries at the same time, the power grid load impact induced by EV charging scenarios could be outside safe boundaries. Presently, the lack of EV charging station infrastructure is a roadblock to successful EV adoption. In the future, this might not be the case as more EVs are deployed and integrated into the smart grid. Thus, it becomes increasingly necessary to investigate and quantify the load impact by combining mobility needs with the power system infrastructure. Grid operation solutions known as optimal power solutions, therefore need to consider electric vehicles in their models as one of the critical issues in power operation. EVs can contribute economically and enhance the security of the power grid due to their flexibility owing to their energy storage or charging controls, where they can be used to fill load valleys or for intermittent generation[186–188]. However, since electric vehicles operate as behind-the-meter devices, visibility is important to balance the economic advantages with electric system reliability. Utilitiesâ major goal is to operate the grid in a smooth and reliable manner while meeting the demands of their consumers. However, increasing EV adoption will add a significant load to the demand profile for each distribution network, posing challenges to its robust operation and infrastructural integrity. The various influencing factors that could impact the EV charging load have paramount importance in modeling grid stability[189]. Intermittent charging patterns induced by the stochastic operations of several EV users will create load variations and imbalances in the grid metrics [190]. Since EVs are considered as distributed energy resources this type of mobile energy demand is highly influenced by several factors. These include EV battery State of Charge (SOC), battery type and capacity, charging duration with charge preferences, etc. EVs can be recharged at home or any public charging station with low operational cost given market incentives and regulations. Residential EV charging demand is fairly predictable in nature as the average userâs driving pattern could be identified on a regular basis. However, public EV re-charging scenarios are stochastic and difficult to predict because they are influenced by EV user decisions. Driver behavior is a key factor that determines the energy usage of an EV which is elemental on weather conditions, traffic density, acceleration rate, and maintaining a minimum safe distance between following vehicles. When several EVs charge simultaneously, there might be severe consequences on the power grid as a huge load is drawn from fast charging stations. The likelihood of rapid EV adoption and the potential shift to an electric transportation system is a major concern for power systems. Mitigating the peak demand through optimized charging strategies is a key solution to not overload the power grid. The impact on the distribution systems accounts for 90% of outages and with the introduction of EV charging load, it will likely increase the

energy impact hence posing a challenge to the stability of the grid. [191], [192]. Determining the Spatial-Temporal Model (STM) of EV charging load across the LV network is critical for the optimal operational efficiency of the entire distribution network. The challenges of large-scale EV integration in the power grid are manifold. First, due to uncontrolled charging schemes adopted by EV users, the power load might increase during peak hours. This can be a source of possible grid failures due to voltage instability, power losses etc. Second, due to the power capacity constraints, the charging stations might not be able to fulfill all EV recharge requests when several EVs recharge at the same time. These interactions between TN and DN pose a complex challenge to the real-time operation and dependencies between the two systems with a higher level of EV penetration, Including the charging load impact of EVs in DN within the mathematical modeling of TN, through coordinated control of coupled networks could improve the operational integrity of the overall system. Thus, coupled systems play an important role in the smart grid ecosystem energy market. Several authors have investigated the effects of large-scale EV integration on power systems. Some studies have been performed on the impacts of electric vehicles on the distribution grid in [190] demonstrated its impact on the secondary voltage of feeders with short circuit capacity. Studies have been done Integrated simulation-based approach to model road traffic and EV battery charging using Multi-agent systems. However, more emphasis has been made on EV agentâs characteristics and behavioral modeling rather than the interrelation between TN and DN. Details of distributed charging station services are not included in the electricity grid. We try to bridge the research gap by considering several aspects of stochastic EV agent behavioral profiles and coupling TN with DN. Moreover, for calculating the cost function of travel time based on traffic flow in transportation network modeling, the current state-of-the-art research in optimal operation of interdependent transportation-power network systems is based on a graph network approach where nodes and edges are represented as the interlinking elements. The functional characteristic metrics of both TN and PDN are measured by considering methods of network analysis. We have combined the optimal power flow solution and an optimization framework to control the charging of EVs, by providing set points through an aggregate controller which is the charging station, and performed a comparative analysis on active and passive controls.

6.2.1 Main Contributions

The technique developed in this section has the following advantages

- Ensures that the energy demand required for electric vehicle charging is met daily.
- Reduces the likelihood of stress on the grid caused by electric vehicles.
- Co-simulation of transmission and distribution network and ensuring no violation of

grid power quality metrics.

The technique main contributions are thus:

- A technique that coordinates the electric charging optimally, to ensure that each electric vehicle load demand is met daily.
- An optimal setpoint control (Passive/ Active) technique for charging stations that allows utilities to participate in coordinating the operations of electric vehicle charging and can assist with integrated resource planning.
- Management of the stochastic nature of EVs charging in an integrated T&D network, our technique ensures that EV's sudden charging behaviors are well managed.

6.2.2 Current Approach

Utilities have the responsibility to ensure that demand is met at all times, bearing in mind the security and stability of the grid. Demand response techniques using customer-side resources have been one of the measures utilities are using to meet the growing demand rather than build new power generation plants or run expensive generators. Since electric vehicles are connected to the distribution network, it is important to develop an integrated T&D model to study its impacts on both transmission and distribution network resources. In the previous chapters, we discussed extensively integrated T&D using an optimization framework (Linear decision rule), using the fundamentals of a heterogeneous network in [138, 139]. Utilities are looking for active ways to control the charging of electric vehicles to manage their stochastic load demand and reduce the operation cost incurred by utilities to meet the growing demand for electricity, as well as reduce the strain on the grid. Here is a structure of what the grid now looks like with respect to EV charging and different controls interplaying at the device level shown in Fig. 6.24.

6.2.2.1 Case studies

Firstly, an analysis was performed to determine the load profile of a typical residential customer without and with electric vehicles. The residential electric vehicle charging curve was obtained from INL [193]. This analysis provided us with the peak demand and EV charging intervals within a 24-hour period. The analysis compared the impact of electric vehicles with respect to generation cost and voltages on the transmission network. Before carrying out the analysis a bus was selected as the aggregate charging bus in the distribution network. The equation that guides the operations of the aggregate charging status bus is discussed as seen in (6.16) and (6.17).

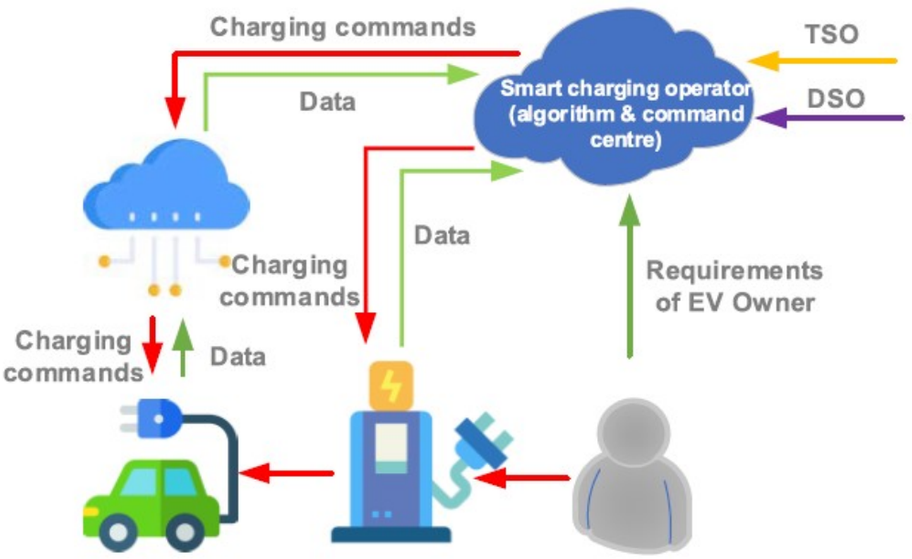

Figure 6.23: A schematic of smart charging infrastructure [1]

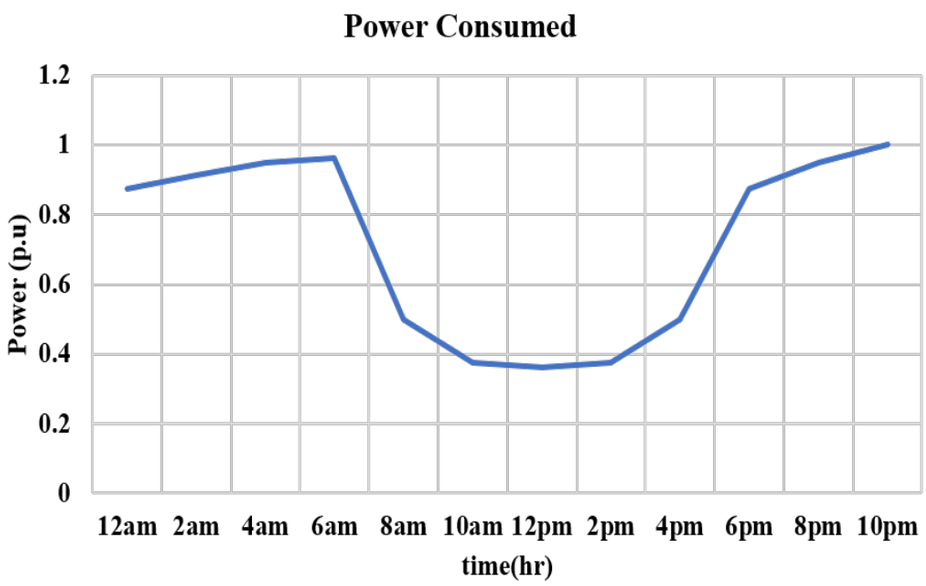

Figure 6.24: Typical EV charging curve

Constraints at each interval

$$\forall \quad t = \{1, ...24\}, P_{agg}(t) \leq min \sum_{n=1}^{k} Pc_n \tag{6.16}$$

$$P_{agg}(t) = min \sum_{t=1}^{ev} P_{ev}(t) \tag{6.17}$$

6.2.3 Proposed EV charging Management technique

A management technique, that provides setpoints for each charging station is developed. The technique allows EVs to change optimally and ensure the objectives of the integrated network are satisfied Two control approaches are been implemented for this management

Algorithm 11: Optimization steps for IOE with EV Charging Management

```
-
Set the tolerance error ϵ
Identify and initialize with set parameters all the devices in the integrated network.
Choose the station EVs aggregate bus in the distribution network.
Select the operational mode of EV charging (active or passive).
Obtain the parameters t_p for TN and d_p for DN
while tol > ϵ do
    forall t ∈ 24 do
        forall t_p ∈ TN do
            Solve the TOPF using SDP-BIM.
            Extract the simulation results. (Voltage and angle)
            Use the boundary bus parameters as setpoints for the DN feeder
        end
        forall d_p ∈ DN do
            Solve the DOPF using SDP-BFM.
            Extract the total demand with losses at DN
            Update the DN load demand at the boundary bus of the integrated
             network.
        end
    end
    Obtain the new tolerance tol
    Check for convergence
    Obtain the X(i) for each interval for the specific mode
end
```

which include the active and passive management of EV charging.

The objectives of each network are written below and are detailed in the appendix, the TN has the objective of minimizing the cost of generation while the DN is to minimize the losses in the system.

$$TOPF = min \sum_{t=1}^{T_t} \sum_{g=1}^{N_G} (f(P_{m,t}^{j})) \tag{6.18}$$

$$where, f(P_{j,t}^{g}) = c_2(P_{j,t}^{g})^2 + c_1(P_{j,t}^{g}) + c_0(t) \tag{6.19}$$

$$DOPF = min \sum_{t=1}^{T_t} Re(S_{pq}(t) - Z_{pq} I_{pq}^2(t)) \tag{6.20}$$

The active power generated is a combination of power flowing in the lines P_{jk}, the line losses P_{jk}^{loss}, and where m is the other bus in the transmission asides the boundary bus which is b.

$$P_j^g(t) = \sum_{k:j \rightarrow k} P_{jk}^M(t) + \sum_{k:j \rightarrow k} P_{jk,loss}^M(t) + xP_j^d(t) + yP_b^d(t) \tag{6.21}$$

$$P_b^d(t) = P_j^d(t) + Re(S_{DN}^d) + X(i))P_{agg,t} \tag{6.22}$$

$$\sum_{t=1}^{T_t}\sum_{i=1}^{24}(X(i))P_{agg,t} = P_{ev,tot} \tag{6.23}$$

The objective of the co-simulation engine is to minimize the boundary bus error mismatch as shown below

$$Min \quad \Delta V_{pcc}(t) = V_j^{pcc}(t) - u_0^{abc}(t) \tag{6.24}$$

The transmission network OPF is solved using the objective function and constraints below

$$min \quad c^T P_G c^T P_G = m_2 P_{G_j}^2 + m_1 P_{G_j} + m_0 \tag{6.25}$$

subject to

$$S_{G_j} - S_{D_j} = diag(\bar{V_j})\bar{Y}_{j_{bus}}^* \bar{V}_j^* \tag{6.26}$$

$$\bar{Y}_{jk}\bar{V}_j \leq I_{jk,max} \tag{6.27}$$

$$\bar{V}_j \bar{Y}_{jk} \bar{V}_j^* \leq S_{jk,max} \tag{6.28}$$

$$0 \leq P_{G_j} \leq P_j^{max} \tag{6.29}$$

$$Q_j^{min} \leq Q_{G_j} \leq Q_j^{max} \tag{6.30}$$

$$V_j^{min} \leq V_j \leq V_j^{max} \tag{6.31}$$

The distribution network OPF is solved using the objective function and constraints below

$$min \sum_{t=1}^{T_t} Re(S_{pq}(t) - Z_{pq} I_{pq}^2(t)) \tag{6.32}$$

$$\sum_{p:p\longrightarrow q} diag(S_{pq} - z_{pq} l_{pq}) + s_q + y_q u_q = \sum_{r:q\longrightarrow q} diag(S_{qr})^{\phi_q} \tag{6.33}$$

$$u_q = u_p^{\phi_{pq}} - (S_{pq} z_{pq}^H + S_{pq}^H z_{pq}) + z_{pq} l_{pq} z_{pq}^H \tag{6.34}$$

Equation (4) is very important as it provides us with a control variable. X(i) can either be a binary output in the case of passive control where it can either be 0 or 1, or it can be an active control where it is a floating value between 0 and 1. The P_{agg} is the summation of all the charging power requirements by all the EVs combined together at each interval. The $P_{ev,tot}$ is the total expected amount of charge requirements by EVs daily. One of the bus in the distribution network is chosen as P_{agg}.

6.2.3.1 Passive control

The operation mode for the charging station aggregator here is an ON/OFF state. When the x(i) is at position 1, it means the aggregator is in an ON state which means vehicles can charge at each charging station while it is OFF when x(i) is at position 0. This is an optimized output dependent on the total energy requirement by all EVs for the 24hr period of time.

6.2.3.2 Active control

The operation mode for the charging station aggregator here is controlled such that x(i) take a value between 0 and 1. This is an optimized output dependent on the total energy requirement by all EVs for the 24hr period of time.

Ultimately both charging management methods operate as a setpoint for the charging aggregator at each time interval while ensuring that the total demand by electric vehicles daily is satisfied.

6.2.4 Results and Discussion

Our multiperiod implementation was tested on integrated networks, and for a 24-hour single-day interval with a daily load profile used as shown below, The EV charging curve as discussed in the previous section is implemented, We implemented the two charging controls algorithms on the integrated grid and compared the performance on grid voltage and other metrics.

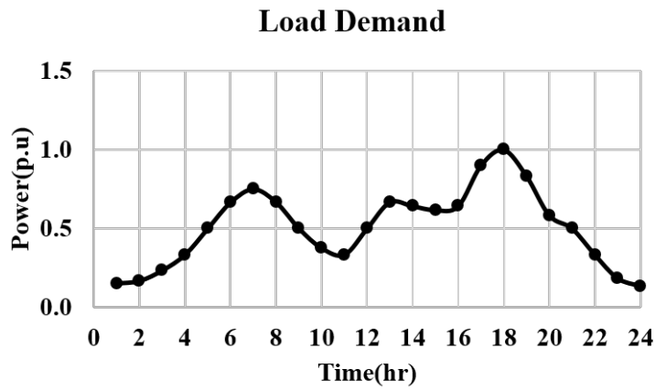

Figure 6.25: Load profiles for 24hr

6.2.4.1 Test System with charging management

The new algorithm is evaluated on the integrated IEEE 9 & 13 bus system, the system architecture is as shown in Fig. 6.26, Our static OPF analysis was performed as well to benched-mark the SDP BIM model with IEEE test cases MATPOWER simulation results. The system was modified to enable the changes in the DN to have a significant impact on the TN. A modification was performed such that 20 times the base load value of the DN was connected to the TN. As seen in the integrated system in Fig. 6.26 the boundary bus is

bus 4. We performed an analysis with no EVs connected to the integrated grid and observed both the cost of generation at each interval and the voltage profiles Fig. 6.27, we then chose bus 645 as the aggregate bus to connect the demand requirement by the EVs,

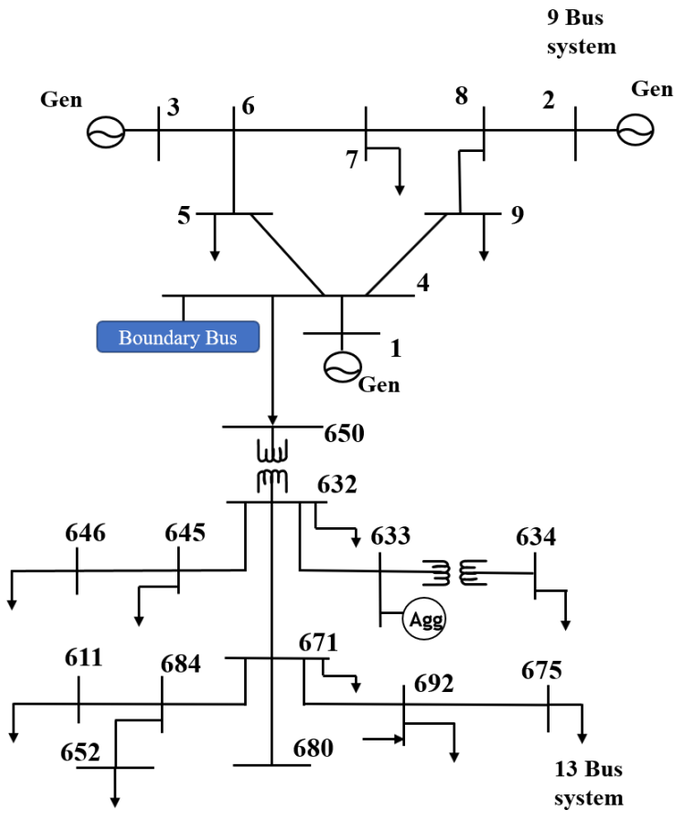

Figure 6.26: Integrated T&D model for IEEE 9bus and IEEE 13bus

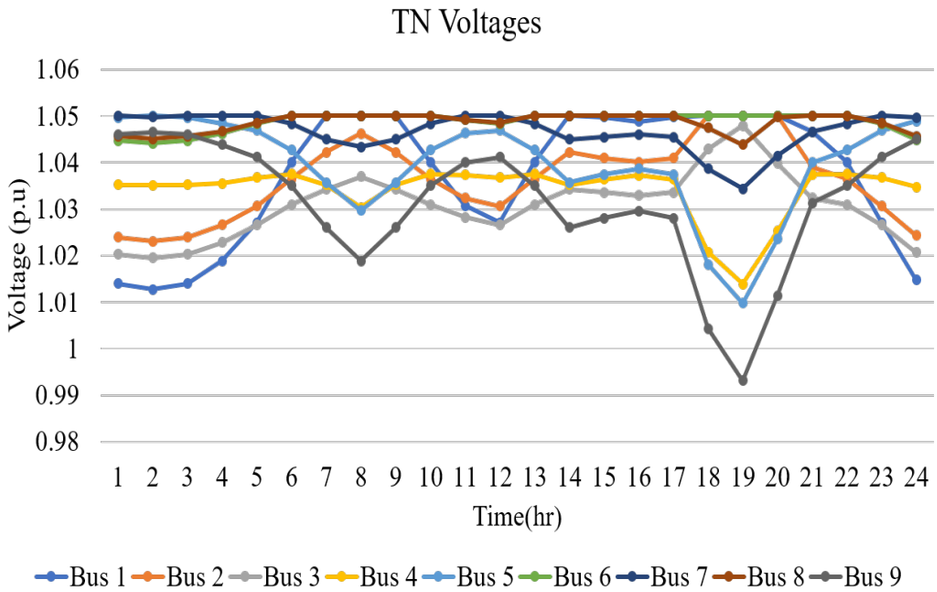

Figure 6.27: 24hr TN bus voltage profiles

6.2.4.2 Integrated T&D with charging management

After performing the base analysis, the charging management technique is added to the integrated network, and the impacts on critical grid objectives as detailed below. The Pagg is the combined aggregate of all the charging stations connected to bus 634 in the distribution

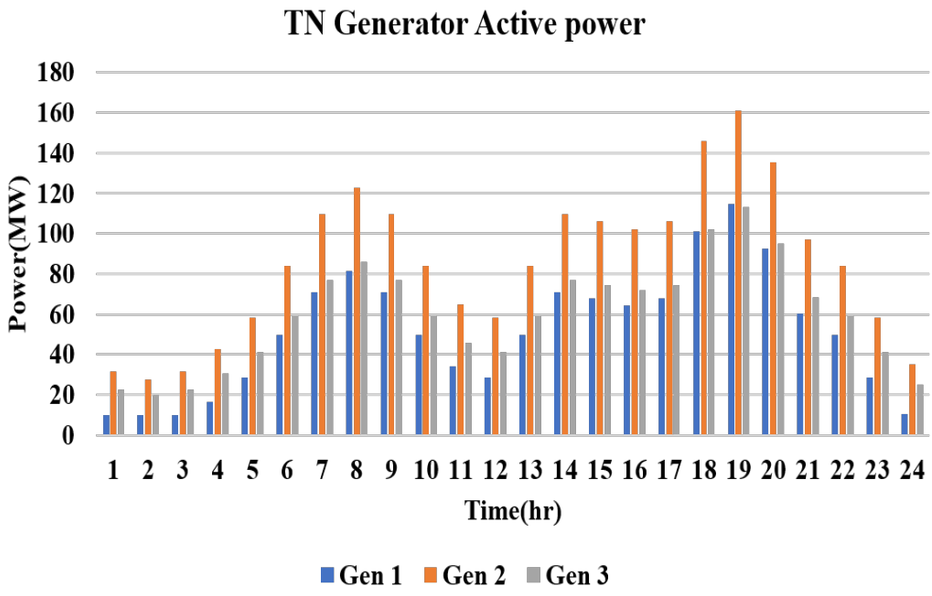

Figure 6.28: 24hr TN generator active power

network, we used level 2 charger types. The data used for the analysis are shown in the table below.

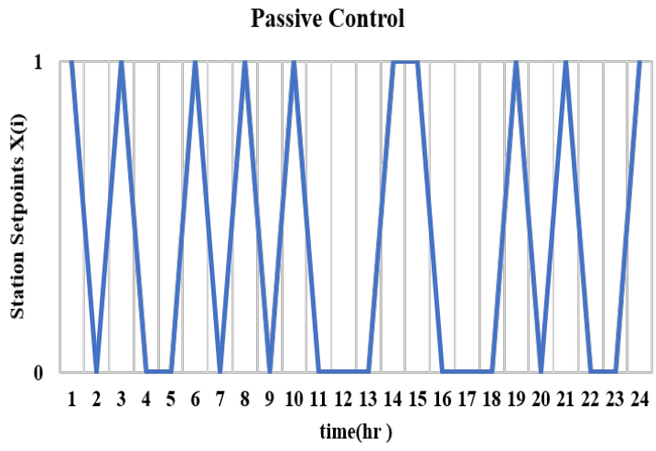

Figure 6.29: Dispatch for charging station passive control

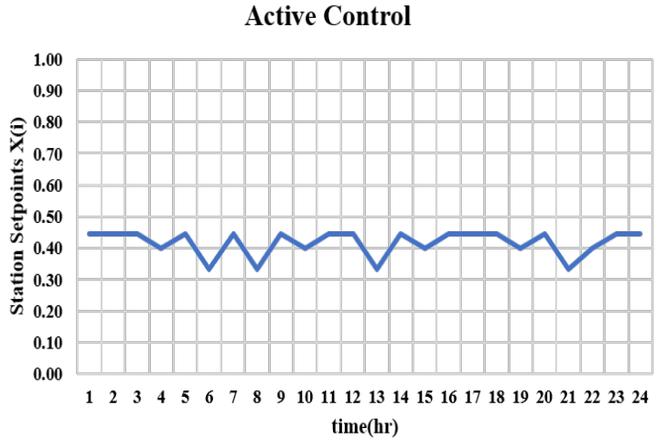

Figure 6.30: Dispatch for charging station active control

Applying the active, passive, and no control setpoint obtained as shown in the figures above

to the integrated T&D simulation the results as seen below, the setpoints were obtained using the forecasted demand of energy consumed by electric vehicle users daily. We made an assumption that Electric vehicle users won't drain their battery from 100% to 0% within a 24-hour period. Our setpoint model was such that each curve determined optimally satisfied the no-control total energy demand which is base energy demand. The total energy demand by all the EVs is 180,000kWh as shown in the cumulative result in Figure 10.

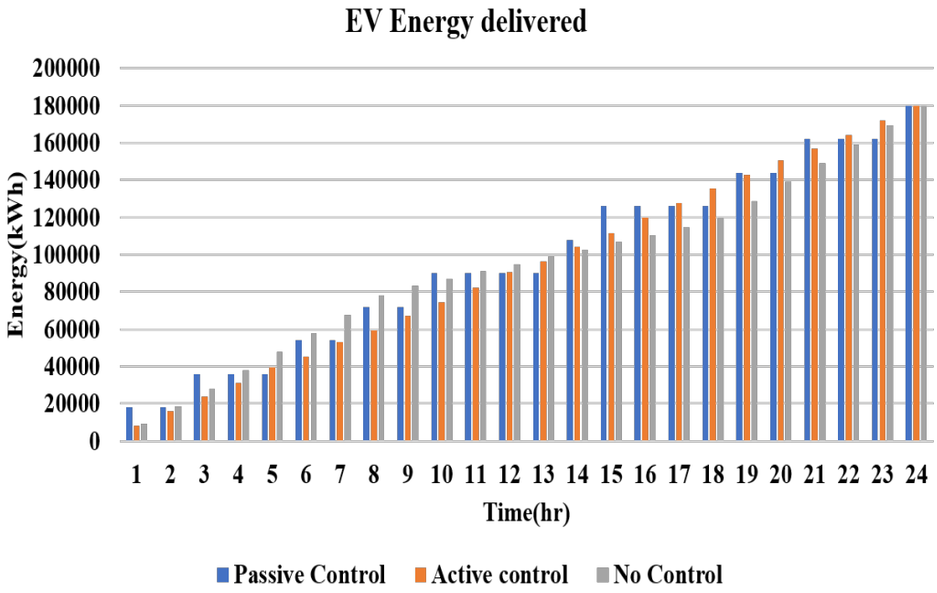

Figure 6.31: Energy delivered with different controls

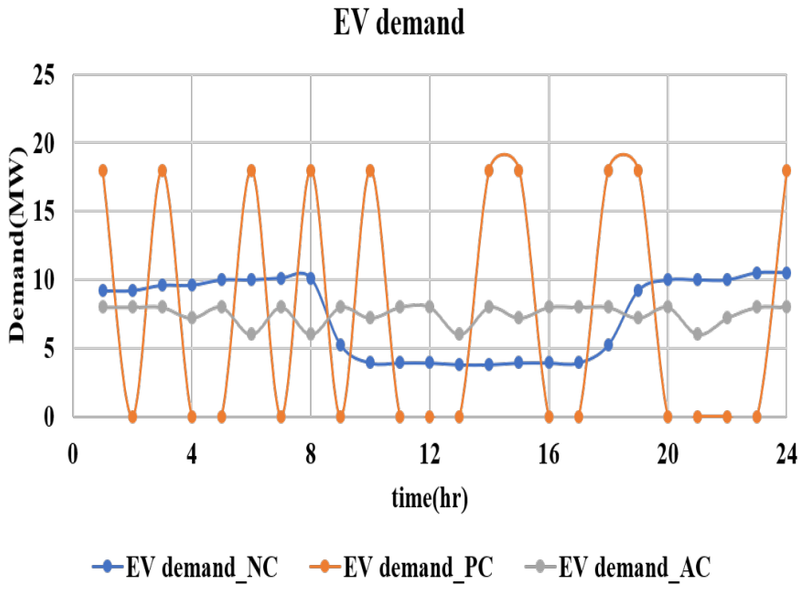

Figure 6.32: Power demand with different controls

TABLE 6.3: Control Comparison

Parameter	No control	Passive control	Active control
Capacity Required (MW)	$\geq$ 397.93MW	406.72MW	395.52MW
Cost (USD)	$\geq$ 518 million	529 million	514 million
EV demand uncertainty	Yes	No	No

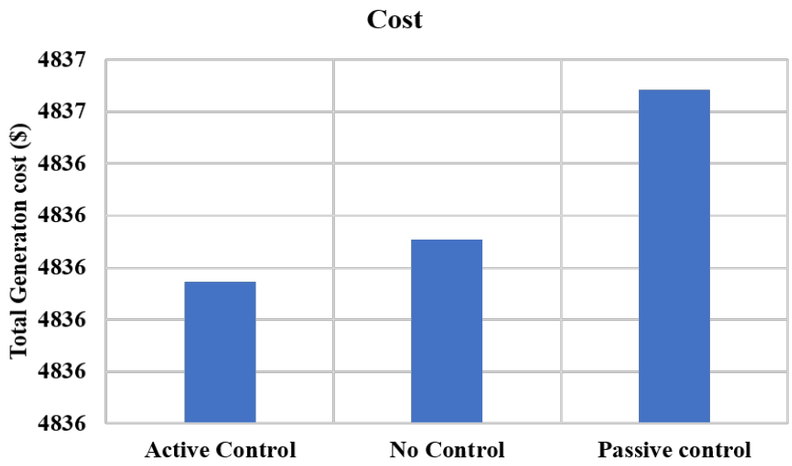

Figure 6.33: Cost impact of different charging controls

The NREL ATB [194] calculator to consider the cost implication of the different charging management techniques discussed, the active control offers the best cost savings of over 4 million USD, compared to no control where utilities might not be willing to take the risk of satisfying the base demand due to stochasticity involved in EV charging.

TABLE 6.4: Parameter

S/N	Parameter	Data
1	No of charging stations	900
2	Each station capacity	20kW
3	Aggregator max Capacity	18MW
4	No of electric vehicles	4500
5	EV battery capacity	40kWh
6	NREL ATB CAPEX	1270.78 $/kW
7	NREL Fixed Cost	30.5 $/kW-yr
8	NREL Capital Cost	133.578 $/MWh

6.3 Summary

A typical charging profile of a residential electric vehicle was implemented, the voltage profile of the TN was observed and the impacts on the cost of generation were observed from the amount of power generated, future steps are exploring the uncertainty in charging by electric vehicle users and comparing a binary variable decision or controlled power consumption when charging. Another direction to be considered in the future direction is to implement decentralized charging setpoints for the stations using a global and local controller to ensure optimal operation of the grid.

CHAPTER 7: CONCLUSIONS AND FUTURE WORK

7.1 Conclusion

This dissertation proposed methodologies for optimal management and control of integrated transmission and distribution electric grid considering distributed renewable energy resources at the distribution system. In Chapter 3 an adaptive control architecture and an optimization framework to help manage the grid under renewable rich operational conditions were discussed extensively, two frameworks were discussed one that considered only the distribution grid, and another that considered both networks and extended the control capabilities to other resources on the grid to help mitigate oscillations during disturbances on the grid, caused by fault occurrences, sudden load changes, capacitor switching, or even the intermittent nature of the energy sources for most renewable systems, considering both integrated transmission and distribution system.

In Chapter 4, a management technique was developed using an integrated optimization engine, the proposed technology ensured that the integrated networks had visibility to each other, and a linear optimization technique was implemented while considering the heterogeneous nature of the boundary variables in an integrated transmission and distribution network. The stochastic integrated linear optimization (SILP) framework is modeled can help utilities achieve optimum operation based on two key objectives of utilities which are the cost of operation and minimization of distribution network loss/voltage deviation.

Chapter 5, extends the study of the integrated grid to the time-varying operations of renewable energy resources, this allows the linear optimization method to be capable of providing efficient operations at different times of operation of the grid, irrespective of the renewable energy resources power generation, the linear decision rule was used to provide the generator real-time outputs of the renewable energy resources, different networks were explored with huge penetration of RERs, in future studies impact of different location of renewable energy resources on the LDR constraints can be studied.

Finally, in chapter 6, the grid of the now (smart grid) is discussed which involves different resources interplaying on the grid, a framework that helps to ensure the grid operates in an efficient manner is developed, especially with all the uncertainties involved which might due to human interference or the sources of the RERs. The management technique developed can accommodate as many renewable energy resources as possible and for the purpose of our work we evaluated the technique with solar PV resources and electric vehicles, our work also modeled how utilities can manage the growing demand concerns caused by electric vehicles.

The main contributions are as follows:

- First an online tuned oscillation damping controller for battery-integrated wind energy systems is proposed. The approach was tested on a grid-connected system, and the simulation results validate the superiority of our proposed control to provide an improved frequency response of the grid during different dynamic conditions.

- Next, an optimal damping control framework is designed and implemented on an integrated transmission and distribution system with bulk power and distributed renewable-based generation. The proposed methodology can manage the frequency oscillation in an integrated transmission and distribution network, with interconnected renewable energy resources. The approach relies on an optimal damping control architecture that is adaptive and at the same time optimal.

- Third, an optimization technique is implemented to help ensure optimum performance of the controller, while minimizing the deviation of the grid frequency. The approach is implemented on synchronous generators that can be used to augment the existing stabilizers or other damping controllers. Also, field implementation of the proposed methodology was discussed. The results from simulations on real-life feeders validate the superiority of the proposed control method, as compared with a conventional control approach, to provide an improved grid frequency response for a range of anticipated dynamic conditions (e.g., wind speed variations, faults, and load changes). Overall an improvement in damping and settling time is observed.

- Fourth, an architecture is illustrated that demonstrates the versatility of a newly formulated stochastic linear optimization to handle the intermittent nature of renewable energy resources capable of affecting grid quality metrics due to their penetration level at any time. The proposed methodology helps with the co-simulation of an integrated T&D system and offers the transmission system capabilities to adequately capture the changes that occur in the distribution system. With our approach, there will be no loss of information during operation between the transmission system and distribution system, and faster action can be performed optimally in case of uncertainties before the operational windows or intervals that most utilities use. Our technique ensures that the grid objectives are achieved for both networks, and the formulation can also be implemented in power flow simulations. The versatility of our technique was established with two different integrated frameworks.

- Fifth, the scope of our stochastic linear optimization (LDR) technique is extended to a multiperiod optimal power flow framework, the integrated optimization operated each

network OPF as an MPOPF and ensures that the grid objective for each on the coupled network is achieved while fully utilizing the offerings of DERs. Our approach offered economic benefits, like the decrease in the cost of generation and voltage deviation as well as eliminating the need for curtailing RERs which if not properly managed can cause variations on the grid.

- Finally, the grid of now was evaluated with several renewable energy resources and several uncertainties,a technique that is capable of managing this phenomenon was discussed, and emphasis was on electric vehicle charging management, a technique which handles the uncertainty of charging and shows significant improvement on the cost of generation efficiency.

7.2 Future Works

Overall, different methodologies and approaches have been discussed on the control and management of grid-connected renewable energy resources. These resources will continue to interact with the grid in much capacity, a few items have been recognized that have the potential to bring value to this research in the future.

1. **Time and Constraint Impacts of LDR technique**

The capabilities of the LDR technique to provide the networks with insights into the operations of renewable energy resources and how to ensure that the generators adjust themselves accordingly, further work can be done on studying the time of response for the generators to adjust themselves including constraints like ramp-time and other generator responsiveness constraints, to validate the swiftness of the technique, this can be studied in a time-scale domain analysis.

2. **Multi-Objective function of the LDR technique**

The LDR technique capabilities have a main objective of eliminating the need to curtail DERs during operations of reverse power flow due to the likelihood of causing challenges on the grid, the scope of this objective should be extended to accommodate the willingness of this market participant in the transmission network, which transforms the objective equation into a multi-objective function.

3. **Decentralized setpoints controllers for charging station management**

A framework for controlling the charging stations using a centralized controller is developed, that receives a setpoints after the optimal power flow simulations have been performed. This can first be evaluated on a hardware simulator and the scope of the work can be extended to the decentralized controller (local controller), which can have similar or different objectives to the centralized (global controller) with different similar set points. Ultimately, this gives utilities the opportunity to participate in EV charging with minimum risk.

4. **Optimal co-ordination or selection between several control and management frameworks**

Several control and management techniques if implemented industry-wide utilities might find it difficult to prioritize which to use or combine, further studies can be done on which is most suited for different grid scenarios and when to combine different approaches bearing in mind the objectives of the utility.

CHAPTER 8: LIST OF PUBLICATIONS

1. O. Ogundairo, S. Kamalasadan, A. R. Nair and M. Smith, "Oscillation Damping of Integrated Transmission and Distribution Power Grid With Renewables Based on Novel Measurement-Based Optimal Controller," in IEEE Transactions on Industry Applications, vol. 58, no. 3, pp. 4181-4191, May-June 2022, doi: 10.1109/TIA.2022.3162565.

2. O. Ogundairo, A. R. Nair, M. Smith and S. Kamalasadan, "Online Adaptive Damping Controller Architecture for Wind Integrated Power Grid," 2020 IEEE International Conference on Power Electronics, Drives and Energy Systems (PEDES), Jaipur, India, 2020, pp. 1-6, doi: 10.1109/PEDES49360.2020.9379689.

3. O. Ogundairo, S. Kamalasadan and B. K, "Integrated Transmission and Distribution Optimal Power Flow Simulation Using Linear Decision Approach," 2022 IEEE International Conference on Power Electronics, Drives and Energy Systems (PEDES), Jaipur, India, 2022, pp. 1-6, doi: 10.1109/PEDES56012.2022.10080002.

4. A. Abbas, O. Ogundairo and O. Adeosun, "Overvoltage Correction in Active Distribution Grids using Smart Inverters and Load Control: A Comparison," 2020 52nd North American Power Symposium (NAPS), Tempe, AZ, USA, 2021, pp. 1-6, doi: 10.1109/NAPS50074.2021.9449679.

5. O. Ogundairo, O. Adeosun and S. K. Srivastava, "A Cost-driven Transition Comparison to improve grid resilience during unusual harsh weather condition operation. âTexas A Case Studyâ," 2021 North American Power Symposium (NAPS), College Station, TX, USA, 2021, pp. 1-6, doi: 10.1109/NAPS52732.2021.9654670.

Accepted

6. O. Ogundairo and S. Kamalasadan, "Stochastic Optimization of Integrated Transmission and Distribution Network Considering Distributed Generation With Uncertainties. Journal Accepted and submitted IEEE Transactions on Industry Applications.

7. O. Ogundairo and S. Kamalasadan, "Multi-Period Integrated Transmission and Distribution Optimal Power Flow Simulation Using Linear Decision Approach. Accepted ETFG to be presented in December 2023

Under Review

8. O. Ogundairo and S. Kamalasadan, "Management of Electric Vehicle Charging Impact on an Integrated Transmission and Distribution Grid. Submitted to IEEE general meeting

9. O. Ogundairo and S. Kamalasadan, "Management and Coordination of Multiple Grid-Connected Renewable Energy Resources.Submitted to IEEE general meeting

REFERENCES

[1] S. Tirunagari, M. Gu, and L. Meegahapola, "Reaping the benefits of smart electric vehicle charging and vehicle-to-grid technologies: Regulatory, policy and technical aspects," *IEEE Access*, vol. 10, pp. 114657–114672, 2022.

[2] Energy.gov, "Federal agency use of renewable electric energy."

[3] US EPA, "State renewable energy resources."

[4] US DOE, NETL, "Backup generators (bugs): The next smart grid peak resource (DOE/NETL-2010/1406)," 2010.

[5] B. Pokharel, O. Ojo, and A. Balogun, "Standalone operation of a dfig-based wind turbine system with integrated energy storage," in *2015 IEEE 6th International Symposium on Power Electronics for Distributed Generation Systems (PEDG)*, pp. 1–5, 2015.

[6] M. Al-Muhaini and G. T. Heydt, "Evaluating future power distribution system reliability including distributed generation," *IEEE Transactions on Power Delivery*, vol. 28, no. 4, pp. 2264–2272, 2013.

[7] T. Ackermann., "Wind power in power systems," 2005.

[8] "Ieee standard for interconnecting distributed resources with electric power systems," *IEEE Std 1547-2003*, pp. 1–28, 2003.

[9] R. R. Nejad, A. Golshani, and W. Sun, "Integrated transmission and distribution systems restoration with distributed generation scheduling," in *2018 IEEE Power Energy Society General Meeting (PESGM)*, pp. 1–5, 2018.

[10] S. Moghadasi and S. Kamalasadan, "Optimal fast control and scheduling of power distribution system using integrated receding horizon control and convex conic programming," *IEEE Transactions on Industry Applications*, 2016.

[11] X. Chen, M. Sim, P. Sun, and J. Zhang, "A linear decision-based approximation approach to stochastic programming," *Operations Research*, vol. 56, pp. 344–357, Mar. 2008.

[12] D. Gayme and U. Topcu, "Optimal power flow with large-scale storage integration," *IEEE Transactions on Power Systems*, vol. 28, no. 2, pp. 709–717, 2013.

[13] W. Tinney, J. Bright, K. Demaree, and B. Hughes, "Some deficiencies in optimal power flow," *IEEE Transactions on Power Systems*, vol. 3, no. 2, pp. 676–683, 1988.

[14] B. Palmintier, E. Hale, T. M. Hansen, W. Jones, D. Biagioni, K. Baker, H. Wu, J. Giraldez, H. Sorensen, M. Lunacek, N. Merket, J. Jorgenson, and B.-M. Hodge, "Final technical report: Integrated distribution-transmission analysis for very high penetration solar pv,"

[15] S. M. Mohseni-Bonab, I. Kamwa, and A. Moeini, "Ic-gama: A novel framework for integrated t amp;d co-simulation," in *2019 IEEE PES Innovative Smart Grid Technologies Europe (ISGT-Europe)*, pp. 1–5, 2019.

[16] R. Maharjan and S. Kamalasadan, "Real-time simulation for active and reactive power control of doubly fed induction generator," in *2013 North American Power Symposium (NAPS)*, pp. 1–6, 2013.

[17] N. Petrovic, L. Strezoski, and B. Dumnic, "Overview of software tools for integration and active management of high penetration of ders in emerging distribution networks," in *IEEE EUROCON 2019 -18th International Conference on Smart Technologies*, pp. 1–6, 2019.

[18] V. Cecchi, S. Kamalasadan, J. Enslin, and M. Miller, "Grid impacts and mitigation measures for increased pv penetration levels using advanced pv inverter regulation," in *2013 IEEE Energy Conversion Congress and Exposition*, pp. 561–568, IEEE, 2013.

[19] M. Baran and M.-Y. Hsu, "Volt/var control at distribution substations," *IEEE Transactions on Power Systems*, vol. 14, no. 1, pp. 312–318, 1999.

[20] J. Tengku, A. Mohamed, and H. Shareef, "A review on voltage control methods for active distribution networks," *Przeglad Elektrotechniczny*, vol. 88, pp. 304–312, 06 2012.

[21] H. V. Padullaparti, Q. Nguyen, and S. Santoso, "Advances in volt-var control approaches in utility distribution systems," in *2016 IEEE Power and Energy Society General Meeting (PESGM)*, pp. 1–5, 2016.

[22] B. Green., "Grid strategy 2011: Conservation voltage reduction and volt var optimization in the smart grid," 2010.

[23] R. R. Jha, A. Dubey, C.-C. Liu, and K. P. Schneider, "Bi-level volt-var optimization to coordinate smart inverters with voltage control devices," *IEEE Transactions on Power Systems*, vol. 34, no. 3, pp. 1801–1813, 2019.

[24] K. Mahmud, M. J. Hossain, and J. Ravishankar, "Peak-load management in commercial systems with electric vehicles," *IEEE Systems Journal*, vol. 13, no. 2, pp. 1872–1882, 2019.

[25] O. Erdinc, N. G. Paterakis, T. D. P. Mendes, A. G. Bakirtzis, and J. P. S. CatalÃ£o, "Smart household operation considering bi-directional ev and ess utilization by real-time pricing-based dr," *IEEE Transactions on Smart Grid*, vol. 6, no. 3, pp. 1281–1291, 2015.

[26] E. Reihani, S. Sepasi, L. R. Roose, and M. Matsuura, "Energy management at the distribution grid using a battery energy storage system (bess)," *International Journal of Electrical Power Energy Systems*, vol. 77, pp. 337–344, 2016.

[27] M. T. Lawder, B. Suthar, P. W. C. Northrop, S. De, C. M. Hoff, O. Leitermann, M. L. Crow, S. Santhanagopalan, and V. R. Subramanian, "Battery energy storage system (bess) and battery management system (bms) for grid-scale applications," *Proceedings of the IEEE*, vol. 102, no. 6, pp. 1014–1030, 2014.

[28] Z. Wang and S. Wang, "Grid power peak shaving and valley filling using vehicle-to-grid systems," *IEEE Transactions on Power Delivery*, vol. 28, no. 3, pp. 1822–1829, 2013.

[29] L. Zhao and V. Aravinthan, "Strategies of residential peak shaving with integration of demand response and v2h," in *2013 IEEE PES Asia-Pacific Power and Energy Engineering Conference (APPEEC)*, pp. 1–5, 2013.

[30] A. Salman, Y. Li, and M. Stewart, "Evaluating system reliability and targeted hardening strategies of power distribution systems subjected to hurricanes," *Reliability Engineering and System Safety*, vol. 144, pp. 319–333, 12 2015.

[31] J. Li, X.-Y. Ma, C.-C. Liu, and K. P. Schneider, "Distribution system restoration with microgrids using spanning tree search," *IEEE Transactions on Power Systems*, vol. 29, no. 6, pp. 3021–3029, 2014.

[32] H. Gao, Y. Chen, Y. Xu, and C.-C. Liu, "Resilience-oriented critical load restoration using microgrids in distribution systems," *IEEE Transactions on Smart Grid*, vol. 7, no. 6, pp. 2837–2848, 2016.

[33] Z. Wang and J. Wang, "Self-healing resilient distribution systems based on sectionalization into microgrids," *IEEE Transactions on Power Systems*, vol. 30, no. 6, pp. 3139–3149, 2015.

[34] S. Poudel, P. Sharma, A. Dubey, and K. P. Schneider, "Advanced flisr with intentional islanding operations in an adms environment using gridapps-d," *IEEE Access*, vol. 8, pp. 113766–113778, 2020.

[35] A. Gupta, "Integration challenges of wind power on power system grid a review," in *2018 International Conference on Advanced Computation and Telecommunication (ICACAT)*, pp. 1–7, 2018.

[36] H. Holttinen, "Wind integration: experience, issues, and challenges," *Wiley Interdisciplinary Reviews: Energy and Environment*, vol. 1, pp. 243–255, 2012.

[37] D. Johnson, "Issues of power quality in electrical systems," *International Journal of Energy and Power Engineering*, vol. 5, p. 148, 01 2016.

[38] X. Liang, "Emerging power quality challenges due to integration of renewable energy sources," *IEEE Transactions on Industry Applications*, vol. 53, no. 2, pp. 855–866, 2017.

[39] M. Chowdhury, N. Hosseinzadeh, and W. Shen, "Smoothing wind power fluctuations by fuzzy logic pitch angle controller," *Renewable Energy*, vol. 38, pp. 224–233, Feb. 2012.

[40] M. Farhoodnea, A. Mohamed, H. Shareef, and H. Zayandehroodi, "Power quality impact of grid-connected photovoltaic generation system in distribution networks," in *2012 IEEE Student Conference on Research and Development (SCOReD)*, pp. 1–6, 2012.

[41] I. Mehouachi and S. Chebbi, "Power quality disturbances and its mitigation in wind energy generation interface to grid system," 07 2018.

[42] S. Mohod and M. V. Aware, "Power quality issues itâs mitigation technique in wind energy generation," in *2008 13th International Conference on Harmonics and Quality of Power*, pp. 1–6, 2008.

[43] M. A. Saqib and A. Z. Saleem, "Power-quality issues and the need for reactive-power compensation in the grid integration of wind power," *Renewable and Sustainable Energy Reviews*, vol. 43, pp. 51–64, 2015.

[44] X. Zhu and Y. Zhang, "Coordinative voltage control strategy with multiple resources for distribution systems of high pv penetration," in *2018 IEEE 7th World Conference on Photovoltaic Energy Conversion (WCPEC) (A Joint Conference of 45th IEEE PVSC, 28th PVSEC 34th EU PVSEC)*, pp. 1497–1502, 2018.

[45] M. A. Tayyab, M. Vaziri, A. Yazdani, and M. Zarghami, "Distributed generation effects on voltage profile of distribution grid with svc and smart inverter," in *2015 IEEE Power Energy Society General Meeting*, pp. 1–5, 2015.

[46] H. Galiveeti, A. Goswami, and N. Choudhury, "Impact of plug-in electric vehicles and distributed generation on reliability of distribution systems," *Engineering Science and Technology, an International Journal*, vol. 21, 02 2018.

[47] J.Alle and F. B. Wollenburg, "Power generation operation and control," 2012.

[48] H. Chen, T. N. Cong, W. Yang, C. Tan, Y. Li, and Y. Ding, "Progress in electrical energy storage system: A critical review," *Progress in Natural Science*, vol. 19, no. 3, pp. 291–312, 2009.

[49] P. Medina, A. Bizuayehu, J. CatalÃ£o, E. Rodrigues, and J. Contreras, "Electrical energy storage systems: Technologies' state-of-the-art, techno-economic benefits and applications analysis," in *2014 47th Hawaii International Conference on System Sciences*, pp. 2295–2304, 2014.

[50] N. Hargreaves, *Extension of IEC 61970 for electrical energy storage modelling*, pp. 135–160. 01 2014.

[51] Y. Zhu, H. Zang, L. Cheng, and S. Gao, "Output power smoothing control for a wind farm based on the allocation of wind turbines," *Applied Sciences*, vol. 8, no. 6, 2018.

[52] A. M. Howlader, N. Urasaki, T. Senjyu, A. Yona, T. Funabashi, and A. Y. Saber, "Output power leveling of wind generation system using inertia for pm synchronous generator," in *2009 International Conference on Power Electronics and Drive Systems (PEDS)*, pp. 1289–1294, 2009.

[53] Y. Hu, W. Wei, Y. Peng, and J. Lei, "Fuzzy virtual inertia control for virtual synchronous generator," pp. 8523–8527, 07 2016.

[54] A. Uehara, A. Pratap, T. Goya, T. Senjyu, A. Yona, N. Urasaki, and T. Funabashi, "A coordinated control method to smooth wind power fluctuations of a pmsg-based wecs," *IEEE Transactions on Energy Conversion*, vol. 26, no. 2, pp. 550–558, 2011.

[55] J. He and Y. Li, "Analysis, design, and implementation of virtual impedance for power electronics interfaced distributed generation," *IEEE Transactions on Industry Applications*, vol. 47, pp. 2525–2538, 2011.

[56] Z. Gao, K. Zhang, X. Zhou, and Y. Ma, "The discussion on active power filter," in *2017 36th Chinese Control Conference (CCC)*, pp. 10646–10651, 2017.

[57] S. Kamalasadan, *A new generation of adaptive control: An intelligent supervisory loop approach.* PhD thesis, University of Toledo, 2004.

[58] Y. Xue, M. Starke, J. Dong, M. Olama, T. Kuruganti, J. Taft, and M. Shankar, "On a future for smart inverters with integrated system functions," in *2018 9th IEEE International Symposium on Power Electronics for Distributed Generation Systems (PEDG)*, pp. 1–8, 2018.

[59] X. Wang, F. Blaabjerg, and W. Wu, "Modeling and analysis of harmonic stability in an ac power-electronics-based power system," *IEEE Transactions on Power Electronics*, vol. 29, no. 12, pp. 6421–6432, 2014.

[60] G. Gaba, S. Lefebvre, and D. Mukhedkar, "Comparative analysis and study of the dynamic stability of ac/dc systems," *IEEE Transactions on Power Systems*, vol. 3, no. 3, pp. 978–985, 1988.

[61] S. Lefebvre and B. Dube, "Control system analysis and design for an aerogenerator with eigenvalue methods," *IEEE Transactions on Power Systems*, vol. 3, no. 4, pp. 1600–1608, 1988.

[62] B. Arbab-Zavar, E. J. Palacios-Garcia, J. C. Vasquez, and J. M. Guerrero, "Smart inverters for microgrid applications: A review," *Energies*, vol. 12, no. 5, 2019.

[63] J. Rocabert, A. Luna, F. Blaabjerg, and P. RodrÃguez, "Control of power converters in ac microgrids," *IEEE Transactions on Power Electronics*, vol. 27, no. 11, pp. 4734–4749, 2012.

[64] S.-H. Hu, C.-Y. Kuo, T.-L. Lee, and J. M. Guerrero, "Droop-controlled inverters with seamless transition between islanding and grid-connected operations," in *2011 IEEE Energy Conversion Congress and Exposition*, pp. 2196–2201, 2011.

[65] T. L. Vandoorn, B. Meersman, J. D. M. De Kooning, and L. Vandevelde, "Transition from islanded to grid-connected mode of microgrids with voltage-based droop control," *IEEE Transactions on Power Systems*, vol. 28, no. 3, pp. 2545–2553, 2013.

[66] T.-V. Tran, T.-W. Chun, H.-H. Lee, H.-G. Kim, and E.-C. Nho, "Pll-based seamless transfer control between grid-connected and islanding modes in grid-connected inverters," *IEEE Transactions on Power Electronics*, vol. 29, no. 10, pp. 5218–5228, 2014.

[67] W. Xian, W. Yuan, Y. Yan, and T. A. Coombs, "Minimize frequency fluctuations of isolated power system with wind farm by using superconducting magnetic energy storage," in *2009 International Conference on Power Electronics and Drive Systems (PEDS)*, pp. 1329–1332, 2009.

[68] Q.-C. Zhong and G. Weiss, "Synchronverters: Inverters that mimic synchronous generators," *IEEE Transactions on Industrial Electronics*, vol. 58, no. 4, pp. 1259–1267, 2011.

[69] H. Beck and R. Hesse, "Virtual synchronous machine," *2007 9th International Conference on Electrical Power Quality and Utilisation*, pp. 1–6, 2007.

[70] Q.-C. Zhong, Z. Ma, W.-L. Ming, and G. C. Konstantopoulos, "Grid-friendly wind power systems based on the synchronverter technology," *Energy Conversion and Management*, vol. 89, pp. 719–726, 2015.

[71] R. Hesse, D. Turschner, and H. Beck, "Micro grid stabilization using the virtual synchronous machine (visma)," *Renewable energy power quality journal*, vol. 1, pp. 676–681, 2009.

[72] Q.-C. Zhong, P.-L. Nguyen, Z. Ma, and W. Sheng, "Self-synchronized synchronverters: Inverters without a dedicated synchronization unit," *IEEE Transactions on Power Electronics*, vol. 29, no. 2, pp. 617–630, 2014.

[73] Q.-C. Zhong, "Power-electronics-enabled autonomous power systems: Architecture and technical routes," *IEEE Transactions on Industrial Electronics*, vol. 64, no. 7, pp. 5907–5918, 2017.

[74] B. B. Johnson, M. Sinha, N. G. Ainsworth, F. DÃ¶rfler, and S. V. Dhople, "Synthesizing virtual oscillators to control islanded inverters," *IEEE Transactions on Power Electronics*, vol. 31, no. 8, pp. 6002–6015, 2016.

[75] J. Alipoor, Y. Miura, and T. Ise, "Stability assessment and optimization methods for microgrid with multiple vsg units," *IEEE Transactions on Smart Grid*, vol. 9, no. 2, pp. 1462–1471, 2018.

[76] M. Ashabani, F. D. Freijedo, S. Golestan, and J. M. Guerrero, "Inducverters: Pll-less converters with auto-synchronization and emulated inertia capability," *IEEE Transactions on Smart Grid*, vol. 7, no. 3, pp. 1660–1674, 2016.

[77] R. R. Behera and A. N. Thakur, "An overview of various grid synchronization techniques for single-phase grid integration of renewable distributed power generation systems," in *2016 International Conference on Electrical, Electronics, and Optimization Techniques (ICEEOT)*, pp. 2876–2880, 2016.

[78] Y. Xue, K. C. Divya, G. Griepentrog, M. Liviu, S. Suresh, and M. Manjrekar, "Towards next generation photovoltaic inverters," in *2011 IEEE Energy Conversion Congress and Exposition*, pp. 2467–2474, 2011.

[79] Y. Xue and J. M. Guerrero, "Smart inverters for utility and industry applications," in *Proceedings of PCIM Europe 2015; International Exhibition and Conference for Power Electronics, Intelligent Motion, Renewable Energy and Energy Management*, pp. 1–8, 2015.

[80] A. Abbas, O. Ogundairo, and O. Adeosun, "Overvoltage correction in active distribution grids using smart inverters and load control: A comparison," in *2020 52nd North American Power Symposium (NAPS)*, pp. 1–6, 2021.

[81] M. Kuzlu, M. Pipattanasomporn, and S. Rahman, "Communication network requirements for major smart grid applications in han, nan and wan," *Computer Networks*, vol. 67, pp. 74–88, 2014.

[82] M. Kuzlu and M. Pipattanasomporn, "Assessment of communication technologies and network requirements for different smart grid applications," in *2013 IEEE PES Innovative Smart Grid Technologies Conference (ISGT)*, pp. 1–6, 2013.

[83] C. Bekara, "Security issues and challenges for the iot-based smart grid," *Procedia Computer Science*, vol. 34, pp. 532–537, 2014. The 9th International Conference on Future Networks and Communications (FNC'14)/The 11th International Conference on Mobile Systems and Pervasive Computing (MobiSPC'14)/Affiliated Workshops.

[84] C. Tankard, "The security issues of the internet of things," *Computer Fraud Security*, vol. 2015, no. 9, pp. 11–14, 2015.

[85] W. Zhang, D. Xu, P. N. Enjeti, H. Li, J. T. Hawke, and H. S. Krishnamoorthy, "Survey on fault-tolerant techniques for power electronic converters," *IEEE Transactions on Power Electronics*, vol. 29, no. 12, pp. 6319–6331, 2014.

[86] P. Weber, P. Poure, D. Theilliol, and S. Saadate, "Design of hardware fault tolerant control architecture for wind energy conversion system with dfig based on reliability analysis," in *2008 IEEE International Symposium on Industrial Electronics*, pp. 2323–2328, 2008.

[87] M. A. Rodriguez, A. Claudio, D. Theilliol, L. G. Vela, and L. Hernandez, "Strategy to replace the damaged power device for fault-tolerant induction motor drive," in *2009 Twenty-Fourth Annual IEEE Applied Power Electronics Conference and Exposition*, pp. 343–346, 2009.

[88] S. Li and L. Xu, "Strategies of fault tolerant operation for three-level pwm inverters," *IEEE Transactions on Power Electronics*, vol. 21, no. 4, pp. 933–940, 2006.

[89] P. Mahat, Z. Chen, and B. Bak-Jensen, "Review of islanding detection methods for distributed generation," in *2008 Third International Conference on Electric Utility Deregulation and Restructuring and Power Technologies*, pp. 2743–2748, 2008.

[90] F. De Mango, M. Liserre, A. Dell'Aquila, and A. Pigazo, "Overview of anti-islanding algorithms for pv systems. part i: Passive methods," in *2006 12th International Power Electronics and Motion Control Conference*, pp. 1878–1883, 2006.

[91] C. Li, C. Cao, Y. Cao, Y. Kuang, L. Zeng, and B. Fang, "A review of islanding detection methods for microgrid," *Renewable and Sustainable Energy Reviews*, vol. 35, pp. 211–220, 2014.

[92] S. Yang, D. Xiang, A. Bryant, P. Mawby, L. Ran, and P. Tavner, "Condition monitoring for device reliability in power electronic converters: A review," *Power Electronics, IEEE Transactions on*, vol. 25, pp. 2734 – 2752, 12 2010.

[93] H. Oh, B. Han, P. McCluskey, C. Han, and B. D. Youn, "Physics-of-failure, condition monitoring, and prognostics of insulated gate bipolar transistor modules: A review," *IEEE Transactions on Power Electronics*, vol. 30, no. 5, pp. 2413–2426, 2015.

[94] V. Nasirian, Q. Shafiee, J. Guerrero, F. Lewis, and A. Davoudi, "Droop-free distributed control for ac microgrids," *IEEE Transactions on Power Electronics*, vol. 31, pp. 1–1, 01 2015.

[95] Y. Wang, P. Zhang, W. Li, W. Xiao, and A. Abdollahi, "Online overvoltage prevention control of photovoltaic generators in microgrids," *IEEE Transactions on Smart Grid*, vol. 3, no. 4, pp. 2071–2078, 2012.

[96] S. Alyami, Y. Wang, C. Wang, J. Zhao, and B. Zhao, "Adaptive real power capping method for fair overvoltage regulation of distribution networks with high penetration of pv systems," *IEEE Transactions on Smart Grid*, vol. 5, no. 6, pp. 2729–2738, 2014.

[97] X. Lu, J. M. Guerrero, K. Sun, and J. C. Vasquez, "An improved droop control method for dc microgrids based on low bandwidth communication with dc bus voltage restoration and enhanced current sharing accuracy," *IEEE Transactions on Power Electronics*, vol. 29, no. 4, pp. 1800–1812, 2014.

[98] J. M. Guerrero, J. C. VÃ¡squez, and R. Teodorescu, "Hierarchical control of droop-controlled dc and ac microgrids â a general approach towards standardization," in *2009 35th Annual Conference of IEEE Industrial Electronics*, pp. 4305–4310, 2009.

[99] N. Yang, D. Paire, F. Gao, A. Miraoui, and W. Liu, "Compensation of droop control using common load condition in dc microgrids to improve voltage regulation and load sharing," *International Journal of Electrical Power Energy Systems*, vol. 64, pp. 752–760, 2015.

[100] J. Guerrero, L. de Vicuna, J. Matas, M. Castilla, and J. Miret, "A wireless controller to enhance dynamic performance of parallel inverters in distributed generation systems," *IEEE Transactions on Power Electronics*, vol. 19, no. 5, pp. 1205–1213, 2004.

[101] J.-W. Kim, H.-S. Choi, and B. H. Cho, "A novel droop method for converter parallel operation," *IEEE Transactions on Power Electronics*, vol. 17, no. 1, pp. 25–32, 2002.

[102] J. He, Y. W. Li, and F. Blaabjerg, "An enhanced islanding microgrid reactive power, imbalance power, and harmonic power sharing scheme," *IEEE Transactions on Power Electronics*, vol. 30, no. 6, pp. 3389–3401, 2015.

[103] J. Guerrero, J. Matas, L. de Vicuna, N. Berbel, and J. Sosa, "Wireless-control strategy for parallel operation of distributed generation inverters," in *Proceedings of the IEEE International Symposium on Industrial Electronics, 2005. ISIE 2005.*, vol. 2, pp. 845–850 vol. 2, 2005.

[104] H. Han, Y. Liu, Y. Sun, M. Su, and J. M. Guerrero, "An improved droop control strategy for reactive power sharing in islanded microgrid," *IEEE Transactions on Power Electronics*, vol. 30, no. 6, pp. 3133–3141, 2015.

[105] S.Heier, *"Grid Integration of Wind Energy Conversion Systems"*. John Wiley and Sons ltd, Chichester England, 2006.

[106] R. Pena, J. C. Clare, and G. M. Asher, "Doubly fed induction generator using back-to-back pwm converters and its application to variable-speed wind-energy generation," *IEE Proceedings - Electric Power Applications*, vol. 143, no. 3, pp. 231–241, 1996.

[107] M. Yamamoto and O. Motoyoshi, "Active and reactive power control for doubly-fed wound rotor induction generator," *IEEE Transactions on Power Electronics*, vol. 6, no. 4, pp. 624–629, 1991.

[108] Haiyan Tang, Wei He, Yongning Chi, Xinshou Tian, Yan Li, and Yukun Wang, "Impact of grid side converter of dfig on sub-synchronous oscillation and its damping control," in *2016 IEEE PES Asia-Pacific Power and Energy Engineering Conference (APPEEC)*, pp. 2127–2130, 2016.

[109] H. Shao, X. Cai, Z. Li, D. Zhou, S. Sun, L. Guo, Y. Cao, and F. Rao, "Stability enhancement and direct speed control of dfig inertia emulation control strategy," *IEEE Access*, vol. 7, pp. 120089–120105, 2019.

[110] Lie Xu and P. Cartwright, "Direct active and reactive power control of dfig for wind energy generation," *IEEE Transactions on Energy Conversion*, vol. 21, no. 3, pp. 750–758, 2006.

[111] R. Yousefian, A. Sahami, and S. Kamalasadan, "Hybrid energy function based real-time optimal wide-area transient stability controller for power system stability," in *2015 IEEE Industry Applications Society Annual Meeting*, pp. 1–8, IEEE, 2015.

[112] R. Yousefian and S. Kamalasadan, "A lyapunov function based optimal hybrid power system controller for improved transient stability," *Electric Power Systems Research*, vol. 137, pp. 6–15, 2016.

[113] A. Thakallapelli, S. J. Hossain, and S. Kamalasadan, "Coherency and online signal selection based wide area control of wind integrated power grid," *IEEE Transactions on Industry Applications*, vol. 54, no. 4, pp. 3712–3722, 2018.

[114] S. Abdelrazek and S. Kamalasadan, "A weather-based optimal storage management algorithm for pv capacity firming," *IEEE Transactions on Industry Applications*, vol. 52, no. 6, pp. 5175–5184, 2016.

[115] A. V. Oppenheim, R. W. Schafer, and J. R. Buck, *Discrete-time signal processing*. Prentice Hall, 2 ed., 1999.

[116] N. Ahmed, T. Natarajan, and K. R. Rao, "Discrete cosine transform," *IEEE Transactions on Computers*, vol. C-23, no. 1, pp. 90–93, 1974.

[117] V. Britanak, P. Yip, and K. Rao, *Discrete Cosine and Sine Transforms: General Properties, Fast Algorithms and Integer Approximations*. Elsevier Science, 2010.

[118] M. Frigo and S. G. Johnson, "The design and implementation of fftw3," *Proceedings of the IEEE*, vol. 93, no. 2, pp. 216–231, 2005.

[119] S. G. Johnson and M. Frigo, "A modified split-radix fft with fewer arithmetic operations," *IEEE Transactions on Signal Processing*, vol. 55, no. 1, pp. 111–119, 2007.

[120] B. Sun and J. Yuan, "Feature extraction from the engine measurement signal of mass characteristic based on wavelet analysis," in *2012 International Conference on Computer Science and Information Processing (CSIP)*, pp. 128–130, 2012.

[121] K. Duda, L. B. Magalas, M. Majewski, and T. P. Zielinski, "Dft-based estimation of damped oscillation parameters in low-frequency mechanical spectroscopy," *IEEE Transactions on Instrumentation and Measurement*, vol. 60, no. 11, pp. 3608–3618, 2011.

[122] M. Elsisi, M. Aboelela, M. Soliman, and W. Mansour, "Design of optimal model predictive controller for lfc of nonlinear multi-area power system with energy storage devices," *Electric Power Components and Systems*, vol. 46, no. 11-12, pp. 1300–1311, 2018.

[123] R. Maharjan and S. Kamalasadan, "Real-time simulation for active and reactive power control of doubly fed induction generator," in *2013 North American Power Symposium (NAPS)*, pp. 1–6, IEEE, 2013.

[124] S. Moghadasi and S. Kamalasadan, "Optimal fast control and scheduling of power distribution system using integrated receding horizon control and convex conic programming," *IEEE Transactions on Industry Applications*, vol. 52, no. 3, pp. 2596–2606, 2016.

[125] S. Ghosh and S. Kamalasadan, "An integrated dynamic modeling and adaptive controller approach for flywheel augmented dfig based wind system," *IEEE Transactions on Power Systems*, vol. 32, no. 3, pp. 2161–2171, 2016.

[126] M. Ramirez-Gonzalez and O. P. Malik, "Power system stabilizer design using an online adaptive neurofuzzy controller with adaptive input link weights," *IEEE Transactions on Energy Conversion*, vol. 23, no. 3, pp. 914–922, 2008.

[127] J. A. O. Lala and C. F. Gallardo, "Adaptive tuning of power system stabilizer using a damping control strategy considering stochastic time delay," *IEEE Access*, vol. 8, pp. 124254–124264, 2020.

[128] P. Zhao and O. P. Malik, "Design of an adaptive pss based on recurrent adaptive control theory," *IEEE Transactions on Energy Conversion*, vol. 24, no. 4, pp. 884–892, 2009.

[129] J. Zhang, C. Y. Chung, C. Lu, K. Men, and L. Tu, "A novel adaptive wide area pss based on output-only modal analysis," *IEEE Transactions on Power Systems*, vol. 30, no. 5, pp. 2633–2642, 2015.

[130] O. Ogundairo, A. R. Nair, M. Smith, and S. Kamalasadan, "Online adaptive damping controller architecture for wind integrated power grid," in *2020 IEEE International Conference on Power Electronics, Drives and Energy Systems (PEDES)*, pp. 1–6, 2020.

[131] R. Huang, R. Fan, J. Daily, A. Fisher, and J. Fuller, "Open-source framework for power system transmission and distribution dynamics co-simulation," *IET Generation, Transmission, Distribution*, vol. 11, 6 2017.

[132] B. Palmintier, E. Hale, T. M. Hansen, W. Jones, D. Biagioni, H. Sorensen, H. Wu, and B.-M. Hodge, "Igms: An integrated iso-to-appliance scale grid modeling system," *IEEE Transactions on Smart Grid*, vol. 8, no. 3, pp. 1525–1534, 2017.

[133] B. Palmintier, E. Hale, B.-M. Hodge, K. Baker, and T. M. Hansen, "Experiences integrating transmission and distribution simulations for ders with the integrated grid modeling system (igms)," in *2016 Power Systems Computation Conference (PSCC)*, pp. 1–7, 2016.

[134] B. Palmintier, D. Krishnamurthy, P. Top, S. Smith, J. Daily, and J. Fuller, "Design of the helics high-performance transmission-distribution-communication-market co-simulation framework," in *2017 Workshop on Modeling and Simulation of Cyber-Physical Energy Systems (MSCPES)*, pp. 1–6, 2017.

[135] H. Jain, A. Parchure, R. P. Broadwater, M. Dilek, and J. Woyak, "Three-phase dynamic simulation of power systems using combined transmission and distribution system models," *IEEE Transactions on Power Systems*, vol. 31, no. 6, pp. 4517–4524, 2016.

[136] M. J. Dolan, E. M. Davidson, I. Kockar, G. W. Ault, and S. D. J. McArthur, "Reducing distributed generator curtailment through active power flow management," *IEEE Transactions on Smart Grid*, vol. 5, no. 1, pp. 149–157, 2014.

[137] M. Farivar and S. H. Low, "Branch flow model: Relaxations and convexificationâpart ii," *IEEE Transactions on Power Systems*, vol. 28, no. 3, pp. 2565–2572, 2013.

[138] H. Sun, Q. Guo, B. Zhang, Y. Guo, Z. Li, and J. Wang, "Masterâslave-splitting based distributed global power flow method for integrated transmission and distribution analysis," *IEEE Transactions on Smart Grid*, vol. 6, no. 3, pp. 1484–1492, 2015.

[139] Z. Li, Q. Guo, H. Sun, and J. Wang, "Coordinated transmission and distribution ac optimal power flow," *IEEE Transactions on Smart Grid*, vol. 9, no. 2, pp. 1228–1240, 2018.

[140] J. Lavaei and S. H. Low, "Zero duality gap in optimal power flow problem," *IEEE Transactions on Power Systems*, vol. 27, no. 1, pp. 92–107, 2012.

[141] Z. Wang, D. S. Kirschen, and B. Zhang, "Accurate semidefinite programming models for optimal power flow in distribution systems," *arXiv: Optimization and Control*, 2017.

[142] H. Jain, K. Rahimi, A. Tbaileh, R. P. Broadwater, A. K. Jain, and M. Dilek, "Integrated transmission distribution system modeling and analysis: Need advantages," in *2016 IEEE Power and Energy Society General Meeting (PESGM)*, pp. 1–5, 2016.

[143] S. M. Mohseni-Bonab, I. Kamwa, A. Moeini, and A. Rabiee, "Investigation of besss' benefits in transmission and distribution systems operations using integrated power grid co-optimization," in *2017 IEEE Electrical Power and Energy Conference (EPEC)*, pp. 1–6, 2017.

[144] H. Sun and B. Zhang, "Distributed power flow calculation for whole networks including transmission and distribution," in *2008 IEEE/PES Transmission and Distribution Conference and Exposition*, pp. 1–6, 2008.

[145] H. Jain, B. Palmintier, I. Krad, and D. Krishnamurthy, "Studying the impact of distributed solar pv on power systems using integrated transmission and distribution models," in *2018 IEEE/PES Transmission and Distribution Conference and Exposition (TD)*, pp. 1–5, 2018.

[146] N. Kang, R. Singh, J. T. Reilly, and N. Segal, "Impact of distributed energy resources on the bulk electric system combined modeling of transmission and distribution systems and benchmark case studies,"

[147] S. Eftekharnejad, V. Vittal, G. T. Heydt, B. Keel, and J. Loehr, "Impact of increased penetration of photovoltaic generation on power systems," *IEEE Transactions on Power Systems*, vol. 28, no. 2, pp. 893–901, 2013.

[148] H. Liu, L. Jin, D. Le, and A. A. Chowdhury, "Impact of high penetration of solar photovoltaic generation on power system small signal stability," in *2010 International Conference on Power System Technology*, pp. 1–7, 2010.

[149] P. Palensky, A. A. Van Der Meer, C. D. Lopez, A. Joseph, and K. Pan, "Cosimulation of intelligent power systems: Fundamentals, software architecture, numerics, and coupling," *IEEE Industrial Electronics Magazine*, vol. 11, no. 1, pp. 34–50, 2017.

[150] K. Anderson, J. Du, A. Narayan, and A. E. Gamal, "Gridspice: A distributed simulation platform for the smart grid," in *2013 Workshop on Modeling and Simulation of Cyber-Physical Energy Systems (MSCPES)*, pp. 1–5, 2013.

[151] H. Jain, B. A. Bhatti, T. Wu, B. Mather, and R. Broadwater, "Integrated transmission-and-distribution system modeling of power systems: State-of-the-art and future research directions," *Energies*, vol. 14, no. 1, 2021.

[152] J. Momoh, R. Adapa, and M. El-Hawary, "A review of selected optimal power flow literature to 1993. i. nonlinear and quadratic programming approaches," *IEEE Transactions on Power Systems*, vol. 14, no. 1, pp. 96–104, 1999.

[153] P. Y. Nugraha, A. Widyotriatmo, and A. Samsi, "Optimization of capacity and operational scheduling for microgrid system using two-stage stochastic linear programming," in *2016 International Conference on Instrumentation, Control and Automation (ICA)*, pp. 178–183, 2016.

[154] S. Dehghan, N. Amjady, and A. J. Conejo, "A multistage robust transmission expansion planning model based on mixed binary linear decision rulesâpart i," *IEEE Transactions on Power Systems*, vol. 33, no. 5, pp. 5341–5350, 2018.

[155] M. J. Hadjiyiannis, P. J. Goulart, and D. Kuhn, "A scenario approach for estimating the suboptimality of linear decision rules in two-stage robust optimization," in *2011 50th IEEE Conference on Decision and Control and European Control Conference*, pp. 7386–7391, 2011.

[156] C. Coffrin and P. Van Hentenryck, "A linear-programming approximation of ac power flows," *INFORMS Journal on Computing*, vol. 26, 06 2012.

[157] D. Molzahn and I. Hiskens, "A survey of relaxations and approximations of the power flow equations," *Foundations and TrendsÂ® in Electric Energy Systems*, vol. 4, pp. 1–221, 01 2019.

[158] P. Parrilo and S. Lall, "Semidefinite programming relaxations and algebraic optimization in control," *European Journal of Control*, vol. 9, pp. 307–321, 12 2003.

[159] J. Löfberg, "Automatic robust convex programming," *Optimization methods and software*, vol. 27, no. 1, pp. 115–129, 2012.

[160] M. ApS, *The MOSEK optimization toolbox for MATLAB manual. Version 9.0.*, 2019.

[161] J. Warrington, P. Goulart, S. MariÃ©thoz, and M. Morari, "A market mechanism for solving multi-period optimal power flow exactly on ac networks with mixed participants," in *2012 American Control Conference (ACC)*, pp. 3101–3107, 2012.

[162] D. Gayme and U. Topcu, "Optimal power flow with distributed energy storage dynamics," in *Proceedings of the 2011 American Control Conference*, pp. 1536–1542, 2011.

[163] R. Li, Q. Wu, and S. S. Oren, "Distribution locational marginal pricing for optimal electric vehicle charging management," *IEEE Transactions on Power Systems*, vol. 29, no. 1, pp. 203–211, 2014.

[164] A. Kargarian and Y. Fu, "System of systems based security-constrained unit commitment incorporating active distribution grids," *IEEE Transactions on Power Systems*, vol. 29, no. 5, pp. 2489–2498, 2014.

[165] X. Wang and Y. Song, "Apply lagrangian relaxation to multi-zone congestion management," in *2001 IEEE Power Engineering Society Winter Meeting. Conference Proceedings (Cat. No.01CH37194)*, vol. 2, pp. 399–404 vol.2, 2001.

[166] A. Conejo, F. Nogales, and F. Prieto, "A decomposition procedure based on approximate newton directions," *Mathematical Programming*, vol. 93, pp. 495–515, 12 2002.

[167] P. Biskas, A. Bakirtzis, N. Macheras, and N. Pasialis, "A decentralized implementation of dc optimal power flow on a network of computers," *IEEE Transactions on Power Systems*, vol. 20, no. 1, pp. 25–33, 2005.

[168] Z. Li, Q. Guo, H. Sun, and J. Wang, "Coordinated economic dispatch of coupled transmission and distribution systems using heterogeneous decomposition," in *2017 IEEE Power Energy Society General Meeting*, pp. 1–1, 2017.

[169] Z. Li, Q. Guo, H. Sun, and J. Wang, "Coordinated transmission and distribution ac optimal power flow," in *2017 IEEE Power Energy Society General Meeting*, pp. 1–1, 2017.

[170] O. Ogundairo, S. Kamalasadan, and B. K, "Integrated transmission and distribution optimal power flow simulation using linear decision approach," in *2022 IEEE International Conference on Power Electronics, Drives and Energy Systems (PEDES)*, pp. 1–6, 2022.

[171] Z. Jiang, H. Tian, M. J. Beshir, S. Vohra, and A. Mazloomzadeh, "Analysis of electric vehicle charging impact on the electric power grid: Based on smart grid regional demonstration project â los angeles," in *2016 IEEE PES Transmission Distribution Conference and Exposition-Latin America (PES TD-LA)*, pp. 1–5, 2016.

[172] N. Hartmann and E. Ãzdemir, "Impact of different utilization scenarios of electric vehicles on the german grid in 2030," *Journal of Power Sources*, vol. 196, no. 4, pp. 2311–2318, 2011.

[173] C. Zhang, F. Wen, Y. Xue, G. Ledwich, and J. Lei, "Impacts of plug-in electric vehicles on distribution networks," pp. 115–120, 11 2012.

[174] S. Rezaee, E. Farjah, and B. Khorramdel, "Probabilistic analysis of plug-in electric vehicles impact on electrical grid through homes and parking lots," *IEEE Transactions on Sustainable Energy*, vol. 4, no. 4, pp. 1024–1033, 2013.

[175] Z. Jiang, L. Shalalfeh, and M. J. Beshir, "Impact of electric vehicle infrastructure on the university of southern california microgrid: Based on smart grid regional demonstration project â los angeles," in *2014 International Conference on Connected Vehicles and Expo (ICCVE)*, pp. 7–11, 2014.

[176] B. Zhou, T. Littler, and H. Wang, "The impact of vehicle-to-grid on electric power systems: A review," in *2nd IET Renewable Power Generation Conference (RPG 2013)*, pp. 1–4, 2013.

[177] W. Kempton and J. TomiÄ, "Vehicle-to-grid power fundamentals: Calculating capacity and net revenue," *Journal of Power Sources*, vol. 144, no. 1, pp. 268–279, 2005.

[178] R. Shi, L. Xu, and Y. Xue, "Research on coordinated charging strategy of electric vehicles based on pso algorithm," in *2018 Chinese Automation Congress (CAC)*, pp. 1269–1273, 2018.

[179] C. Xu, J. Shi, X. Han, J. Ma, and D. Lv, "Research on coordinated charging and influence of ev based on distributed charge control," in *2017 Chinese Automation Congress (CAC)*, pp. 5766–5769, 2017.

[180] M. Li, X. Su, X. Yan, Y. Zhang, F. Wu, D. Li, and X. Liu, "Coordinated charging and discharging of plug-in electric vehicles based on multi-layered and multi-regional optimization," *Dianwang Jishu/Power System Technology*, vol. 39, pp. 3556–3562, 12 2015.

[181] L. Qin, L. Yujiao, X. Shi, and F. Shi, "Study on coordinated charging strategy for electric vehicles based on genetic algorithm," in *2020 IEEE/IAS Industrial and Commercial Power System Asia (ICPS Asia)*, pp. 1523–1527, 2020.

[182] W. Yao, J. Zhao, F. Wen, Y. Xue, and J. Xin, "A charging and discharging dispatching strategy for electric vehicles based on bi-level optimization," vol. 36, pp. 30–37, 06 2012.

[183] X. Wang, J. Zhao, K. Wang, J. Yao, S. Yang, and S. Feng, "Multi-objective bi-level electric vehicle charging optimization considering user satisfaction degree and distribution grid security," *Dianwang Jishu/Power System Technology*, vol. 41, pp. 2165–2172, 07 2017.

[184] M. Khan and K. M. Kockelman, "Predicting the market potential of plug-in electric vehicles using multiday gps data," *Energy Policy*, vol. 46, pp. 225–233, 2012.

[185] W. Kempton and J. TomiÄ, "Vehicle-to-grid power implementation: From stabilizing the grid to supporting large-scale renewable energy," *Journal of Power Sources*, vol. 144, no. 1, pp. 280–294, 2005.

[186] C. Guille and G. Gross, "A conceptual framework for the vehicle-to-grid (v2g) implementation," *Energy Policy*, vol. 37, no. 11, pp. 4379–4390, 2009.

[187] B. K. Sovacool and R. F. Hirsh, "Beyond batteries: An examination of the benefits and barriers to plug-in hybrid electric vehicles (phevs) and a vehicle-to-grid (v2g) transition," *Energy Policy*, vol. 37, no. 3, pp. 1095–1103, 2009.

[188] H. Lund and W. Kempton, "Integration of renewable energy into the transport and electricity sectors through v2g," *Energy Policy*, vol. 36, no. 9, pp. 3578–3587, 2008.

[189] J. Taylor, A. Maitra, M. Alexander, D. Brooks, and M. Duvall, "Evaluation of the impact of plug-in electric vehicle loading on distribution system operations," in *2009 IEEE Power Energy Society General Meeting*, pp. 1–6, 2009.

[190] A. Dubey, S. Santoso, and M. P. Cloud, "Understanding the effects of electric vehicle charging on the distribution voltages," in *2013 IEEE Power Energy Society General Meeting*, pp. 1–5, 2013.

[191] A. Mohammad, R. Zamora, and T. T. Lie, "Integration of electric vehicles in the distribution network: A review of pv based electric vehicle modelling," *Energies*, vol. 13, no. 17, 2020.

[192] J. Taylor, J. W. Smith, and R. Dugan, "Distribution modeling requirements for integration of pv, pev, and storage in a smart grid environment," in *2011 IEEE Power and Energy Society General Meeting*, pp. 1–6, 2011.

[193] "NREL ATB fossil energy technology." `https://avt.inl.gov/sites/default/files/pdf/EVProj/CharacterizeEnergyDemandResidentialEVSE.pdf`. Accessed: 2023-08-15.

[194] "NREL ATB fossil energy technology." `https://atb.nrel.gov/electricity/2023/fossil_energy_technologies`. Accessed: 2023-09-15.

APPENDIX A: THEOREM PROOF

In this section, the proof of the LDR- model is discussed.

A stochastic model can be formulated as below:

$$\begin{aligned} min \quad & \mathbf{c}'\mathbf{x} + E(Q(\mathbf{x}, \bar{\mathbf{z}})) \\ s.t. \quad & \mathbf{A}\mathbf{x} = \mathbf{b} \\ & \mathbf{x} \geq \mathbf{0} \end{aligned} \tag{A.1}$$

with the $\mathbf{x}$ as vectors and other bold lower case, $\tilde{x}$ as a random variable, bold upper case such as $\mathbf{A}$ are the matrices.

where,

$$\begin{aligned} Q(\mathbf{x}, \mathbf{z}) = min \quad & \mathbf{f}'\mathbf{w} + \mathbf{f}'\mathbf{b} \\ s.t. \quad & \mathbf{T}(\mathbf{z})\mathbf{x} + \mathbf{W}\mathbf{w} + \mathbf{B}\mathbf{b} = \mathbf{h}(\mathbf{z}), \\ & w_i \geq 0, \quad \forall i \in I \subseteq \{1, ...n_2\} \\ & b_i \geq 0, \quad \forall i \in I \subseteq \{1, ...n_2\} \end{aligned} \tag{A.2}$$

Additionally, $\mathbf{c}$, $\mathbf{f}$ and $\mathbf{b}$ are known vectors in $\Re^{n_1}$, $\Re^{n_2}$ and $\Re^{m_1}$, $\mathbf{T}(\tilde{z})$, $\mathbf{h}(\tilde{z})$ are assumptions for affine data dependency.

$$\mathbf{T}(\bar{\mathbf{z}}) = \mathbf{T^0} + \sum_{\mathbf{k=1}}^{\mathbf{N}} \mathbf{T^k}\tilde{\mathbf{z}}_\mathbf{k}, \quad \mathbf{h}(\tilde{\mathbf{z}}) = \mathbf{h^0} + \sum_{\mathbf{k=1}}^{\mathbf{N}} \mathbf{h^k}\tilde{\mathbf{z}}_\mathbf{k} \tag{A.3}$$

$$\begin{aligned} Z_{STOC} = min \quad & \mathbf{c}'\mathbf{x} + E(\mathbf{f}'\mathbf{w}(\bar{\mathbf{z}})) + E(\mathbf{f}'\mathbf{b}(\bar{\mathbf{z}})) \\ s.t. \quad & \mathbf{A}\mathbf{x} = \mathbf{b}, \\ & w_i(\tilde{\mathbf{z}}) \geq 0, \quad \forall i \in I, \\ & b_i(\tilde{\mathbf{z}}) \geq 0, \quad \forall i \in I, \\ & \mathbf{x} \geq \mathbf{0} \\ & \mathbf{w}(\tilde{\mathbf{z}}) \in \mathcal{Y} \\ & \mathbf{b}(\tilde{\mathbf{z}}) \in \mathcal{Y} \end{aligned} \tag{A.4}$$

Translating into LDR

$$\mathbf{w}(\bar{z}) = \mathbf{w}^0 + \sum_{k=1}^{N} \mathbf{w}^k \bar{z}_k \tag{A.5}$$

$$\mathbf{b}(\bar{z}) = \mathbf{b}^0 + \sum_{k=1}^{N} \mathbf{b}^k \bar{z}_k \tag{A.6}$$

The stochastic model approximation is then written in the LDR

$$\begin{aligned} Z_{LDR} = min \quad & \mathbf{c'x} + \mathbf{f'w^0} + \mathbf{nf'b^0} \\ s.t. \quad & \mathbf{Ax} = \mathbf{b}, \\ \mathbf{T^k x} + \mathbf{W w^k} + \mathbf{B b^k} = \mathbf{h^k} \quad & \forall k \in \{0, ...N\}, \\ w_i(\mathbf{z}) \geq 0 \quad & \forall \mathbf{z} \in W, \forall i \in I, \\ b_i(\mathbf{z}) \geq 0 \quad & \forall \mathbf{z} \in B, \forall i \in I, \\ & \mathbf{x} \geq \mathbf{0}, \\ & \mathbf{w}(.) \in \mathcal{L} \\ & \mathbf{b}(.) \in \mathcal{L} \end{aligned} \tag{A.7}$$

$$\begin{aligned} w_i(\mathbf{z}) \geq 0 \quad & \forall Z \in W \\ w_i^0 \geq \sum_{j=1}^{N} (z_j s_j + \tilde{z}_j t_j) \end{aligned} \tag{A.8}$$

If the solution at equation(A.7) is feasible, then it will be in equation(A.4), $Z_{STOC} \leq Z_{LDR}$, with $\mathcal{W}$ = [-z, $\tilde{z}$]. for some **s**,**t** ≥ 0 satisfying s_j-t_j = w_i^j. The variables that are implemented above can be translated to our operation of the integrated T&D model with several renewable energy resources connected to the grid. By correlation, the variable w is the P_{PG}, the variable x is the $\mathrm{P}_{k,RP}$, while the uncertainty $\tilde{Z}$ is the P_{PV}, the variable b can be a binary variable which can be a decision of an electric vehicle user to charge or not.

APPENDIX B: SIMULATION TOOLS

The dissertation was performed using the following system parameters, simulation tools, and solvers.

1. HP Computer with RAM 16GB, speed 2.7GHz, and storage 450GB windows OS.
2. Simulink and MATLAB R2019-R2022.
3. Python in Jupyter notebook.
4. Mosek, Gurobi and Yalmip solvers.
5. GridAppsD with Linux OS.